UNIVERSITY OF SOUTHAMPTON

Experimental and Analytical Techniques for the Assessment of *In Vitro* Implant Migration in Polymer Foam Models

by

Vinu Palissery

A thesis submitted in partial fulfillment for the degree of Doctor of Philosophy

in the

Faculty of Engineering and Applied Science

School of Engineering Sciences

April 2004

Acknowledgements

I would like to express my sincere thanks to .....

Dr Mark Taylor and Dr Martin Browne, my supervisors, for their invaluable guidance, care, encouragement and patience shown at all productive discussions have helped me a lot in shaping up this thesis.

Wright Medicals (UK) for financially supporting this research work.

The technicians in the Engineering Materials and EDMC labs, and especially to Eric Bonner, for their help and technical assistance in carrying out the experimental work.

Eric Bonner for taking up the tough task of being my guardian and for standing by me in good and bad times.

My colleagues and staff members of the department, who always rendered their help, support and co-operation.

Ros & Dave for the warm and homely atmosphere during my stay with them.

Dr R. P. R. Nair and Dr Chandra Kishen for motivating me to study further and for their valuable advises.

My friends at Southampton and far away places, for their timely help, sweet inspiration, pleasant company and much treasured friendship.

My family and other relatives for their love, understanding and support in all my endeavours.

Whatever I have accomplished, I owe it to my parents, teachers and mainly to GOD.

UNIVERSITY OF SOUTHAMPTON

ABSTRACT

FACULTY OF ENGINEERING AND APPLIED SCIENCE
SCHOOL OF ENGINEERING SCIENCES

Doctor of Philosophy

by Vinu Palissery

In vivo studies on implant migration indicate that migration in the first two years after implantation could be used as a predictor of failure by aseptic loosening. Currently there are no preclinical methods capable of predicting the risk of migration and hence the risk of aseptic loosening. A possible cause of migration is fatigue failure of the cancellous bone, which is in direct contact with the prosthetic components.The aim of this study was to develop a preliminary *in vitro* tool, using a combined experimental and numerical approach, for simulating migration.

The first phase of this thesis examined the use of two polymer foams as a suitable analogue material to cancellous bone. Fatigue characterisation of the polymer foam materials showed the materials to be qualitatively similar to cancellous bone in their behaviour. However, quantitative differences existed as compared to cancellous bone and also between the analogue materials themselves; the foams showed less modulus degradation and accumulated strain compared to cancellous bone. Relationships were established for life, secondary strain rate, modulus reduction and accumulated strain in terms of normalised stress and life fraction. In the absence of established data for the fatigue properties of cancellous bone/analogue materials, the approach employed here could form the basis for the selection of a suitable analogue *in vitro* test medium for assessing the performance of implants.

A combined Finite Element and Continuum Damage Mechanics method was used for the fatigue/migration simulation. Life fraction was used as the damage parameter and a coupled analysis was conducted based on the relationships for modulus and accumulated strain. The algorithm used an iterative procedure where each iteration simulated a number of cycles. The models were capable of simulating the given input behaviour satisfactorily for uniaxial compression tests of both the materials. However, under very high stress levels the models were sensitive to localisation of damage, and underpredicted life. The method was extended to a bonded, foam and metal plate model of migration, simulating an idealised model of the implanted proximal tibia. In the simulations, the effect of the stress concentration near the plate edges was found to dominate the model behaviour; it caused a significant underprediction of migration. However, a similar trend was observed between the FE models and the experiments in terms of migration pattern and how it varied with load.

The research has proposed a suitable methodology for migration simulation and the FE methods for simulation have been qualitatively validated using the experimental results. Further refinements to the models need to be made in order to produce a validated quantitative predictive tool.

List of Figures

List of Tables

Nomenclature

Definitions for the abbreviations and symbols and terms used in this thesis are presented here.

Abduction	A movement away from the midline of the body or the segment
ACL	Anterior Cruciate Ligament
Adduction	The return movement of the segment back toward the midline of the body or segment
AML implant	Anatomic Medullary Locking implant
Anisotropic	Having material properties that are different in different directions, or having no planes of material symmetry
Anterior	An anatomical term meaning situated before or to the front
A-P	Anterior-Posterior
Atrophy	A wasting away, a diminution in the size of a cell, tissue, organ or part
CDM	Continuum Damage Mechanics
CT	Computerised tomography
Diaphysis	The shaft or slender part of the bone
Distal	A position away from the reference point
Epiphysis	The enlarged ends of long bones
Extension	a straightening movement where the relative angle between two adjacent segments increases as the joint returns back to the zero, anatomical position
FEA	Finite Element Analysis
Femur	The large bone in the thigh that articulates with the pelvis above and the knee below
Flexion	A bending movement where the relatives angle between two adjacent segments decreases
Frontal plane	This is a flat vertical plane passing through the body from side to side, dividing it into a front half and a back half
HA	Hydroxy-apatite
HCF	High Cycle Fatigue
Hypertrophy	The enlargement or overgrowth of an organ or part due to an increase in size of its constituent cells
Internal rotation	The act of turning about an axis passing through the centre

continued on next page

	of the leg
Isotropic	Having material properties independent of direction
Lateral	Away from the sagittal plane
LCF	Low Cycle Fatigue
Lesser trochanter	A large process that projects from the posteromedial surface of the femur just distal to neck
Medial	Towards the sagittal plane or closer to the midline
Metaphysis	The flared end of diaphysis where the shaft merges with the epiphyses
M-L	Medial-Lateral
MTPM	Maximum Total Point Motion
OA	Osteo Arthritis: Noninflammatory degenerative joint disease of the articular cartilage, occurring chiefly in older persons, characterised by degeneration and changes in the synovial membrane.
Orthotropic	orthotropic material has at least 2 orthogonal planes of symmetry, where material properties are independent of direction within each plane
Osteoporosis	A pathologic condition leading to reduction in the amount of bone mass, leading to fractures
PCA	Porous Coated Anatomic
PCL	Posterior Cruciate Ligament
PFC	Press Fit Condylar
Posterior	Situated behind or to the back; designated the hinder part, as of a foot
Proximal	A position closer or nearer to the reference point
PMMA	Poly methyl methacrylate
RA	Rheumatoid Arthritis: It is characterised by the inflammation of the membrane lining the joint, which causes pain, stiffness and swelling. The inflamed joint lining can invade and damage bone and cartilage
RSA	Roentgen Stereophotogrammetric Analysis
Sagittal plane	This is a flat vertical plane passing through the body from front to back, dividing the body into a right and left half
Sensitivity	The sensitivity of a test can be described as the proportion of true positives it detects of all the positives
Specificity	The specificity of a test can be described as the proportion of

continued on next page

	true negatives it detects of all the negatives. It is thus a measure of how accurately it identifies negatives.
THR	Total Hip Replacement
Tibia	The large bone between the knee and foot
TKR	Total Knee Replacement
Transverse plane	This is a flat horizontal plane passing through the body, dividing the body into a upper and lower half
Valgus	An abnormal position in which part of a limb is twisted outward away from the midline
Varus	An abnormal position in which part of a limb is twisted inward toward the midline
Upper trochanter	large prominence projecting upward from shaft on lateral aspect of the junction of neck body of femur
UHMWPE	Ultra High Molecular Weight Polyethylene
σ	Stress component
ω	Damage
$\triangle\omega$	Damage increment
ϵ_{acc}	Accumulated strain
$\frac{\epsilon_{acc}}{dN}$	Steady state accumulated strain rate
N	cycle number
N_f	number of cycles to failure
E_*	Secant modulus from the preconditioning tests
E_o	The secant modulus from the first cycle of fatigue
E	The secant modulus at any cycle of fatigue
E_{N_f}	The modulus at N_f, number of cycles to failure

Chapter 1

Background, Aim and Objectives

1.1 Introduction

Total hip replacement (THR) and total knee replacement (TKR) have become a routine operation for many disorders and diseases of the respective joints, allowing pain reduction, improved movement and increased activity levels for the patient. The surgery involves removal and replacement of the affected joint with artificial parts called prostheses. Approximately 40,000 hips and 30,000 knees replacement operations are carried out per year in UK. Arthroplasty registries report an approximate 100 surgeries per 100,000 inhabitants[68, 115, 118]. However joint replacement does not guarantee long term success, and an artificial joint may eventually fail, requiring a revision surgery. An estimated 10% of all joint replacements performed each year are revision operations[68, 115, 118, 176].

1.1.1 Anatomical Terms and Description of Movement

This section explains the terminology used to describe human movements including planes and axes of motion and joint actions; these terms may repeatedly appear in the literature review. Anatomical position is the position of the body in its erect posture with the arms hanging along the sides of the body and the palms looking forwards. Three imaginary orthogonal planes through the human body in its anatomical position are normally used for the reference system.

- Sagittal or Antero-posterior(A-P) - divides the body into right and left halves.
- Frontal or coronal - divides the body into front and back halves

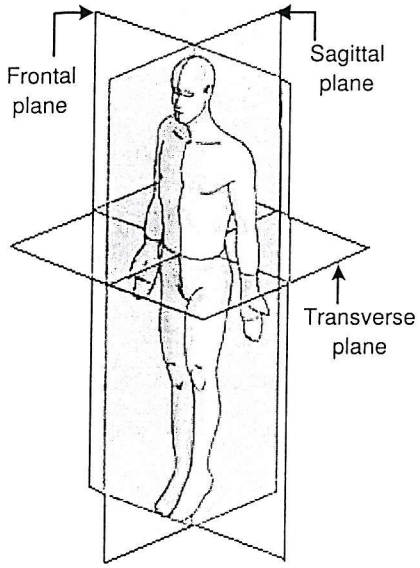

FIGURE 1.1: A Schematic of the anatomical planes, which are used as reference planes for describing anatomical position and movement. http://www.spineuniverse.com/displayarticle.php/article1023.html

- Transverse or horizontal - divides the body into top and bottom halves

To describe the location on the body some directional terms are used normally in pairs.

- Anterior and posterior - nearer to the front and back surface of the body respectively
- proximal and distal- nearer and further from the trunk respectively
- medial and lateral - closer and further from the midline respectively

The movements of the body are described about axes normal to the anatomical reference planes. These axes and corresponding reference planes are

- Frontal axis - sagittal plane
- A-P axis - frontal plane
- Longitudinal or vertical axis - transverse plane

A few more terms in relation to the anatomical movements are given below.

- Flexion and extension -The movement at a joint which decreases the angle between two adjacent body segments is know as flexion. The opposite action is extension, where the angle between body segments is increased
- Adduction and abduction - Movement of the leg or arm away from the midline and towards the midline respectively
- Medial and lateral rotation - Rotating the leg inward and outward about a vertical axis respectively

1.1.2 Anatomy of the Hip and Knee

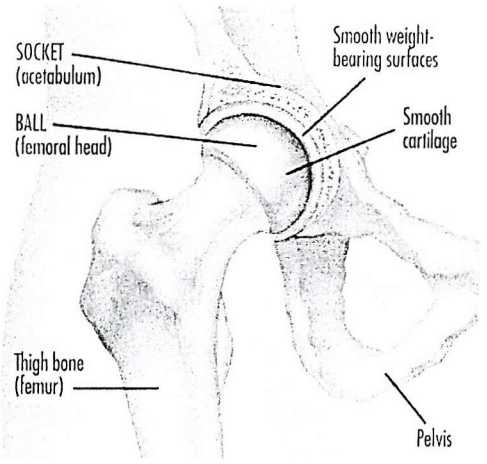

FIGURE 1.2: Anatomy of normal hip (www.mapletonhill.com/Hip%20Anatomy.html)

The hip joint, the largest ball and socket joint in the body, is located where the thigh bone (femur) meets the pelvic bone. The ball or the upper end of the femur (the head of the femur) articulates within the cavity in the pelvic bone or the socket (acetabulum). A smooth surface called cartilage covers the articulating surfaces. The head narrows distally into the neck of the femur. The projection lateral to the neck is called the greater trochanter, while the projection medial and inferior to the neck is known as the lesser trochanter. These are the locations for the muscle attachments. The hip allows movements in all three planes of motion including flexion-extension, abduction-adduction and medial-lateral rotations.

The knee is the largest joint in the body. It is a hinge type joint which is formed by two bones, the proximal tibia and distal femur, held together by flexible ligaments. In addition to the hinge type motion the joint surfaces can glide and roll which makes the knee a very complex joint. The knee cap (patella) which glides over the end of the femur as the knee bends also forms part of the knee joint. Again, the articulating surfaces are covered by the cartilage. The joint is kept stabilised by ligaments and tendons. The collateral ligaments along the sides of the knee provide stability when the knee moves from varus/valgus rotation. The anterior cruciate ligament (ACL) and posterior cruciate ligament (PCL) control the front to back motion of the knee joint.

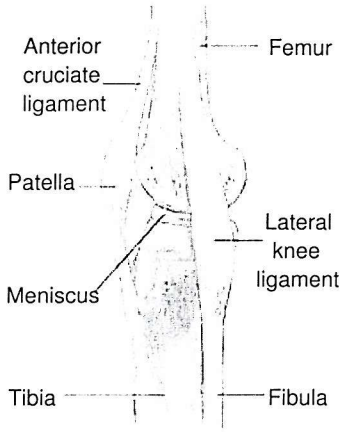

FIGURE 1.3: Anatomy of normal knee in lateral view (www.celebrationjointreplacement.com/ knee.htm)

1.1.3 Diseases/Causes of Joint Replacements

As we age, disease and injury may cause the cartilage to thin or break and the bone surfaces to rub against each other causing pain. To relieve pain, surgery is often performed to replace the worn part of the joint. The most common disease resulting in hip and knee replacement surgery is arthritis. The most common types of arthritis are Osteoarthritis (OA), Rheumatoid Arthritis (RA) and Post-traumatic arthritis. Osteoarthritis (OA), or sometimes known as degenerative arthritis, causes the cartilage between the bones to gradually deteriorate leading the bones to rub together causing pain, swelling and reduction in range of motion. There are primary and secondary causes for osteoarthritis, where primary arthritis is linked to the break down of cartilage due to the natural wear and tear of the joint over years. Secondary osteoarthritis results from conditions like obesity and congenital deformities. Rheumatoid Arthritis is the inflammation of the tissue which lines the inside of the joint resulting in hot, swollen, stiff and painful joints. Arthritis resulting from an injury to the joint is referred as post-traumatic arthritis. Replacement surgery is suggested in cases of joint pain due to conditions like injury, bone tumor and avascular necrosis (bone death due to insufficient blood supply). Hip replacement surgery is also suggested in cases of proximal femoral fracture. According to various national registries on hip replacement, for more than 70% of the patients osteoarthritis is the main indication for an operation[68, 115, 118] while for the rest of the patients diagnosis of fracture, RA, secondary arthritis and other reasons were the reasons. According to the reports by the Swedish knee arthroplasty register[176] more than 80% of the primary operations for knee replacement are done for cases of OA, while nearly 10% of the operations are done for RA and the remaining

operations are done for cases like post traumatic arthritis, osteonecrosis and other reasons.

1.1.4 Total Hip replacement

During the surgery the femoral head is replaced with a metal ball attached to a metal stem where the stem is fixed into the prepared hollow space inside the femur, which provides stability. The worn out hip socket is lined with a plastic or metal socket. The metal part of the components are made of titanium, stainless steel or cobalt/chromium alloys and the plastic parts are made of ultrahigh-molecular weight polyethylene (UHMWPE). While the basic design remains the same, each part of the implant components comes in various sizes, shapes and degrees of roughness. A pictorial representation of total hip replacement is given in Figure 1.4.
Not all hip joints need total hip replacement and sometimes alternative hip operations are carried out. For example, in surface replacement, instead of removing the whole femoral head both hip joint surfaces are replaced by two concentric spherical cups.

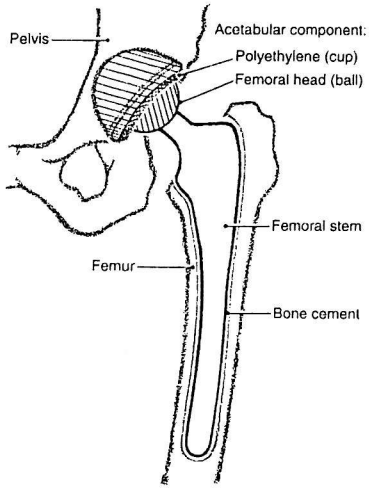

FIGURE 1.4: A schematic representation of the elements of total hip replacement (http://www.consensus.nih.gov/ cons/098/098hip.htm)

1.1.5 Total Knee Replacement

In the replacement surgery thin layers of bone are removed from the damaged surface of the distal femur and proximal tibia. A metallic femoral component and a polyethylene tibial component replaces the removed bone of the distal femur and the proximal tibia

respectively. The tibial component may or may not include a metal back. The main design types of TKR give the option of either a fixed bearing or a mobile bearing design or a cruciate retaining or cruciate substituting design. In the fixed bearing design the metallic tibial tray and the polyethylene insert are fixed together so that there is no significant movement between them. In the case of mobile bearing knee replacement, both the metallic femoral and tibial components articulate against the polyethylene insert. The tibial component is provided with additional fixation arrangements like a stem or screws in some designs. The posterior part of the knee cap (patella) may also be resurfaced with a polyethylene component. The metal part of the components are made of titanium or cobalt/chromium alloys and the plastic parts are made of ultrahigh-density polyethylene.

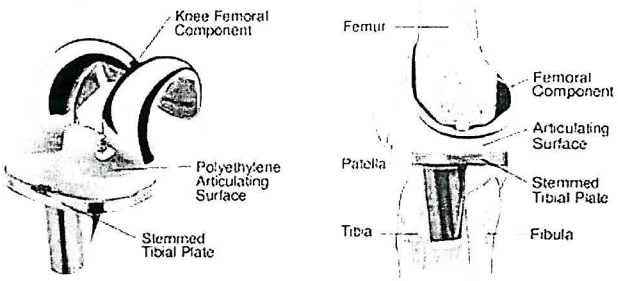

FIGURE 1.5: A schematic representation of the elements of total knee replacement(www.celebrationjointreplacement.com/ knee.htm).

1.1.6 Classification of Implants Based on Fixation

The most commonly reported components in terms of aseptic loosening are the femoral component of THR and tibial component of TKR. The further literature review in this chapter will focus only on the femoral and tibial components of THR and TKR respectively while discussing various issues related to THR and TKR. Based on the type of fixation to the bone, both THR and TKR prostheses can be classified as cemented and uncemented.

In the case of cemented implants, the components are fixed to bone using a grout referred to as bone cement or polymethylmethacrylate (PMMA). A stable interface and good contact between the components are important in this case. Although cemented implants allow increased activity initially, poor cement quality/techinique or/and poor bone quality and repeated loading effects can lead to failure of the cement mantle interface. Also cement debris particles at the interface can cause osteolysis, an inflammatory reaction to wear and debris particles.

Cementless implants have been introduced to encourage prosthesis attachment directly to the bone. The implants have a surface which is either rough or porous or with beads or a meshed surface to provide a platform for the bone to grow into and fix the implant stably to the bone. The newer versions of cementless implants are coated with Hydroxyapatite (HA coated implants). The HA coating has a similar chemical composition to bone, and this is considered to enhance the bone growth. The term press-fit is used for uncemented implants, when an oversized implant is fixed into an undersized cavity in the bone. The prestress created by press-fitting is considered to provide the equilibrium of forces to keep the implant in place. Cementless implants are considered to be suitable for younger (under 50 years of age), more active patients and patients with good bone quality where bone ingrowth into the components can be predictably achieved. Uncemented implants with porous coatings and HA coatings have comparable results to those of cemented implants [47, 93, 166]. At present, however, cemented prostheses are the most widely used implants with the national registries reporting more than 90% of currently used implants as cemented[115, 118, 176]. Though the basic designs of THR and TKR remain the same, changes between designs are seen in the form of size, shapes, region and extent of coating.

1.1.6.1 Causes of Revision Surgery

There are a number of conditions which necessitate revision of a prosthesis. These include aseptic loosening, infection, dislocation, wear, osteolysis, component failure and instability [68, 176]. Aseptic loosening is the major cause accounting for 75% and 45% of revisions of hip and knee replacements respectively[68, 176]. Only a brief explanation is given here for causes other than aseptic loosening, as aseptic loosening is the mode of failure of interest.

Infection following total joint replacement can be categorised as either superficial or deep infection of the tissues surrounding the implant. While late chronic infections are usually treated by removal of the prosthesis, some early post-operative infections can be treated with the retention of the prosthesis[187]. Dislocation occurs when the fit between the components is poor or when the orientation is such that it cause the component to slip from its normal position. Excessive wear of the polyethylene component, errors in positioning and other surgical factors could cause dislocation of the implant.

Wear occurs when particles of material are removed from the bulk material due to the articulation of surfaces or due to micromotion at the interfaces of the implanted construct.

An inflammatory response to wear particles at the interface, which causes the removal

or resorption of bone is called osteolysis; this can weaken the surrounding bone and cause loosening. Osteolysis may occur secondary to wear or due to mechanical effects of loosening at the interface.
Fracture of bone most commonly occurs in cementless implants where too big a component has been forced into too small a cavity. Fracture of the surrounding bone can occur during or after surgery, due to errors in manipulating bone during surgery, or the presence of stress raisers in the bone such as screw holes or osteoporosis, which weakens the bone. Corrosion of materials and biological reactions to these corroded materials can also lead to failure in some cases.
Instability of the replaced knee joint is a cause of revision, and is considered due to malalignment, poor restoration of the proper joint level and collateral ligament imbalance[49, 126].

Aseptic loosening is a gradual process, where the mechanical integrity of the implant-bone construct is lost through various mechanical and biological failure scenarios, resulting in observation of symptoms of such as severe pain and the presence of radiolucent lines at interfaces, relative movement of the implant with respect to bone, cement fracture (if present) and osteolytic lesions. Over years the biological and mechanical failure processes can be interconnected resulting in the acceleration of both processes. Many survival analysis studies of implanted joints use aseptic loosening as the end point as it is the major cause of revision. It is also noticeable that there may be variations in aseptic loosening mechanisms based on design, type of fixation and age. Cemented implants in general perform well with a revision rate of less than 10% after 10 years. For patients under the age of 50 there are different reports on the performance of cemented implants[11, 167]. While Sharp and Porter[167] observed a higher incidence of failure for cemented THA patients under the age of 40, Boeree et al.[11] reported a similar revision rate to that reported for elderly patients. Uncemented implants have varying results; many of the early generations of uncemented implants were reported to have poor results[44, 134, 141]. However, the newer versions of uncemented implants with porous coatings and HA-coatings have comparable results to those of cemented implants[17, 47, 93, 166]. Revision rates may vary depending on a variety of factors including age, sex, diagnosis and these vary as the demography of the study group varied. Results from a few survival analysis studies by registries and individual groups are summarised in Table 1.1.

1.1.6.2 Mechanical Failure Scenarios of Replacement

The local mechanical environment is altered by the implantation of a total joint replacement. In the intact femur load is transferred from the femoral head to the stiffer

TABLE 1.1: Survival analysis results from National Arthroplasty Registries and clinical trials

Results from arthroplasty registries				
Register& location	Diagnosis for THR/TKR	Major reason for revision	Revision rate	Comments
Swedish Arthroplasty Register, THA (1979-1998)[118]	OA(75%) fracture(11%)	aseptic loosening(75.7%) deep infection(7.2%)	cemented(7%) uncemented(13%)	100 THR/100,000 inhabitants, 93% cemented implants, outcome of modern uncemented implants not known
Danish Arthroplasty Register, THA, (1995-1998)[115]	OA(75%) fracture(11%)	aseptic loosening(64%) dislocation(12%)	3%	93 primary THR/100,000 inhabitants, 64% primary THR cemented implants, lowest survival rate(94%) in young men with hyrid implant
Swedish Arthroplasty Register, TKA[176] (Annual report, 1999)	OA RA	aseptic loosening(43.7%) infection(11.2%)	5-10%	80% of TKR cemented implants, survival rate varied with age, diagnosis etc
Results from clinical trials				
Location & study period	Type of fixation (No. of implants)	Aseptic loosening	Revision or survival rate	Comments
THR, 10 to 15 years[93]	Porous coated(311)	10 stem out of 17 hips revised	90% (survival)	thigh pain and an increasing prevalence of osteolysis , variation in survival rate with sex
THR, 11 years [54]	Two different cemented implants(410)	5 stem out of 15 cases of revision	94.5% (survival)	with patient dissatisfaction as end point, survival rate 83%, loosening rate different for two implants
THR, 10 to 18 years[11]	Two different cemented implants(51)	6 stem out of seven failure cases	12.7% revision at 12 years	patients avg. age less than 50, clinical signs unreliable in determining failure, high activity level for revised cases
TKA, 10 to 12 years[192]	cemented(130)	3 tibial loosening out of 6 cases of revision	6.8% (revision)	failure to achieve alignment, proximal tibial bone resection lead to loosening, radiological and clinical signs showed poor correlation
TKA, 10 years[166]	Porous coated(114)	3 tibial component loosening out of 3 revisions	97% (survival)	survival rate 87% when pain and radiologic loosening were considered, no progressive osteolysis

cortical bone of the diaphyseal bone via network of trabecular bone. In total hip replacement load is transferred through contact at the bone-implant interface, along the length of the prosthesis, by tension, compression and shear, depending on the mode of fixation. Therefore bone is loaded abnormally from the inside. In the case of knee replacement the distribution of applied load is the same, however, the harder subchondral bone is replaced by the tibial plate, exposing the trabeculae at the interface to take the load transmitted at the interface. An effective load transfer similar to intact condition depends on factors like the design of the component, interface condition and the material properties.

Sharing and distribution of load between implant and bone depends on the implant shape, rigidity and type of fixation, interface conditions and quality of the supporting bone. A bone/prosthesis structure can be considered as a composite structure with different elastic and geometric properties, where the stress pattern in the structure is dependent on the bonding characteristics at the interface and the relative magnitudes of the elastic modulii[82]. The frictional and adhesive characteristics of the surfaces and the orientation of the interface relative to the dominant direction of loading are important factors in the stress transfer in composite structures. A successful distribution of load at the interface is based on assuring integrity of the interface in terms of initial fixation and its maintenance over time. Bones are subjected to a variety of loading patterns which can be instantaneous or repetitive and can vary in direction, magnitude, frequency and mode. At the same time, bone is continuously being remodelled according to the mechanical environment. The response of bone, the biological component of the composite structure, to the mechanical environment at the interface is important in this respect. A decrease in the experienced stress/strain stimulus causes bone to resorb (atrophy), while an increase in stress/strain stimulus result in an increased building up of new bone cells (hypertrophy). This is commonly referred to as Wolff's law. The presence of foreign particles causes osteolysis, an inflammatory reaction to remove the particles which also causes the removal or resorption of some bone. An implant coating such as HA can enhance bone ingrowth, known as osseoinduction. Relative movements taking place at the interface are also important as it is considered that there is an optimum movement which is ideal for bone rebuilding stimulus[145]. A movement in excess of this can cause bone resorption.

Huiskes et al.[80] summarised various contemporary failure theories for the hip replacement which included accumulation of damage, particulate reaction, failed bonding, stress-shielding, stress by pass and destructive wear. Accumulation of gradual damage occurs over time under dynamic loading. In the case of cemented implants, for which this failure scenario is considered to be more relevant, damage occurs with cement cracking and debonding of the stem-cement and the cement-bone interface. With time

this can result in further debonding, interface micromotion, cement failure, bone resorption, fibrous interposition and gross loosening. In the case of uncemented implants the accumulation of damage may lead to disruption of the coating. The stress pattern and the strength of materials and interface bonding are the major factors which determines the progression of this failure scenario.

Cement debris and polyethylene wear particles accumulate at the interface subsequent to the damage accumulation scenario and from the articulating surfaces causing bone resorption and gradual debonding of the bone-implant interface.

In the case of uncemented implants, the failed bonding scenario is considered to be valid when bone ingrowth or osseous integration does not take place after implantation, normally due to an excessive relative micromotion at the interface causing bone resorption, fibrous tissue formation and eventual loosening. Relative micromotion above $150\mu m$ is considered to prevent bone ingrowth[145]. Poor initial fit and high initial relative interface motions are the major factors considered to cause the failed bonding scenario.

Stress shielding occurs when the bone is shielded from load by the prosthetic component causing resorption of bone. Stress shielding is not directly related to loosening, though it can cause loss of bone stock and can cause bone or stem fracture. It depends on the effectiveness of load transfer between implant and bone in maintaining the stress/strain distribution close to that of the intact bone. Stress by-pass is caused when stress is by passed through another route and causes a similar effect as stress shielding. Stress by-pass is similar to stress shielding, in that bone is shielded from the applied load, but is a result of poor fixation. For example, over-reaming the proximal femur may result in poor proximal contact resulting in the load being transmitted more distally than intended. Destructive wear can occur when the articulating surfaces wear out and unable to maintain the mechanical integrity any further.

Tibial components are designed mainly for compressive load bearing. Because the hard subchondral bone of the tibia is removed during a knee replacement, loads are absorbed by the softer cancellous bone and the peripheral cortical bone that remains. If loads are heavier than the underlying bone can bear over a long period of time, the prosthesis will begin to sink into or loosen from its attachment to the bone. Though many of the above mentioned failure scenarios of hip replacements are present in the case of tibial components, the most commonly observed failure modes in tibial component loosening are the failure of the component materials, compressive failure of trabecular bone and fragmentation of cement[21, 43, 197]. Thus the stress pattern and mechanical properties of the materials involved and their interface bond are the most important factors affecting loosening in tibial implants. A non-uniform axial load distribution across the medial and lateral condyles along with the torsional load experienced at

the joint, can lead to bending, rotation and sinkage of the tibial component/plateau [21]. Eccentric and tangential loads can cause shear stress at the interfaces and lift off can occur with eccentrically applied loads in the absence of sufficient anchorage. Larger compressive stresses in over loaded regions, micromotion, tensile and shear forces at implant-cement interfaces and failure of bone ingrowth follows, resulting in a progressive loosening at the interfaces. Bone resection, alignment of the component, achievement of normal tibiofemoral alignment and knee function after implantation, activity levels and the rigidity, shape and fixation of the tibial component are major factors affecting the success of tibial implants[43, 146, 192, 200]. Firm fixation against movements and sufficient strength against the applied stresses are the most important factors in the case of tibial fixation. Stems, screws, and pegs are used for firm fixation of the components into the bone, though in some cases sharing of load by the can cause stress-shielding in the proximal region.

1.1.7 *In Vivo* Evaluation of Implant Performance

While the individual prosthetic components undergo many standard tests before implantation to ensure its biocompatibility, resistance to corrosion, degradation and wear and mechanical properties, there are no standardised preclinical methods to ensure the *in vivo* performance of total joint replacements. Present methods for the evaluation of an implant's performance are based on results of clinical studies.
Survival analysis is a statistical tool used to determine the success of joint replacements by determining the cumulative survival rate of implants usually with revision surgery as an end parameter [68, 176, 115, 118, 155]. The Swedish Arthroplasty Register, Norwegian Arthroplasty Register and Danish Arthroplasty registers [68, 176, 115, 118, 155] are examples of such analyses on a national basis; other than that, there are studies carried out by hospitals and individuals on smaller populations. Usage of national registries for survival analysis are encouraged as they give a nation's experience in arthroplasty based on a large data set and improve the quality control and assurance on a national basis. Survival analysis along with clinical follow-ups of implants can give more information about the failure and clinical symptoms of failure. However, survival analysis studies cannot provide any details of primary causes and/or mechanisms of failure. In the case of survival analysis with clinical follow ups performance bias between centers of excellence and routine surgery is possible as such studies are often conducted by a limited group of surgeons who are likely to be superior from the general population of surgeon and are well aware of the implant design philosophy[54, 80].
Conventional clinical methods of implant assessment are based on radiological observations of incidence and progression of radiological signs and changes in pain and

functional levels[45]. Using radiological methods, X-rays of the respective joints are taken at regular intervals, normally anterior-posterior(A-P) and lateral views, and bone implant interfaces are observed for changes in alignment, the presence of radiolucent lines and their density and progression, cement fracture, gaps at the interface, osteolysis, bone resorption and movement of implant[3, 43, 45, 61, 66, 114]. The failure stage is evaluated based on these signs. A progressively migrating or moving implant with or without radiolucent lines is always considered to indicate an impending failure. In the case of porous coated and HA coated implants the radiographs are evaluated for the status of biological fixation[46, 93]. The absence of radiolucent lines around the porous-surfaced portion of the implant and presence of new bone bridging the gap between the bone and porous surface of implant are considered as a sign of good implant fixation while progressive radiolucency and migration are indicators of instability. Assessment of pain and function is based on patient interview/questionnaires. Patients are asked to answer questions regarding levels of pain, function and range of motion and are asked to rate them in a respective scale as suggested by the method of scoring[23]. A considerable increase in postoperative score compared to preoperative score is a qualitative indication of success of arthroplasty in terms of patients' comfort.Severe pain is a common indication for revision surgery due to aseptic loosening. Conventional clinical methods use combinations of clinical signs for the failure criteria making the prediction complex and often the criteria varies in different studies[23]. Factors like non-standardisation of radiographs for the proper alignment and reduction of 3-D reality into a 2-D radiograph and the limited ability of radiolucency for failure prediction in the absence of gross evidence are considered as problems associated with radiological assessment of implant performace[3, 45, 46, 192]. A standardised procedure to follow the progressive changes in radiolucent signs is required. Although progressive migration is a definite indicator of aseptic loosening, it can only be recorded after considerable movement of the implant has occurred.

However, *in vivo* migration studies of implants, with accurate measurement techniques like radiostereometric analysis (RSA) and standardised radiograph techniques, have shown that migration, permanent movement of implant with respect to bone, within two years after implantation can be used to predict failure due to mechanical loosening[53, 159]. Migration studies of implants have shown that all prostheses migrate to some extend, irrespective of design, location and fixation, and it is those implants which continue to migrate and migrate at a higher rate which are bound to fail[5, 92, 101, 127, 161]. A detailed discussion of results from migration studies are given in Chapter 3. While accurate *in vivo* migration studies are a good short term predictive tool of aseptic loosening these techniques are not widely in use as they are expensive, tedious and demand good technical support.

Observations from migration studies suggest aseptic loosening is initiated by a mechanical cause at the very early stage after implantation. The conventional theories on mechanical failure scenarios of implants, as described in previous section, are unable to explain the fact that migration is observed at least in the early stage after implantation, irrespective of whether they are successful or not in later years. Besides, with various theories to explain different failure scenarios, a single theory is unable to predict the common nature of migration patterns and their occurrence irrespective of design, location and fixation of implants. The possibility is that these failure scenarios/theories are a consequent effect of migration rather than the cause of migration[127].
Many *in vitro* tests on cortical and cancellous bone have reported considerable modulus degradation and accumulation of strain in these materials under cyclic loading. The effect of accumulation of strain is a permanent displacement in the materials while modulus reduction causes an increase in the elastic displacement. Although the mechanism of migration is not fully understood, Taylor and Tanner [181] postulated that micromotion (relative movement between implant and bone) and migration (permanent movement of the implant from its initial position with respect to the bone) could be due to the fatigue failure of the supporting bone. It is the spongy cancellous bone, which fills the inside of the proximal and distal ends of the long bones (i.e. the femur and tibia), that is in direct contact with the prosthetic components. The mechanical properties of cancellous bone are influenced by many factors including age, location, deformities and degenerative diseases[8, 50, 60, 83, 94]. Similarly, *in vitro* studies have expressed concern over the elevated stress levels in the supporting bone for some implanted joints [140, 81, 149, 180, 182, 193]. Factors such as higher stress levels in the bone surrounding an implant as compared to that of the intact bone, poor bone quality and lower metabolic rate can cause accumulation of fatigue damage. Bone tends to repair damage occurring in the material, however, a condition of damage rate higher than the repair rate could result in permanent damage of the bone leading to implant migration. The patterns of implant migration and accumulation of strain in bone exhibit similarities with both having an initial rapid phase followed by a steady rate of migration/strain accumulation. It indicates the possibility of representing migration as the global effect of accumulated strain.

1.1.7.1 The Need for a Short Term Method for Performance Evaluation

Methods that attempt to predict *in vivo* performance of implants are important because:

- Revision surgeries of TJRs are complicated, time consuming, expensive and less successful compared to the previous surgery.

- The number of patients, especially young patients undergoing replacements is increasing; therefore the increase in number, activity level and life expectancy of patients demand assurance of long term success of total joint replacements.
- While large numbers of prostheses are developed and implanted worldwide many of them do not have established performance data of more than five years[113, 133].
- Present methods of evaluating *in vivo* performance of implants are based on clinical studies in which patients are put at the risk by using an implant which may not be proven.
- With the normal life of prostheses being 10-15 years[68, 176], conventional methods take a long time to study the outcome of a new technique, design and fixation.
- Conventional methods require a large patient population to be studied to identify significant statistical conclusion regarding the superiority of one design or fixation technique over another[70, 100].

Despite its clinical relevance, very few studies have attempted to simulate migration, as a preclinical method for implant performance assessment. Most of the reported *in vitro* studies on implant migration are confined to cemented implants, and they merely state the observations on magnitude and pattern of migration, and their comparisons for various implants, without an insight to the cause of migration. At present there are no preclinical methods which have attempted to explain migration in terms of the fatigue behaviour of cancellous bone and a suitable method to address this issue is required.

1.2 Aim of the Study

It has been observed that the measurement of the rate of migration within two years of implantation is a good predictive tool for aseptic loosening. Hips and knee joints are subjected to cyclic loads in day-to-day activities. Measurement of micromotion (relative movement between implant and bone) and migration of the implant-bone construct under cyclic loading is one of the major preclinical tests to assess the possible performance of the implant *in vivo* and to compare the performance of different implants. However, these studies are not based on the possible mechanisms causing migration. A possible cause of migration is considered to be the fatigue failure of supporting cancellous bone.
Synthetic bone models of the respective joints, which use analogue materials instead of bone, are used in many *in vitro* tests due to the consistency in their properties and

convenience in using them compared to cadaver bone. Polymer foams are most commonly used as substitute materials for cancellous bone in synthetic models. In almost all these studies the substitute materials are chosen based on a similar structure and static behaviour to that of cancellous bone, irrespective of their use in fatigue studies. Almost all the studies which use substitute materials never take account of the fact that the fatigue behaviour of the substrate material can be different from the fatigue behaviour of bone. A similar structure and static behavior may not result in similar fatigue behavior of the two materials and in that case the observed *in vitro* performance may be significantly different to the *in vivo* performance.
The aim of this project is to develop a validated preliminary level *in vitro* tool to simulate implant migration in a worst case scenario with no bone remodelling, based on the assumption that migration is due to the fatigue failure of the supporting cancellous bone. The experimental and analytical models of migration are based on simple metal-foam models representing the implant and cancellous bone respectively.

1.3 Objectives and Procedures

Any attempt to develop an analytical model of implant migration in terms of fatigue failure of cancellous bone has three requirements. The first requirement is to develop a model to represent the fatigue behaviour and its characteristics as a function of stress/strain experienced at any time. In the absence of established fatigue data for the fatigue behaviour of cancellous bone, and due to difficulties in conducting experimental fatigue tests on cancellous bone and the wide variation in its properties, there are major problems to be faced in achieving this requirement. The second requirement is to develop a model to relate the migration over time with the fatigue characteristics of the bone. This requires a model which can progressively monitor implant migration, cancellous bone stress distribution and update the changes in cancellous bone response and migration. The third requirement is validation of the analytical model.
Analogue materials will be selected based on comparable fatigue and creep behaviour to cancellous bone. Once characterised, these material models can be used to develop an analytical model which can predict the creep and stiffness loss of the analogue material during its life. The present work aims to develop a model based on an analogue cellular material with qualitatively similar properties to cancellous bone.
The major requirements for the selected analogue material in this study are:

- A cellular material consistent in its mechanical properties with low inter specimen and intra specimen variation

- A similar pattern of accumulation of strain and modulus degradation to that of cancellous bone

Once a suitable material is selected, an *in vitro* biomechanical test model and an FE model are required. A simplified idealised model, avoiding the complexities and uncertainties associated with geometry and material property and loading conditions would be an ideal choice in the development and validation of the model. The test method requires consistent test geometry, material properties and loading conditions and these have to be represented in an accurate FE simulation. The material properties, constitutive relationships and cycle dependent behaviour under fatigue are required for the FE model. The FE model should also be able to reflect the changes in mechanical behaviour due to the accumulation of fatigue damage. The chosen procedures to achieve the objectives are:

- Selecting suitable substitute materials to develop material model of fatigue
- Identifying relationships to express modulus degradation and accumulated strain of the material coupled with fatigue damage. This involves
  - Defining a damage parameter and its evolution law
  - Expressing the variation in modulus and accumulated strain as the damage evolves for tests carried out at various stress levels
- FE modelling of fatigue behaviour of the material
  - Defining the protocol for a Continuum Damage Mechanics approach to model fatigue behaviour of materials in an FE model
  - Verification and validation of the FE model in simulating the prescribed input material behaviour under fatigue
- Selection of an *in vitro* migration model
  - Choosing a test protocol
  - Monitoring migration at different load levels
  - Analysis of the results in terms of pattern, magnitude and load dependence
- FE simulation of a migration test
  - Choosing a failure criteria
  - Extension of the uniaxial test results to multiaxial load state
  - A parametric study of migration
- Comparison of the experimental and analytical models and assessing performance of the model

1.4 Thesis Layout

A background for the main motivation for the present work and the approach is presented in Chapter 1.
Chapter 2 reviews the mechanical properties of cancellous bone and details of substitute materials to cancellous bone as used in many *in vitro* studies.
Chapter 3 deals with studies on migration as a tool to predict aseptic loosening. Trends in the migration patterns of the components are discussed.
Chapter 4 deals with the experimental work carried out to characterise the analogue materials for their fatigue behaviour.
Chapter 5 gives a general description of the combined Finite Element (FE) and Continuum Damage Mechanics (CDM) concept adopted to model the fatigue behaviour of the materials.
Chapter 6 details the fatigue simulation of the material using a combined FE and CDM concept.
Chapter 7 discusses the experimental and finite element simulation of migration using simplified models.
Chapter 8 presents a discussion of the findings of this work along with ideas for future work in this area.

Chapter 2

Cancellous Bone/Analogue Materials and Their Mechanical Behaviour

2.1 Introduction

There are mainly two types of bone structure, dense cortical bone and porous cancellous bone, each having the same chemical composition. The main difference between these two forms of bone is their relative density. Bone with a volume fraction less than and greater than 70% is classified as cancellous and cortical bone respectively. Bone tissue is considered to be a two-phase composite material consisting of mineral salts (Hydroxyapatite) within an organic matrix of collagen. As mentioned earlier (Section 1.1.7) fatigue failure and the inability to compensate for damage accumulation in cancellous bone is considered to be a possible cause of migration. As this thesis is interested only in the consequences of the failure of spongy cancellous bone, the review of the mechanical properties will be restricted to cancellous bone.

2.2 Cancellous Bone

In a typical long bone the cortex or exterior of the shaft (diaphysis) and flared ends (metaphysis) are composed of cortical bone. The inner cavity, especially near the articulating ends, is filled with spongy cancellous bone which is continuous with the inner shell of cortical bone. Cancellous bone distributes the loads from the articulating

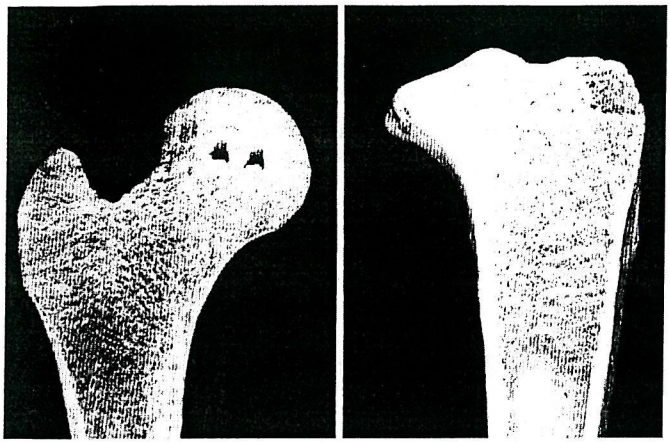

FIGURE 2.1: Cross sectional view of (a) proximal femur and (b) proximal tibia. The porous cancellous bone covered by the outer shell of dense cortical bone[57].

surfaces of the joints to the cortical bone. Figure 2.1 shows a cross sectional view of the proximal femur and the proximal tibia.

Cancellous bone, also known as trabecular bone, has a complex internal structure made of a network of interconnected struts and plates known as trabeculae. A network of rods produces an open cell structure, while plates produce a closed cell structure. The density of the bone is determined as the density of the tissue alone or the density of the trabecular structure including the pores (apparent density). While the tissue density of human trabecular bone is in the range of 1.6-2.0 g/cm^3 the apparent density varies substantially in the range of 0.05-1 g/cm^3[7, 57, 94]. At low densities the bone forms an open structure and it shows a transition from an open to a closed cell structure as the density increases. At locations with complex stress patterns the cancellous bone structure is also found to be complex, with anisotropic properties. Based on elastic symmetry, cancellous bone is classified as isotropic, transversely isotropic, or orthotropic. The structure and mechanical behaviour of cancellous bone is similar to that of man made cellular materials; however living bone has a complex and evolving structure and it continues to modify its mechanical properties and structure by the process of removal and replacement of bone in response to factors such as injury and damage, and the mechanical environment.

2.3 Mechanical Behaviour of Cancellous Bone

The most commonly reported parameters to describe the mechanical properties of bone are strength and modulus. The strenght and modulus depend on the quality and quantity of bone tissue. The properties are determined by direct mechanical testing or by non destructive methods such as ultrasound (for modulus only). There are also theoretical and analytical works to determine elastic properties of cancellous bone.

These methods are based on reconstructing an idealised or CT scan based trabecular architecture in which the trabeculae are assigned the mechanical properties of cortical bone[153].

2.3.1 Elastic Properties of Cancellous Bone

The tissue level modulus of cancellous bone, which has been estimated to be between 3-20 GPa, is considered to be less than or equal to that of cortical bone[7, 36, 94]. This is thought to be due to the differences in microstructure and mineralization between the two tissues[94]. At apparent level the density, strength and modulus of cancellous bone fall into wide ranges. Keller et al.[98] reported that over the range of apparent dry density ($0.05g/cm^3 - 1.89g/cm^3$) there can be 3000 fold variation in strength and 20,000 fold variation in modulus. Strength and modulus are normally taken as the values of ultimate stress and the tangent to the steepest part of the stress-strain curve respectively[112]. Though the apparent density alone cannot account for the wide variation in mechanical properties, it is the primary factor and the most widely used structural parameter to show relationships between structural and elastic properties. There are linear, square and cubic power law relationships describing the effect of density on elastic properties of cancellous bone [25, 56, 74, 152]. Modulus and strength of trabecular bone are related to strain rate by a powerlaw relationship, demonstrating that trabecular bone is a viscoelastic material. However, the exponent of strain rate in the relationship is small, between 0.03 to 0.07[25, 111]. In this respect for strain rates during normal daily activities, cancellous bone can be considered to behave as an elastic material, rather than viscoelastic[79].

The reported compressive modulus of cancellous bone varies from as low as 4MPa to as high as 3350MPa with the mean modulus falling in a range of 200-600MPa[7, 8, 60, 95, 97, 121]. The compressive strength has been reported to range from 0.4MPa to 50MPa with the mean strength falling in the range of 3 to 10MPa[121]. There is a consensus of opinion that the tensile and compressive moduli of cancellous bone are equal or linearly related[8, 156]. However, there is a considerable debate as to whether the compressive strength is greater than, equal or less than the tensile strength[24, 90, 97, 156, 175]. Theoretical analysis of cancellous bone suggests that any one of these possibilities could be valid, depending on the structure of cancellous bone and the bulk properties of the trabeculae. The reported shear strength of cancellous bone falls in a range of 1 to 6 MPa[52, 175]. A summary of cancellous bone properties is presented in Table 2.1.

Studies on cancellous bone properties of the proximal tibia and the proximal femur have shown a large variation in properties within one tibia or hip and also among individuals. There exists a pattern of property distribution across the normal joint

TABLE 2.1: Mechanical properties of cancellous bone

Location, donor and number of specimen	Test	Density(ρ) kg/m^3	Strength, σ(MPa)	Modulus, E(MPa)	
				Young's modulus	Shear modulus
Tibial plateau and femoral condyle(100), human and bovine(24) cylindrical specimen [25]	compression test at various strain rates	310	4.1 at strain rate 0.01 (adjusted) $= 68\dot{\epsilon}^{0.06}\rho^2$ $\dot{\epsilon}$, strain rate	75.5 at strain rate 0.01 (adjusted) $= 3790\dot{\epsilon}^{0.06}\rho^3$	
Human proximal tibial epiphysis 60 cylindrical specimens[111]	Compression test at various strain rate	230-590	$= 40.2\rho^{1.65}\dot{\epsilon}^{0.073}$ (r=0.93) $= \rho^{1.53}(25.0 + 2.26\dot{\epsilon})$ (r=0.93)	$= 2232\rho^{1.56}\dot{\epsilon}^{0.047}$ (r=0.84) $= \rho^{1.43}(1534 + 103\dot{\epsilon})$ (r=0.89)	
Human proximal femur(head), cube specimens[121]	compression test in three directions		9.3 ± 4.5 10.2 ± 3.3 4.9 ± 1.27	900 ± 710 811 ± 604 403 ± 65	
Human proximal femur(neck), cube specimens[121]	compression test in three directions		6.6 ± 6.3 2.8 ± 1.3 0.965 ± 0.33	616 ± 707 174 ± 84 63 ± 7.1	
Human proximal tibia and distal femur, cylindrical specimens (107 from OA and 27 from RA patients)[201]	Compression test		5.9 ± 3.6(OA) 4.7 ± 2.8(RA) 6.9 ± 3.6(medial tibia) 4.8 ± 2.8(lateral tibia) 3.5 ± 2.6(anterior tibia)	154 ± 104(OA) 145 ± 103(RA) 181 ± 105(medial tibia) 134 ± 100(lateral tibia) 102 ± 83(anterior tibia)	
Bovine proximal tibia, 59 reduced section cylinders[97]	Tensile and compressive tests	610 ± 120	16.9 ± 4.24(tension) 23.6 ± 8.28(comp.)	2630 ± 727(tension) 2380 ± 777(comp.)	

Table 2.1 Mechanical properties of cancellous bone - Contd..

Location & Donor & specimen	Test	Density(ρ) kg/m^3	Strength, σ(MPa)	Modulus, E(MPa)	
				Young's modulus	Shear modulus
Human proximal tibia, 60 specimens with ends embedded in resin[156]	Tensile and compressive test	1049 ± 57	2.54 ± 1.18(tension) 2.22 ± 1.42(compression)	487 ± 329(tension) $489 \pm (331)$compression	
Bovine proximal humerus, 48 reduced section specimens [90]	Tension and compression test	262-1136	7.6 ± 2.2(tension) 12.4 ± 3.2(compression) $S_T = 14.5\rho^{1.71}$ $S_C = 32.4\rho^{1.85}$		
Human proximal tibia (using ultrasonic techniques) [8]	Tension and compression in 3 orthogonal directions	263.4 ± 135		346.8 ± 218 457.2 ± 282 1107±634	98.3 ± 66.4 132.6 ± 78.1 165.3±94.4
Bovine humeri,butterfly shaped specimen[175]	Shear test	480	6.6 ± 1.66(shear) $= 21.6\rho^{1.65}$		
Bovine proximal tibia, 48 dumb bell cylindrical specimens[52]	Torsion test for longitudinal and transverse shear properties	500±110 (longitudinal) 590±110 (transverse)	6.35±2 (long.) 4.92±1.48 (trans.)	2470±789 (long.) 719±241 (trans.)	349±128 (long.) 296±103 (trans.)

where the pattern matches the functional requirement of the joint[8, 10, 16, 60, 83, 121]. At the proximal tibia, cancellous bone has an orthotropic anisotropy with the major axis oriented in the axial direction[8]. Anisotropy and differences in it for different regions of cancellous bone at the upper femoral region[16, 121, 201] is also reported. Deformities like varus and valgus alignment disrupt the normal pattern of property distribution and aging or degenerative diseases can cause a reduction in the mechanical properties of cancellous bone [50, 83, 94]. Osteoporosis, a pathological condition leading to an increasing porosity of bone and loss of bone mass can lead to a reduction in mechanical strength of the bone.

2.3.1.1 Ultimate Strength, Post-yield Behaviour and Other Properties of Cancellous Bone

The stress-strain curve of cancellous bone (Figure 2.2) is similar to that of an engineering cellular material. The stress strain curve of a cellular material[25, 69] has three distinct regions in compression; the first regime is linear elastic, where the cell walls bend or compress axially. At high enough loads the cells begin to collapse by elastic buckling, plastic yielding, or brittle fracture of the walls. In the second phase the collapse progresses under almost a constant load until the cell walls meet and touch. The final increasingly steep portion of the stress-strain curve is due to the resistance to load as the cell walls press over each other. In tension, the initial linear region is due to the elastic bending or extension of trabeculae. The stress-strain curve becomes non-linear as the trabeculae start to deform irreversibly and crack and finally fails by

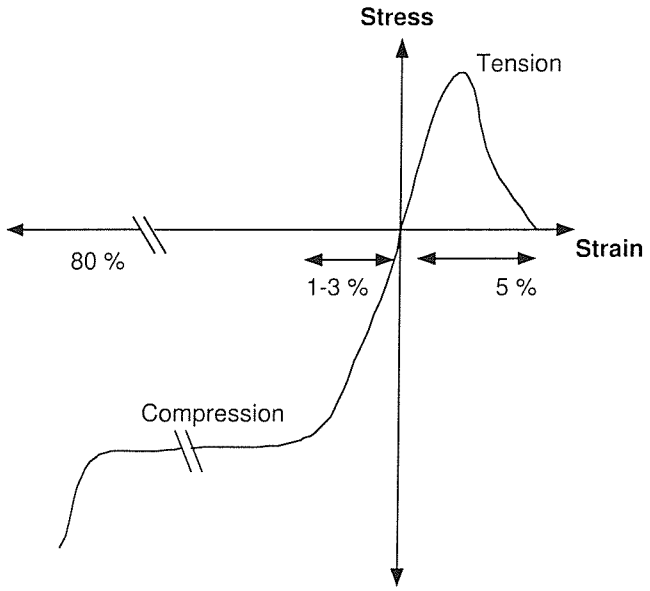

FIGURE 2.2: Stress-strain behaviour of cancellous bone in tension and compression[24, 56].

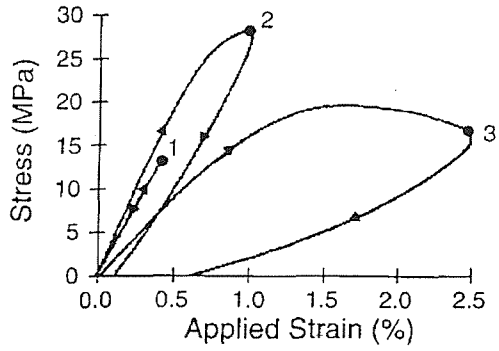

FIGURE 2.3: The loading/unloading stress-strain behaviour of cancellous bone. On reloading cancellous bone showed degradation in mechanical properties which depended on the previous loading strain. The numbers 1, 2, 3 correspond to tests at three levels of strain [198]

tearing and fracturing.

Determining the yield point of cancellous bone is difficult and in many studies the criteria for defining the point at which yielding occurs is not defined. While in some other cases the yield point is taken as a noticeable change of the stress-strain curve from linear to non-linear or by using a 0.2% offset strain criterion[112]. A uniform, isotropic, (i.e., independent of loading direction) and asymmetric (not equal in tension, compression, shear) uniaxial yield strain is reported for cancellous bone in some studies, though there are arguments against it[33, 52, 97, 102, 131, 186]. Kopperdahl et al.[102] tested low and high density human vertebral specimens and reported that tensile yield strain appeared to be independent of anatomic site and apparent density. The compressive yield strain was linearly correlated to apparent density, but it may appear to be constant over a small density range.

The presence of microcracks in bone has been observed under monotonic loads, repetitive loads and creep loads[6, 18, 198]. Wachtel et al.[198] tested trabecular specimens to one of the three levels of strain by grouping the tests as elastic, yield and post yield corresponding to strain levels of 0.4, 1.0 and 2.5%. The stress-strain behaviour of cancellous bone under loading and unloading for these three strain levels is shown in Figure 2.3. The trabecular damage for each group was quantified, and they observed that the amount of damage, when bone is loaded beyond the elastic range, depended on the applied strain. They pointed out that substantial amounts of damage in trabecular bone occur within trabeculae at yield, causing substantial modulus reduction, and hypothesized the presence of densitometrically normal but mechanically compromised cancellous bone which may also play role in increased risk of bone fracture. Zilch et al.[206] studied the viscoelastic nature of cancellous bone by taking specimens obtained from the head and condyles of pairs of cadaveric femora and subjecting them to constant axial load or deformation over a time period of 40 minutes. They observed creep, an increase in deformation over a period of time, and stress-relaxation, a reduction in the stress level when the deformation is held constant over a longer time period. They

observed considerable variation in these properties between regions of one particular bone in addition to patient to patient variability. They could not find any correlation between the time independent properties and time dependent properties. They recommended that the study of time dependent properties are important as it is not possible to determine one group of properties from the other.

Cancellous bone is subjected to multiaxial stresses *in vivo*. A few studies compared the multiaxial test results of cancellous bone with different failure criterion for materials[52, 175]. The von-Mises stress criterion, which assumes both isotropic and symmetrical material behaviour, is not suitable for cancellous bone which has anisotropic and asymmetric strength values. Stone et al.[175] used Hoffman's failure criteria, isotropic but asymmetric (accounting for different tensile and compressive strength), while extrapolating pure shear and shear-compression test results to determine the tensile properties of cancellous bone. For a plane stress and isotropic condition, using this failure theroy it can be written that,

$$\frac{1}{S_t.S_c}(\sigma_{xx}-\sigma_{yy})^2+(\frac{1}{S_t}\frac{1}{S_c})(\sigma_{xx}+\sigma_{yy})+\frac{1}{S_s^2}{\sigma_{xy}}^2=1 \tag{2.1}$$

where S_t and S_c are uniaxial tensile and compressive strengths respectively, S_s is shear strength and σ_{xx} and σ_{yy} are normal and shear strength respectively. The Tsai-Wu criteria, which accounts for anisotropic and asymmetric yield strengths of materials, has also been suggested for cancellous bone[52]. The Tsai Wu Criterion states that failure occurs when

$$A_{11}{\sigma_1}^2+2A_{12}\sigma_1\sigma_2+A_{22}\sigma_2^2+A_{66}\tau_{12}+B_1\sigma_1+B_2\sigma_2\geq 1 \tag{2.2}$$

The coefficients are determined according to the material strength as follows

$$A_{11}=\frac{1}{X_tX_c}\quad B_1=\tfrac{1}{X_t}-\tfrac{1}{X_c} \tag{2.3}$$

$$A_{22}=\frac{1}{Y_tY_c}\quad B_2=\tfrac{1}{Y_t}-\tfrac{1}{Y_c} \tag{2.4}$$

$$A_{66}=\frac{1}{S^2} \tag{2.5}$$

where X_t, X_c, Y_t, Y_c are axial and transverse strengths in tension and compression respectively, S is shear strength.

2.3.2 Fatigue Behaviour of Cancellous Bone

Fatigue is the progressive failure of a material under cyclic or fluctuating loads. *In vivo*, joints are subjected to millions of load cycles and in many cases the load cycles are not fully reversed (in a fully reversed load cycle the stress varies from tension to compression and back again). In *in vitro* studies to quantify the effect of cyclic loading on mechanical behaviour, specimens are subjected to cyclic loads or displacements (in many cases uniaxial) such that they are subjected to normally a particular constant or sometimes a variable amplitude stress/strain. One important reason for studying the fatigue behaviour of cancellous bone is to understand how the microcracks and microfractures propagate under various load levels and their effect on overall mechanical properties. Microlevel studies are carried out to estimate the microfracturring and microcracking behaviour, while macrolevel studies are carried out to understand the mechanical property degradation and its relationship with various parameters. Quantifications of relationships between loading levels and time, for the apparent mechanical behaviour of the bone would provide a basis for non-linear time dependent modelling of trabecular bone.
In vitro research on the fatigue behaviour of cortical bone and cancellous bone [14, 25, 26, 27, 63, 124, 130, 139, 183, 207, 208] has demonstrated that repeated loading of bone can cause a progressive loss of stiffness and ultimate strength along with accumulation of strain. The accumulated strain is referred to in each study as either permanent strain, residual strain or creep strain. Accumulation of strain in bone has been studied with either cyclic or constant loads. Features of fatigue and creep of cortical bone are given in Table 2.2. These studies show that cortical bone exhibits:

- a negative power law correlation between the stress/strain amplitude with fatigue life
- a positive power law correlation between the stress/strain amplitude with rate of steady state creep/accumulation
- a positive relation between density and fatigue life

Although limited in number and restricted to compression testing only, *in vitro* studies have shown that cancellous bone exhibits complex fatigue behaviour with degradation of strength, modulus and accumulation of strain/creep when subjected to cyclic loading[13, 14, 63, 124]. Considerable variability in fatigue results are reported which are caused by the variability due to experimental design and by the bone itself. It is noted that normalising stress with the initial Young's modulus results in more statistically stable results[94, 95]. A schematic representation of the stress-strain behaviour,

TABLE 2.2: Features of fatigue and creep of cortical bone

Fatigue and creep characteristics	Relationships	Remarks
Number of cycles to failure in fatigue(N_f) as function of stress range(σ),initial strain range(ϵ),normalised stress,($\frac{\sigma}{E}$) [26, 29, 183, 208]	$N_f = A(\sigma)^B$	B (-7.4,-11.9, -14.7)
	$N_f = A(\epsilon)^B$	B (-5.3, -13.88)
	$N_f = A(\frac{\sigma}{E})^B$	B (-19.3, -28.2)
Modulus reduction w.r.t. number of cycles in tension fatigue[183, 139]	$E_n = A\omega^3 + B\omega^2 + C\omega + E_o$ $1 - \frac{E(n)}{E_o} = \alpha_1[log(n)]$ $= \alpha^{'} + \alpha_1[log(\frac{n}{N_f})]$	$E_n, E(n)$ - Modulus at n^{th} cycle E_o- Initial Young's modulus from first cycle or pretest. $A, B, C, \alpha_1, \alpha^{'}, \beta_1$- Linear functions of $\frac{\sigma}{E}$ $\omega = \frac{n}{N_f}$
Modulus Reduction w.r.t number of cycles in compression fatigue [139]	$1 - \frac{E(n)}{E_o} = \beta_1 log[\frac{1}{1-\frac{n}{N_f}}]$	
Creep in tension fatigue [183]	$\epsilon_{pn} = d(\omega)^e$	d, e - Linear functions of $\frac{\sigma}{E}$
Modulus as a function of cyclic stress, σ[144]	$E(\sigma) = \alpha log(\sigma)$	$E(\sigma)$- Modulus at cyclic stress range σ
Creep life, t_f [15, 51, 154]	$t_f = A(\frac{\sigma}{E})^B$	Range of B -15.6 to -16.7 Range of A 2.51×10^{-35} to 2.56×10^{-15}
	$t_f = A(\frac{d\epsilon}{dt})^B$	Range of A 0.0042 to 0.0293 Range of B -0.91 to -1.03
Steady state creep rate[15, 51, 154]	$\frac{d\epsilon}{dt} = A(\frac{\sigma}{E})^B$	Range of A 3.38×10^{38} to 6.74×10^{12} Range of B 15.5 to 18.9
In a Log-log plot a power law relationship is a straight line ($log(Y) = log(A) \pm Blog(x)$), with a negative or positive slope depending on negative or positive powers respectively.		

creep pattern and modulus reduction under cyclic loading are given in Figures 2.4 to 2.5. Michel et al.[124] studied the fatigue behaviour of bovine trabecular bone under cyclic compressive load. The stress ranges were selected such that the minimum

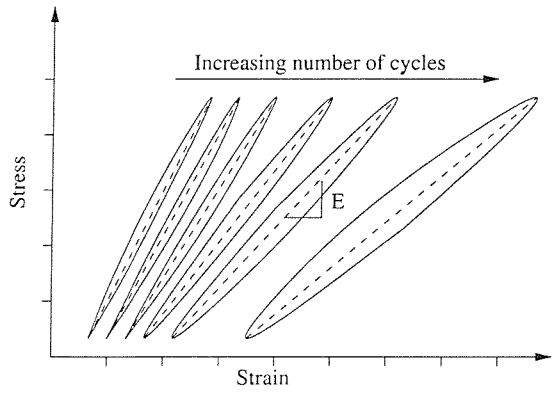

FIGURE 2.4: A schematic of the typical stress-strain pattern at various cycles observed for compressive cyclic loading of cancellous bone; Cancellous bone exhibits an increase in hysteresis, decrease in the slope and translation of the curves along the strain axis with increase in cycles (adapted from Bowman et al. [14]).

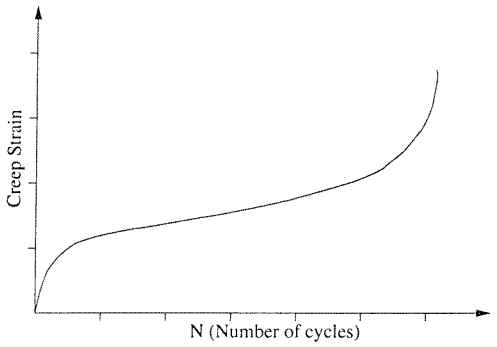

FIGURE 2.5: A schematic of the accumulation of strain/creep strain pattern observed under compressive cyclic loading of cancellous bone; The curve resembles a standard creep curve with initial, secondary and tertiary regions (adapted from Bowman et al. [14]).

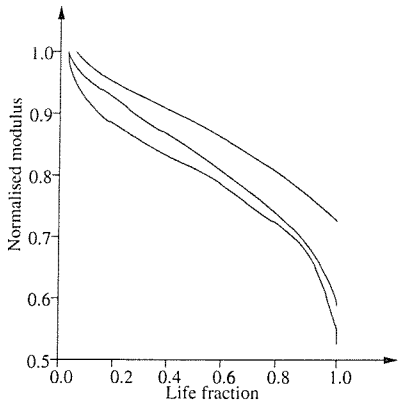

FIGURE 2.6: A schematic of the pattern of modulus reduction observed for cancellous bone under compressive cyclic loading (adapted from Haddock et al.[63]).

strain was 0.6% and maximum strain between 0.8% to 2.1%. The number of cycles to failure correlated with initial maximum global strain by a power law relationship. They observed a difference in modulus reduction with number of cycles at low and

high cycles. The high cycle fatigue showed an initial increase in modulus with a rapid drop of modulus in the final stage. The initial increase in modulus was considered due to the end effects associated with the specimens. A continuous drop in modulus from the beginning was observed for low cycle fatigue. Bone was considered to fail by creep and slow crack growth at low and high cycle fatigue respectively, and they attributed this difference in failure mechanism to the different pattern of modulus reduction at low and high cycle tests.

Bowman et al.[13, 14] studied the creep and fatigue characteristics of trabecular bone. They identified a power law relationship between the normalised stress and both the time to failure t_f and steady state creep rate $d\epsilon/dt$, and found a qualitatively similar creep behaviour to that of cortical bone. The bone underwent creep when subjected to stress levels of approximately 50% of the ultimate strength. They suggested that the existence of creep deformation at such low normalised stress levels may act as stimulus for bone remodelling or may play a role in the progressive weakening of trabecular bone. There was no distinct low and high cycle regimes, with the data described well by only one regression. They considered that creep and slow crack growth are not separate processes at high and low load cycles respectively, but are present throughout all stages of fatigue.

Haddock et al.[63] conducted fatigue tests on cylindrical specimens of human vertebral trabecular bone. Four specimens out of seven were tested at a normalised stress level of 0.5% and the rest at 0.4%. The modulus reduction at the time of failure was in the range of 25-55% while strains at failure were in the range of 1.58-2.65%. The reduction in modulus and failure strains were observed to be higher for cases of both higher initial modulus and lower test load levels. A summary of cancellous bone fatigue properties is presented in Table 2.3.

Moore and Gibson[130] studied the damage accumulation pattern in bovine trabecular bone under compressive fatigue. Specimens were tested at various normalised stress levels and terminated when a predetermined final strain was reached. The modulus of the reloaded specimen was used to determine modulus reduction. Modulus reduction increased with increase in chosen final strain for both low and high stress levels while there were differences in the amount of modulus reduction for a particular final strain for low and high stress levels. Based on an optical examination of the tested specimens they reported that there was no statistically significant difference between total amount of damage per unit area in specimens tested to the same final strain at different normalised stress levels. There was a difference in pattern of damage observed at different normalised stress levels, with specimens tested at low stress levels having more damage in the form of trabecular fracture.

The limited studies on fatigue behaviour of cancellous bone have demonstrated a rela-

TABLE 2.3: Fatigue characteristics of cancellous bone

Ref.,location and specimen geometry	test details	Number of cycles to failure in fatigue and creep (N_f, t_f)	Creep rate $\frac{d\epsilon}{dt}$	Comments
[124] Bovine trabecular bone, cubes (24)	Uniaxial fatigue test at various normalised compressive stress$(\frac{\sigma}{E_o})$	$N_f = 3.18 \times 10^{-23}(\epsilon_{max})^{-13.8}$ ϵ_{max}, maximum initial strain		Specimen end effects present, different fatigue behaviour at low and high load cycles
[13],bovine proximal tibia, reduced section cylinder(24)	Uniaxial creep test at six normalised compressive stress ranges $(\frac{\sigma}{E_o})$	$t_f = 9.66 \times 10^{-33}\frac{\sigma}{E_o}^{-16.18}$	$\frac{d\epsilon}{dt} = 2.21 \times 10^{33}\frac{\sigma}{E_o}^{17.6}$ or $\frac{d\epsilon}{dt} = 0.0257(t_f)^{-1.09}$	creep qualitatively similar to cortical bone
[14],bovine proximal tibia, reduced section cylinders 40-fatigue test 40-creep test	Uniaxial fatigue test at various normalised compressive stress $(\frac{\sigma}{E_o})$	$N_f = 1.77 \times 10^{-23}(\frac{\triangle\sigma}{E_o})^{-11.19}$ $t_f = 1.71 \times 10^{-24}(\frac{\triangle\sigma}{E_o})^{-11.56}$	$\frac{d\epsilon}{dt} = 8.47 \times 10^{16}\frac{\triangle\sigma}{E_o}^{9.94}$ $\frac{d\epsilon}{dt} = 0.0295(t_f)^{-1.1}$	Similar relationships for creep from fatigue and creep test Role of creep in fatigue failure
	Uniaxial creep test at various normalised compressive stress$(\frac{\triangle\sigma}{E_o})$	$t_f = 9.94 \times 10^{-53}(\frac{\triangle\sigma}{E_o})^{-15.05}$ $\exp^{-15600/T}$ T - temperature	$\frac{d\epsilon}{dt} = 1.99 \times 10^{52}(\frac{\triangle\sigma}{E_o})^{15.56}$ $\exp^{-16400/T}$ $\frac{d\epsilon}{dt} = 0.0178(t_f)^{-1.05}$	
[63] human vertebra (7)	cylinders (low cycle tests, at two normalised stress levels$(\frac{\sigma}{E_o})$)	Life was less compared to bovine cancellous bone		Behaviour consistent with cortical bone and bovine trabecular bone
Fatigue failure and the relationships were based on 5% or 10% of reduction in modulus though cancellous bone has been shown to have a large amount of modulus reduction. Creep failure at the intersection of 0.5% offset of secondary regime with tertiary regime of creep curve				

tionship between applied stress/strain level and the fatigue characteristics for uniaxial tests. There are no reported relationships describing the modulus reduction pattern of cancellous bone from these *in vitro* studies other than the observations that modulus reduction occurs with number of cycles. Creep was shown to be related to stress/strain levels, though other comparisons were not reported.

2.3.3 Analytical Models on Fatigue of Cancellous Bone

While the mechanical test results on cancellous bone are insufficient to develop a continuum model of the fatigue behaviour of cancellous bone, analytical methods have derived models at trabecular level to predict apparent mechanical behaviour of trabecular bone under cyclic loading[184, 62]. There are only two studies, to the best of author's knowledge, and both models used an idealised 2-dimensional honeycomb structure to model trabecular bone; the properties of the trabeculae were considered as isotropic and with the modulus of cortical bone. The effect of fracture, property degradation and creep of trabeculae under various applied cyclic compressive loads were quantified to determine the overall modulus reduction, the S-N relationship, and the accumulated strain of the model. The results were compared with experimental results. The difference between these two models were in the method of simulating the failure of individual trabeculae.

In the first method, Guo et al.[62], through an iterative procedure, allowed pre-existing distributed cracks in trabeculae to grow under cyclic loading cycles until fracture. The moduli of the trabeculae were considered to remain the same until fracture. The fractured trabeculae were removed and forces and moments in the structure were redistributed. This procedure was repeated until an overall 10% reduction in modulus of the structure had occurred. In another simulation trabeculae were considered to fail by creep. The trabeculae were assigned a creep behaviour similar to that of cortical bone. Creep load was taken as the mean of cyclic load and time to failure was taken as the time for a 5% increment in apparent strain. The S-N relationship developed from the creep and trabeculae fracture simulations were comparable to low-cycle and high cycle tests respectively. They proposed that the primary failure mechanisms at low and high cycle fatigue were failure of trabeculae by creep deformation and crack propagation respectively. The accumulation of strain with number of cycles was not considered in the fatigue analysis of the model. They hypothesised that modulus degradation for trabecular bone under cyclic loading is due to a combination of fracture, buckling and creep of individual trabeculae.

In the other method, Taylor et al.[184] used a Continuum Damage Mechanics based method where the trabecula failure was considered to occur progressively by prop-

erty degradation. For trabeculae, the property degradation and the accumulation of strain were considered to be the same as cortical bone. Stress and cycle dependent relationships of modulus degradation of cortical bone[183] were used to simulate the failure of trabeculae. They observed that tissue level permanent strain and modulus degradation resulted in little apparent modulus reduction and negligible apparent permanent strain. A probable reason for the observed difference could be a difference in the failure mechanism of trabecular tissue and cortical bone which has been reported in some studies[36]. Understanding and modelling fatigue behaviour of cancellous bone therefore requires further studies in fields of both experimental and analytical studies.

2.4 Analogue Materials to Model Cancellous Bone in *In Vitro* Tests

As discussed, the reported mechanical properties of cancellous bone show a wide variation depending on location, age and sex. Additionally, possible errors and variations exist in the measured values due to the use of different specimen geometries, test protocol and methods of data collection [10, 16, 74, 94, 96, 136]. As a result, when assessing the mechanical performance of orthopaedic devices, large numbers of bone samples are required to obtain statistically significant differences between designs. Availability, preparation and preservation of the bone samples make it a difficult material to work with. Alternative materials to cancellous bone, such as polymer foams for use in *in vitro* biomechanical tests, [37, 168, 170, 177, 178] would appear to be attractive due to their consistent material properties, ease of use and availability. These materials are chosen based on similar cellular structure and mechanical properties (i.e. strength, stiffness and strength/stiffness ratio) falling in the same order as that of cancellous bone.

2.4.1 Previous Works Using Analogue Materials

Szivek [177, 178] reported the mechanical properties for two-component polyurethane foams. He characterised the material for use in the study of acetabular subsidence based on the measurement of their elastic modulus, yield and compressive strength. By varying the ratio of the two components, resin and isocyanate, different foam densities were prepared thus providing a range of mechanical properties. The foam structure and the mechanical behaviour were studied for the different foam samples. The compressive modulus and strength were consistent, with a standard deviation of less than 10%, and

the properties fell within the lower range of that observed for cancellous bone. The compressive stress-strain curves had an initial linear phase and a plateau region after peaking. The average values of strength and modulus were in a range of 3.28 to 5.61MPa and 110.1 to 134 MPa respectively for three different formulations of foam [178]. The modulus fell in the lower range of that for cancellous bone. They suggested that synthetic foam was an attractive alternative to cancellous bone as a test substrate. Shirazi-adi [168] used a polyurethane foam as a substitute for tibial cancellous bone in an experimental and finite element comparison of various designs. They justified the use of polyurethane foam in place of cancellous bone in biomechanical testing due to its availability, homogeneity and relative control of the material properties and resemblance to cancellous bone in its porous structure and mechanical properties. Although this study included an experimental investigation of various fixation systems subjected to repetitive cyclic loads, only static tests were performed to characterise the foam. Commercially available synthetic bone models for the tibia and femur (for example bone models by Pacific Research Labs, Inc) are used as a substitute to cadaver bones in *in vitro* biomechanical tests. Rigid polyurethane foam is used as a substitute to cancellous bone in such models[37]. While composite femur models are used in cyclic loading tests[116], comparisons of the properties of the synthetic bone models and cadaveric bones under cyclic loads have not been performed. ASTM standards[2] give specifications for rigid polyurethane foam for use as a substitute material in orthopaedic tests. The specification provides mechanical properties, strength and modulus in shear and compression, for five different grades of foam in the solid form, but again the required fatigue behaviour of the foam has not been defined.

2.4.2 The Need to Characterise Fatigue Behaviour of Analogue Materials

The measurement of micromotion and migration of the implant-bone construct under cyclic loading has the potential to assess the possible performance of the implant *in vivo* and to compare the performance of different implants. Synthetic bone models of the respective joints, made of substitute materials to bone, are used in many of these tests. The degree of micromotion (relative movement between implant and bone) and migration (permanent movement of implant from its initial position with respect to the bone) are dependent on the behaviour of the substrate materials under cyclic loading. Almost all the studies using substitute materials do not attempt to compare the the fatigue behaviour of the substrate material to that of cancellous bone.

The fatigue and creep behaviour of foams themselves requires more detailed study. An

overview of the available literature on fatigue behaviour of foams is discussed in the following section.

2.4.2.1 Fatigue and Creep of Foams

Gibson and Ashby[57] brings together an understanding of the structure and properties of cellular foams in the book *Cellular Solids: Structure and Properties.* They expressed an obvious need for more detailed studies on the fatigue of foams. No qualitative or quantitative description of compressive fatigue is given, other than the statements that *repeated compression damages some flexible foams* and *Flexible polyurethane, particularly, suffers from flex-fatigue: a loss of strength and permanent decrease in volume, caused, it is thought, by changes in the chemical structure.* Regarding tensile fatigue of foams, only one study (by Fleck and Parker, 1988) is mentioned in the book. Fleck and Parker based on available equations for the solid cell wall material for number of cycles to failure and crack growth per cycle, derived relationships for foams, and compared them with experimental results. The derived model had predicted a strong dependency on relative density through a power equation. However, the experimental results showed differences in the value of the power exponent, for different polymer foams, for the same relative density. It suggested a possible difference in the mechanism of fatigue crack growth in foams from that in true solids.

There are similar studies on fatigue and creep which derived expressions for foam behaviour based on solid cell structure and its properties[1, 75, 77]. The differences between these studies were mainly in terms of factors like arrangement of cellular structure, solid cell wall behaviour and load type. In general these studies indicate the influence of the structural and solid cell material properties on the fatigue behaviour of the foams. Some of these studies compares the predicted behaviour with experimental data. There are also a few studies which examined the fatigue behaviour of polymer and metallic foams[67, 88, 89, 205]. Foams are used as the core material in many sandwich constructions, and in this respect the fatigue/creep of core materials is studied as a part of the sandwich structures for the better performance of sandwich constructions[19, 99, 169]. Most of these studies were concentrating on determining the differences in S-N relationship and fracture mechanism for foams with different densities/cellular arrangement.

Huang and Lin [75] derived the macrocrack growth rate of honeycombs and foams based on dimensional arguments. They considered three cases based on the presence/absence of a microcrack in the first unbroken solid cell wall close to the macrocrack tip. In the case of presence of a microcrack in the wall, the macrocrack propagation rate in the foam was derived based on the microcrack growth rate in the solid wall. In the absence

of a microcrack in the solid cell wall, the fatigue failure life of the solid cell wall was used for a derivation considering cases of low and high cycle fatigue. They arrived at a generalized expression for the microcrack growth propagation irrespective of cell structure and cyclic stress intensity range. The constants in the derived expression were different for conditions of microcrack propagation and conditions of LCF (low cycle fatigue) and HCF (high cycle fatigue); however the constants depended on the cell size, relative density of the material and the fatigue parameters of the solid cell wall materials. They suggested that by knowing experimental data of one particular density, cellular material with a similar cell structure and the same solid cell wall material, fatigue of foam of any density of the material can be predicted.

Huang and Gibson[76] derived the relationships for creep of polymeric foams for cases of solid cell wall material with linear viscoelastic and non-linear viscoelastic properties. The models were based on relationships which incorporated the solid cell properties and relative density of the foam. They compared the results of creep of polyurethane foam under constant shear stress, with the creep model for linear viscoelastic case and the model predicted creep strain to within 10% in all cases. Creep tests of the rigid foam specimens at various densities were carried out for applied stresses of 10, 20, 30 and 40% of the shear strength. The creep pattern was best represented by equations of form

$$\gamma = \gamma_0 + mt^n \tag{2.6}$$

where γ is the amount of creep and γ_0, m and n are material constants. For the tested stress levels, n was a constant, showing the linear viscoelastic nature of the material at these stress levels, while m and γ_0 were linear functions of stress.

Andrews and Gibson[1] studied, using FE simulations, the effect of various cellular structures in creep of two-dimensional cellular solids. The two-dimensional models included regular and random honeycombs and plane sections of an available closed cell foam with and without the curvature of cell walls. In the analysis it was assumed that the secondary state creep of solid cell wall obeyed a powerlaw creep. The results showed the influence of the cellular structure on creep, with a regular honeycomb showing the least amount of creep while the plane section with curved cell walls showed maximum creep. In a similar study the effect of random removal of struts was studied[77]. Removal of a few percentage of struts was found to increase the creep rate by one or two orders of magnitude.

Kanny et al. [88, 89] has reported the static and dynamic characterization of polymer foams under flexural and shear load. Shear fatigue tests were conducted on two different closed cell polymer foams (linear and cross-linked PVC foams) at room temperature at a frequency of 3 Hz and at a stress ratio of R=0.1. The S-N diagram (stress normalised with shear strength against logarithm of number of cycles) was represented

by a power function curve fit. The foams were of the same density, however, the linear foam was stronger in fatigue than the cross-linked foam. The damage formation process was similar in both the foams, with the formation of numerous small cracks in the beginning, which coalesced to form dominant cracks. In both foams, major cracks were visible only after 80% of the life. The higher strength of linear foam was attributed to its smaller cell size, thicker cell edges and the uniform distribution of cells.

In flexural fatigue studies[89], four PVC foams of four different densities were examined. The beams failed by crack initiation from the tension side of the beam. The flexural strength (static and fatigue) and modulus increased with density. However, fatigue strength normalised by static strength showed a negative relationship with density. Viscoelastic parameters of the foams were determined, and it was observed that over a range of frequency of 1-10Hz the viscoelastic properties can be considered independent of the frequency. In two foams, cycling of the foams resulted in stiffening of the materials. SEM analysis showed cell collapse on both the tension and compression side of the beam. The damage concentrated at regions near the surfaces, and on increasing number of cycles they formed a dense band of collapsed cells, resulting in the stiffening of the foam. The flexural modulus was presented through a micromechanical expression

$$E = E_s[\rho^{*2}\phi - \rho^*\phi + \rho^*] \tag{2.7}$$

where E^* is the Young's modulus, ρ^* is the relative density of the foam and ϕ is the ratio of material thickness at the cell wall to cell edges. However, the variation of flexural modulus in cyclic loading was not measured or mentioned in the study.

Harte et al.[67] has reported the fatigue failure of aluminium foam. The tension-tension and compression-compression cyclic properties were measured for two foams. The studies showed that foam with relatively uniform microstructure undergoes homogenoeus straining, while the other foam with more irregular structure exhibited crush band formation which then broadened with additional cycles. Progressive lengthening/shortening of the specimens were reported in both tension-tension and compression-compression fatigue, however, no attempt was made for quantitative representation of the lengthening/shortening.

In general these studies indicate the influence of the structural and solid cell material properties on the fatigue behaviour of the foams, thus emphasising the need for comparison of the fatigue behaviour of the analogue materials with that of cancellous bone. However, the present study does not involve a detailed characterisation of the fatigue properties of the solid cell material in the derivation of the foam behaviour; rather, focuses on the applicability of commercially available commonly used materials for studies involving fatigue and creep.

Chapter 3

Early Implant Migration and its Relationship with Aseptic Loosening

3.1 Migration of Implants

Migration is a gradual micromotion over time by which the prosthesis moves from its original position to a new resting position[157]. Excessive migration is always considered as an indication of definite loosening of implants. It should be noted that conventional radiographic measurements, with random orientation of patients and no specific landmarks on the implant to aid measurements, the minimum detectable level of migration is 4mm-10mm subsidence for femoral stems, and a 3mm sink or 3 degree tilt for the tibial components. The development of accurate methods such as radiostereometric analysis (RSA) and standardised radiographs to measure migration of implants has enabled the identification migrations of 0.5mm to 1mm within two years of implantation at both the hip and knee, irrespective of design and type of fixation.

3.1.1 Methods to Detect *In Vivo* Migration

The introduction of RSA has enabled 3-D measurements of prostheses migration with great accuracy. The method is based on the principle that the a change in the relative position of an implant can be monitored by the migration of at least three of its

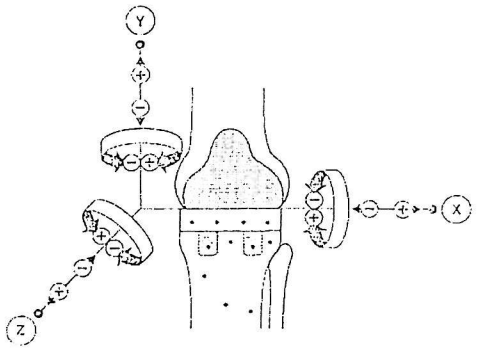

FIGURE 3.1: Rotations and translations in 3-D migration measurement for a tibial implant using RSA. Translations along x, y, z can be interpreted as medial-lateral, anterior-posterior and longitudinal movements, while rotations can be interpreted as anterior-posterior tilt, varus-valgus tilt and internal-external rotation respectively. [4]

identifiable points and that the spatial coordinates of points in the body can be reconstructed from two radiographic images. Relative movements of pre-inserted tantalaum markers in bone and prostheses are measured by determining their 3-D positions from radiographs taken by simultaneous exposure of two X-ray tubes. The 3-D co-ordinates are defined with respect to a known laboratory co-ordinate system. The motion of the prosthesis with respect to bone is expressed as a rotation about and translation along the three co-ordinate axes. Figure 3.1 shows the axes and directions of 3-D measurement of migration for a tibial implant using RSA. The length of the translation vector for the marker with the largest total motion is denoted as the maximum total point motion (MTPM), which is a scalar quantity representing the magnitude of motion. The accuracy of the method is determined by repeated examinations of the objects studied. The accuracy of the method is determined by repeated trials. RSA, when applied to knee arthroplasty, has an accuracy of 0.3^o in rotation, and 0.2mm in translation which is 10 times better than the accuracy of conventional radiographs[157]. An accuracy of 0.25 to 0.5mm/year in translations, and an accuracy of 0.2 to 0.8 degree/year in rotation has been reported for femoral stems[101]. Use of RSA to study migration behaviour of various femoral and tibial components has enabled relationships to be made between migration at two years and aseptic loosening. It has also identified differences in migration for various designs and methods of fixations. RSA, though accurate is expensive, tedious and demands good technical support. As a result of this, the technique is not widely available.

Attempts to standardise the radiograph measurements had increased the accuracy and power of predictability of the method[22, 53, 114, 194]. A major step was to ensure a fixed orientation of the patient relative to x-ray beams. The attempted methods of standardisation slightly varied between studies, however, were based on choosing identifiable landmarks and reference lines, systematic measurements, video imaging of radiographs and its digitisation for analysis. Most of these standardised radiograph

methods only measure the vertical movement of prostheses. Standard radiographs are able to differentiate prostheses performance within two years, similar to RSA, within the permissible limits of accuracy. Compared to RSA, however, the accuracy of this method is reduced (0.5mm to 1mm).
Ryd et al.[159] and Grewal et al.[58] suggested a different concept on aseptic loosening, with the possibility of observation of migration from the very early stage. They suggested that aseptic loosening is initiated at the very early stage of implantation, than the conventional concept of the event occurring a number of years after implantation with a rapid break down of the fixation. Ryd et al.[159] suggested migration as a representation of an adverse biological process established very early, where, on situations of prolongation of the adverse effect for a longer period resulted in observations of clinical significance.

3.1.2 Pattern, Magnitude and Rate of Migration

Migration studies have shown that there is an initial rapid stage with a large amount of migration[42, 53, 101, 104, 158, 159]. The initial rapid phase of migration is reported up to four months[127], six months[53, 91] or one year after surgery[101, 161]. After this period, implants either cease to migrate or migrate at a slower rate, while a few continue to migrate excessively. Evidence for this initial unstable and stable secondary stage has been reported for both femoral stem[53, 127, 135] and tibial implants[73, 158, 159], which included different types of fixation methods and designs. Krismer et al.[104], in their study of hip stem migration, observed a third stage of increasing rate of migration for a few implants at the end of 6 years(Figure 3.2). They identified four patterns of migration; early onset followed by continued subsidence (A), early onset followed by subsequent stabilisation (B), initial stability with late onset of subsidence (C) and stability through out the whole period of observation (D). While some studies have used the rate of migration from a linear fit to the secondary stage, others have used

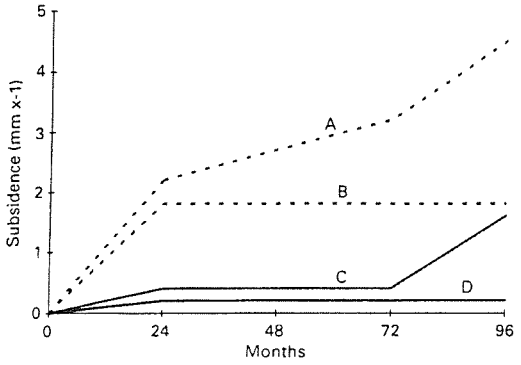

FIGURE 3.2: Observation of various patterns of subsidence from a hip stem migration study[104]. A, B, C, D represents the identified four patterns.

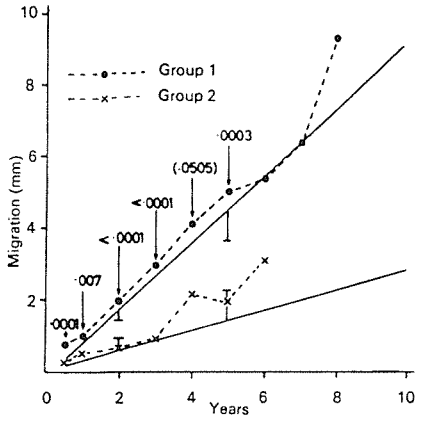

FIGURE 3.3: Difference in migration rates for cemented and uncemented femoral stems[53]. Group1 consist of 125 smooth surfaced press-fit stem and group2 represents 85 cemented stem.

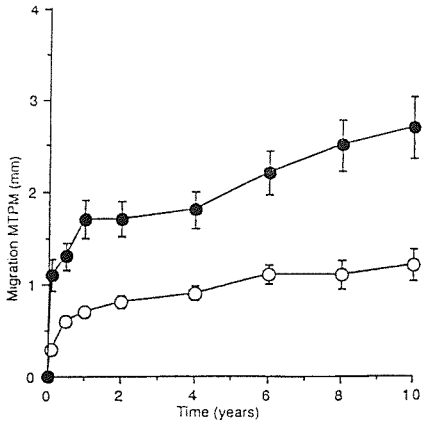

FIGURE 3.4: Difference in migration rates for cemented and uncemented tibial components (97 cemented and 46 uncemented implants) [159]. Black dotted lines represent uncemented implants

the amount of migration after a particular time period for comparisons. Individual studies have differed in terms of chosen landmarks, reference lines, method of analysis and description of migration. In terms of fixation cemented implants migrated less as compared to uncemented implants, especially smooth-fit [42, 53, 157]. Figure 3.3 and 3.4 show migration patterns for cemented and uncemented(smooth fit) proximal femoral and tibial components of hip and knee replacements respectively. At a particular location, the amount of migration measured after the initial stage was able to show significant differences between implants in terms of fixation and design. Summaries of these observations are presented in Table 3.1 and Table 3.2. Normally it is the translations or MTPM which are used to describe migration.

TABLE 3.1: Migration at different stages after implantation

Implant& location	Period of study	Migration(in MTPM) rate or magnitude	Comments
Cemented, femoral stem[101]	0-1 1-4 (years)	0.4mm/year, 1.22°/year 0.15mm/year, 0.22°/year (overall migration and rotation)	Migration unstable in the first year with varus tilt, internal rotation, subsidence. No change in orientation in further years
Uncemented femoral stem [135]	0-3 3-6 6-12 12-18 24-36 (months)	0.41mm, 1.4° 0.6mm, 1.4° 0.47mm, 0.8° 0.35mm, 0.8° 0.37mm, 0.8° (subsidence, rotation)	Rate of subsidence slows over time, but rotation continued to be present in further years
Cemented and uncemented tibial implant [159]	0-1 1-10 (years)	1mm 1.5mm	Most migration in first year, direction of migration scattered, some outward rotation and subsidence about vertical axis

3.1.3 Migration and Aseptic Loosening - Femoral Stem

Subsidence or vertical sinkage is the most reported component of femoral stem migration. Subsidence in excess of 1 to 2mm at two years is used to detect femoral stems at risk of loosening. RSA studies have reported various components of migration, like distal, medial and posterior migration for the femoral head[91] and rotational components of migration for the centre of stem[92].

Freeman et al.[53] have suggested that vertical subsidence of implants in the first two years after implantation could be used to predict the incidence/risk of late aseptic loosening. Using standard radiographs, vertical migrations of four implant configurations were followed for up to nine years. Each configuration was grouped into two as cemented and non-cemented. While survival analysis failed in showing any significant difference between cemented and non-cemented groups at six years, the migration study showed that irrespective of type of fixation, hips destined for revision migrated more rapidly than the remainder, from the initial stage onwards (Figure 3.5). They noted that a rapid migration in the initial six months was followed by a linear migration. A threshold migration of 1.2mm/year during the first two years after implantation identified hips that were likely to fail with a specificity of 86% and a sensitivity of 76%. Severe pain requiring analgesia or revision was considered as the end point of aseptic loosening. Donnelly[42] used similar criteria to identify prostheses that were likely to undergo late aseptic loosening.

TABLE 3.2: Comparison of implant migration within two years after implantation

Location	Method	Comparison feature (No. of implants)	Mean rate or magnitude	Comments
Femoral stem [53]	Standard Radiographs	Cemented(81) smooth press-fit(125) HA-coated(34)	0.27mm/year 0.78mm/year 0.2mm/year	Rate from linear fit of migration from six months onwards
Femoral stem[42]	Standard radiograph	Cemented(223) Ridged and HA coated(115), smooth(145) ridged and smooth(55)	0.3mm/year 0.3mm/year 0.6mm/year 0.8mm/year	Rate from linear fit of migration from six months onwards
Femoral stem[171]	RSA	Ti coated (13) & HA coated (15) (at one year)	3.9 &1.7mm(MTPM)	All implants migrated at 3 months, HA coated stabilised after that, continue to migrate, subsidence 0.2 mm
Tibial implant[159]	RSA	cemented& uncemented mean migration at one year(143 implants)	0.7 & 1.7mm(MTPM) 1mm(subsidence, uncemented)	Most migration in first year, no subsidence for cemented ones, direction of migration erratic,presence of rotational migration
Tibial implant[4]	RSA	uncemented with and without metal backing and stem (25 implants, migration at 2 years)	1.3& 2.4mm(MTPM) 0.6^o&1.8^o (transverse rotation)	Migration in all direction, principal direction vertical subsidence($\approx$ 0.1mm), clinically implants successful, significant reduction in rotation for stemmed ones
Tibial implant[5]	RSA	Proximally cemented(13) & uncemented(16)(mean migration at 12 months)	0.5& 1.5mm(MTPM) 0.7mm& 0.02mm (subsidence)	Most migration in first 6 months, no other pattern of migration no relation between clinical variables
Tibial implant[195]	Standard radiograph	cemented(14), HA coated(12), press-fit(14) (at two years)	upto 0.5mm, 1 mm and 2mm respectively	Most migration in first 6 months varus-valgus tilt, medial lateral tilt was also present
Tibial implant[73]	RSA	Three cementless tibial components (MTPM at two years)	1.4mm(MTPM) which was about the same for all three implants	Considerable variation in components of migration largest component of migration subsidence and outward rotation about vertical axis

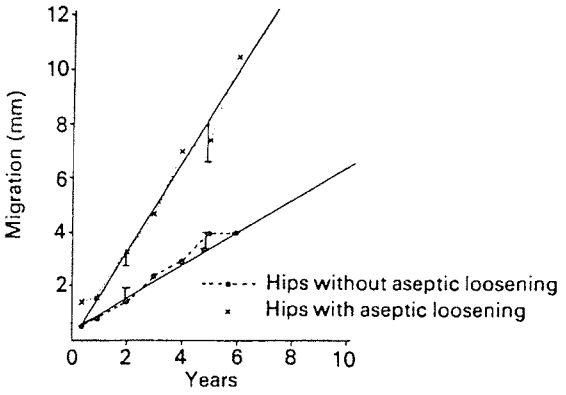

FIGURE 3.5: Difference in subsidence pattern of hip stems without and with aseptic loosening[53].

Karrholm et al.[91] studied subsidence of the femoral head in primary and revised cemented hip arthroplasties using RSA. Two cemented designs (51 Charnley stems and 57 Stanmore stems) followed for eight to nine years, showed identical curves for mean migration. They reported that the probability of revision was greater than 50% if the subsidence at two years was 1.2mm or more. It was migration at two years which could best predict the five to eight years performance. The cut off values for the probability of revision to exceed 50% and 95% were respectively 1.2mm and 2.6mm of subsidence at two years. The magnitude and pattern of migration at two years of those that failed during the study period and those that were successful were very different. The successful implants had a mean migration of 1.45 mm and the failed implants had a mean migration of 4.32 mm at two years post-operatively. Only 5% of prostheses which migrated above 2.6 mm in two years were successful in the long term.
Based on a critical amount of migration of 1.5mm at two years, Krismer et al.[104] were able to predict aseptic loosening of femoral components, which included cemented, straight uncemented and porous coated anatomic stems, with a sensitivity of 69%, a specificity of 80% and an accuracy of 79%.
Walker et al[194] studied the migration pattern for two different cemented hip stems with a minimum follow up of eight years. The the mean migration rates at two years for the successful and failed stems were 1.45mm and 4.32mm respectively, similar to the Karrholm study.

3.1.4 Migration and Aseptic Loosening - Tibial Plate

Tibial components were monitored using RSA for a period of 13 years by Ryd et al.[159]. Migration patterns for 1 to 11 years of two groups of tibial components were compared. The base group consisted of 143 implants which were not aseptically loose in this time period, and the failure group comprised of 15 implants which were revised

for aseptic loosening. Patients included males and females and mean age ranged from 63 to 75. Patients were diagnosed for OA or RA. Seven different designs of both cemented and uncemented fixation were present. Comparisons were carried out between designs, fixations within the base group and failure group, and the group as a whole. A criterion of 0.2mm MTPM at any follow up after one year was used to identify continuously migrating implants in the base and failed group. In the base group differences in migration rates were observed between designs and the method of fixation. Uncemented implants migrated more than cemented ones. While the mean subsidence of the base group was 1mm, for the revised group it was 2.7mm after one year. Based on the criteria followed in classifying continuously migrating implants, migration at two years of the revised implants could be used to predict their late failure with 85% accuracy. They pointed out that implants, which were later revised, would be identified by RSA at one or two years after operation, even though the implant was clinically asymptomatic at that time. Loosening occurred exclusively in those which migrated continuously(Figure 3.6).

Grewal et al.[58] carried out a survival analysis of three configurations of a knee prosthesis, for which one year migration data was available. The criterion for failure was a change in position detected as a 3^o tilt detected by radiographs taken at each review. Tibial components were of similar design but used different methods of fixation, and were classified into three groups. Group 1 consisted of uncemented polyethylene tibial components, group 2 had an additional metal backing and a stem, while group 3, in addition to metal backing and stem, were cemented. RSA studies were carried out only on a sub group of knees studied for survival analysis. The rank order of the components judged by survival analysis was the same as that determined by RSA after one-year on a smaller subgroup. Migration levels at one year were 2.3 mm, 1.5mm and 0.5 mm and survival rates at five years were 79%, 86% and 100 % respectively for

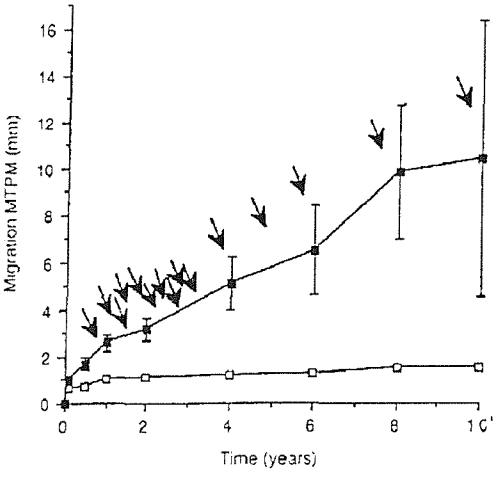

FIGURE 3.6: Difference in the amount of migration of tibial implants without and with aseptic loosening[159]. Arrows indicate year of revision.

groups 1, 2 and 3. It should be noted that a comparatively long time was taken to detect the instability by conventional radiographs.

A critical amount of MTPM of 0.2mm at the second year after implantation has been used to detect tibial implants under the risk of loosening[159]. It has to be noted that MTPM, other than the magnitude of the 3-D migration vector, is not associated with any directions of movement. Tibial implants showed rotation and translation about all three axes, though there were considerable scatter in directions about axes and magnitudes of individual components. Vertical subsidence was found to occur more exclusively for uncemented implants[4, 73, 159], while cemented implants seldom subsided. An internal/external rotation about the vertical axis, varus-valgus tilt, anterior-posterior tilt are commonly reported [4, 5, 159, 161]. The addition of a stem on tibial components (even though it did not show differences in terms of subsidence) was reported to reduce other components of migration, especially rotation[4]. There was no correlation between clinical variables such as clinical score, alignment and component position with migration[5, 72, 73, 157]. Hilding et al.[72] showed a relationship between knee joint loading and implant migration. An increased risk of loosening was associated with certain gait patterns, which were also present in the pre-operative stage, causing increased flexion moments. Albrektsson et al.[5], considered that similar migration patterns observed for RA and OA patients are probably due to the poor bone quality that was compensated for by lower activity levels and loading in RA patients.

3.2 Possible Cause of Migration

The commonly reported failure scenarios (discussed in Chapter 1) of aseptic loosening are unlikely to cause migration in the very early stages (one to two years) after implantation. Wear of the articulating surfaces is low and the possibility of wear induced resorption at the interfaces are possible only at a later stage when the integrity of interface is lost and particles infiltrate into the interface. Stress shielding is considered to cause bone resorption resulting in bone loss, but this is unlikely to cause loosening in the early stage after implantation. Mjoberg et al.[127] considered that bone cement itself is not a weak link with adequate bone support, though an inadequate support can cause stress concentration and subsequent fracture in cement. They also pointed out that some of the resorption pattern described as stress-shielding could be due to the rotational movement of the implant. Micromotion occurring at the interface during the initial stage after implantation, causing bone resorption or prevention of bone ingrowth are also considered as a cause of aseptic loosening. This theory cannot support

the fact that, even most of the successful implants migrated in the initial stage. In addition, it cannot support the fact that migration is observed for cemented implants, which do not show micromotion because of the immediate fixation provided by the cement. While the concept of press-fitting implants theoretically should reduce the initial micromotion, the highest failure rates are observed for such implants.

3.2.1 Failure of Biological Supporting Structure: A Possible Cause of Migration

Migration studies do not propose a mechanism by which migration occurs, but only report observations. While many explanations for migration were trying to relate it to the design or fixation, only a very few studies have mentioned the importance of the biological structure in the migration of implants.
The initial rapid phase has been considered to be due to bone resorption/remodelling taking place at the interface to repair the damaged bone (necrotic bone) during preparation and due to heat generated at cement polymerisation[135, 127, 160, 161, 181]. The initial process was found to depend on the mode of fixation and on design factors, however, was unrelated to the future loosening or continuous migration[158].
Many *in vitro* studies on cortical bone and recent studies on cancellous bone have shown that under cyclic loading the material shows damage accumulation with time indicated by accumulation of strain, modulus degradation and reduction in strength[13, 14, 139, 183]. There is a striking similarity between the migration patterns and the material's creep curve or accumulation of strain over time. Taylor and Tanner[181] suggested that a possible explanation for the migration is the fatigue failure of supporting cancellous bone where inability to compensate for the the damage accumulated through fractures and cracks of trabeculae cause an increased migration rate. They tried to explain the stages of migration and its variation with type of fixation, in terms of the differences in the local load transfer at the prosthesis-bone interface for these fixations as discussed in the following section. The higher the local stresses, the higher the damage accumulation rates and the corresponding migration rates. A stable migration rate would thus depend on the ability of the bone to compensate for the damage suffered.

3.2.1.1 Methods of Local Load Transfer and Its Influence on Migration for Various Type of Fixations

In the case of press-fit implants higher stresses are generated in the surrounding bone, with the implant's wedging effect and the early weight bearing, causing fracture of

a large number of trabeculae leading to high migration rates in the initial phase. The lower initial phase migration rates for HA coated implants compared to press-fit implants, even though they behave similarly to press-fit implants in this phase, was explained[181] based on the fact that there is no weight bearing for these implants in the first few post-operative weeks. In the case of cemented implants, with immediate fixation due to cement interdigitating with the cancellous bone and thus having a large load bearing area, the stresses in the necrotic bone are less compared to other types of fixation, thus resulting in the least amount of migration among them. Once the necrotic layer was resorbed and replaced, the rate of migration will depend on the ability of cancellous bone to repair the accumulated damage by remodelling. In the case of press-fit implants, the local stress levels will still be high with the wedging effect of the implant causing damage to the trabeculae. In the case of an HA coated implant, with the interface bonding with bone ingrowth to the implant, these local stress levels are lower than press-fit; the rate of damage accumulation will be lower and consequently leads to a lower migration rate for these implants compared to the press-fit implants. The lowest migration rates observed for cemented implants, are explained similarly to HA coated implants, with the least local stress levels at the interface experienced for the cemented implants compared to other two fixation methods.
Fatigue of cancellous bone and its repair is dependent on many factors related to the patient and prostheses: design, type of fixation etc of prostheses; age, sex, activity level, bone quality and its ability to remodel. While some of these factors influence the stress/strain magnitude in cancellous bone, other factors affect the remodelling. An increase in stress/strain magnitude increases the risk of fatigue failure. Combinations of these factors resulting in an increased stress/strain level with a decreased remodelling rate could lead to excessive migration.

3.2.2 *In Vitro* studies of Implant-Bone Constructs

In vitro tests of implanted joints are performed to understand the differences in performance of implant design and fixation without the complication of biological factors. There are biomechanical test methods and analytical methods which are used for this purpose. Each method has its own advantages and disadvantages in reproducing the *in vivo* mechanical situation from an *in vitro* analysis. In the case of biomechanical tests the stress-strain data and micromotion are monitored only at a few predefined points on the outer surface of bone and at the interface to avoid any possible damage to the continuity of the implant-bone system by attachment of measuring devices. In addition, preparation and preservation of the bone-implant constructs and application of correct and consistent boundary conditions are also important. In this respect

analytical methods have an edge over biomechanical tests as they can provide better control over study parameters, though FE analyses face problems in reproducing the actual structural and material property distribution.

In vitro studies on implant-bone constructs have observed differences in stress-strain patterns and micromotions for various designs and methods of fixation for implanted joints and intact bone. A brief review of these studies is given in the following section in order to emphasize the fact that there is a change in the stress strain condition in the implanted joint with respect to the intact condition. However, a direct comparison between studies is not possible as the objectives, designs investigated and methods used in each study varied. In many cases these studies reported merely comparisons or observations. In the case of biomechanical tests, the reports on uncemented implants represent only the behaviour at the initial stage after fixation, as there is no bonding between implant and bone by bone ingrowth. Additional insight into the differences in behaviour of different type of fixations and the load transfer at the interface for these fixations are given by analytical studies, using simplified and idealised models.

3.2.3 Observations from *In Vitro* Biomechanical Studies of Implanted Femurs

Quantitative and qualitative differences in stress-strain patterns of intact and implanted femurs are reported from many biomechanical studies[122, 137, 142, 143, 165, 196]. The strain patterns of the loaded femur were reported to change inconsistently after prosthesis implantation[196], and there were large differences in strain pattern between individual femora[137]. A quantitative variation in the amount of subsidence under cyclic loading between cemented and uncemented implants was reported; the uncemented implants subsided significantly more than the cemented implants[143, 165]. Maher et al.[116] proposed a preclinical test to differentiate loosening of cemented implants in terms of migration. The implanted composite bone models were subjected to 3 million cycles of compressive load (0.23 to 2.3 kN) at 5Hz frequency. They observed considerable variation in the migration behaviour among the tests and attributed it to possible variation in strength and porosity of the cement. They observed a non-linear pattern of migration with time and compared it to the creep curve of cement. However, their hypothesis cannot explain the observed migration of uncemented implants.

3.2.4 Observations from Finite Element Studies of Implanted Femurs

Analytical methods like finite element give a more detailed understanding of the stress-strain patterns of implant bone constructs for the chosen model parameters. Huiskes et al.[81] used finite element analysis to understand the load transfer and stress patterns of three types of fixation, cemented, bone ingrown and press-fit using a 2-D model. They observed that stress transfer in the case of cemented implants take place mainly through proximal and distal regions. Uncemented implants, bonded by bone ingrowth, showed a similar load transfer pattern, though the bending stress was less than that of cemented and more load was transferred distally and less proximally; this could be attributed to the higher rigidity of the stem. The load transfer in both cases can be characterised by shear and normal stress components. The effect of decreasing stem modulus showed a pronounced effect for ingrown implants as compared to cemented implants, with a decrease in stem stiffness resulting in an increase in proximal load transfer. Compared to fully coated implants, partly coated implants transferred more load proximally. The stress patterns of cemented and osseointegrated cementless implants were qualitatively similar but quantitatively different. In the case of smooth implants load transfer depended on compression. The compressive force required for equilibrium was developed by the interface compressive stress as a result of subsidence of stem into the bone. Friction, if present, also contributed in equilibrating the external force. In the case of press-fit implants the smaller the taper angle, the larger the compressive contact force required to equilibrate the applied load. For same amount of subsidence a stiffer bone will generate higher compressive stresses. *In vivo*, as bone stiffness varies the compressive forces are also non-uniform. The friction and the initial interference contact and many other factors influence in equilibrating the applied forces. Besides, with the surgical variations in preparation of bone, it could result a less predictable performance for uncemented stems.

Ramamurti et al.[149] studied the relative displacement at the bone-implant interface for cementless implant for combinations of implant motion, coefficient of friction, degree of interference and modulus of surrounding bone. Their study concluded that there is no unique implant motion corresponding to prevention of bone ingrowth at interface, rather the critical amount of micromotion is a combined effect of various factors like degree of press-fit and coefficient of friction. They also highlighted the fact that a micromotion below a critical limit may be achieved at the expense of losing mechanical integrity of bone adjacent to the implant as the bone may become overstressed. The effective stress of cancellous bone was highest at the interface and decreased sharply with increasing radial distance from the interface.

Taylor et al.[180] analysed an intact femur and femur implanted with press-fit, HA coated and cemented implants. Cemented implants were modelled using a perfect bond between the stem-cement and cement-bone interfaces. The HA coated implant was modelled as perfectly bonded over half the stem length. The press-fit implant was modelled as frictionless or with a coefficient of friction of 0.25. The cancellous bone stresses with a press-fit implant were shown to be 6.5 times higher than the other two methods of fixation and they were near or above the elastic limit of the cancellous bone. They hypothesised that an increased stress level can result in progressive failure in the form of fatigue failure of cancellous bone and cause migration. The rank/order of stress levels in the cancellous bone between implants and the order of migration risk observed clinically were similar.
Visnic et al.[193] carried out a parametric study to study the effects of different sizes of implant and bone diameters. For femoral components assembly strains adjacent to the distal end of the porous coating of the implant were well above yielding in many cases. Cancellous bone in the proximal region was completely yielded, indicating local failure during insertion of the implant. They pointed out that assembly stresses associated with press-fit should be considered in any analysis to predict the true state of strain in bone.
A detailed review of stress analyses of the femoral hip prostheses[85] concludes that:

- A significant difference in load transfer in an implanted femur from an intact femur.
- The load transfer can be manipulated with the properties and geometry of the prostheses.
- A stiff implant causes stress-shielding while reducing interface micromotion and interfacial stress. A flexible implant results in higher bone stresses, but at the cost of higher relative motion and/or higher interfacial stresses
- The interface conditions affect the mode of load transfer affecting proximal stress-shielding and the relative motion

3.2.5 Observations from *In Vitro* Biomechanical Studies of Implanted Tibia

The major load at the knee joint is compression and the tibial components are designed mainly for compressive load bearing. Because the hard subchondral bone of the tibia is removed during a knee replacement, loads are absorbed by the softer cancellous

bone and the peripheral cortical bone that remains. Many *in vitro* biomechanical tests have reported the tilt and sinkage of tibial component under axial cyclic loading, and how they vary with design, fixation, alignment and initial fixation[12, 105, 106, 151, 162, 188, 197, 199]. The tilt and sinkage depends on the asymmetry of the loading, the strength of the supporting bone and also on the stability of the implanted joint[105, 106, 188]. In a normal knee 60% of the total load is transferred through the medial part of the knee[132] causing an asymmetric axial distribution of the load, and for an implanted joint this could lead to lift off on one side and sinkage on the other, if adequate initial fixation is not achieved. While lift off inhibits bone ingrowth, on the medial side it increases the compressive stresses causing an increased subsidence which in turn could cause overstressing of cancellous bone. The role of bone quality was studied in a test, where a combination of high, low and medium density foam representing medial, central and lateral portions of tibial cancellous bone respectively were used to substitute cancellous bone[105]. The stability of the construct was directly proportional to the foam density. For a poor quality foam a cemented implant gave an enhanced stability. Subsidence was reported higher for the tibial tray with cancellous bone screw fixation than cortical bone screw fixation[106]. An increase in subsidence for the tibial tray with cancellous bone screws was considered due to the microfractures of the underlying trabecular bone. Sala et al.[162] studied the effect of a combination of physiological torsional and axial load on rotational micromotion of tibial plates. From their results they concluded that under physiological loading rotational micromotion was unlikely to cause failure of bone ingrowth in the case of uncemented implants, though at low axial loads, representing an immediate postoperative condition, they observed that the micromotion can exceed the accepted limits for bone ingrowth. For a poor bone quality they suggested the use of a cemented implant to provide sufficient rotational stability. Whiteside et al.[199] studied the load transfer characteristics of a noncemented total knee arthroplasty by a laboratory strain measurement of the implant-cadaver bone construct along with a prospective clinical roentgenographic study of implanted joints. In clinical study cancellous bone hypertrophy bridging from the undersurface of the tibial component to the metaphyseal cortical bone was observed. It indicated load transfer through cancellous bone to this area. Sinkage of implants was found to change according to the rigidity of fixation of stem, as it was noted that for a changed design with rigid stem fixation, sinkage was less.

3.2.6 Observations from Finite Element Studies of Implanted Tibia

There are FE studies which have compared the performances of various designs and fixations and the stress distribution patterns for implanted tibial constructs. Cheal et al.[34] studied the effect of a tibial plate surface cover, cement injection depth and structural rigidity of metaphyseal cortical shell for a cemented tibial component with four peripheral posts using a 3-D model of proximal tibia. The results showed that compressive axial loads directly transferred to the proximal trabecular bone and transferred more distally through the fixation posts. The maximum stress in trabecular bone was immediately distal to the posts. Decreasing the metal tray width increased the peak compressive stress in trabecular bone, though they observed that unlike in other reports, it did not result in an increase in the compressive stresses in the proximal tibial trabecular bone. Overestimating the structural contribution of the cortical shell, by assuming the same modulus for the shell as that of diaphyseal cortical bone can drastically alter the proximal load distribution. Analyses of the model by assuming the same modulus for the upper cortical shell as that of the diaphyseal cortical bone (as normally assumed in FE analyses) and by assigning a reduced modulus as measured in another study. Reduction in modulus resulted in reduction in the load carried by the cortical shell and a corresponding increase in the load carried by the trabecular bone. Tissakht et al.[185] analysed a 3-D model of an uncemented tibial implant for interference fit and close fit fixation of tibial trays, with either pegs or screws. The study concluded that preparation of host bone and method of fixation appears to be important in the case of immediate post-operative displacements. They mentioned that biological variability between specimens, size, shape and variation in material property with age and loading conditions have to be accounted for in studies.
Garg et al.[55] analysed a 2-D model of the sagittal slice of implanted tibia to determine the stresses immediately beneath the tibial plate as functions of the amount of bone resection, implant-bone contact and interface material. They observed that cement or direct metal on bone interfaces created similar stresses in the bone, while a compliant interface reduced the stresses in regions of high elastic modulus gradient. They also pointed out that areas of irregular contact possible in the case of rigid interfaces could lead to areas of over and understressing of bone. Rakotamanana[150] used a 3-D model for, for a cemented and porous coated tibial implants. The maximum relative displacement at the centre was greater for PCA implants. The interface deflections, and deflections in the plate vary considerably under asymmetric loading with respect to the symmetric loading. There was no significant difference between implants in tilting and displacements under asymmetric loading. Absence of cortical support caused localised

overloading under the plateau edges causing plastic deformation of trabecular bone. Taylor et al.[182] used a 3-D finite element analysis of three implants, for which *in vivo* migration data and survival rates were available. They showed that the cancellous bone stresses in the implanted joint showed a positive relation between the migration and survival data. The press-fit implants which were shown to perform poorly in clinical studies produced the largest cancellous bone stresses, while cemented implants showed lowest cancellous bone stresses. In another study[140], the risk ratio (von Mises stress/ultimate compressive strength) determined by analysing four patient specific finite element models of proximal implanted tibia was the highest for the two press-fit implants. The other two implants were cemented and HA coated. The results of RSA study, which followed these patients, showed that the press-fit implants migrated the most. In short, from these studies it can be summarized that:

- Tibial implants showed vertical subsidence under axial or cyclic loads
- Tilt and sinkage under asymmetric loading were higher for uncemented tibial components
- Tilt and sinkage caused over stressing of some regions of cancellous bone
- For a given substrate bone property, stresses in the bone were highest for press-fit implants
- Initial fit, alignment, type of design have been shown to influence the stresses in bone and also micromotion of the implant

3.3 Summary

The presence of migration, at least in the initial stage after implantation, has been observed for implants, irrespective of whether they were successful or not in later years. This is against the conventional concept that a sound anchorage in the initial stage is required for the success of an implant. At a particular location, whether it is hip or knee, it was the type of fixation which was more influential [53, 73, 194]; additionally differences in migration in terms of factors such as design and diagnosis have also been reported in some studies. Uncemented implants normally show a comparatively higher amount of initial migration than the cemented ones[101, 104]. In the secondary stage, migration of cemented, HA coated and porous coated implants are satisfactory and in many cases HA coated designs are reported to have a comparable migration to that of cemented implants[91, 104, 171]. In the case of smooth, press-fit implants the

migration rate is generally higher in both the initial and secondary stages. Based on migration studies within two years of implantation, it was possible to differentiate risk free and at risk groups by the magnitude of migration alone. Within this time other conventional clinical symptoms were not present or if present, were not able to make a similar prediction[4, 92]. Clinical symptoms of mechanical loosening were associated with those implants which migrated more in the initial two years[32]. Reports of loosening years after implantation can be considered as late detection rather than late occurrence of the failure[127]. Observations from *in vitro* studies of implanted joint constructs indicate the possibility of an altered stress-strain condition in the cancellous bone which supports the implant. At present there are no preclinical methods to quantify the mechanical environment to which cancellous bone is subjected; thus a suitable methodology which will address this shortcoming is required.

Chapter 4

Characterising the Properties of Cancellous Bone Analogue Materials

In this chapter, the experimental work performed to characterise the mechanical behaviour of some rigid polymer foams, as an attempt to use them as analogue materials for cancellous bone, are detailed. These polymer foams have been used in other studies as cancellous bone substitutes[37, 170].

4.1 Selection of Materials

Two polymer foams were chosen for the experimental work. Herex ®C70.55 is a commercially available rigid, closed cell, cross-linked PVC foam with a high modulus and strength to weight ratio and is used as a core material for light-weight sandwich structures with applications in the fields of marine, road and rail, and aircraft industry. It has been previously used in some *in vitro* experiments as an alternative to cancellous bone as its cellular nature and modulus/strength ratio in compression falls into the range of cancellous bone[170] properties.
Solid rigid polyurethane foam is commercially available, and is marketed by Pacific Research Laboratories, INC. as an alternative test substrate to cancellous bone in the *in vitro* performance evaluation of orthopaedic implants and instrumentation. These products aren't intended to replicate the mechanical properties of human bone, however, it does provide consistent and uniform material with properties in the range of human cancellous bone. In composite synthetic models of bone polyurethane foam is

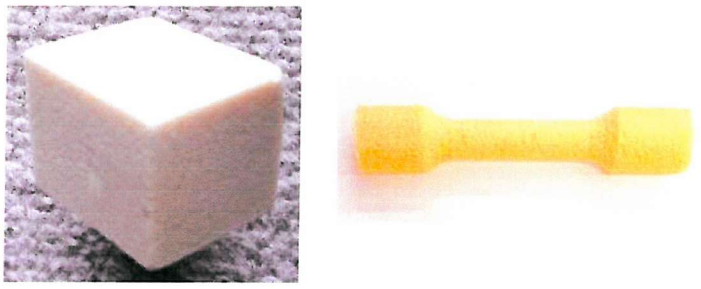

(a) (b)

FIGURE 4.1: Samples of the two foam materials used in the present study (a) Solid Rigid PU foam (b) Herex foam.

normally used as a cancellous bone substitute. It is a closed cell foam. The solid rigid foam ($160kg/m^3$) is equivalent to Grade 10 as per ASTM standards grade specification for Rigid PU foam for use as a standard material for testing orthopaedic devices and instruments[2]. The ASTM standards provides the physical and mechanical requirements for five grades of foam, where grade designation refers to the nominal density of the foam.

Figure 4.1 shows pictures of the two polymer foam material samples. The reported densities of solid polymers of PVC and Rigid PU foam are $1200kg/m^3$ and $1400kg/m^3$[57] and thus the apparent densities fall in a range of 0.043 and 0.13 for PVC and solid rigid PU foam respectively. The relative density of cancellous bone varies between 0.05 to 0.7[57]. As per the manufacturer's literature the strength of Herex®C70.55 is higher in tension than in compression, while for solid rigid polyurethane foam the strength in tension and compression are equal. The static properties of the foams as reported by the manufacturers are given in Table 4.1.

Herex®C70.55 foam was available the earliest and was comparatively cheap and thus most of the preliminary trial and error experiments were carried out with this material. The experience and information obtained while testing the material and its fatigue behaviour were used to develop a consistent procedure for further experiments.

TABLE 4.1: Properties of foams from their manufacturer's literature.

Foam	Density (Kg/m^3)	Strength (MPa)			Modulus (MPa)		
		Tension	Compr--ession	Shear	Tension	Compr--ession	Shear
Herex®C70.55	60	1.3	0.85	0.8	45	58	22
Solid Rigid PU foam	160	2.2	2.2	1.4	57	77	23

4.2 Methods

All tests were performed on waisted cylindrical dumb bell shaped specimens. A waisted cylindrical shape will bias the failure of specimens towards a region of relatively high, uniform stress, where strain data are sampled, thus reducing experimental artefacts[95]. The specimens were machined using a lathe. The waisted region of the specimens had a diameter of 15mm and an approximate gaugelength of 17mm. The geometry of the specimen was identical for tension and compression tests. The specimen ends had a diameter 20mm and were approximately 20mm long; these were glued into metal end caps. This facilitated gripping of the specimen within the collets of the experimental jig without crushing the foam (Figure 4.2).

The experiments were carried out on a computer controlled Instron servo hydraulic load frame (Figure 4.3). Five specimens each were tested in static tension and compression to assess the modulus and strength of each foam material. All static tests were performed in strain control with a crosshead movement rate of 0.1 mm/sec, which corresponded to a strain rate of approximately 0.003/sec within the gauge length. The

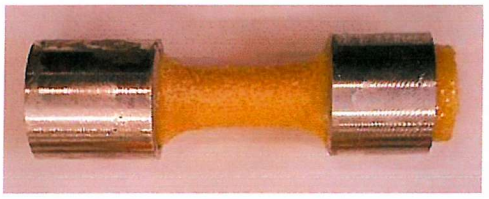

FIGURE 4.2: Reduced section cylindrical specimen of the foam with metal end caps.

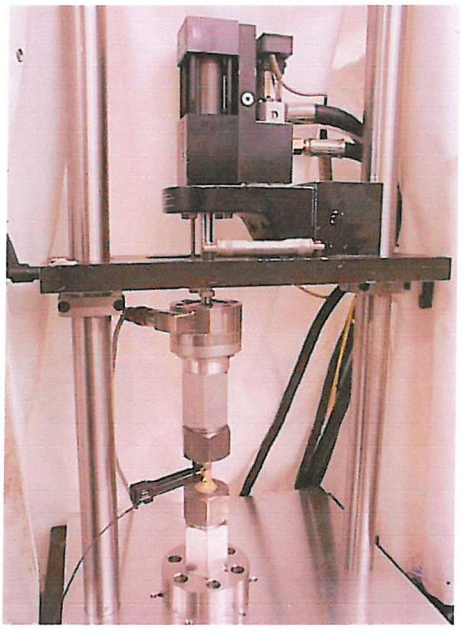

FIGURE 4.3: The experimental set-up for uniaxial tests; the extensometer, attached directly to the mid-section of the specimen, was used to measure the deformation at various load cycles.

load was recorded using a calibrated load cell and the deformation over the gauge length was measured using an extensometer attached to the mid section of the specimens (Figure 4.3). The stress was calculated as the ratio of the load range to the cross section area of the specimen within the gauge length. Strain was calculated as the ratio of elongation of extensometer from its initial position to the gaugelength of the extensometer. Modulus was determined from the initial linear portion of stress-strain curve, by a linear fit of stress-strain curve between 0.1 to 0.4% strain[95, 124]. The ultimate strengths in tension and compression were determined from the respective peak loads recorded in the corresponding tests.

The fatigue behaviour of the foam was characterised in both tension and compression. Prior to the fatigue tests, all specimens were pre-conditioned, by applying 10 cycles at a lower stress level ($\approx$ 1/3rd of ultimate strength) to determine the initial secant modulus in the elastic range,E_*. Fatigue tests, zero to compression and zero to tension were carried out at various stress ranges at a frequency of 2Hz. The load and extensometer position data at minimum and maximum load amplitudes were collected at regular cycle intervals using a PC controlled data acquisition system. The secant modulus E and accumulated strain ϵ_{acc} at various cycle intervals during the test, were calculated using the following protocol (Figure 4.4). The secant modulus at any cycle was defined as the ratio of stress range divided by the strain range or the slope of the line connecting the minimum and maximum stress values of that particular cycle. The accumulated strain at any load cycle N, ϵ_{acc}, was defined as the translation of the stress-strain curve along the strain axis with respect to the first cycle. To assess the variation in modulus reduction, the modulus was normalised with the first cycle modulus E_o and can be represented as

$$\text{Normalised modulus} = \frac{E}{E_o} \tag{4.1}$$

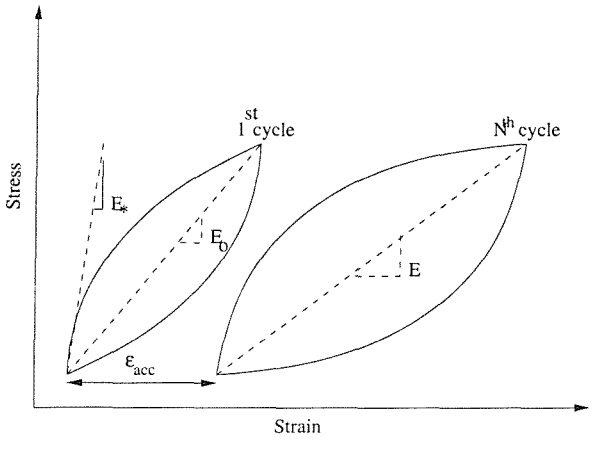

FIGURE 4.4: Schematic drawing of the method used to analyse the fatigue data. The initial secant modulus in the elastic range, determined from the pre-conditioning test is represented as E_*. The secant modulus from the first cycle and at any cycle N and accumulated strain at any cycle N are represented as E_o and E and ϵ_{acc} respectively.

The parameter, normalised stress, defined as the ratio of applied stress (σ) to the initial secant modulus from the pre-conditioning test (E_*), was used as a variable to help describe the fatigue behaviour. In order to assess the influence of the normalised stress, the data was analysed in terms of the life fraction (ω), which is defined as

$$\text{Life fraction, } \omega = \frac{N}{N_f} \tag{4.2}$$

where $N =$ current loading cycle, and N_f is the number of cycles to failure

$\omega = 0$ when $n = 0$, and $\omega = 1$ when $N = N_f$

In the case of the tensile fatigue tests, the specimens failed by a total fracture at the midsection, and the corresponding number of cycles was taken as the number of cycles to failure. For the specimens tested in compression, fracture of the samples rarely occurred. There are no standard criteria defined for the failure in compression fatigue. A large reduction in modulus has been reported for cancellous bone in compression fatigue, however, in previous studies when defining a failure criteria a smaller percentage (5 to 10%) of modulus reduction was chosen [14, 124]. In the present study, failure was defined as the number of loading cycles to reach a particular percentage reduction in modulus and/or a observation of a rapid increase in the deformation rate. The specimens which failed outside the gaugelength were discarded while analysing the data.

4.3 Uniaxial Tensile and Compressive Testing

The static tests showed that for Herex®C70.55, the modulus and strength were higher in tension than in compression. For the solid rigid PU foam the modulus and strength

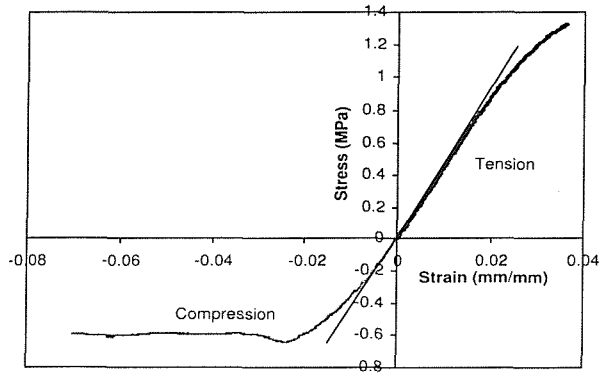

FIGURE 4.5: Stress-strain behaviour of Herex®C70.55 under uniaxial loading. The foam was stronger in tension than compression. The modulus was calculated as the slope of a linear fit to the initial portion of the curves.

in tension and compression were in a similar range. Typical stress-strain curves of the Herex®C70.55 and the solid rigid PU foam are given in Figure 4.5 and Figure 4.6. The modulus and strength of the foams in tension and compression are tabulated in Table 4.2. In all cases the standard deviation was less than 10% of the mean value.

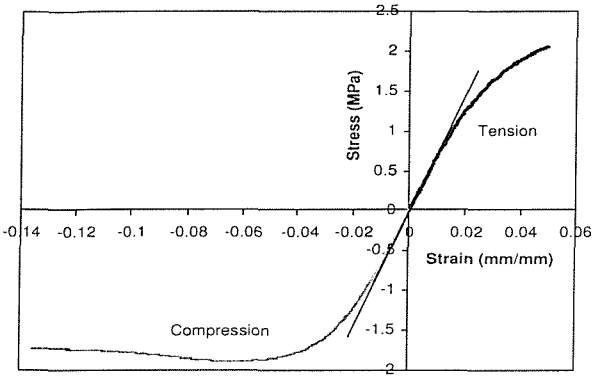

FIGURE 4.6: Stress-strain behaviour of solid rigid PU foam under uniaxial loading. The strength and modulus of the foam were similar in tension and compression. The modulus was calculated as the slope of a linear fit to the initial portion of the curves.

TABLE 4.2: Properties of the foams determined from the uniaxial tests.

Foam	Strength (MPa)		Modulus (MPa)	
	Tension	Compression	Tension	Compression
Herex®C70.55	1.45 ± 0.087	0.64 ±0.024	48.9 ± 3.25	39.6 ± 1.23
Solid Rigid PU foam	1.95 ± 0.12	1.91 ± 0.06	69.5 ± 0.79	70.6 ± 3.8

4.4 Fatigue Behaviour of Foams

The fatigue behaviour of Herex®C70.55 foam was characterised in both tension and compression while that of solid rigid PU foam was characterised only in compression. The Herex ®C70.55 foam results and its analyses are discussed in detail, and for solid rigid foams the results are briefly discussed as the analyses are similar to that of Herex®C70.55.

4.4.1 Tensile Fatigue Test Results of Herex®C70.55 Foam

Details of nine successful tensile fatigue tests are given in Table 4.3. The number of cycles to failure varied from 34 to 132252 for stress levels ranging from 93% to 46% of the ultimate strength. Figure 4.7 shows logarithmic plot of normalised stress(σ/E_*)

TABLE 4.3: Tensile fatigue test results of Herex®C70.55 foam.

Sl No.	N_f	Stress(σ) (MPa)	E_* (MPa)	E_o (MPa)	Initial Strain(ϵ_o)	Normalised Stress (σ/E_*)
1	34	1.35	50.3	45.3	0.0298	0.0268
2	155	1.14	42.7	40.1	0.0284	0.0267
3	533	1.15	46.4	43.7	0.0263	0.0248
4	719	1.05	48.0	45.5	0.0231	0.0219
5	3381	1.05	49.1	46.5	0.0233	0.0213
6	17780	0.93	49.7	49.4	0.0188	0.0187
7	34033	0.81	50.2	50.7	0.0160	0.0161
8	115700	0.73	52.8	53.3	0.0137	0.0138
9	132252	0.67	49.0	48.8	0.0133	0.0140

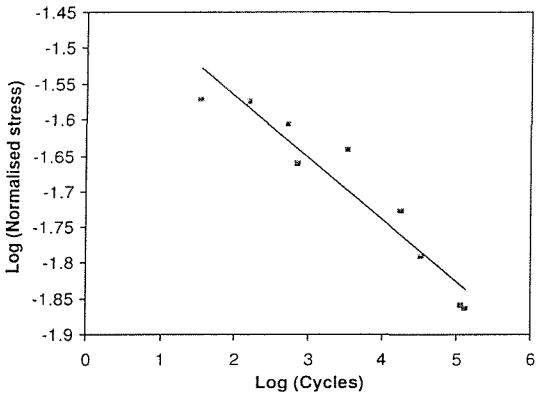

FIGURE 4.7: A logarithmic plot of normalised stress versus number of cycles from the tensile fatigue test results of Herex®C70.55 foam. A linear relationship existed between the variables, in the logarithmic plot, indicating a power law relationship between the variables.

against the number of cycles to failure,N_f. The relationship can be written as

$$N_f = 6 \times 10^{-17}(\sigma/E_*)^{-11.6} \qquad R^2 = 0.92 \tag{4.3}$$

4.4.1.1 Accumulated Strain Under Tension Fatigue Loading

The variation in accumulated strain with number of cycles is shown in Figure 4.8. The accumulated strain pattern followed a classical creep curve, consisting of an initial rapid phase of deformation of decreasing rate, followed by a phase of linear deformation and a final phase of rapid deformation of increasing rate. As the final stage was very rapid and may not be uniform, it was difficult to capture the strain pattern at this stage, especially for the low cycle tests. The accumulated strain, ϵ_{acc}, was calculated with respect to the position of the stress-strain curve of the first load cycle along the strain axis. The variation of accumulated strain with life fraction of the specimens is given in Figure 4.9. The maximum accumulated strain was within 25% of the initial strain

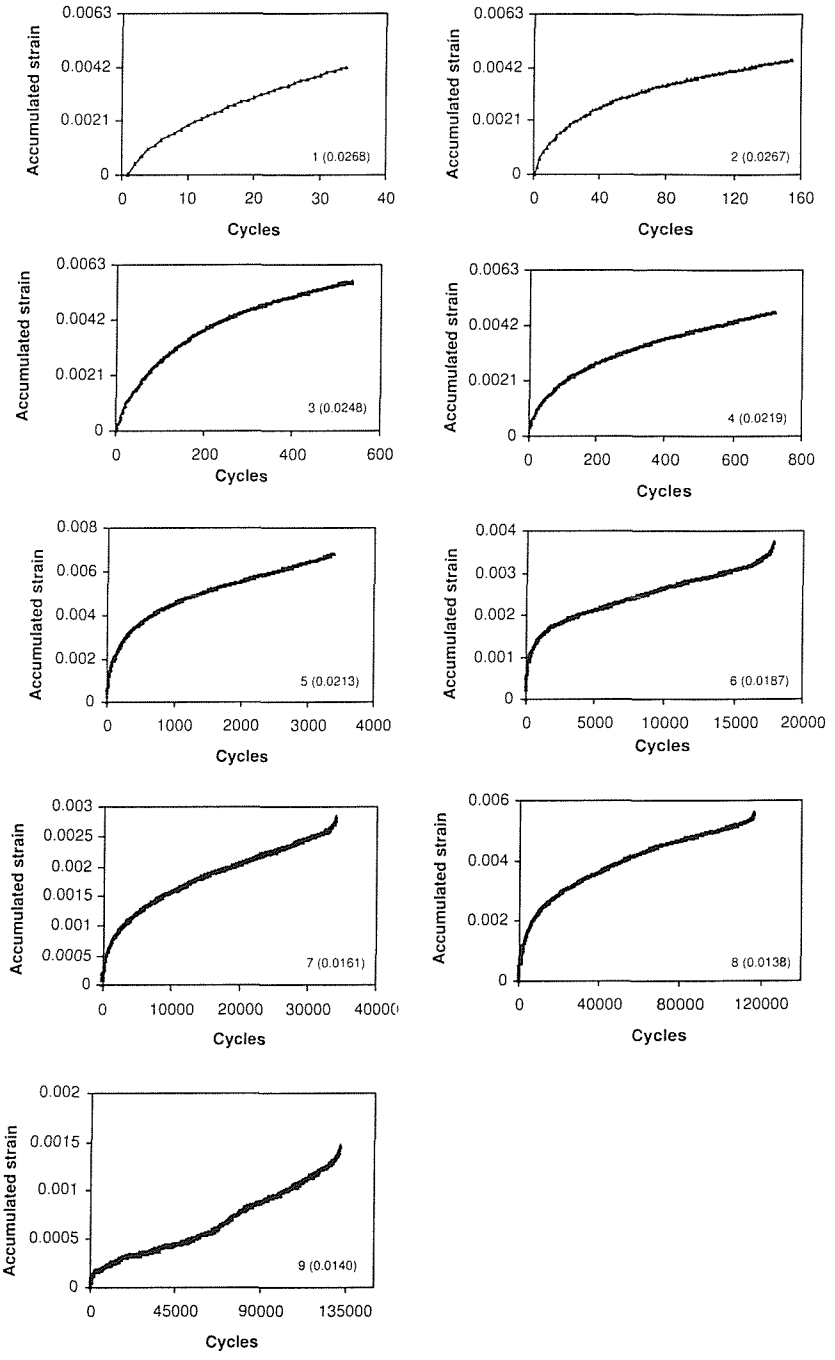

FIGURE 4.8: Variation in accumulated strain with number of cycles for specimens of Herex®C70.55 foam tested in tensile fatigue. The serial number and corresponding normalised stress are marked in each plot.

range. At first inspection, there appeared to be no relationship between the degree of permanent strain accumulated during the test and the magnitude of the applied normalised stress. Visual inspection showed that the linear phase was between life fractions of 0.2 and 0.8. For each test, the constant rate of strain accumulation during

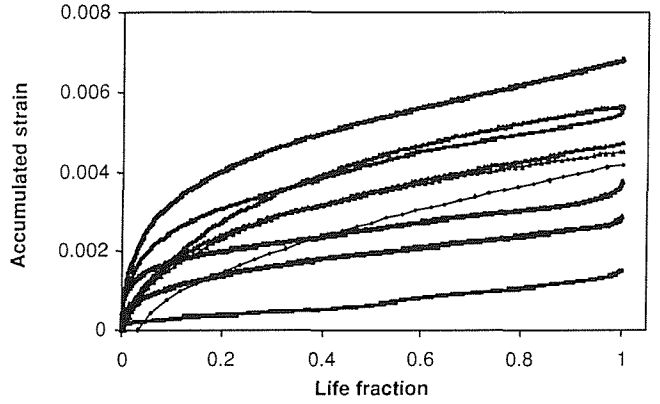

FIGURE 4.9: The pattern of accumulated strain against life fraction from the tensile fatigue tests of Herex®C70.55 foam. The pattern of accumulated strain resembled standard creep pattern.

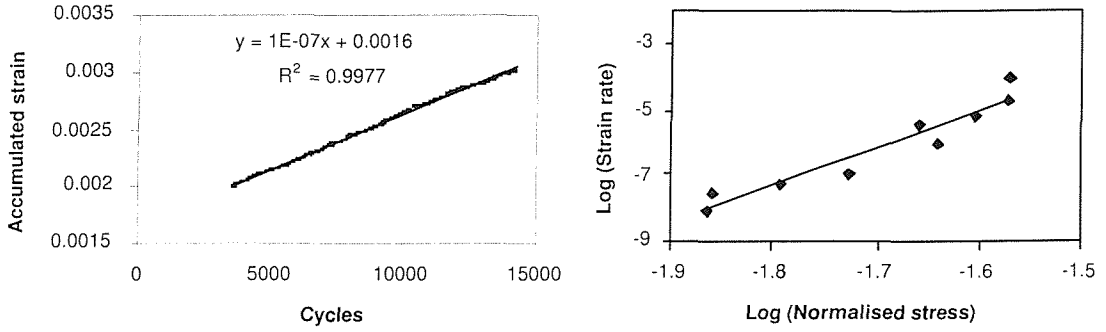

FIGURE 4.10: (a) An example of linear/steady state pattern of accumulated strain between life fraction of 0.2 and 0.8 for tensile fatigue specimen of Herex®C70.55 foam at an applied normalised stress of 0.0188 (b) logarithmic plot of normalised stress versus steady state accumulation rate.

the secondary stage was determined by a linear fit to the accumulated strain over the life fraction range from 0.2 to 0.8. The rate of strain accumulation at a steady state, $\frac{d\epsilon_{acc}}{dN}$, and its relationship with normalised stress is shown in Figure 4.10. The relationship between $\frac{d\epsilon_{acc}}{dN}$ and σ/E_* can be written as

$$\frac{d\epsilon_{acc}}{dN} = 4 \times 10^{13}(\sigma/E_*)^{11.6} \quad R^2 = 0.90 \tag{4.4}$$

4.4.1.2 Modulus Reduction Under Tensile Fatigue Loading

The material exhibited modulus reduction as a result of cyclic loading. Figure 4.11 shows the variation in modulus against number of cycles for the nine specimens. The variation of normalised modulus, (E/E_o) as a function of life fraction (N/N_f) is shown in Figure 4.12. From Figure 4.12 there appears to be two regimes for modulus degradation. A pattern of rapid reduction in the modulus at the very beginning of the tests followed by a linear rate of modulus degradation at higher stress levels. At lower stress

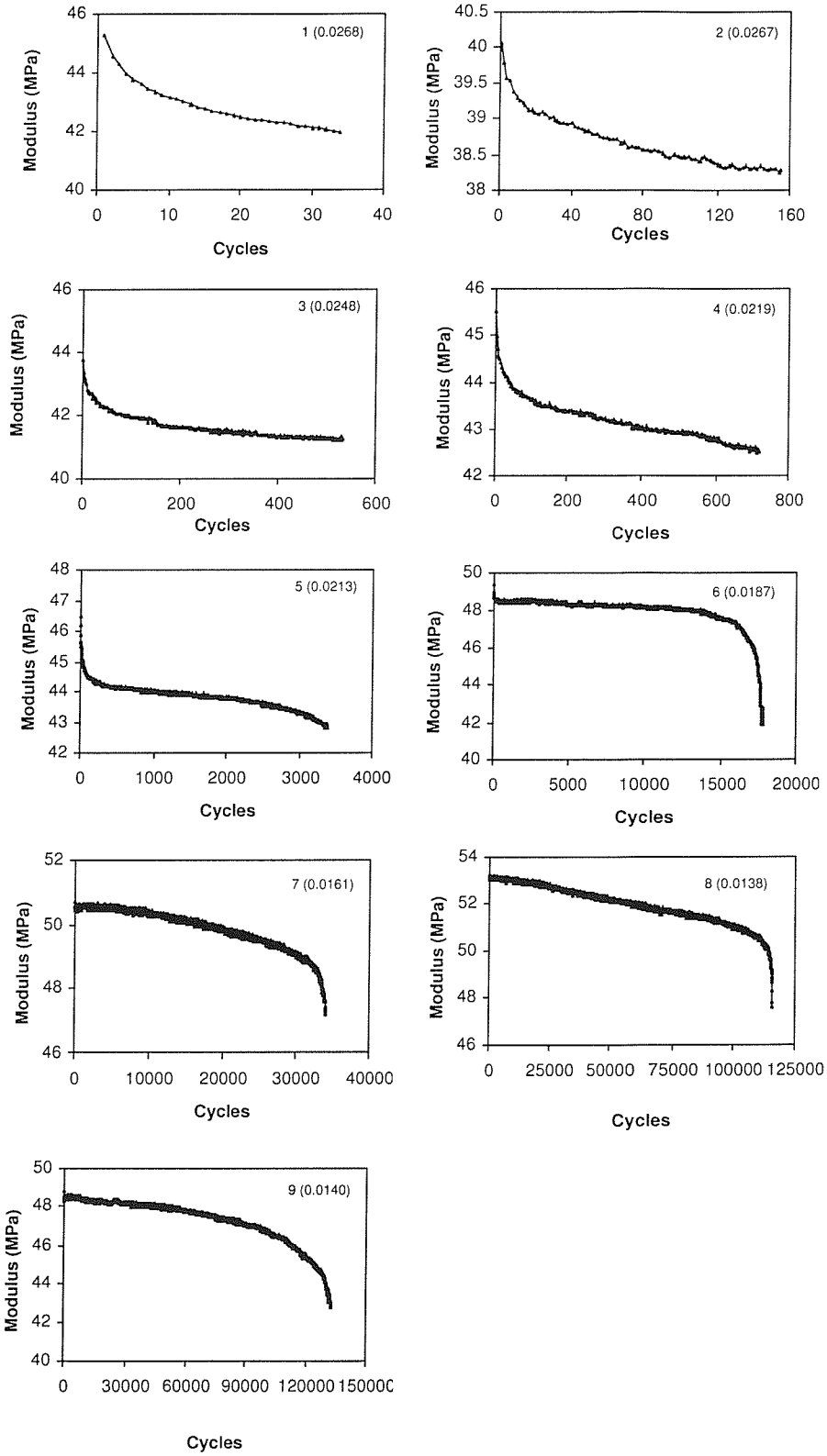

FIGURE 4.11: Pattern of variation of modulus reduction with number of cycles for specimens of Herex®C70.55 foam tested in tensile fatigue. The serial number and normalised stress are marked in each plot.

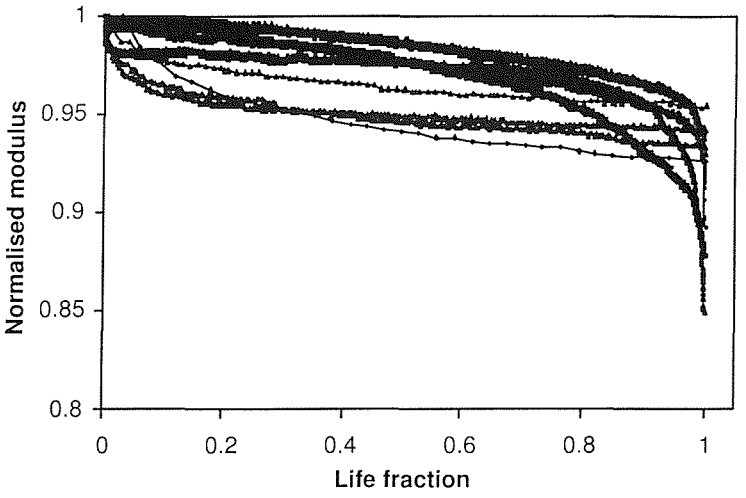

FIGURE 4.12: The pattern of normalised modulus against life fraction from the tensile fatigue tests of Herex®C70.55 foam.

levels the modulus reduction pattern was linear and slow up to 90% of the life and was followed by a rapid reduction in modulus. The maximum modulus reduction at the time of failure was within 15% of the first cycle modulus.

4.4.2 Compressive Fatigue Test Results of Herex®C70.55 Foam

In compression fatigue there was no failure by fracture as observed in tension. In general, failure was considered to occur when there was a rapid increase in the deformation under the loading. A definition of failure as a 30% reduction in modulus compared to the initial modulus, E_* was chosen in the present analysis. Most of the specimens had experienced a rapid phase of deformation (tertiary stage) in the deformation pattern by this time (Figure 4.13). Details of the ten successful tests are given in Table 4.4. For tests carried out at various stresses, from 67-100% of the ultimate strength, the respective number of cycles to failure varied from 5 to 142380. The failure life, N_f exhibited power law relationship with the normalised stress(σ/E_*) as shown in Figure 4.14; the relationship could be written as

$$N_f = 2.2 \times 10^{-53}(\sigma/E_*)^{-29.4} \qquad R^2 = 0.91 \tag{4.5}$$

The material exhibited modulus reduction and accumulation of strain under compressive cyclic loading. As the first three specimens failed in a very few cycles the results from these tests were not used in the analysis of modulus reduction and accumulation of strain.

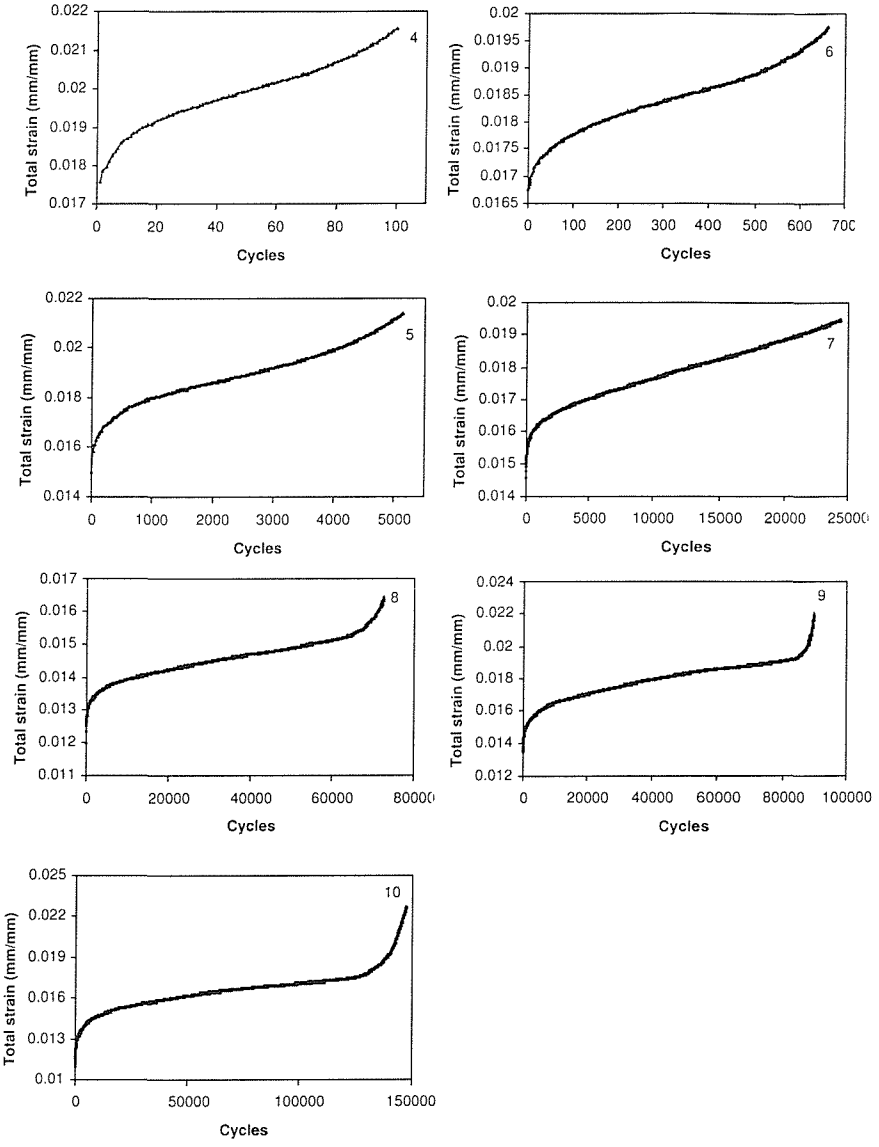

FIGURE 4.13: Total strain versus number of cycles from the compressive fatigue tests of Herex®C70.55 foam, using a failure criteria of 30% reduction in modulus. The serial number is marked in each plot.

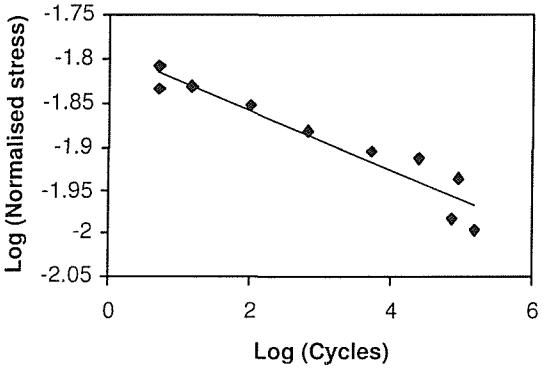

FIGURE 4.14: A logarithmic plot of normalised stress versus number of cycles from the compressive fatigue test results of Herex®C70.55 Foam. A linear relationship existed between the variables, in the logarithmic plot, indicating a power law relationship between the variables.

TABLE 4.4: Compressive fatigue test results of Herex®C70.55 foam.

Sl No.	N_f 1	Stress (σ) (MPa)	E_* (MPa)	E_o (MPa)	Initial Strain (ϵ_o)	Normalised Stress (σ/E_*)
1	15	0.64	43.2	32.1	0.0198	0.0148
2	5	0.68	43.8	31.7	0.0214	0.0155
3	5	0.62	42.2	30.6	0.0203	0.0147
4	100	0.58	41.9	33.2	0.0177	0.0140
5	662	0.61	46.7	36.8	0.0167	0.0131
6	5140	0.55	44.4	36.8	0.0150	0.0125
7	24490	0.49	39.9	33.4	0.0146	0.0122
8	72429	0.46	44.1	37.2	0.0123	0.0104
9	89524	0.51	44.2	37.8	0.0135	0.0116
10	147710	0.43	42.2	37.8	0.0112	0.010

4.4.2.1 Accumulated Strain Under Compressive Fatigue Loading

Accumulation of strain was observed (similar to a standard creep curve) for all the specimens tested in compressive fatigue (Figure 4.15). The pattern of accumulation of strain against life fraction is given in Figure 4.16. The rate of the secondary stage (between a life fraction of 0.2 and 0.8) was strongly related to the normalised stress by power law relationship (Figure 4.17) which could be written as

$$\frac{d\epsilon_{acc}}{dN} = 7 \times 10^{31}(\sigma/E_*)^{20.1} \quad R^2 = 0.85 \tag{4.6}$$

A power law relationship was able to describe the accumulation of strain as a function of life fraction. The relationships of the constants A and B to normalised stress was best represented by a linear fit (Figure 4.18). Figure 4.19 shows the comparison of experimental and analytical prediction of accumulated strain for the normalised stress levels at which the tests were carried out. At some normalised stress levels, the analytical and experimental results were very similar, while for the rest the analytical model either under predicted or over predicted the experimental observations. As mentioned earlier in this section, the relationships of the constants in the power-law relationship showed a positive relationship with normalised stress levels, but a strong dependence on normalised stress was not observed from the available data. A larger number of samples, with a number of tests at each stress level, would have given a better idea of the dependence of the constants; however, in the present study more tests were not carried out with constraints on availability of material and time for specimen preparation and testing.

A wide scatter in the fatigue data of materials is expected, with the microstructural

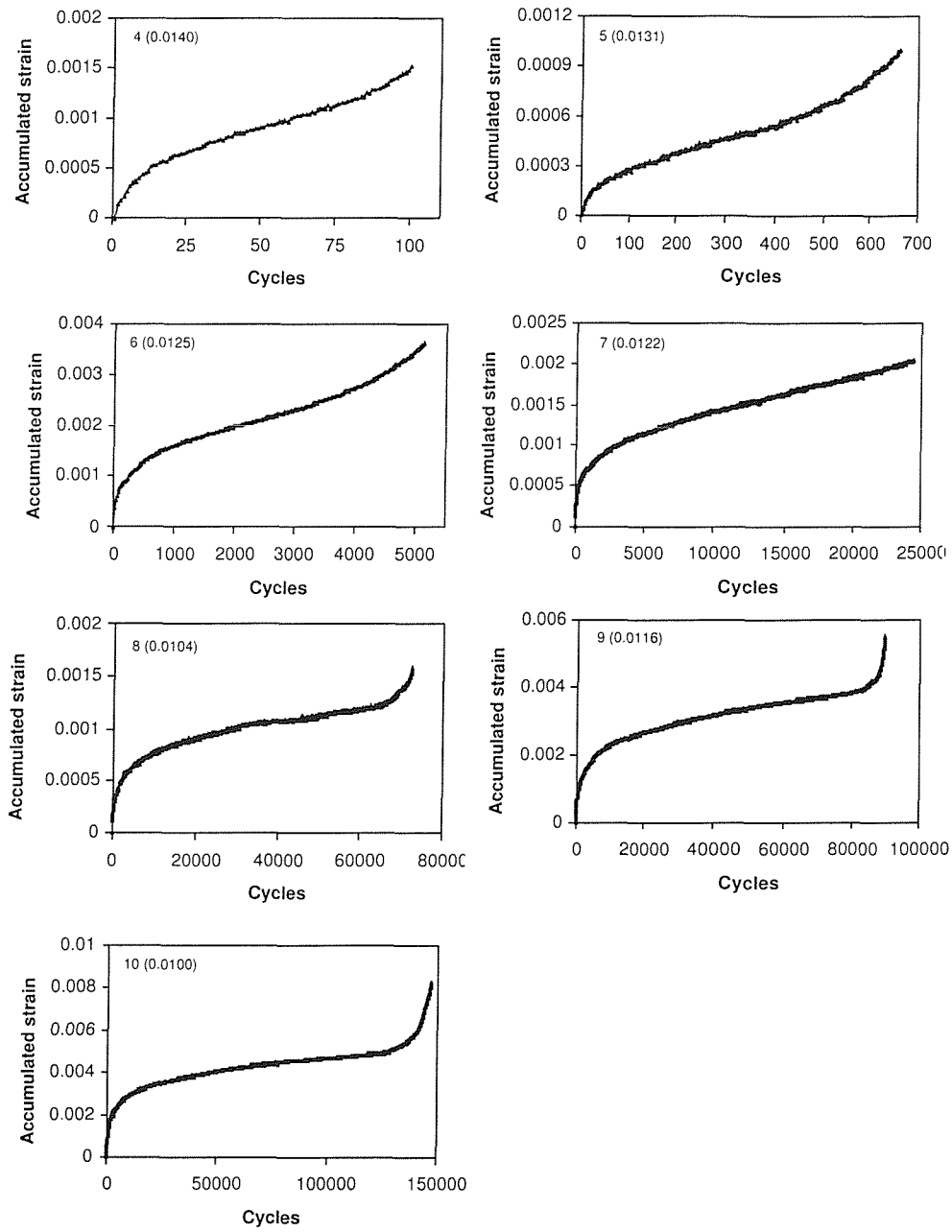

FIGURE 4.15: Pattern of variation of accumulated strain with number of cycles for specimens of Herex®C70.55 foam tested in compressive fatigue. The serial number and normalised stress are marked in each plot.

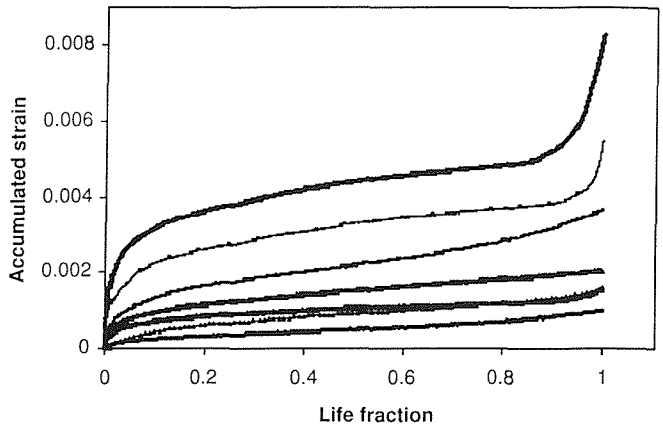

FIGURE 4.16: The pattern of accumulated strain against life fraction from the compressive fatigue tests of Herex®C70.55 foam. The pattern of accumulated strain resembled standard creep pattern.

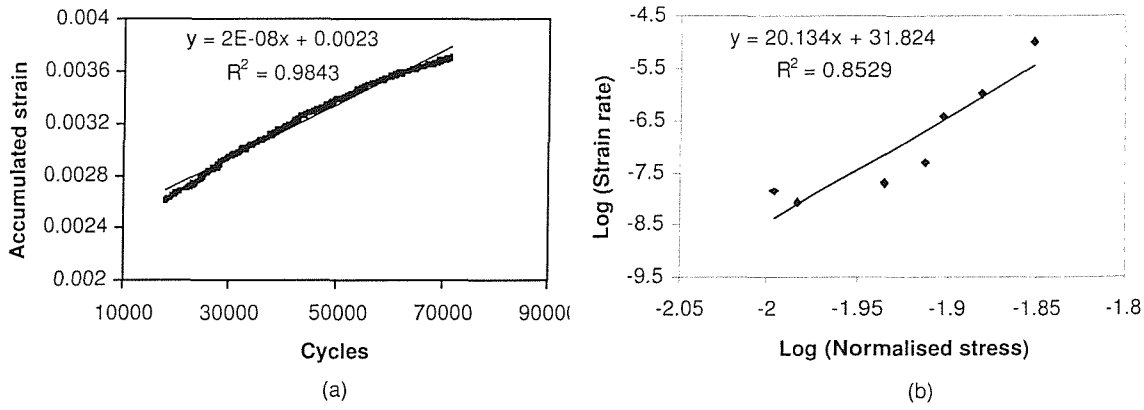

FIGURE 4.17: (a) An example of linear/steady state pattern of accumulated strain between life fraction of 0.2 and 0.8 for compressive fatigue specimen of Herex®C70.55 foam at an applied normalised stress of 0.0116 (b) logarithmic plot of normalised stress versus steady state accumulation rate.

inhomogeneity in the material properties and test conditions of the specimens. In the case of foams, with structural inhomogeneity in terms of structural arrangement of cellular structure, the scatter in the fatigue data could be higher. It would thus result in the requirement of a larger sample size for deriving at the S-N relationship for the material. However, from the fatigue tests of the present material, with a comparatively smaller sample size (approximately 10) a good correlation was observed between the number of cycles to failure and the normalised stress levels. In deriving the relationships for the accumulated strain/modulus as a function of stress level, the scatter would be higher with the variability in the strain experienced in the guagelength. It could be possible that the material was not uniformly strained in all the tests, with

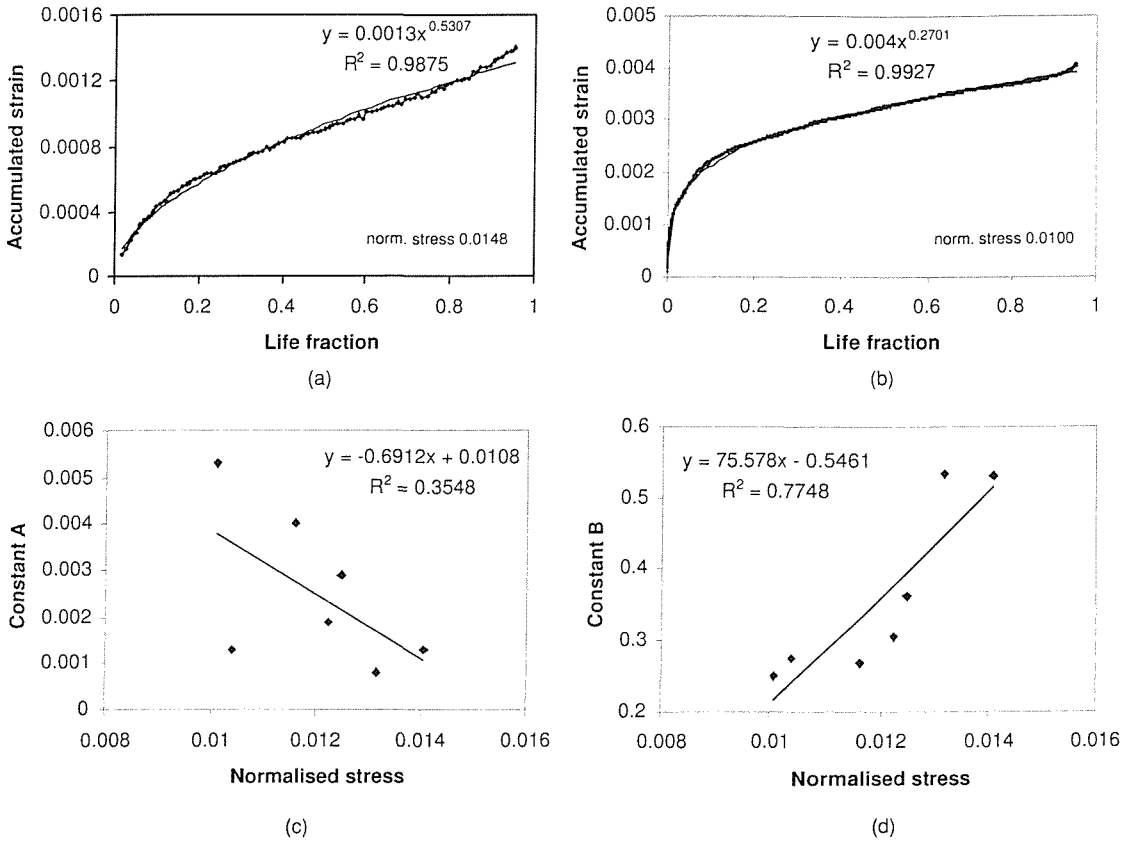

FIGURE 4.18: Examples of strong power law relationship between accumulated strain and life fraction of form $A\omega^B$ for compressive fatigue specimens of Herex®C70.55 foam for a normalised stresses of (a) 0.0148 and (b) 0.010. The relationship between (c) constant A (d) constant B and normalised stress levels.

structural inhomogeneity of the foam, and there could be have been some errors from the method of strain measurement as well.

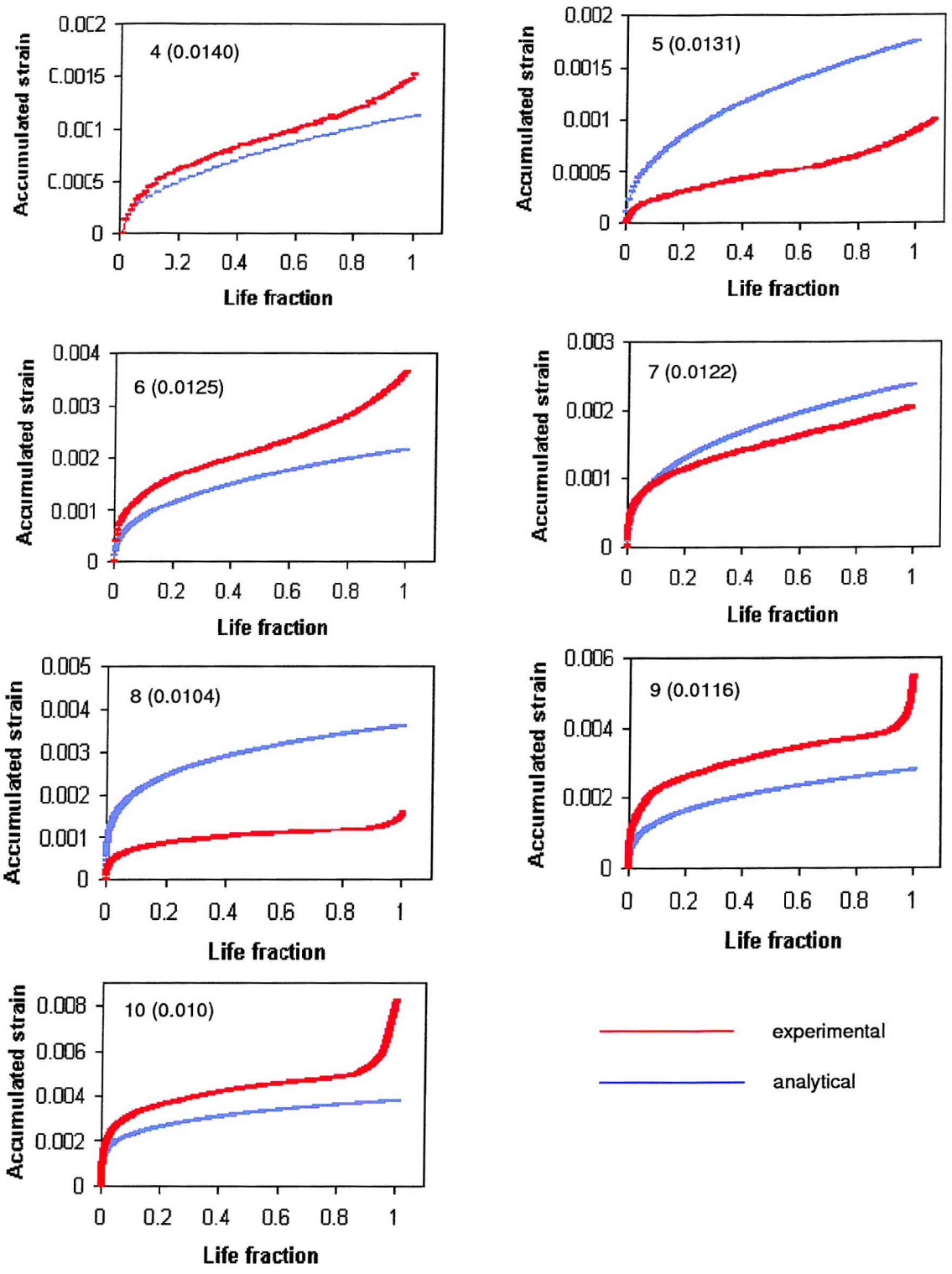

FIGURE 4.19: Comparison of analytical and experimental values of accumulated strain for Herex ®C70.55. in compression fatigue.

4.4.2.2 Modulus Reduction Under Compressive Fatigue Loading

Plots of modulus reduction against number of cycles for specimens tested at various stress levels are shown in Figure 4.20. The material showed modulus reduction with number of cycles at all stress levels. The pattern of normalised modulus E/E_o against life fraction is shown in Figure 4.21. The patterns were similar at all stress levels, while modulus reduction was faster at higher stress levels. In general there was a rapid

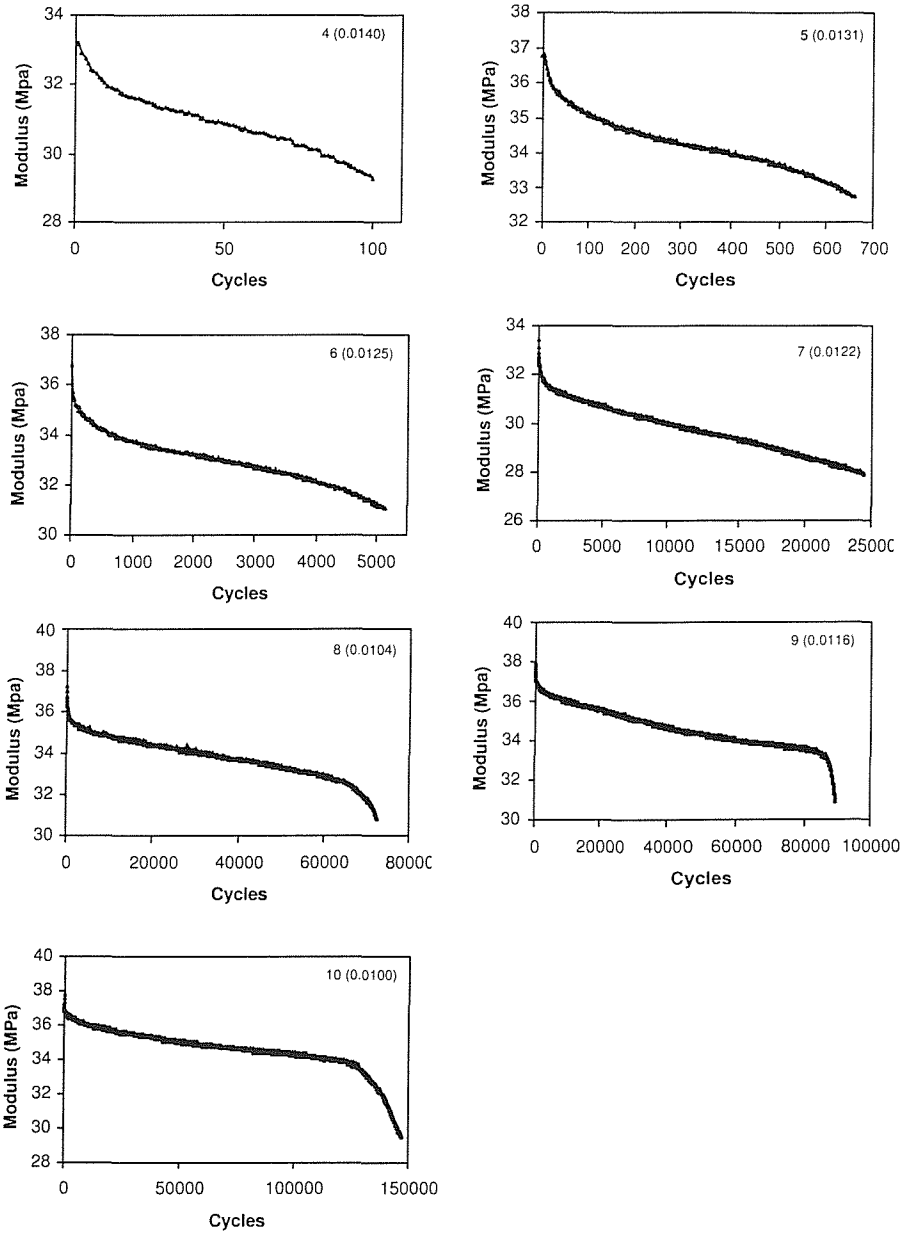

FIGURE 4.20: Pattern of variation of modulus reduction with number of cycles for specimens of Herex®C70.55 foam tested in compressive fatigue. The serial number with respective normalised stress in bracket as from Table 4.4 is marked in each plot.

reduction in modulus up to 10% of life, a linear region between 10-90% of life followed by a rapid phase again. The modulus reduction showed a power law relationship with life fraction (up to 95%) for all tests. The constants in the relationship showed a positive linear relation with normalised stress levels (Figure 4.22). Figure 4.23 shows a comparison of the analytical and experimental values of modulus reduction. In most of the cases analytical and experimental values were similar, while in some cases the

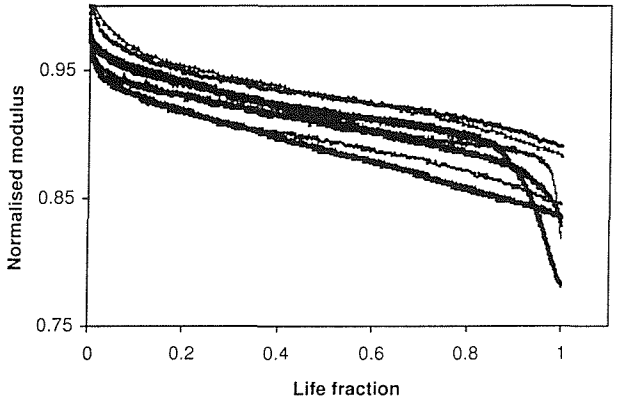

FIGURE 4.21: Normalised modulus (E/E_o) against life fraction for compressive fatigue specimens of Herex®C70.55 foam.

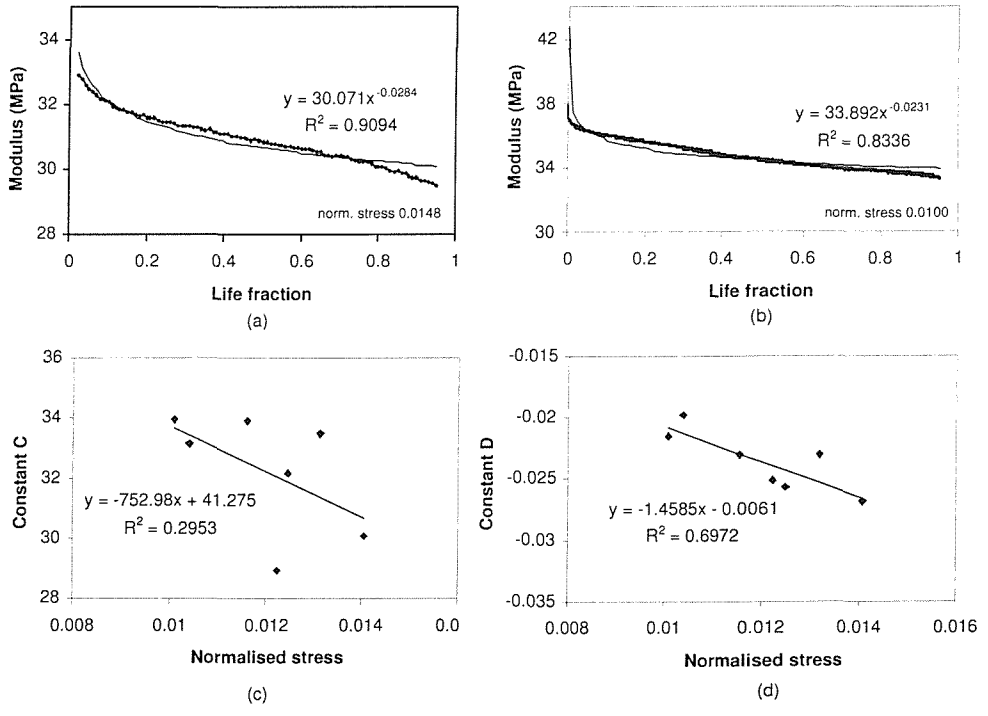

FIGURE 4.22: Examples of power law representation of modulus of form $(E = C\omega^D)$ for the compressive fatigue specimens of Herex®C70.55 foam at normalised stress levels of (a) 0.0148 and (b) 0.010. Also shown are the relationships between the (c) constant C and (d) constant D and normalised stress level.

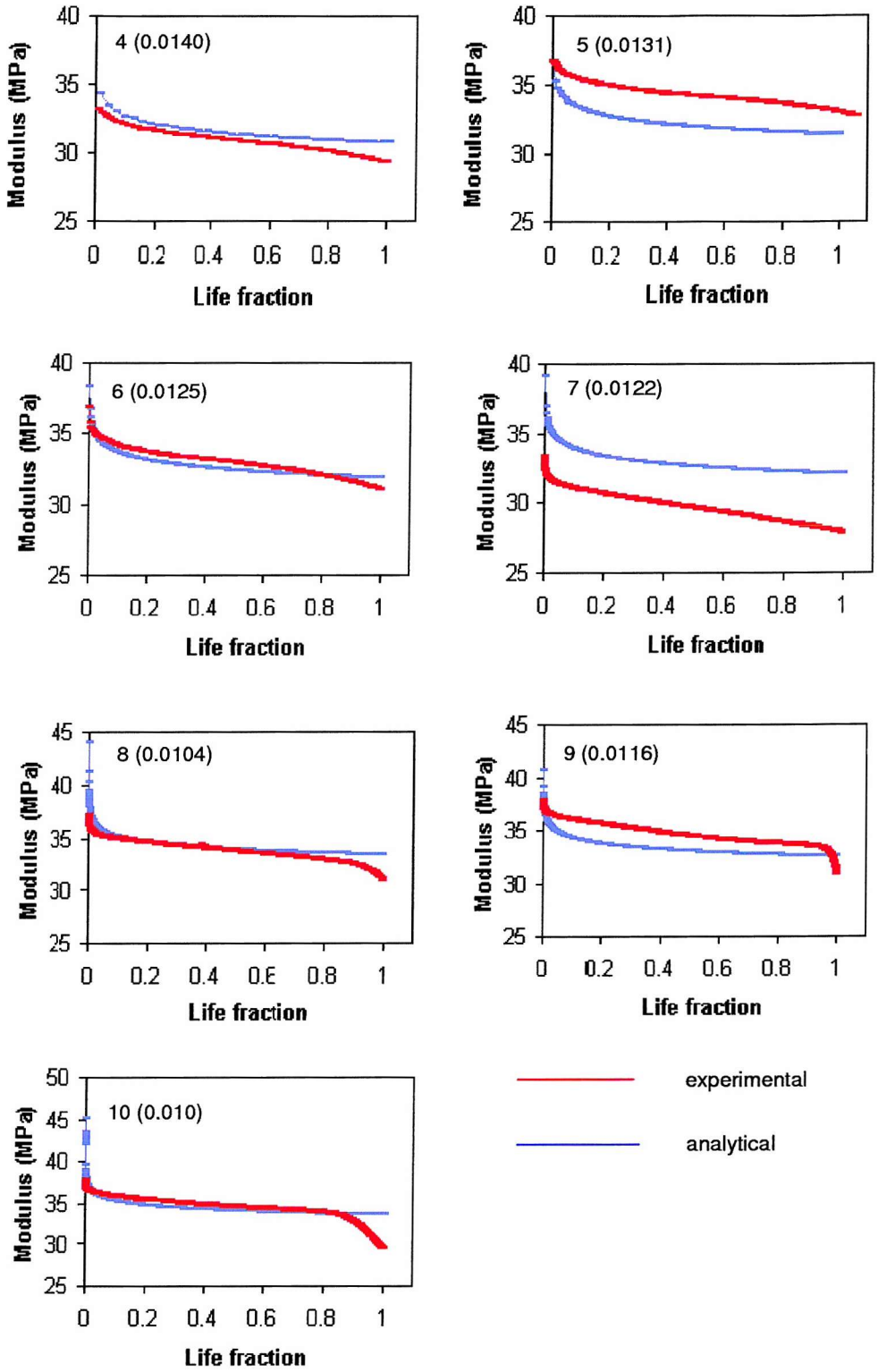

FIGURE 4.23: Comparison of analytical and experimental values of modulus reduction for Herex ®C70.55. in compression fatigue.

analytical model over/under predicted the experimental results.

4.4.2.3 Comparison of Tensile and Compressive Fatigue Behaviour of Herex Foam

The constants and exponents in the expressions for S-N relationship and secondary strain rate were distinctly different for the foam material in tension and compression. The magnitude of the exponent in the power law expressions (for both S-N and secondary strain rate) was almost the double in compression compared to that in tension. However, with the material being stronger and stiffer in tension, the range of normalised stress levels at which tests were carried out in tension and compression were different (Table 4.3 and Table 4.4). The pattern of accumulated strain and the range of its magnitudes (Figure 4.9 and Figure 4.16) were similar in tension and compression. However, the material accumulated higher amount of strain in compression than in tension, at a given normalised stress level. Considering modulus reduction, in tension there were two distinct patterns, for higher and lower stress levels. In compression the modulus degradation pattern was similar at all the tested stress levels (Figure 4.12 and Figure 4.21).

4.4.3 Compressive Fatigue Test Results of Solid Rigid PU Foam

The methods used to test and analyse the Solid Rigid PU foam fatigue behaviour were similar to those used for Herex ®C70.55 foam. At very high stress levels the failure was too rapid to record any data. The main details of ten successful tests are given in Table 4.5. Similar to Herex®C70.55 foam, the failure life, N_f, of the Solid Rigid foam showed a power law relationship with normalised stress(σ/E_*) (Figure 4.24):

$$N_f = 4.3 \times 10^{-36}(\sigma/E_*)^{-23.6} \qquad R^2 = 0.82 \tag{4.7}$$

The criteria of a percentage reduction in modulus was found not applicable for specimens tested at lower stress levels as they showed a negligible modulus reduction. The number of cycles to failure, N_f was taken as the number of cycles at which the deformation rapidly increased after the secondary phase of deformation (Figure 4.25).

TABLE 4.5: Compressive fatigue test results of Solid Rigid PU foam.

Sl No.	N_f	Stress (σ) (MPa)	E_* (MPa)	E_o (MPa)	Initial Strain(ϵ_o)	Normalised Stress (σ/E_*)
1	450	1.51	62.7	51.3	0.0295	0.0241
2	3000	1.64	71.4	59.7	0.0275	0.023
3	6000	1.61	73.0	62.3	0.0259	0.0221
4	6000	1.51	65.2	52	0.0290	0.0231
5	11000	1.41	62.8	53.5	0.0263	0.0224
6	11100	1.36	64.9	56	0.0243	0.0209
7	30000	1.42	71.2	62.5	0.0226	0.0199
8	48000	1.36	71.4	62.5	0.0217	0.0190
9	110178	1.36	68.0	58.9	0.0231	0.020
10	180000	1.425	73.1	67.3	0.0212	0.0195

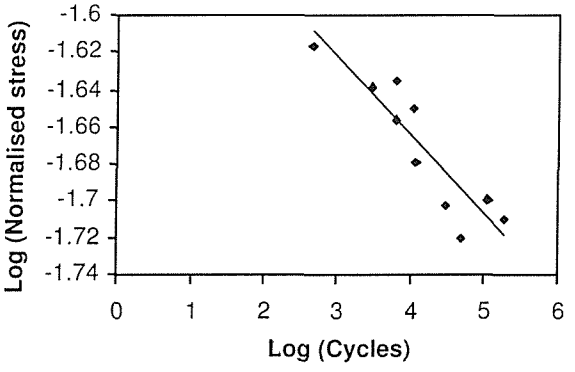

FIGURE 4.24: A logarithmic plot of normalised stress versus number of cycles from the compressive fatigue test results of Solid Rigid PU foam. A linear relationship existed between the variables, in the logarithmic plot, indicating a power law relationship between the variables.

4.4.3.1 Accumulated Strain Under Compressive Fatigue Loading

The patterns of accumulated strain against life fraction for all specimens are shown in Figure 4.26. In general, the accumulated strain and the normalised stress level were directly related by a linear relationship (Figure 4.27). Again, the pattern of accumulated strain was similar to that of a creep curve and the slopes of the secondary stage of the accumulated strain curves were related to the normalised stress levels by powerlaw relationship as given in Equation 4.9.

$$\frac{d\epsilon_{acc}}{dN} = 6.85 \times 10^{48}(\sigma/E_*)^{33.169} \quad R^2 = 0.90 \tag{4.8}$$

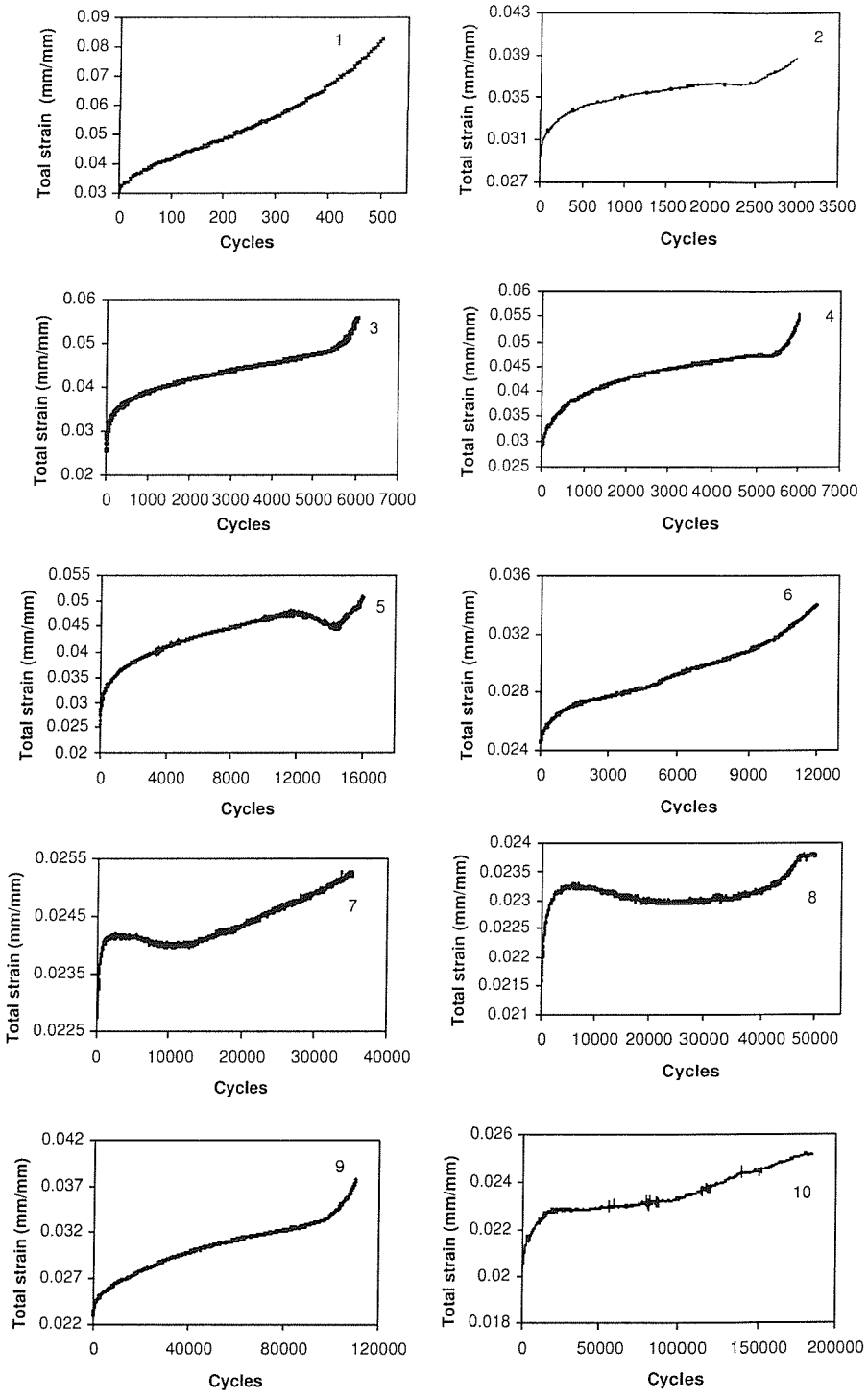

FIGURE 4.25: Total strain versus number of cycles for compressive fatigue of Solid Rigid PU foam.

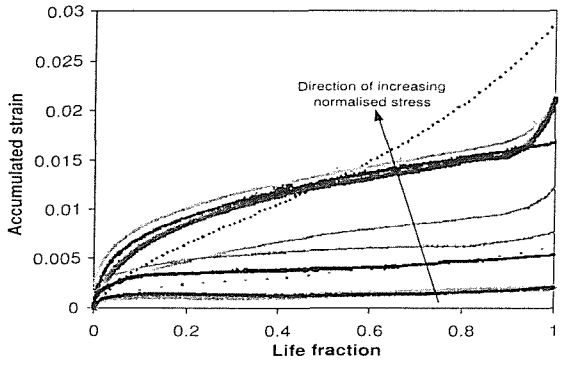

FIGURE 4.26: Plot showing accumulated strain against life fraction from the compressive fatigue tests of Solid Rigid PU foam. In general higher normalised stress level resulted in higher amount of accumulated strain.

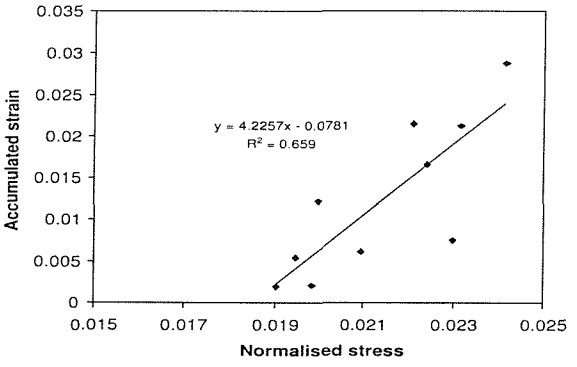

FIGURE 4.27: A plot showing accumulated strain at failure against normalised stress from the compressive fatigue tests of Solid Rigid PU foam. There is a direct relationship between the normalised stress level and the total accumulated strain.

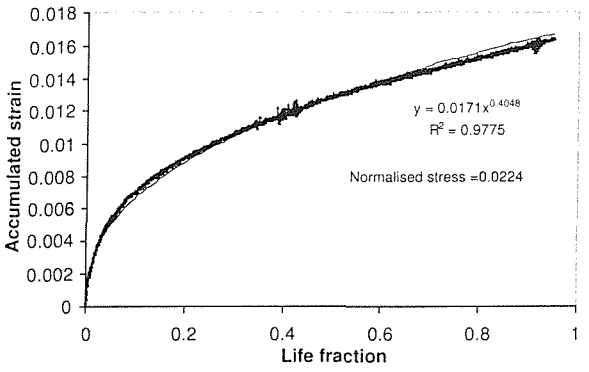

FIGURE 4.28: An example of strong power law relationship between accumulated strain and life fraction of Solid Rigid PU foam specimens of form $A\omega^B$, for any particular normalised stress level.

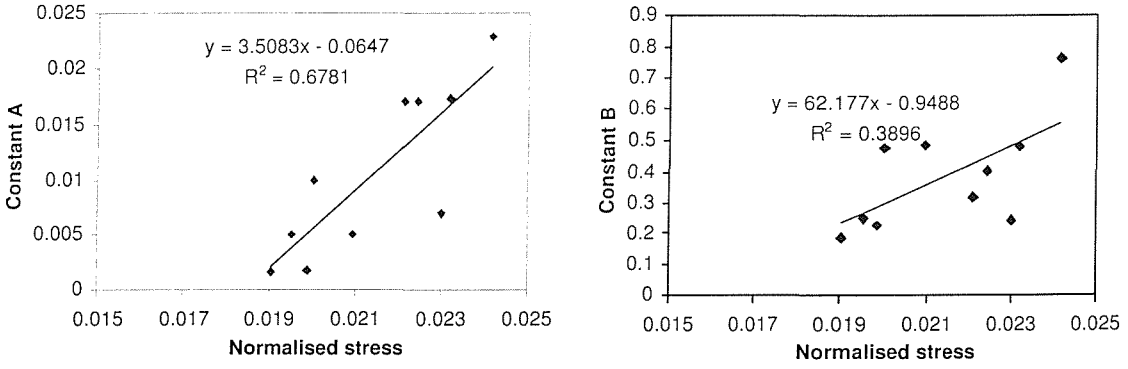

(a) (b)

FIGURE 4.29: The relationships between (a) Constant A and (b) Constant B with the respective normalised stress levels for the compressive fatigue tests of Solid Rigid PU foam.

The accumulated strain curves were related to the life fraction ω by relationships of the form $A\omega^B$ (Figure 4.28). Again, the constants were best fitting to a linear fit in showing their relationship with normalised stress levels (Figure 4.29). A comparison of the analytically predicted and experimental values of the accumulated strain is given in Figure 4.30. The experimental and analytical values of accumulated strain were similar in most cases, with a few exceptions where the model under/overpredicted the experimental results.

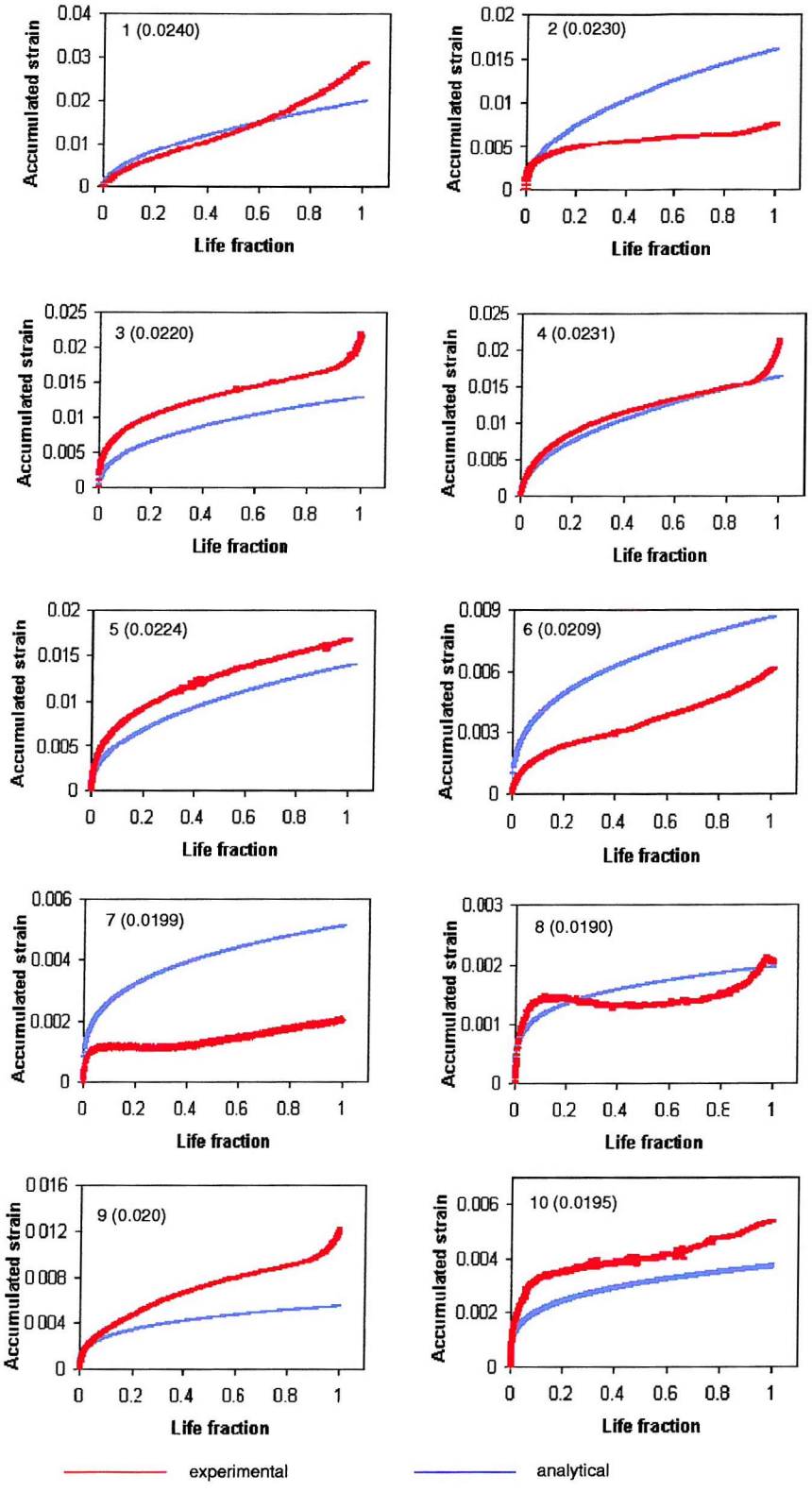

FIGURE 4.30: Comparison of analytical and experimental values of accumulated strain for Solid Rigid PU foam in compression fatigue.

4.4.3.2 Modulus Reduction Under Compressive Fatigue Loading

The modulus reduction pattern was similar to the pattern of strain accumulation, with a rapid reduction in the modulus at the initial stage followed by a steady state and a rapid phase of modulus reduction. The variation in normalised modulus with life fraction for the tests are shown in Figure 4.31. The modulus pattern could be described in the form of $E = C\omega^D$. Figure 4.32 shows the relationships between constants C and D and the normalised stress level. Figure 4.33 gives a comparison of the modulus reduction, experimental and analytical, for Solid Rigid PU foam. The analytical model was similar to the experimental results in most of the cases, however, in a few cases the model under/overpredicted the results.

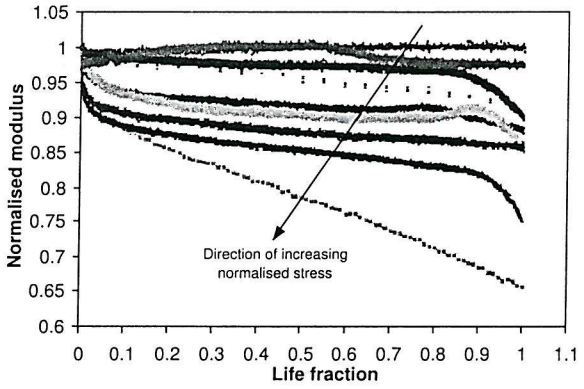

FIGURE 4.31: Pattern of variation of normalised modulus with life fraction for the compressive fatigue test specimens of Solid Rigid PU foam. In general, higher normalised stress level resulted in higher amount of modulus reduction

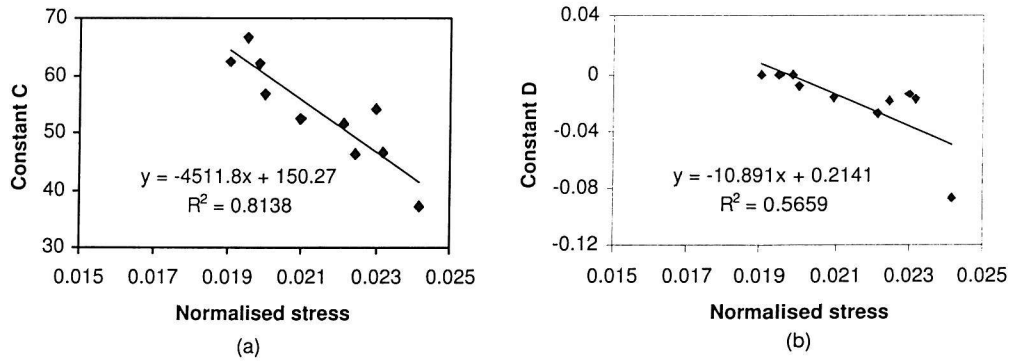

FIGURE 4.32: The relationship between the (a) Constant C and (b) Constant D with normalised stress levels for compressive fatigue of Solid Rigid PU foam.

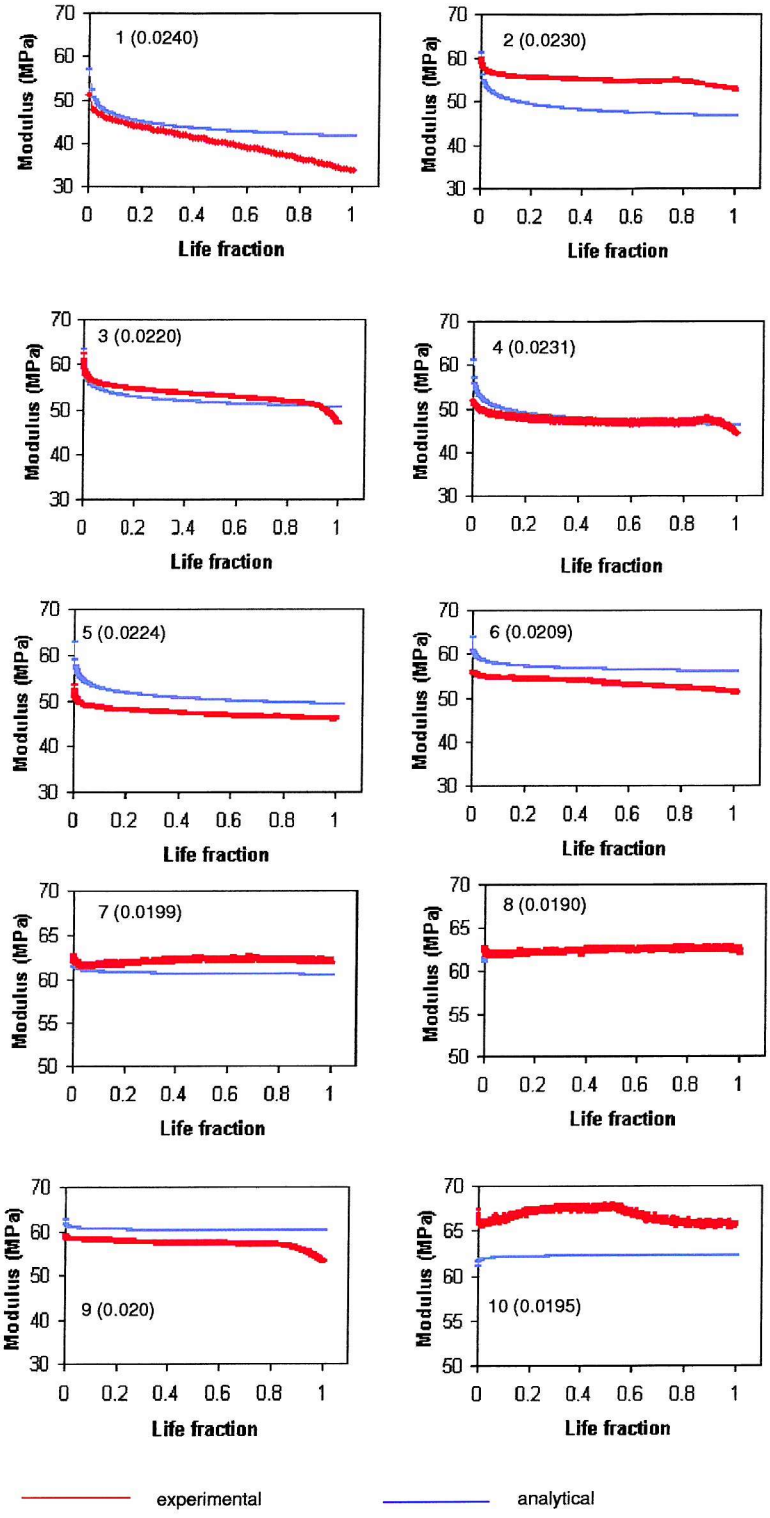

FIGURE 4.33: Comparison of analytical and experimental values of modulus reduction for Solid Rigid PU foam in compression fatigue.

4.5 Discussion

The present study proposes a methodology for the selection of suitable analogue materials to cancellous bone for studies involving fatigue loading.

The wide variation in properties and the difficulties involved in working with cancellous bone has resulted in synthetic foams being widely used as an alternative in many *in vitro* biomechanical tests [37, 168, 170, 177]. Rigid Polyurethane foam is commonly used as a cancellous bone substitute in synthetic bone models[37, 177] and there are standards specified for their use as a cancellous bone substitute[2]. PVC foams have also been used in some *in vitro* studies related to cancellous bone[170]. The ranges of strength (0.45 to 5 MPa) and modulus (30-150MPa) of the foams used in these studies was small, and fell into the lowest range of that for cancellous bone; for cancellous bone the ranges of strength and modulus were 0.4 to 50 MPa and 3 to 3350 MPa[7, 8, 60, 95, 97, 121]. However, the major importance while using these materials as cancellous bone analogue was given for the cellular structure, the consistency in properties and the resemblance of the tensile and/or compressive stress-strain curves to that of cancellous bone.

Initial monotonic uniaxial tests of the materials (Chapter 4, Section 4.3) showed that for both the materials the strength and modulus were consistent with a standard deviation less than 10% and the values fell in the lowest range for cancellous bone[94, 121]. Herex foam was stronger in tension than compression. Most of the reports on cancellous bone have found equal compressive and tensile modulus but higher strength in compression, compared to tension [8, 24, 156, 90, 97, 156, 175]. This suggests that for tests involving both tension and compression loading, the strength and modulus inequalities of the foam material may be significant. In the present work, importance is given to compressive loading of the foam. Solid Rigid PU foam had similar strength and modulus values in tension and compression.

The performance of the foams were qualitatively similar to the fatigue behaviour of cancellous bone in compression, with the materials exhibiting reduction in strength, modulus degradation and accumulation of permanent strain with number of cycles. There are no studies on the tensile fatigue behaviour of cancellous bone. There are no standard criteria defined for failure in compression fatigue of foam/bone, as in compression the material, even after crushing may still take further load. The foams did not fail by fracture(as in tension) and were observed to take load by undergoing large deformation. In the studies on cancellous bone fatigue, to draw the relationship between life and stress level, failure life was taken as number of cycles corresponding to a 5% reduction in modulus[124] or 10% reduction in modulus [13]; however as reported in these studies, cancellous bone was able to take load in further cycles and undergo

large modulus reductions (to the level of 60% of initial modulus) and accumulation of strain. Most of the studies on cortical bone are confined to tensile fatigue, and the other studies do not give any information on the chosen failure criteria. In the case of creep tests the starting phase of tertiary curve was taken as the failure point[13, 14]. These studies, only reported the S-N relationships and secondary strain rate-stress relationships. However, the present study, attempted to determine modulus reduction and accumulation of strain, as a function of cycles and stress level for input into the migration simulation. The chosen failure life is important, as accordingly the amount of modulus reduction and accumulated strain varies, and thus the amount of migration. Harte et al.[67] discussed the need for an alternative definition for compression fatigue failure of metal foams, where the foam could undergo progressive crushing while achieving large strains. They chose failure criteria to be the number of cycles when the foam begins to crush, the first point of failure. This was identified as the formation of a knee in the strain curves, corresponding to the formation of the first crush band across the specimen. Shenoi et al.[169] used a criteria of change in slope of deflection curve (point of change of deformation pattern from a progressive to rapid phase) in defining the failure. In the present study, for Herex foam a 30% reduction in modulus was chosen, within which most of the specimens experienced a tertiary phase. In the case of the Solid Rigid PU foam there was no obvious modulus reduction at lower stress levels. Failure was taken as the starting point of the tertiary phase of deformation. It may be necessary to define alternative failure criteria, dependent on the comparison of simulated and experimental results of migration.

The foams showed power law relationships for life with normalised stress level. Studies on cancellous bone fatigue has reported a similar relationship for number of cycles to failure (N_f) with normalised stress/strain levels of form

$$N_f \propto X^{-y} \tag{4.9}$$

where X is normalised stress/strain level. Reported magnitudes of y are 11.9[124] and 12.99[13] from fatigue studies on cancellous bone. In those studies, they have reported that the value of the constant fell into a similar range to that of cortical bone. For the foam materials studied, they were 29.4 (Herex foam) and 23.6 (Solid Rigid PU foam). The difference in the constants could be attributed to many factors, as the fatigue/creep of cellular foam is dependent on the fatigue/creep of solid cell wall material, the density, cellular shape and arrangement[75, 76].

In this work, modulus values, in general, showed an initial reduction, a steady phase and a tertiary phase of rapid reduction in compression. For both the foams, the tertiary phase of modulus reduction was observed by the time a modulus reduction of 20

to 30% (with respect to the initial modulus) has occurred. In the case of Solid Rigid PU foam, at lower stress levels there was no apparent modulus reduction. For specimens tested at the lower stress levels, some stiffening effect was observed towards the end of the test (observed as a slight increase in modulus and decrease in accumulated strain with cycles). Michel et al.[124] observed a progressive increase in the modulus, in the initial stage of high cycle fatigue tests of cancellous bone, and they attributed this to a possible end effects associated with a compliant end layer of trabeculae near the specimen surface. However, in the present work, with the reduced section model this effect could not be influential. Kanny et al.[89] in their study on flexural fatigue of PVC foams, reported an increase in the flexural modulus of some foams which then started to decrease again as the specimens approached the end life. From an SEM analysis they observed that cells collapse on the tension and compression side of the beam, and damage concentrate at regions near the surfaces where the stresses are high. They attributed the stiffening effect to the increase in the damaged area with number of cycles, which formed a dense band, towards the neutral axis. Micromechanical/optical analysis of the specimen failure was not carried out in the present study. Some of the tests (high cycle tests) spanned over two-three days; however the effect of variation in temperature (which was within 4 degree Celsius) was not considered in the present study. It could be possible that, localised crushed zones/deformation regions were present, and the possible temperature effect and associated strain recovery, resulted in the stiffening of the foam.

For the Herex foam, the maximum amount of accumulated strain at the time of failure, in both tension and compression, was less than half of the initial applied strain. In the case of the Solid Rigid PU foam, the maximum amount of accumulated strain at higher stress levels was close to the initial applied strain; the percentage of accumulated strain with respect to the initial applied strain decreased for the lower normalised stress levels. There was a direct relationship between the total accumulated strain and the normalised stress level. The magnitude of accumulated strain was approximately three times higher than that of Herex foam. For both foams, modulus reduction and accumulated strain were best represented by means of a power equation of the form $A\omega^B$, where ω is the life fraction. The constants in the relationship were best related to the normalised stress levels by a linear relationship, however the relationship in some cases was weak. In most cases the analytical model was similar to the experimental results, however, in some cases they over/underpredicted the results. As explained in section 4.4.2.1 a few factors could have influenced the predicted analytical/experimental model mismatch, such as the sample size and non-uniform strain and the strain data extraction.

Michel et al.[124] reported an increase in the hysteresis and decrease in secant modulus,

and a rapid drop in the modulus towards the final stages of cancellous bone fatigue; however no attempt was made to quantify the amount of modulus reduction and its relationship with stress level and life fraction. They merely observed that there were two distinct patterns of modulus reduction in high and low cycle tests. However, the presented plots of modulus reduction and cyclic stress-strain, indicated modulus reduction up to 60% and accumulation of strain to almost double the initial elastic strain. In their study, Bowman et al.[13], compared the accumulated strain from fatigue and creep tests of cancellous bone, to specify the importance of accumulation of strain on fatigue. They noted an increase in the secant modulus, reported as an increase in the fatigue strain (a term used to describe the increase in elastic strain with cycles). The amount of accumulated strain was higher than the increase in elastic strain, throughout the test. Cancellous bone was reported to accumulate strain to a large degree (in one case the accumulated strain had a magnitude higher than the initial strain). Haddock et al.[63] reported a reduction in magnitude by 60% with respect to the initial modulus. The failure strain was more than three times the initial strain, and throughout the tests, they reported similar components of accumulated and fatigue strain. Pattin et al.[139] compared the tensile and compressive fatigue behaviour of cortical bone. The study concentrated more on the distinction between the S-N and modulus reduction patterns of the material in tension and compression fatigue. The study presented plots of stress-strain behaviour that showed a large increase in accumulated strain, and considerable modulus reduction. The patterns of modulus reduction in tension and compression were different. For cortical bone, in compression, they reported no apparent modulus reduction in the initial half of the life, while in tension most of the modulus reduction occurred in the first and last quarter of the life. The observed pattern of modulus reduction for the foam was more similar to the tensile modulus reduction pattern of cortical bone. In spite of the observations patterns and magnitudes of modulus reduction and accumulated strain for cancellous bone and cortical bone [13, 14, 124, 139] very few studies have attempted to represent their relationship with cycles/life fraction and stress level. The available relationships were mainly for the tensile fatigue of cortical bone (Chapter 2, Table 2.2). Taylor et al.[183] fitted a third order polynomial ($a\omega^3 + b\omega^2 + c\omega + d$) and a power law representation ($a\omega^b$) respectively to represent modulus reduction and accumulated strain for the tensile fatigue test results. The correlation coefficients of the curve fit were higher than 0.9 for all the specimens. The constants in the relationships were linearly related to stress level, and the correlation coefficients from the regression analysis were, for all constants, higher than 0.7. Pattin et al.[139] represented modulus as

$$1 - E(n)/E_o = \beta_1 log[\frac{1}{1 - n/N_f}] \tag{4.10}$$

where $E(n)$ is the n^{th} cycle modulus, E_o is the first cycle modulus and n/N_f is the life fraction. For all the specimens, the curve fitted with a good correlation coefficient (higher than 0.97). However, a linear fit for the constant β_1 to the effective strain gave a poor correlation coefficient (r^2=0.06).

Most of the fatigue/creep studies of foams concentrate more on relating the microlevel mechanisms of deformation to the apparent level mechanical behaviour; and not much information is available on quantitative representation of modulus reduction and accumulation of strain of these materials, at apparent level. As mentioned earlier, in the present study, the mechanical behaviour of the materials were compared to that of cancellous bone only at apparent level. However, with studies showing the relationship between factors like the solid cell properties[1, 57, 75, 77] the structural arrangement of the cells and the cell size on foam behaviour, it would be advantageous in further work to consider foams with similar microlevel properties to that of cancellous bone, depending on the experimental requirements. Fatigue of polymers could be different from fatigue of bone, a composite material at the microlevel. In fatigue of polymers, the fracture is considered as a result of initiation and propagation of a crack[163], with influential factors such as polymer structure, molecular weight, crosslinking and filler type. Cyclic softening is reported for polymers[163], attributed to the changes in microstructure (packing rearrangement) and generation of defects. Many optical observations on specimens of cancellous bone under fatigue/creep and static loading has shown extensive microcracking/fractures in the trabeculae, depending on the strain level to which they are subjected[6, 130, 203]. However, further studies are required to understand the micromechanism of microcracking/fracturing of trabeculae. Similarly, further understanding/studies of analogue materials, for similar material composition and micromechanism of failure would be helpful in choosing appropriate alternatives to cancellous bone in *in vitro* studies.

Chapter 5

FE Model Development

A combined Finite Element (FE) and Continuum Damage Mechanics (CDM) procedure is used for modelling the observed fatigue behaviour of the material. In this chapter a brief introduction to the concepts of FE and CDM is given.

5.1 Finite Element Analysis (FEA)

Finite element analysis is a numerical procedure for obtaining approximate solutions to mathematical models of physical problems. The method is widely used in engineering analyses and design. The mathematical model of the physical problem is stated in terms of geometry, loading, boundary conditions, material properties and their constitutive relationships[9, 39]. Only a brief explanation of the process of finite element analysis is given here as there are many standard literature sources available for further reference[9, 39].

The method is based on the concept that an approximate solution to a problem can be achieved by subdividing the problem into smaller units (elements) and solving the problem from these finite element levels. The geometry of the model is divided into a number of units called elements which are considered interconnected to each other at joints called nodes. Simple displacement functions are chosen to assume the distribution of actual displacement over each element. Equilibrium equations are derived for each element from its material and geometric properties, based on the variational principle of mechanics. The coefficients of the equilibrium equations for the elements (stiffness matrix) relates the nodal displacements to the nodal forces. The equilibrium

relation can be expressed through a set of equations

$$[k]\{q\} = \{Q\}$$

where $[k]$ is the stiffness matrix, $\{q\}$ is the nodal displacement vector and $\{Q\}$ is the nodal force vector. The equilibrium equations for the entire body are obtained by combining the equations of individual elements in such a way that continuity of displacement is preserved at the interconnecting nodes. These equations are modified for the given boundary conditions and then solved to obtain the unknown displacements. The overall equilibrium relation for the entire body can be thus represented as

$$[K]\{r\} = \{R\}$$

where $[K]$ is the global stiffness matrix formed by the assemblage of elemental stiffness matrix, $\{r\}$ is the global nodal displacement vector and $\{R\}$ is the global nodal force vector. The equilibrium equations are solved for the unknown displacements. With known displacements other unknowns like stresses and strains are calculated. There are different methods for solving the set of equations which depend on many factors such as the type of constitutive relationships which can be linear or non-linear, computational load, computational time and cost and the results of interest. The availability of a computer assisted solution process and computer based packages for the analysis make finite element methods very popular in the engineering field. The main advantage of FEA is its suitability to take into account complex geometries and boundary conditions, various material properties, non-homogeneity of the continuum and its control over the variables. A realistic numerical solution depends on the presentation of the mathematical problem, justification of the statement of the problem, assumptions and their justifications. In this respect assumptions and justifications have to be validated against theoretical or experimental results. A pictorial representation of the process of finite element analysis[9] is given in Figure 6.1. The efficiency of the analysis is evaluated in terms of the computational time/cost and accuracy of the results and in this respect the statement and solution procedure chosen for the problem is normally a trade off between these factors.

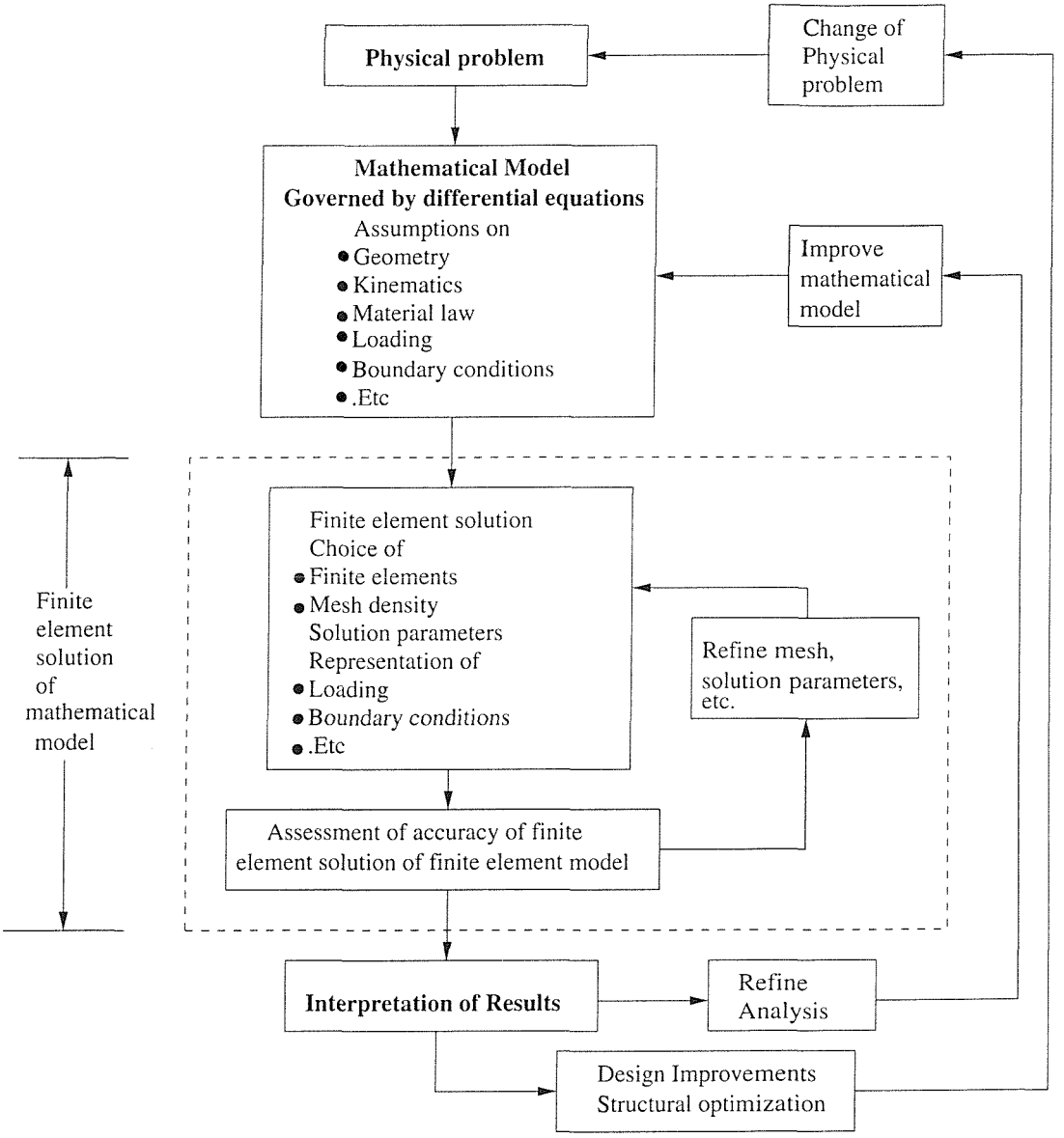

FIGURE 5.1: The process of FE analysis[9].

5.2 Application of Continuum Damage Mechanics (CDM) To Model Fatigue

Repeated loading causes the initiation and growth of micro and macrocracks. On reaching a critical level of damage, failure of the material occurs, normally at a stress level lower than its strength under monotonic loading and this phenomenon is known as fatigue. Understanding the accumulation and progression of fatigue damage in materials and its effect on the overall structural behaviour under varying loads of varying durations are important in formulating life time predictions and assessment of cumula-

tive damage. The results of laboratory fatigue experiments are often used to formulate the cumulative damage laws of fatigue. As damage accumulation is reflected through the mechanical response of the specimen, related parameters can also recorded in these experiments. One of the most simple and straight forward measures of damage is the remaining life or cycle ratio (ratio between number of cycles of loading versus number of cycles to failure) and one of the simplest forms of cumulative law is Palmgren-Miner's linear cumulative damage law[125] which states that equal time intervals lead to equal damage increments and the total damage will always be equal to 1. Based on this law if a material subjected to m number of load levels the total damage D can be written as

$$D = \sum_{i=1}^{m} \triangle D_i = \sum_{i=1}^{m} \frac{n_i}{N_i} \tag{5.1}$$

where $\triangle D_i$ represents the damage accumulation during the i^{th} load level n_i is the number of cycles of operation and N_i is the number of cycles to failure at that load level. $D = 0$ represents the undamaged state and failure occurs when $D = 1$. This method is widely used for its simplicity, however, it has been observed that the damage accumulation is not linear always and is dependent on the load sequence. Various studies on fatigue damage accumulation has resulted in a number of damage parameters and many cumulative laws in terms of these parameters. Fatemi [48] and Yang [202] give a detailed review of cumulative fatigue damage mechanisms, quantifying parameters for damage and cumulative damage theories mainly used for homogeneous materials, especially metals. They discuss many methods of quantifying the damage, D, which includes surface crack measurements, mechanical parameters like stress, strain, hardness, elastic modulii and total strain energy and physical measures using optial, acoustic, thermal and magnetic techniques. They point out that each damage model accounts for one or several phenomenological factors such as load dependence, multiple damage states, non linear damage evolution and load sequence and the interaction and applicability of each model varies from case to case which consequently makes the simpler Palmgren-Miner rule a dominant choice for designs.

Continuum mechanics deals with the response of materials to various loading conditions based on the assumptions that the material is continuous where fine details of discontinuity or heterogeneity of matter at a very small scale compared to the structural level of the material can be neglected. Every portion of continuum, however small, is assumed to exhibit the global physical properties of the material. The size of the elementary unit is such that it is large enough to smooth the effect of the discrete nature of the matter at a finer scale, and at the same time small enough to represent a continuous distribution of the field variables. The scale of the elementary unit of continuum depends on the scale of discontinuity and the structural scale of the

material considered and as long as the scale of interest is not below the elementary unit level the material can be treated as continuum and analysed using continuum mechanics. In this respect many heterogenous materials like concrete, rock, wood, cement, bone, foams and composites can be treated as continuum materials. The description of mechanical behaviour of a solid has two parts where the first part deals with the governing equations such as the strain displacement relations, equations of static equilibrium and the description of boundary conditions which are based on principles of physics universally applicable to any material. The second part describes the material specific aspects where stress-strain constitutive relationships and appropriate material constants for that particular material are used. The constitutive relationships are derived based on the principles of thermodynamics. The thermodynamic state of a material at any point and instant is described by the knowledge of the values of certain state variables at that instant. These state variables are two types, observable and internal, and the choice of them depends on the phenomena to be described. For defining the mechanical state of a system the observable variable is the total strain. There are no rules for choosing the internal variables, however they are usually chosen based on the application, experience and the phenomena to be described.
The stress-strain constitutive relationship of an isotropic elastic material can be written as

$$\sigma = E\epsilon \tag{5.2}$$

where σ is the stress components, E is the Hooke's elasticity matrix and ϵ the strain components.
Considering the fact that damage may accumulate without forming a major crack through most of the life time, conventional methods of prediction of life based on measurement of an existing flaw (fracture mechanics) or prior estimation of the life time (S-N diagram) could be difficult in the case of sophisticated structures and where complex damage mechanisms are present. Kachanov[86, 87] was the first to introduce the concept of a continuous parameter $0 \leq D \leq 1$ to characterize the gradual deterioration of a material's microstructure under creep loading. While the exact nature of cracks and their evolution cannot be quantified, their effect on material damage can be averaged on a representative volume as a macroscopic variable giving it a continuum variable identity. The damage is defined in terms of the density of the microcracks in a unit volume or the reduction in the effective area for load transfer. An assumption that microracks are uniformly distributed without any specific orientation gives a scalar dimension to the damage. Later the use of effective stress and effective strain concepts based on damage gave the framework to include the damage parameter directly to the stress strain constitutive relationships[109]. The concept of effective stress(σ) states that the stress on a damaged section is same as the stress acting on a undamaged sec-

tion over the effective area. The constitutive law for damaged materials is commonly derived from the principle of strain equivalence which states that any strain constitutive equation of a damaged material is written exactly as for the virgin material except that the stress is replaced by an effective stress.

$$D = 1 - A/A_o \tag{5.3}$$

where A is the effective area and A_o is the initial area of the concerned section. The effective stress is

$$\tilde{\sigma} = \frac{\sigma}{(1-D)} \tag{5.4}$$

The stress-strain relationship thus can be written as

$$\epsilon = \tilde{\sigma}E = \frac{\sigma E}{(1-D)} \tag{5.5}$$

and the effective modulus is:

$$\tilde{E} = E(1-D) \tag{5.6}$$

which gives a form of measurable variable for determining the damage. Since damage is an irreversible process, the thermodynamics of irreversible processes gives the necessary scientific basis for deriving the stress-strain relationships of damaging material in a continuum mechanics framework[30]. While conventional methods do not couple the stress-strain behaviour of the material with the accumulated damage, Continuum Damage Mechanics allows the damage field in the structure along with the relevant stress-strain fields to be evaluated.

In short, Continuum Damage Mechanics (CDM) is a branch of continuum mechanics representing the mechanical property degradation at a continuum level while taking into account the macrolevel effect of micromechanisms of damage by means of a macroscopic field variable, the damage parameter. The constitutive relationship couples damage accumulation to the mechanical response of the structure under loading. CDM can be applied to high cycle and low cycle fatigue, creep, and creep-fatigue. This requires the identification of a suitable damage parameter to represent damage mechanism under consideration, expressing the damage evolution law in terms of it and and inclusion of the damage parameter into the constitutive relationships. Cheng [35] and Lemaitre [107] gave different measurement parameters of damage by using direct and indirect and destructive and non-destructive methods. Krajcinovic, [103] discusses issues in damage mechanics, focusing on the criteria for choosing the damage parameter. Damage measures through physical parameters such as density change, resistivity change, change in fatigue limit, change in mechanical behaviour are other options. Effective modulus is mentioned as an appropriate measure of damage during

fatigue, as long as the damage is distributed uniformly over the strained volume. Paas et al.[138] describes the characteristics of a proper evolution law for damage:

- Damage is considered to be the relevant dissipative mechanism
- The irreversible nature of damage or rate of change of damage is always positive
- There is a non-linear dependence of damage growth on loading and current damage state
- If D approaches the critical value damage growth becomes infinite
- There exist a threshold below which no damage occurs

While Palmgren-Miner's law is the most used linear damage accumulation law, there are some non-linear damage accumulation models in fatigue. Chaboche et al. [31] proposed a nonlinear damage law in which the damage rate was expressed as a function of the present damage; the mean stress level and the maximum stress level by $dD = f(\sigma_m, \overline{\sigma}, D)dN$, i.e., a non linear evolution of damage. He formulated a damage evolution equation:

$$D = 1 - [1 - r^{1/(1-\alpha)}]^{1/(1+\beta)} \tag{5.7}$$

Where β is a material constant and α is a stress dependent function and r is the life fraction. The function had unseparable variables σ_m and D which described the non linear damage accumulation and load sequence effects.

If constitutive equations can represent elasticity, plasticity, creep and micromechanisms of damage by continuous variables, the behaviour of a crack may be obtained by structure calculations using, for example finite element method, without any reference to concepts taking into account the material discontinuity of the cracks as stress intensity factors or strain energy release rate[108]. Since the damage variables are formulated in terms of field variables they are normally easy to represent in FE procedures. As many of the fatigue experiments are based on uniaxial test data, in order to generalise the results, equivalent quantities are introduced. The concept of CDM has found application in many engineering fields like civil and mechanical engineering and material science.

A rupture analysis using damage mechanics concepts can be based on two approaches, coupled damaged zone calculations and coupled strain damage calculation. In an uncoupled analysis it is assumed that the stress tensor is not influenced by the damage state until a critical damage state is reached at which local rupture occurs; in a coupled analysis the stress-strain and damage fields are determined simultaneously. A pictorial representation of these concepts is given in Figure 5.2. For materials showing

property degradation with damage a coupled analysis is used to describe the change in properties. For example using elastic modulus as a damage parameter, an uncoupled analysis can be written as

$$E = E_o, \text{ if } D < 1.0 \tag{5.8}$$

$$E = 0.0 \text{ or } E_c, \text{ if } D > 1.0 \tag{5.9}$$

For a coupled analysis

$$E = E_o, \text{ if } D = 0 \tag{5.10}$$

$$E = (1 - D)E_o, \text{ if } D \leq 1.0 \tag{5.11}$$

where E is the initial modulus and E_o is the effective modulus.
A coupled analysis requires the modelling of every single cycle of the step which will be computationally an enormous task. A 'cycle jump' option is used in such situations using an iterative procedure where each iteration represents a predetermined number of cycles[138]. It is assumed in this case that the changes in the mechanical behaviour within the step are negligible. Memon et al.[123] used a procedure of additional load method for the prediction of crack initiation and fatigue life thus avoiding a reassem-

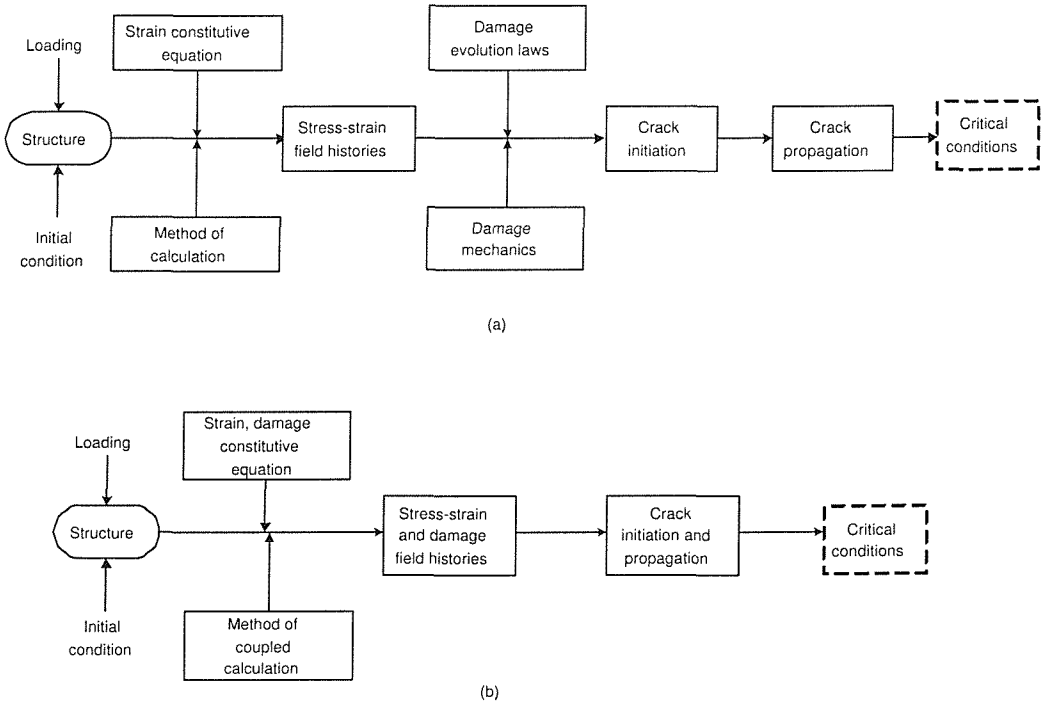

FIGURE 5.2: Differences between coupled and non-coupled rupture analysis [108, 31]. Scheme of (a) non-coupled damaged zone analysis (b) coupled strain damage calculations.

blies of stiffness matrix. The effect of reduction in stiffness was represented by an additional load vector.

There are a few studies in orthopaedic field which have used the concept of CDM. Verdonschot et al.[191] used simple CDM concepts for pre-clinical testing of cemented hip prostheses. When only the load level is varied in the damage process under cyclic loading the amount of damage becomes a function of the number of cycles n and the applied load level S. The relationship between load level S and the number of cycles to failure N is represented using S-N curve obtained by fatigue tests. They used a Miner's linear damage accumulation law, and an uncoupled analysis based on the assumption that bone cement is brittle. They extended the method to include the creep behaviour of cement in later studies and to include a tensorial representation of damage[189, 190].

Carter and Caler [28] proposed a cumulative fatigue damage model for bone fracture by adding up the damage due to the time dependent effect of creep damage (D_C) and the cycle dependent effect of fatigue damage (D_F). If the time to failure in creep (T_B) and time to failure in fatigue (N) are related to the stress level (σ) by relationships

$$T_B = A\sigma^{-B} \tag{5.12}$$

$$N = F\sigma^{-G} \tag{5.13}$$

where A, B, F and G are empirical constants determined from experiments; then it can be written that,

$$D_C + D_F = 1 \tag{5.14}$$

$$\int_0^{t_b} \frac{dt}{A\sigma(t)^{-B}} + \frac{\omega t_b}{F\triangle\sigma^{-G}} = 1 \tag{5.15}$$

where ω is the frequency of cyclic load. Taylor et al.[183] used a combined FEM and continuum damage mechanics (CDM) approach to predict the fatigue behaviour of cortical bone. The damage parameter (ω) was taken as the cycle ratio with a linear damage rule. Expressions were derived from the uniaxial test data relating the modulus and accumulated strain with the damage parameter.

5.3 Summary

Finite Element Method is a widely used numerical procedure to analyse engineering problems. The computer assisted solution process makes it popular. FE is an approximation technique, however, it can provide the stress-strain field, displacement and reaction forces at any point inside a structure of arbitrary geometrical and material

complexity. The technique allows absolute control over the problem, which is its major advantage over experimental biomechanical tests, in the present study. Development of a validated FE model for migration would be thus advantageous while conducting many parametric and comparative studies on various implant migration.

In fatigue, cancellous bone/analogue materials behaves like a continuously damaging material, showing reduction in strength, modulus reduction and accumulation of strain and they were related to the applied stress levels (as derived from experimental test results). In this respect, CDM techniques can be used to represent the damage and its progression and associated property degradation. Thus a method combining FE and CDM may be useful in representing the fatigue behaviour of the materials, and thus migration due to damage accumulation. FE can be used to determine the stress strain fields, and CDM to determine the levels of damage and associated changes in the material properties in terms of the stress levels.

Chapter 6

Finite Element Simulation of Uniaxial Fatigue Tests

In this chapter, the methods and procedures chosen for the analytical simulation of the uniaxial fatigue tests are described. All data used for the analytical model are taken from the experimental results (Chapter 4). The efficiency of the model in reproducing the fatigue behaviour is verified, along with parametric studies on factors which could possibly influence the model behaviour.

6.1 The FE Model

The uniaxial specimens could be represented as an axysymmetric model in the FE analyses. The 3-D model was replaced by a 2-D model of that plane, which on revolution about the axis of symmetry resulted in the solid model. As the model was symmetric about the horizontal mid plane of the longitudinal axis it required only one half of the 2-D axysymmetric model. The creation of the geometry and mesh descretization was carried out using the software I-DEAS. The finite element analysis and post processing used the commercial software MSC.Marc and Mentat. The cellular material was modelled as a continuum, where the mechanical behaviour at an apparent level was considered to be valid at any element level. The load was applied as a pressure on the top edge of the model, equivalent to the applied load divided by the area of cross section of the specimen head. Symmetric boundary conditions were used where necessary (Figure 6.1). The end caps of the specimen were omitted in the FE model. The presence/absence of the end caps at the far ends of the specimen was assumed to have no significant contribution to the reduced midsection of the specimen,

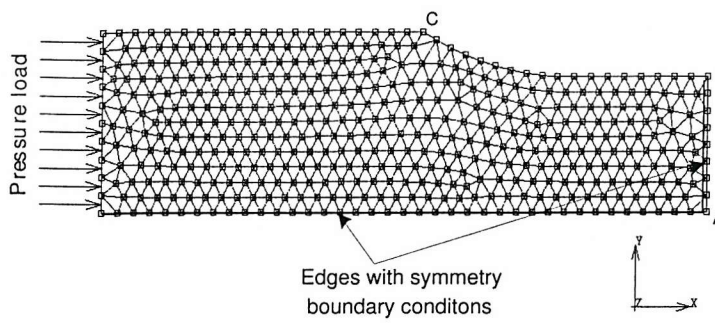

FIGURE 6.1: The FE model for the simulation of uniaxial tests. An axysymmetric quarter model of the cylindrical specimen with an applied load on top edge and appropriate symmetry boundary conditions was used as a representative model of the experimental set-up.

the region of interest in the FE simulations.

Initially, a few analyses were carried out to decide on the mesh size and to check the convergence of parameters of interest. The stress at the uniform midsection, the theoretical value of which could be calculated, was taken as the parameter for comparison. The magnitude of the von Mises stress was the same as that of the axial compressive stress, as expected for a uniaxial model. In order to compare the effect of mesh size on the results, three models, each meshed with first order triangular elements of sizes 2 mm, 1 mm and 0.5 mm respectively, and two models meshed with rectangular elements of sizes 1mm and 2mm respectively, were used. The models were analysed with the material properties of Herex®C70.55 foam. A Young's modulus of 38.9 MPa (obtained from the static tests) and Poisson's ratio of 0.3 (data from personal communication with the manufacturer) were used in the linear static analyses. A pressure load of 0.36 MPa was applied on the top edge which, theoretically, gave a stress of 0.64 MPa at the mid section. Figure 6.2 shows the von Mises stress at midsection (along edge AB shown in Figure 6.1). For all the models the differences between stress values from FE and analytical values were within 1%. The pattern of stress distribution was the same for all the meshes with only a slight deviation for the coarse (2 mm) mesh

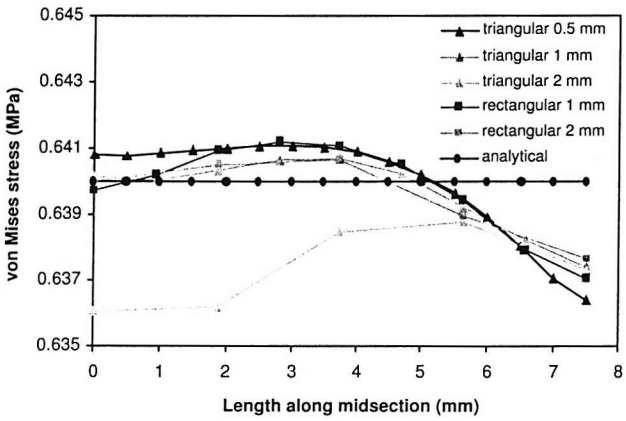

FIGURE 6.2: von Mises stress distribution along the midsection (edge AB in Figure 6.1) for five different meshes, from linear static analyses along with the analytical value of stress for the uniaxial models of Herex®C70.55 foam.

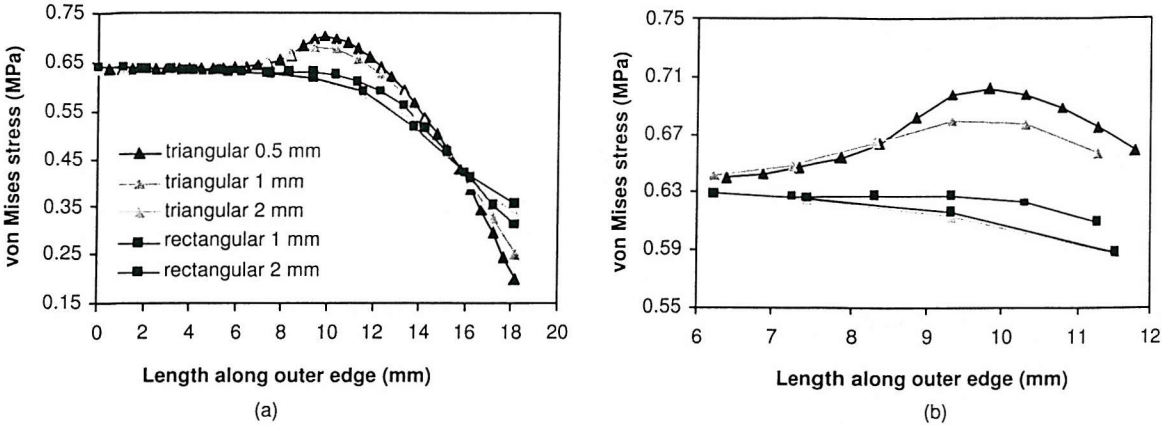

FIGURE 6.3: (a) von Mises stress distribution along the outer edge BC (in Figure 6.1) of the uniaxial model for five different meshes, from linear static analyses and (b) shows the von Mises stress distribution more focused on the region of shape transition, from the uniaxial models of Herex®C70.55 foam.

using triangular elements. The stress distribution along the outer edge of the model (along edge BC in Figure 6.1), was compared for the models (Figure 6.3). A stress concentration was expected at the region where the uniform section met the starting point of the curve, due to the sudden change in geometry. The chosen mesh size had to be sufficient to capture this. As seen from the Figure 6.3, all the models were able to predict the uniform stress at the midsection, while the finer meshes produced a smoother representations of stress distribution in the transition region. An attempt to further refine the mesh to less than 0.5 mm was not carried out, as the 0.5 mm element size gave a smooth stress distribution. For all subsequent analyses an FE model with a mesh of 0.5 mm triangular elements was used. It is notable from Figure 6.3 that the peak stress at the region of stress concentration using a linear elastic analysis, was above 0.64 MPa, the compressive strength of the Herex®C70.55 foam. The axial strain at the midsection, which was 1.4% from the linear analysis for an axial stress of 0.64 MPa, was less than the experimentally observed value of the strain (2.4%) for this stress. The FE model was thus analysed with the experimentally determined non-linear material properties assigned to it. A step wise elastic-plastic material behaviour was defined in MSC.Marc to describe the material properties and the input data was taken from the observed non-linear stress strain behaviour of the material. The von Mises yield criteria was chosen for the analysis.

Figure 6.4 shows the stress distribution along the outer edge after accounting for the non linear stress-strain behaviour of the material. The stress-concentration effect was eliminated resulting in a more uniform stress distribution over the uniform cross sectional area. The non-linear FE results were comparable to the experimental results

of Herex®C70.55 foam. Figure 6.5 compares the stress-strain pattern from the linear and non-linear static analyses with the experimental results. Using the same FE models, with the material properties of Solid Rigid PU foam, static analyses (linear and non-linear) were carried out. The observations from the analyses were similar to that of Herex® foam.

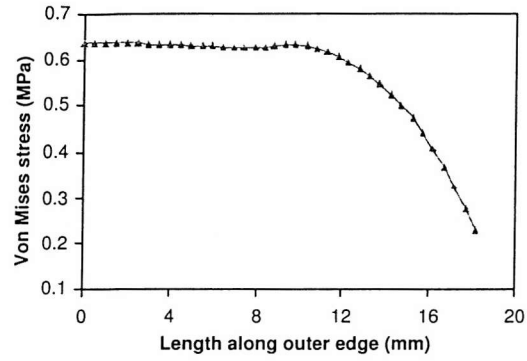

FIGURE 6.4: The Von Mises stress distribution along the outer edge from the non-linear analysis of uniaxial model of H ®C70.55 foam. The non-linear model caused material softening at the higher stress region resulting in a more uniform stress distribution.

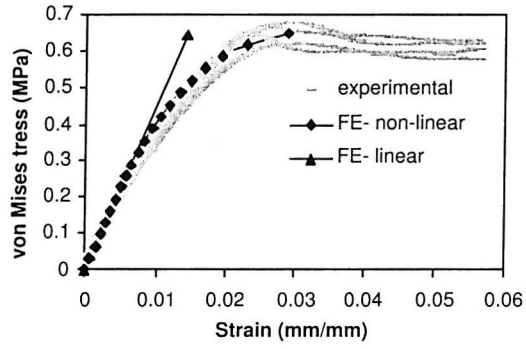

FIGURE 6.5: A comparison of the stress-strain curves from the linear and non-linear FE analyses and the experiments (five samples) for the uniaxial model of Herex®C70.55.

6.2 A Combined FE and CDM Approach to Model Fatigue Behaviour of Analogue Materials

An approach similar to that used by Taylor et al. [183] for modelling cortical bone fatigue behaviour was followed in this study. The required material properties for the undamaged state, assuming an isotropic material condition, were the elastic modulus and the Poisson's ratio. In order to define the fatigue behaviour, the parameters derived from the results of S-N experiments and the stress dependent constants representing the modulus reduction and accumulated strain as a function of the damage ω (life fraction) were used. The cellular material was considered as a continuum and the

mechanical behaviour observed at apparent level are considered to be valid at the level of an individual element.

6.2.1 The General Concept of the Algorithm Used for Fatigue Damage Simulation

A scalar damage parameter ω, a function of life fraction N/N_f, was used to represent the damage at integration point of each element. N is the number of loading cycles and N_f is the number of loading cycles to failure. A linear cumulative damage law was chosen, stating the damage as a linear function of damage parameter. A coupled analysis was performed to represent the changes in mechanical behaviour with damage accumulation. The derived relationships from experiments for modulus and accumulated strain as functions of life fraction, the chosen damage parameter, was used for this purpose. Thus, a linear damage parameter,

$$\text{damage, } \omega = f(N/N_f) = N/N_f \tag{6.1}$$

and with a linear cumulative law, damage at any number of cycles n is:

$$\omega(n) = \sum_{i=1}^{n} \triangle\omega_i \tag{6.2}$$

modulus and accumulated strain were coupled with damage:

$$\text{modulus, } E = f(\omega) \tag{6.3}$$

$$\text{accumulated strain, } \epsilon_{acc} = f(\omega) \tag{6.4}$$

The model predicted the number of cycles to failure and the variation of modulus and accumulated strain as number of cycles increased. The FE analysis of fatigue simulation was carried out iteratively. An iteration consisted of two load increments, the first increment represented the specimen with the peak compressive load and the subsequent increment represented the unloaded state. Accordingly, in the iterative procedure, odd and even increment numbers represented loaded and unloaded states of the model respectively. Figure 6.6 shows a pictorial representation of the method. In the first step, the stress-strain fields were determined in the FE analysis for the loading increment and corresponding to the stress levels the number of cycles to failure for each element, at its integration point, was calculated. The relationship between the normalized stress level σ/E_* and N_f, where σ is the applied stress and E_* is the initial

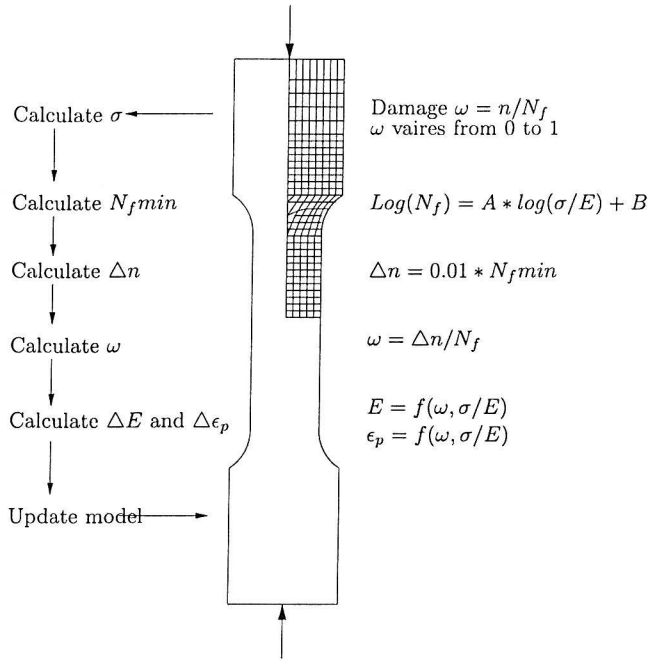

FIGURE 6.6: A pictorial representation of the algorithm for describing the combined FE and CDM method employed for the fatigue simulation of uniaxial models. The axysymmetric quarter model used for the FE analysis is shown in mesh.

Young's modulus, was used for the calculation. In the iterative analysis, each iteration stood for a chosen number of cycles and the effect of damage suffered in these cycles was updated to the model at the end of each iteration. The rules for choosing the size of the cycle step in each iteration was defined. The number of loading cycles represented in any iteration ($\triangle N$) was calculated as a percentage of the lowest number of cycles to failure ($N_f min$) and for that $\triangle N$ damage level ($\triangle \omega$) at the integration points of each element were calculated ($\triangle N/N_f$). In the first iteration the total damage (ω) was the same as $\triangle \omega$ while for the consecutive iterations the total damage was the sum of damage in the present iteration with the total damage until the previous iteration. In other words

$$\omega = \omega_{N-1} + \triangle \omega_N \tag{6.5}$$

where N is the present iteration and N-1 is the previous iteration. The modulus and accumulated strain were calculated as a function of the normalised stress level (σ/E_*) and damage (ω). The next iteration started with the FE analysis of the loading increment, with an updated stiffness matrix and the additional strain from the previous increment. The iterations continued until the model became unstable or when most of the elements at mid-uniform section were completely damaged, i.e., all elements had reached a damage value of one. In order to generalise the uniaxial stress state to an equivalent quantity, the von Mises stress was used in the calculation of normalised stress.

In the FE analysis the material was considered as linear elastic. However, the use of secant modulus, and updating the model with the accumulated strain and new mod-

ulus after each iteration, in effect, represented the total strain irrespective of whether the material was in linear or non-linear regime.

The changing fatigue parameters at the element level with number of iterations was reflected globally in the change in displacement of the model. The modulus reduction caused a change in the elastic displacement of the model, while accumulated strain caused a permanent displacement in the model on unloading. While updating the fatigue parameters to the model in each iteration, accumulated strain was updated during the unloading increment while modulus degradation was updated at the beginning of next iteration. By updating the modulus and accumulated strain separately, through two different load increments, it was possible to independently observe the effect of modulus reduction and accumulated strain on the global model behaviour. This was advantageous while analysing models with a non-uniform stress distribution, where the global displacement would not be as a direct result of fatigue changes within any given element, but rather a combination for the structure as a whole. The FE analysis of unloading increment was carried out only to include the accumulated strain in the model.

The MSC.Marc program has in built programs for the model definition and analysis; it also allows them to be replaced with user defined subroutines using appropriate control set ups. These facilities were used to incorporate the CDM algorithm into the FE analysis and for updating the modulus and accumulated strain in the models. The sequence of using the subroutines and their purpose in the present analysis, along with the algorithm, is given in Appendix A.

Once an element has failed, i.e. damage $w = 1$, suitable limiting conditions were provided in the algorithm so that there is no further modulus degradation and accumulation of strain in that element. Sufficient checks were included in the algorithm to ensure that damage was always positive and additive. Similar checks were required and appropriately defined to preserve the incremental nature of accumulated strain and decremental nature of modulus. The analyses reported are based on the material model of Solid Rigid PU foam, and the analyses results for Herex ®C70.55 foam are presented in the Appendix A. The Solid Rigid PU foam was chosen as it showed comparatively closer behaviour to cancellous bone than Herex®C70.55 foam, as discussed in Chapter 4.

6.3 Simulation of Compressive Fatigue of Solid Rigid PU Foam

An initial Young's modulus and Poisson's ratio of 68.4 and 0.3 respectively were assigned to the axysymmetric quarter model of the uniaxial specimen. The derived relationships for modulus and accumulated strain could not be extrapolated to any arbitrary normalised stress levels, with the relationships valid in a given normalised stress range. Thus, upper and lower limits were determined within which these relationships were valid and specified in the algorithm; if the normalised stress level at any particular integration point in any increment was above the upper limit, the calculations would be based on the upper level and if the normalised stress was less than the lower limit then it was assumed that there was no modulus reduction or accumulated strain for that stress level in that increment.

Finite element analysis is only an approximate method of solving a problem. The present work had used analytical relationships for fatigue parameters (derived from the experimental results) and assumed that the behaviour at an apparent level was valid at any finite element level of the material. In the case of a uniaxial model any changes and modifications in the CDM algorithm were directly reflected at the element level, while at the same time the effects at a global level (over the uniform section) were the same as that at the element level. In this respect, for the uniaxial model, the element level and global results from the FE analysis were expected to match the analytical results. Validation and fine tuning of the fatigue simulation could be carried out using the uniaxial model as it was a simple model for the simulation of bench mark tests. In many cases, it is the global effect which is of interest and can be directly measured for the validation of the model, especially in models which are expected to have a non-uniform stress distribution. For complex models it may not be possible to validate the observed global behaviour by relating the effects at element level because of the possible non-uniform distribution of stress and fatigue parameters over the elements. In the present work, it was convenient to use the uniaxial model to verify whether the chosen algorithm could be implemented to give the observed behaviour.

From a number of static analyses, an FE model was chosen (Section 6.1), which satisfactorily reproduced the geometry, boundary conditions and applied loading and gave converged results. The following series of analyses concentrated on achieving converged results in reproducing the element level variation of parameters, and comparing the global behaviour against the input models via further tuning, and validation of the FE model for fatigue simulation.

The relationships and constants which were used as input parameters in the CDM al-

TABLE 6.1: Details of the input relationships and constants in the CDM algorithm for fatigue simulation of Solid Rigid PU foam.

Relationships	Constants	Comments
Life $logN_f = C_1\ log\frac{\sigma}{E_*} + C_2$	$C_1 = -23.64$ $C_2 = -35.37$	σ is von Mises stress and E_* is 68.4, initial Young's modulus assigned to the material
Accum. strain $A\omega^B$	$A = 3.5083\frac{\sigma}{E_*} - 0.0647$ $B = 62.177\frac{\sigma}{E_*} - 0.9488$	The relationships are valid within a normalised stress range of 0.0188 and 0.030
Modulus $C\omega^D$	$C = -4511.8\frac{\sigma}{E_*} + 150.27$ $D = -10.89\frac{\sigma}{E_*} + 0.214$	The relationships are valid within a normalised stress range of 0.0198 and 0.030

gorithm are given in Table 6.1. Five load cases were simulated in the FE analyses. The load cases were chosen such that the axial compressive stress at the midsection varied from 1.4 to 1.9 MPa, similar to the range of stress levels at which the experiments were carried out. A few initial analyses were performed, to select suitable cycle step size, mesh size and Poisson's ratio for converged and consistent results. A common node on the midsection (location B in Figure 6.1, further referred to as node B in this Chapter) was chosen for comparison of results. In all the anlyses, for higher load cases (for axial stresses of 1.8 MPa and 1.9 MPa) the failure occurred prematurely, within 10 cycles, for the default model option. This made it difficult to compare the effect of the model variables. The issue of high stress, low cycle test simulations are dealt with in a later section, leaving the discussion of results in the following sections excluding data from low cycle simulations. Details of the default model are given in Table 6.2. The results from the FE simulations were compared with analytical results. The analytical value of N_f, for each load case, was determined by substituting the respective axial stress into the relationship for N_f (see Table 6.1). For each load case, for cycles from $N = 1$ to $N = N_f$, the axial stress and life fraction corresponding to each cycle (N/N_f) were substituted into the relationships (given in Table 6.1) to calculate the analytical values of accumulated strain and modulus degradation. The calculations were done using an excel spreadsheet.

TABLE 6.2: The default FE model details for uniaxial fatigue simulation of Solid Rigid PU foam.

The default FE model details	
Model	Axysymmetric quarter model of the uniaxial specimen
Type of elements	Linear, triangular elements
Element size	0.5 mm
Number of elements	3121
Initial Young's modulus and Poisson ratio	68.4 MPa and 0.3
Number of load increments in each iteration	2, peak load applied at compressive load direction and opposite
Type of FE analysis	Linear static analysis
Chosen load cases	Five load cases such that axial compressive stress at the midsection over these five load cases varied from 1.4 to 1.9 MPa, analytically
Stress component for normalised stress calculation	von Mises stress
Termination point of revising fatigue parameters at integration points	total damage till that increment, $\omega = \sum \triangle\omega_i = \sum \frac{n_i}{N_{f\,i}} = 1$

6.3.1 Case 1: Effect of Chosen $\triangle N$

Since each iteration represents a number of load cycles ($\triangle N$), it was necessary to ensure that the non-linear variation of modulus and accumulated strain with damage, ω, was reproduced smoothly in the FE model between each iteration. In this respect, $\triangle N$, as a chosen percentage of number of cycles to failure was also a variable whose effect on the model behaviour needed to be checked. For a particular load case, the models were analysed for four cases of $\triangle N$ as 10, 5, 2 and 0.5% of $N_{f_{min}}$, while all other factors (default model options) were kept constant during these analyses. Figure 6.7 shows the variation of modulus reduction and accumulation of strain from these analyses as a function of number of cycles, at node B. The use of factors 5, 2 and 0.5% gave converged values for number of cycles to failure (the total number of cycles at which $\omega = 1$ at node B), modulus reduction and accumulated strain, for all but the low cycle tests (or tests at higher stress levels). Since factors of 2 and 0.5% gave the required smooth transition of both modulus reduction and the accumulation of strain over cycle steps, in further analyses these two factors were used to determine the cycle steps for these load cases.

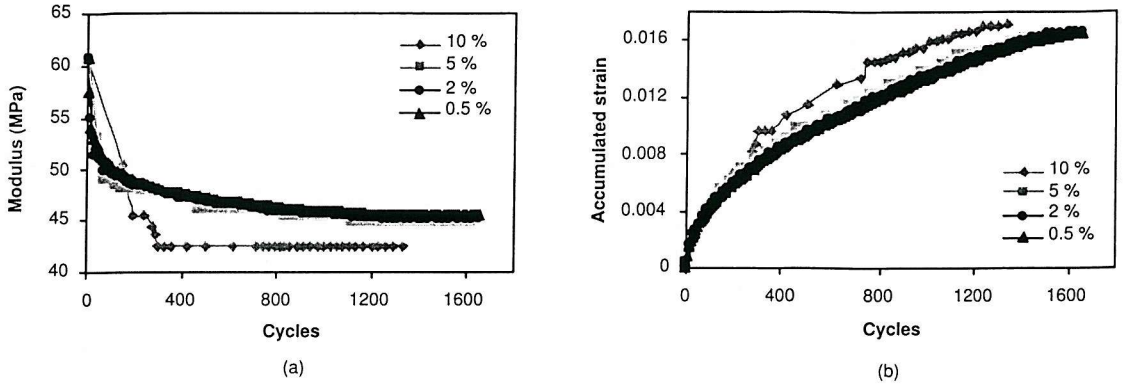

FIGURE 6.7: Variation of (a) modulus and (b) accumulated strain with number of cycles for four chosen values of cycle steps ($\triangle N$) in the iterative FE simulation of uniaxial fatigue of Solid Rigid PU foam. The axial stress at midsection was 1.6 MPa.

6.3.2 Case 2: Effect of Mesh Size

The effect of mesh density was evaluated using 0.5 and 1 mm element edge lengths. The two models were analysed for fatigue behaviour for an axial stress of 1.6 MPa. The meshes gave converged results for number of cycles to failure, modulus variation and accumulated strain. For example, Figure 6.8 compares the accumulated strain variation at node B.

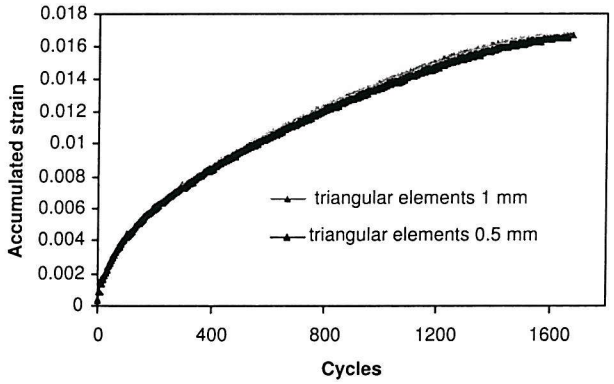

FIGURE 6.8: Comparison of effect of mesh density on uniaxial fatigue simulation of Solid Rigid PU foam. The axial stress at midsection was 1.6 MPa. The results showed that the chosen mesh densities were good enough to produce consistent results in fatigue simulation.

6.3.3 Case 3: Effect of Poisson's Ratio

The effect of Poisson's ratio was verified using two load cases for Poisson's ratios of 0.25, 0.3 and 0.35. The range of chosen Poisson ratio was the range in which the material Poisson's ratio was considered to fall (0.25 to 0.35). Figure 6.9 shows plots of accumulated strain against number of cycles for an applied axial stress of 1.6 MPa at midsection. It shows that over the Poisson's ratio range there was no significant effect on the accumulated strain, modulus reduction and cycles to failure.

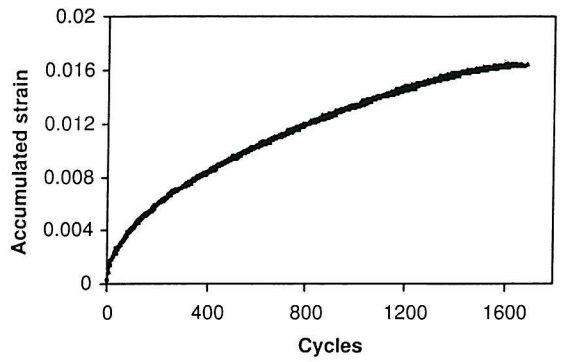

FIGURE 6.9: Variation in accumulated strain with number of cycles for three cases of Poisson's ratios 0.25, 0.3 and 0.35 in the uniaxial fatigue simulation of Solid Rigid PU foam. The axial stress at midsection was 1.6 MPa.

6.3.4 Case 4: Axial stress VS von Mises Stress

In order to generalise the fatigue simulation to more complex stress states, the von Mises stress was chosen for the normalised stress calculation in the default model. It was checked whether the use of axial stress instead of von Mises stress would affect the outcome. The results were similar with both stress components, which is expected for a uniaxial stress state. However, in the multiaxial stress state, the axial stress and the von-Mises stress could be different; then the choice of the stress component has to be verified again, against the experimental results. Figure 6.10 shows the comparison of the modulus variation with cycles for the two stress components, at node B. The patterns were similar, while the difference in variables, number of cycles to failure, modulus and accumulated strain, between the two analyses was less than 10%.

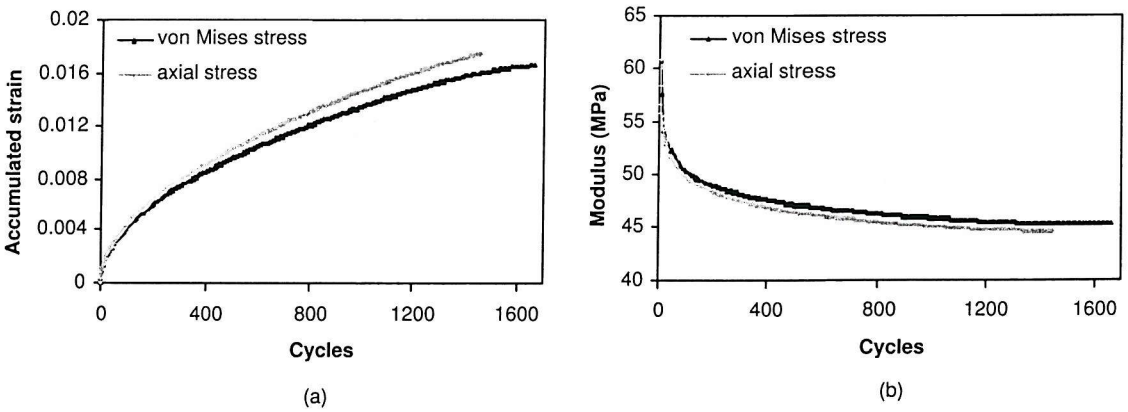

FIGURE 6.10: A comparison of modulus reduction with number of cycles for cases of stress component as von Mises stress and axial stress in the algorithm, from the uniaxial fatigue simulation of Solid Rigid PU foam. The axial stress at midsection was 1.6 MPa.

6.3.5 Validation of the FE model of Fatigue Simulation

The analyses reported in the above four cases, confirmed that the default model had a suitable mesh density, Poisson's ratio, chosen stress component for analysis and that a cycle step factor of either 0.5 or 2% was appropriate. This section describes the validation of the model. For the local comparison of the results, node B on the midsection was again chosen. For the global comparison of results, over the uniform section, the displacement at a node on the outer surface within the gaugelength (at a distance of 5.89 mm from the midsection) was used. The chosen node location was the closest in position to the gaugelength used in experiments (at 6.25 mm from the midsection) for displacement measurement. The displacement variable was used as a basis for the calculation of other parameters (for example strain). Using the default model and with a cycle step factor of 0.5% analyses were carried out for five load cases. For low cycle fatigue (for failure within 100 cycles), as mentioned earlier, the FE models were not successful. The remaining load cases are discussed here.

Figure 6.11 shows the gradual accumulation of damage in the FE simulation, for a particular load case (1.4 MPa), at various stages of the simulated fatigue test. The

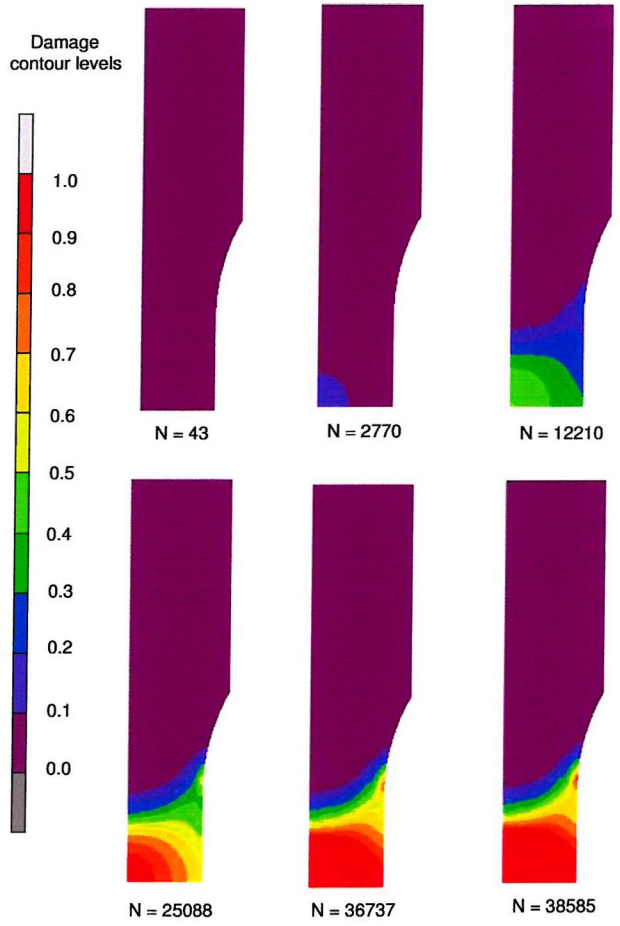

FIGURE 6.11: Patterns of gradual accumulation of damage at various stages of the uniaxial fatigue simulation of Solid Rigid PU foam at an axial stress of 1.4 MPa.

first location of damage initiation was the transition region of the geometry (which showed stress concentration). However, in the next few cycles the resultant reduction in modulus transferred the the load to the uniform midsection, where the damage accumulated gradually until failure of the whole midsection. As mentioned earlier (in Section 6.1), the effect of end caps was neglected in the model. It is possible to have an influence for the end cap constraints at the transition region. However, as observed in the FE simulation, after the first few cycles at which damage occurs at the transition region, the region of high stress and damage accumulation was always the midsection, where the end cap effect could not be influential. The damage, which initiated at the midsection, gradually extended to the whole uniform section. However, a satisfactory relationship between damage accumulation and mechanical behaviour, at element and global level, had to be verified. The number of cycles to failure at a global level, similar to the definition of failure in the experiments, was defined as the point at which the pattern of maximum displacement/ strain (axial displacement/strain at peak load) changed from the secondary to tertiary region. There was no tertiary region in the strain patterns, rather the strain pattern changed to a steady state of constant strain. This change occurred at the same time at which the local failure at the mid section (at node B) occurred.

The variation of maximum strain (global) and damage with number of cycles are shown in Figure 6.12. The location used for measuring the global axial displacement is marked on the model. At the time of local failure (at cycle 1655), the mid section had failed completely. The observation supported the fact that, the mid-section, with

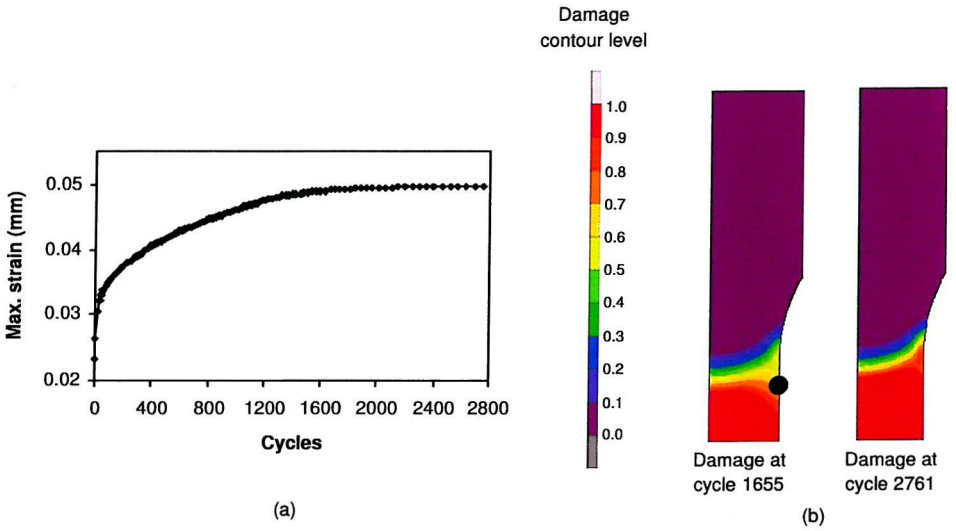

FIGURE 6.12: (a) Variation of global maximum strain with number of cycles (b) Damage distribution over the specimen at cycles 1655 and 2761, from the uniaxial fatigue simulation of Solid Rigid PU foam. The axial stress at midsection is 1.6 MPa. The location for global displacement measurement is noted using a dot.

a uniform stress, failed locally and globally together and justified the selection of the gaugelength as a region for extracting stress-strain data. Unlike the experimental data no tertiary region of failure was observed in the simulations. This is because the input model was derived assuming that failure occurred at the start of the tertiary region. In addition, in the default modelling option both modulus reduction and accumulated strain were terminated once damage had reached a value of 1.

A comparison of the local, global and analytical values of modulus and accumulated strain, for an applied axial stress of 1.6 MPa, is shown in Figure 6.13. The modulus and accumulated strain differed slightly from the analytical value (the analytical value being higher), and this difference increased towards the end of life. At the time of the analytically predicted failure, the difference for the local variables was within 10% for all the load cases except the low cycle tests. In this respect, the FE model was capable of reproducing the experimentally observed material behaviour. Globally, in all the load cases, it was observed that the maximum displacement/strain and the accumulated strain followed the same trend as the local variables and the variation of displacement/strain was almost constant, from the time of local failure onwards. The predicted global strain and modulus values were slightly less than the local and analytical values. A comparison of the number of cycles to failure from the FE simulation with analytical values is given in Table 6.3. The FE models overestimated the number of cycles to failure for high cycle tests; the issue of low cycle test is dealt with in a later section.

It has to be remembered that the analytical predictions were based on an assumption of constant value of peak axial stress over the uniform section throughout the simulation which may not be strictly true. The changing modulus and accumulated strain with damage progression can result in variations in the axial stress distributions (the

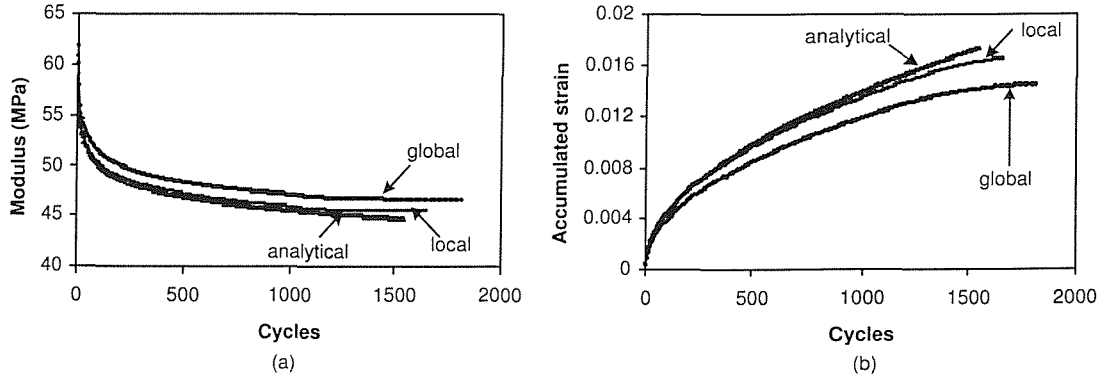

FIGURE 6.13: A comparison of the local, global and analytical values of (a) modulus reduction and (b) accumulated strain with number of cycles from the uniaxial fatigue simulation of Solid Rigid PU foam. The axial stress at midsection was 1.6MPa.

assumed constant value) thus causing the observed variability of results.
A comparison of the axial stress at the local node, with the theoretical constant value (1.6 MPa) is shown in Figure 6.14. Towards the end of the life, there was a gradual decrease in the stress experienced at the mid section. The difference between the accumulated strain and modulus reduction when compared with the analytical values, towards the end of the life, could be attributed to the observed variation in the stress. In the experiments it was not possible to measure the slight variations in the axial stress, as the damage accumulated.

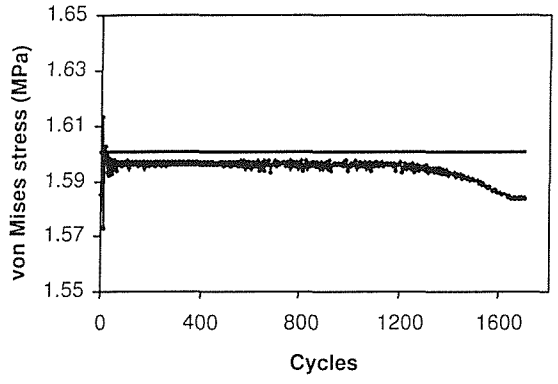

FIGURE 6.14: Variation of von Mises stress at local node B, for an applied load which was assumed to cause a constant axial stress of 1.6 MPa. The straight line was the assumed axial stress from the analytical calculation.

TABLE 6.3: Comparison of number of cycles to failure from analytical and FE simulation results, for five load cases, using the default model.

Load case	Stress (MPa) (analytical)	N_f (analytical)	N_f from FE simulation	
			local	% of over/under estimation
1	1.9	26	3	-88
2	1.8	95	7	-92
3	1.6	1532	1655	+8
4	1.5	7046	8657	+22
5	1.4	36000	40945	+14

6.3.6 Effect of Modulus Reduction Factor

In the default model, the status of an element was left unchanged in further iterations, once that element had theoretically failed. It was verified whether a change in the element status after it had failed (damage, ω=1), had any influence on bridging the slight difference between the local and global behaviour. A total loss of structural integrity

could be attributed to an element in tensile failure (as the material failed by a total fracture) by either removal of that element or by reducing the elemental modulus to a very low value in such a way as to remove the effect of that material volume and redistribute the load among other elements. It should be noted that in compression, there was no total loss of structural integrity of the material as there was still a smaller volume of material that could take load. A few analyses were performed to determine the influence of modulus reduction factor which could suitably represent the reduced volume of the material after complete damage had occurred.

The modulus reduction factor was defined as the factor by which the modulus at the next increment after failure (E_{N_f+1}) was reduced. Two values of $\triangle N$ (2 and 0.5 %) were again included in these analyses to check whether the cycle step, coupled with modulus reduction factor had any influence on the results. The initial analyses showed that the modulus reduction factor had an effect on the parameters of interest in the fatigue simulation. The cycle step factor was not influential. The reduction of modulus to a small value resulted in, at the later stage of life, a faster rate of damage progression and a sudden increase in the maximum displacement and underestimated the life. Figure 6.15 shows the variation of maximum strain (global), with cycles, for the default model and the model with large modulus reduction factor. Analysis 1 was the default model, and in Analysis 2, E_{N_f+1} was reduced by 90% of E_{N_f}. It is clear from these plots that, the modulus reduction factor affected the model behaviour. At

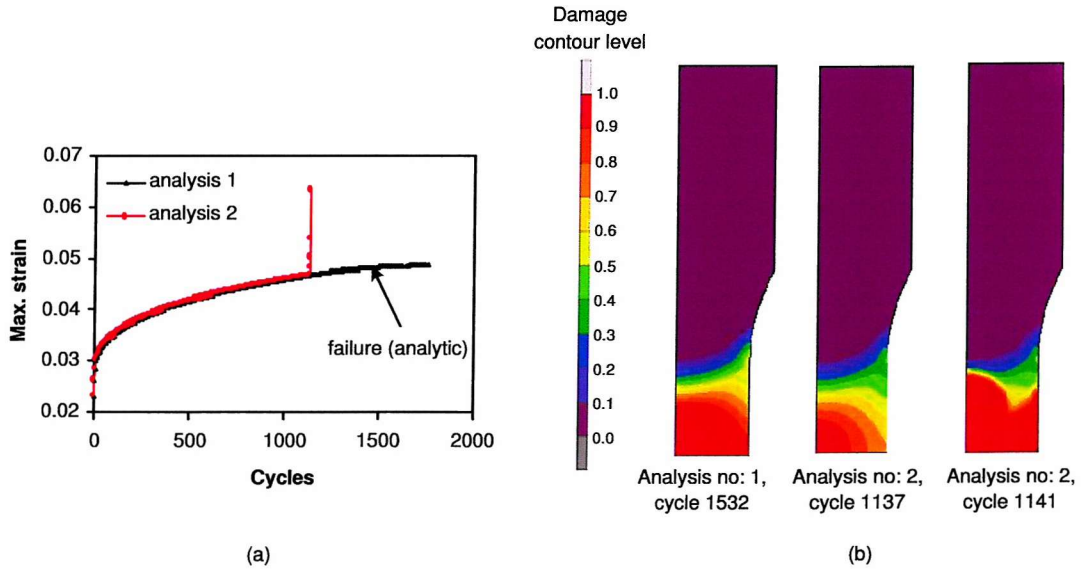

FIGURE 6.15: (a) variation of global maximum strain with the number of cycles from **Analysis no: 1& 2** (b) The damage contour levels in the model at cycles 1532 for Analysis no:1 and at cycles 1137 and 1141 for Analysis no:2. Applied axial stress is 1.6 MPa.

TABLE 6.4: Details of various modulus reduction factors used in the fatigue simulations of Solid Rigid PU foam.

Parameter	Analysis number						
	1	2	3	4	5	6	7
E_{N_f+1}	E_{N_f} (E_{N_f})	$90\%E_{N_f}$ $E_{N_f}/10$	$50\%E_{N_f}$ $E_{N_f}/2$	$33\%E_{N_f}$ ($E_{N_f}/1.5$)	$17\%E_{N_f}$ ($E_{N_f}/1.2$)	$9\%E_{N_f}$ ($E_{N_f}/1.1$)	$5\%E_{N_f}$ ($E_{N_f}/1.05$)

TABLE 6.5: Comparison of number of cycles to failure from analytical and FE simulation results, for various modulus reduction factors used in the analyses.

Load case	Stress (MPa) (analytical)	N_f (analytical)	N_f from FE simulation for analysis number						
			1	2	3	4	5	6	7
3	1.6	1532	1655	1143	1212	1298	1445	1511	1586
4	1.5	7046	8657	5696	6388	7024	7421	7815	8172
5	1.4	36000	40564	26073	29061	31364	34178	37006	38585

approximately 70-75% of the total life a few elements in the midsection had already failed (at cycle 1137). In Analysis 1, damage accumulation gradually progressed further. In the case of Analysis 2, the reduction of modulus of the elements which had failed, drove the damage accumulation faster causing failure of the whole midsection within the next 10 cycles.

Further analyses were performed where the modulus was reduced by a range of factors (Table 6.4). A comparison of number of cycles to failure from analytical and FE simulations (at node B) is given in Table 6.5. For the number of cycles to failure, analysis numbers 5&6 gave a closer value (within 10%) to the analytical results. The variation of pattern of modulus reduction and accumulated strain locally, for various modulus reduction factors is shown in Figure 6.16. The pattern and magnitude of modulus degradation and accumulated strain, for all the modulus reduction factors were the same for up to 70-75% of the cycles to failure (from the analytical calculation). Following this the steepness of the tertiary curve, in modulus and accumulated strain were directly related to the modulus reduction factor. This effect was consistent for all the load cases analysed. It is noticeable that the modulus reduction factor also affected the local values, with a rapid increase in the reduction of modulus and accumulated strain towards the end of the failure.

The global level variation reflected the local variations in a similar fashion. The modulus variation, calculated from the global displacement for a particular load (axial stress 1.6 MPa), for various modulus reduction factors, is shown in Figure 6.17. A similar

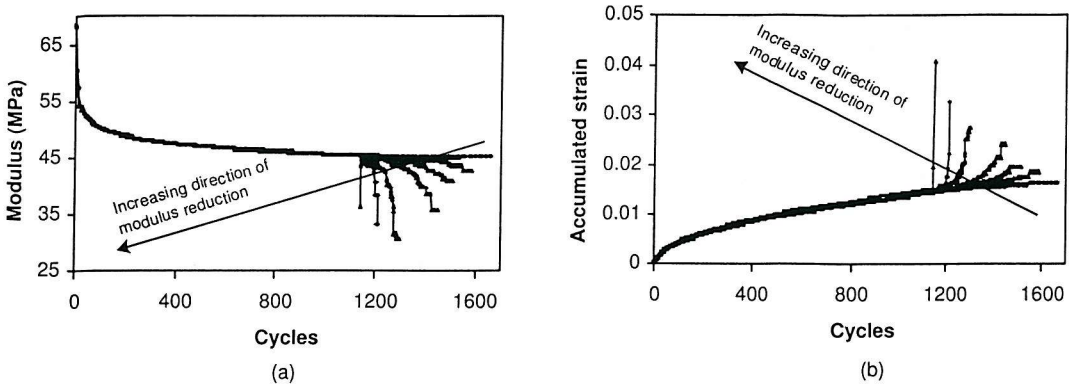

FIGURE 6.16: Effect of various modulus reduction factors on pattern of (a) modulus reduction and (b) accumulated strain at local node B from uniaxial fatigue simulations of Solid Rigid PU foam. The applied axial stress at midsection was 1.6 MPa.

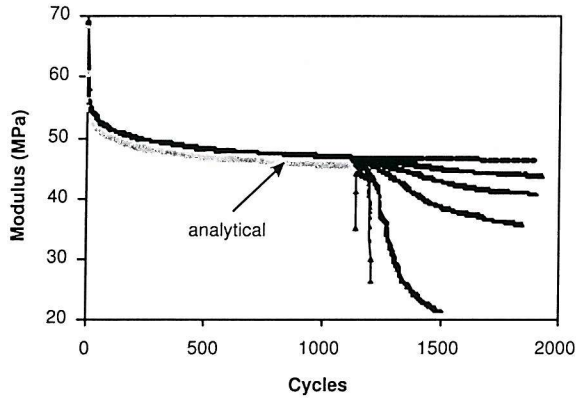

FIGURE 6.17: Variation of modulus at global level for various modulus reduction factors from the uniaxial fatigue simulations of Solid Rigid PU foam. The axial stress was 1.6 MPa.

pattern of variation was observed for accumulated strain. The pattern and magnitude of modulus and accumulated strain, for all the modulus reduction factors were the same, for up to 70-75% of the cycles to failure, similar to the observation at local node B. However small the reduction in the modulus, it still caused a change in the pattern, once a few elements at midsection had reached failure. A comparison of the stress distribution at local node B for the default model and model with modulus reduced to 10% of E_{N_f} (analysis 1 and 2 in Table 6.4) shows that when there was a sudden change in modulus and accumulated strain pattern there was a sudden catastrophic rise in the stress distribution at local node B (Figure 6.18).

From the default model (see Figure 6.11) it could be seen that at approximately 3/4 of the expected life, the elements at the inner midregion had nearly reached failure. The effect off any change in modulus would be the redistribution of load. Thus, a reduction in modulus of these elements when damage reached a unit value resulted in a shift of load to the outer stiffer elements. As the change was sudden, rather than gradual, it

could have caused the large stress rise in the elements. A reduction in cycle step could not alter this, because at chosen factor (0.5%) only one cycle was being simulated at each iteration in the latter stages. Again, the default model was the closest in the various case studies carried out, to the observed mechanical behaviour of the model.

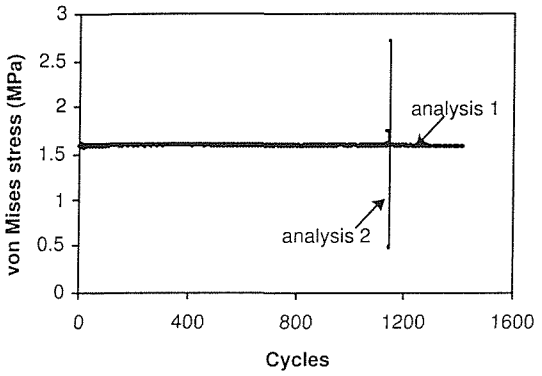

FIGURE 6.18: Variation of von Mises stress at local node B from Analysis no: 1 &2, for an applied load which was assumed to cause a constant axial stress of 1.6 MPa.

6.3.7 Fatigue Simulation with Non-Linear FE analysis

The analyses described in previous sections were unable to simulate low cycle tests as they underestimated the life by a significant margin. This could be due to the fact that the damage accumulation and associated changes in the fatigue parameters at the element level occurred too quickly over the initial cycles. This resulted in a sudden rather than gradual localised stress rise/damage accumulation and sudden failure. The choice of a smaller cycle step was not valid, as at the chosen cycle step of only one cycle was simulated at each iteration.

A linear elastic analysis was used for the default model, based on the assumption that the accumulated strain and modulus reduction, combined with the elastic behaviour, could represent the non-linear stress-strain behaviour. In the case of low cycle tests, it was observed that, with sudden large changes in the fatigue parameters at element level the linear assumption resulted in unrealistically high stresses and caused rapid failure. Therefore in order to capture the non-linear material behaviour of high stresses, non-linear stress-strain behaviour was assigned to the material model in the FE analysis. These models were able to simulate the low cycle tests close to the input models, although the convergence tolerance had to be reduced to carry out the analysis. Convergence tolerance is the limit specified for the ratio of the maximum residual force compared to the maximum reaction force, to achieve a converged solution in the FE analysis. The tolerance had to be loosened as, with the large residual forces created due to the plastic strain, the residual/reaction force converged to a higher value than the specified tolerance. The effect of cyclic increments (0.5% and 2%) was also

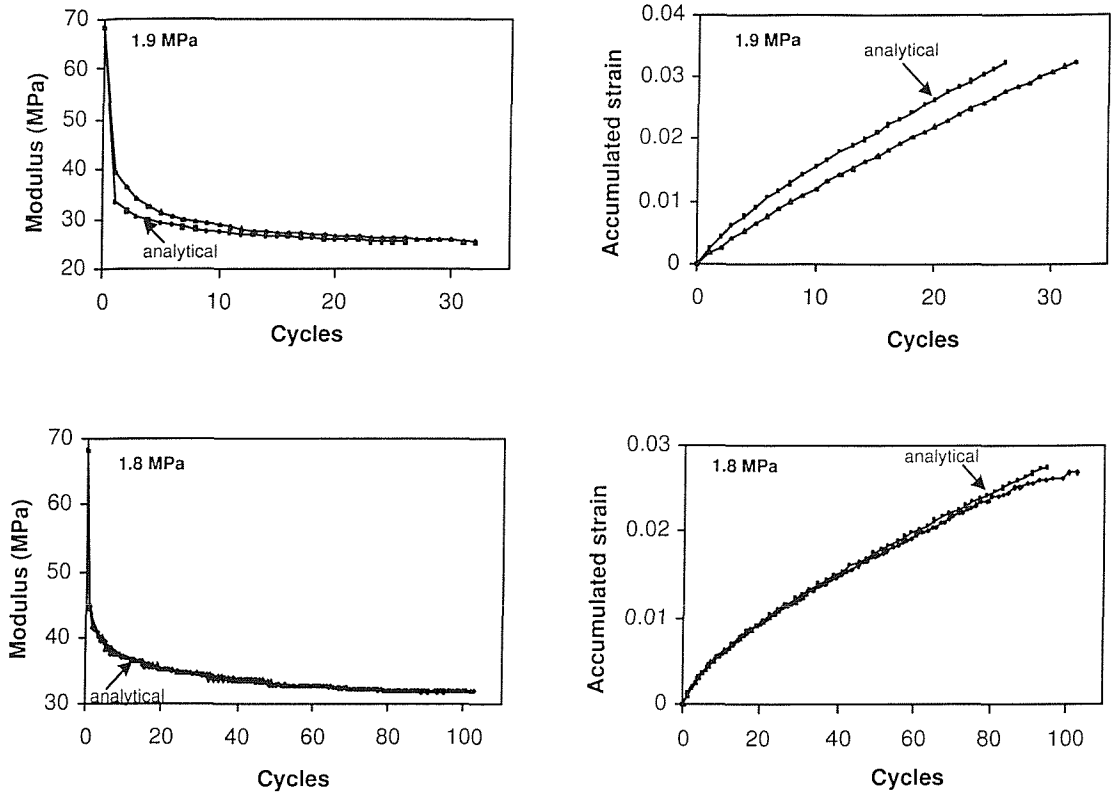

FIGURE 6.19: Comparison of pattern of modulus and accumulated strain from the simulations of low-cycle fatigue of Solid Rigid PU foam with non-linear material properties, with analytical values. The axial stresses were 1.9 MPa and 1.8 MPa.

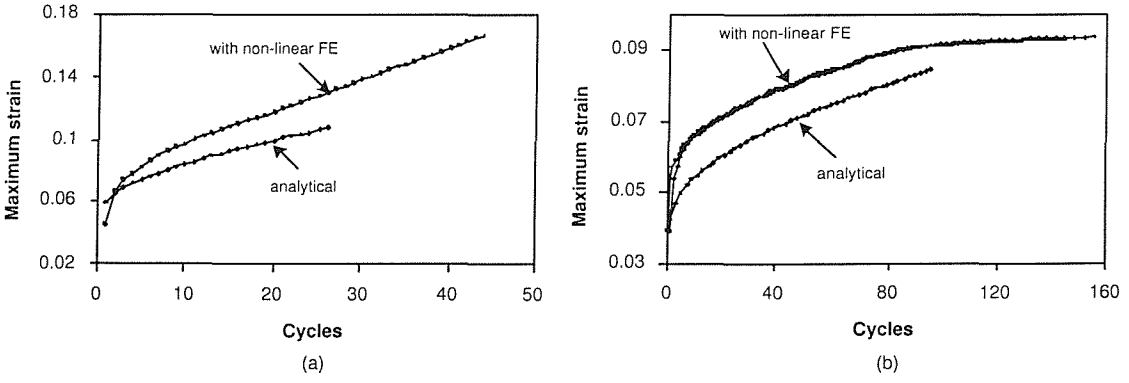

FIGURE 6.20: Comparison of the global maximum strain from simulations with non-linear material properties for low-cycle uniaxial fatigue simulation of Solid Rigid PU foam, for an applied axial stress of (a) 1.9 MPa and (b) 1.8 MPa.

examined and showed no effect.

The pattern and magnitudes of modulus reduction and accumulated strain, at the local node were similar to the analytical results (Figure 6.19). The global maximum strains for low cycle tests were higher than the analytical values (Figure 6.20). At

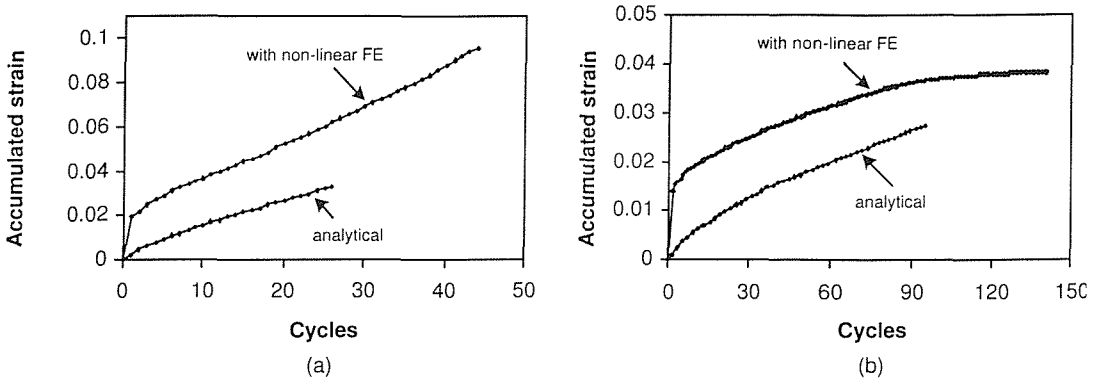

FIGURE 6.21: Comparison of the global accumulated strain variation from the results of simulation with non-linear material properties with analytical representation, for an applied axial stress of (a) 1.9 MPa and (b) 1.8 MPa.

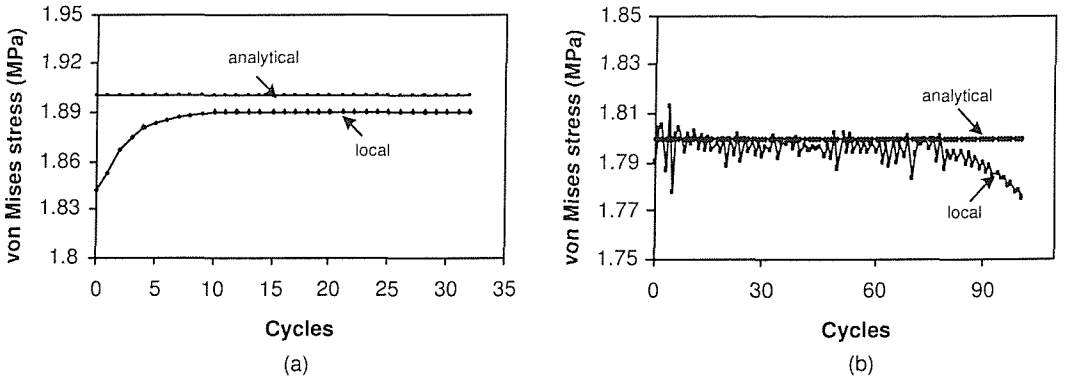

FIGURE 6.22: Comparison of the von Mises stress variation at local node B from the simulations with non-linear material properties for low-cycle uniaxial fatigue of Solid Rigid PU foam with analytical values, for an applied axial stress of (a)1.9 MPa and (b) 1.8 MPa.

1.9 MPa, the global strain continued to increase even after local failure (the end point of analytical curve). At 1.8 MPa, the global strain pattern became a constant steady state after the local failure. The pattern of accumulated strain also followed a similar pattern, and was higher in magnitude than the analytical values, in contrast to the default model. Figure 6.21 shows the variation of accumulated strain for the higher stress load cases. The variation of axial stress at local node B, for these two load cases were compared with the analytical values (Figure 6.22). At 1.8 MPa, the pattern of variation of stress was consistent with the default model results for other load cases. For the highest load case (1.9 MPa) the stress variation pattern was unique; there was an increasing stress in the early stage which then reduced to a constant value.

For the remaining load cases (high cycle/low stress) the results of non-linear FE analysis were similar to the default models, in terms of number of cycles to failure, pattern of modulus reduction and accumulated strain. However, the pattern of global varia-

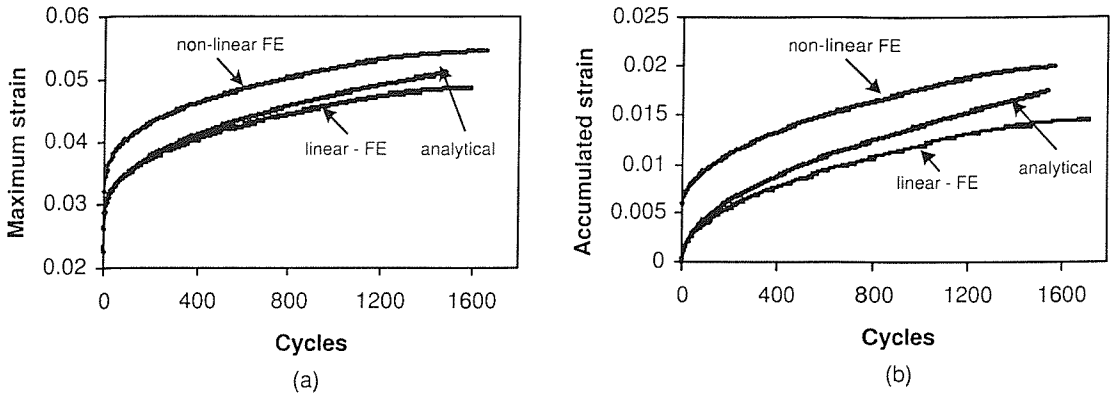

FIGURE 6.23: Comparison of the globa maximum strain and accumulated strain from the simulations with linear and non-linear material properties in the uniaxial fatigue of Solid Rigid PU foam with analytical values, for an applied axial stress of 1.6 MPa (a) variation of maximum strain (b) variation of accumulated strain.

tion of the accumulated strain and maximum strain differed from the default model results. A comparison of the global variation of maximum strain and accumulated strain from the linear and non-linear FE analyses is given in Figure 6.23. The linear and non-linear strains were observed to differ by set permanent strain from the initial cycles onwards. The stress variation from the simulations with linear and non-linear FE analysis, for load case 3 (applied stress 1.6 MPa) is shown in Figure 6.24. The stress patterns, in general, were similar for linear and non-linear analysis. However, during the initial cycles there was a larger scatter in stress in the linear analysis which then evened out to a constant value within a few cycles on further softening of the material through accumulated strain and modulus reduction. In the case of non-linear models, the stress rise was more controlled giving a comparatively smoother variation of stress. The permanent displacement/strain accumulated through the non-linear deformation in the initial cycles caused the offset in the strain patterns. By accounting for this offset in the first cycle a pattern and magnitude of strain exactly similar to that of linear analysis resulted.

The observations from the non-linear FE analyses highlight the importance of assuring a gradual variation in fatigue parameters for a smooth transition of stress over elements and over cycles.

6.4 Discussion

In general, the experimental characterisation of fatigue behaviour of cortical bone[36, 25, 26, 27, 139, 207, 208] has received the most attention and in comparison there is little published data for cancellous bone[13, 63, 124]. As a result of this, there have

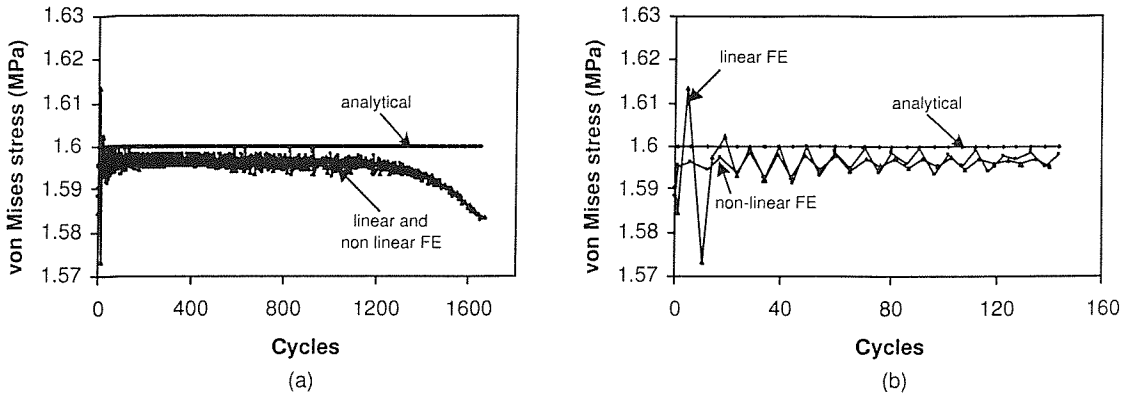

FIGURE 6.24: Comparison of the von Mises stress at local node B from the linear and non-linear FE analyses, for an applied axial stress of 1.6 MPa (a) variation with number of cycles (b) variation at the initial cycles.

been various attempts to develop numerical models to describe the fatigue behaviour of cortical bone[59, 139, 183]. Similar studies on cancellous bone are limited and confined to a micromechanical approach by performing the simulation at the trabecular level, by assigning the cortical bone material properties to the trabeculae. However, at present there are no numerical/analytical techniques which have attempted to simulate the fatigue/creep behaviour of cancellous bone at a continuum level. For the present work, a continuum level model is required to simulate migration based on the global effect of modulus reduction and accumulation of strain under cyclic loading of cancellous bone/analogue material. Microlevel modelling of the implant bone construct could be computationally expensive and technically tedious. In this respect it would be worth attempting to develop techniques for modelling fatigue behaviour of cancellous bone at continuum level, and for their application to simulate cases of bone fracture and migration.

This chapter has dealt with the use of a numerical approach to simulate the fatigue of analogue foam materials (using FE and CDM concepts). The approximations of geometry and its mesh descretization and boundary conditions for the FE model were validated based on convergence studies to get a uniform stress (theoretical value) at the midsection, from static elastic analysis. The chosen model based on this convergence study was able to reproduce the non-linear stress-strain behaviour of the material. The model was satisfactory for fatigue analysis, for convergence studies carried out for the choice of cycle steps, Poisson's ratio and stress component. The default model was defined with the given input parameters as obtained from the analytical model of experimental results. While the models were able to reproduce the analytical models, at very high stress levels there was premature failure while using a linear elastic analysis. The models reproduced the analytical model satisfactorily, at local and global level, for high cycle tests.

In the fatigue simulations it was assumed that the the non-linear strain could be quantitatively represented, in effect, by the inclusion of the accumulated strain and degradation of secant modulus. The assumption was found valid in most of the analysed cases, with the models successful in reproducing the global strains (both permanent strain and maximum strain) comparable to the analytical values. However, a gradual accumulation of the damage and coupled properties had to be assured to simulate the non-linear nature through a linear analysis. Problems were faced in situations where sudden and large changes occurred in an individual element or small group of elements (like the low cycle tests and modulus reduction after failure). With its path independent nature, a linear material model predicted a very high stress, for a given deformation. Figure 6.25 depicts a schematic of the difference between a linear and non-linear stress strain behaviour of a material. For a given strain, e1, the linear and non-linear material model results in stresses S1 and S2 (S2 higher than S1). The S-N relation thus underestimates the life for the linear model, and for a given cycle step in that iteration, it overpredicts the damage suffered by that element, which in turn results in larger changes in the material behaviour coupled with damage. When the predicted stresses are unrealistically high in the initial cycles, this could produce an immediate failure or a significant accumulation of damage. In reality, the material would have relaxed that stress through non-linear deformation. The derived relationships used for the fatigue simulations were extrapolated to the possible higher stress levels for the specimens, based on the experimental stress ranges (Chapter 4). It could be possible that the material had a different behaviour at these higher stress levels, from that described by the extrapolated relationships.

The assignment of a non-linear stress-strain behaviour to the material gave a good correlation with the analytical results in terms of the predicted life and the modulus degradation while it produced a set permanent displacement in the model due to plastic deformation, in addition to the permanent strain accounted through the CDM method. The advantage of the non-linear model was in its ability to control the initial

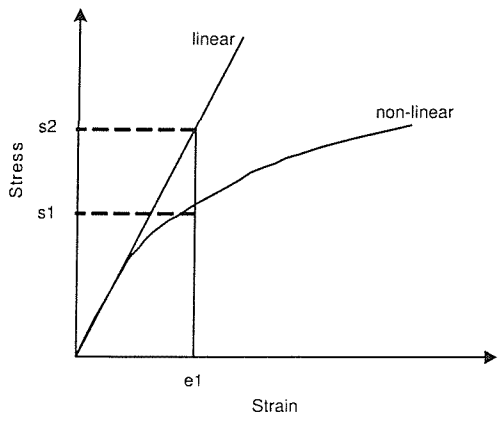

FIGURE 6.25: A schematic of linear and non-linear stress-strain behaviour.

scatter in stress patterns due to the sudden changes in the mechanical behaviour; this controlled the localisation of damage growth. The fatigue simulation with non-linear FE analyses was carried out by assigning the non-linear material properties obtained from the static tests. In the fatigue experiments, it was the maximum and minimum displacement which were recorded at each cycle corresponding to the loading-unloading cycle. These data were sufficient to provide the amount of accumulated strain and secant modulus at each cycle or cycle intervals, and no other data was recorded and no information was available on the variation of the non-linear path of stress-strain behaviour with cyclic loads. In the present frame work of the algorithm, the addition of non-linear material properties resulted in an additional set displacement in the material. In this respect, a detailed attempt to represent the non-linear material model in the algorithm was not carried out.

Damage accumulation in cancellous bone, along with modulus reduction and accumulation (as observed from *in vitro* experimental studies) could be influential in orthopaedic situations like bone fracture and implant migration[181]. There are models (only two to the best of author's knowledge) which had attempted to simulate modulus reduction/creep and life of cancellous bone, based on assumed micromechanisms of failure at trabecular level[62, 184]. Both methods used, idealised 2-dimensional (honeycomb) structures and mechanical behaviour of trabecular material was considered similar to that of cortical bone. These methods and their associated drawbacks were discussed in Chapter 2, Section 2.3.3. Guo et al.[62] modelled each trabeculae as linear elastic beam with cortical bone properties. They conducted two studies with the model; a fatigue simulation and creep simulation. In the fatigue simulation microcracks were randomly distributed in the trabeculae and were allowed to grow based on the Paris law. Life was calculated for various stress levels, where life was defined as the number of cycles at which there was a 10% reduction in apparent modulus. In the second study, trabeculae were allowed to only creep (creep under mean fatigue stress level), with the assigned creep behaviour of cortical bone, and the life was determined as number of cycles for an apparent 5% increase in strain. The S-N curves were compared with the experimental data, and they observed that the S-N curves from creep and fatigue analysis were similar to the low cycle and high cycle S-N curves respectively. Taylor et al.[184] used a similar 2-D model, however, the trabeculae was considered to fail by progressive strength and modulus reduction and accumulation of strain in a similar fashion as that of cortical bone. The fatigue simulations of trabeculae were carried out for three cases (i) only damage accumulation (ii) damage accumulation with modulus reduction and (iii) damage with modulus reduction and accumulation of strain. Inclusion of modulus reduction increased the fatigue life, while addition of accumulated strain increased the fatigue life even further. The inclusion of material property

degradation resulted in the redistribution of peak stresses, delaying the fatigue life of individual trabeculae. They stressed the need for including the accumulated strain in the simulation (which is normally neglected in other studies), which played an important role in reducing the localised peak stresses and in redistributing the loads. However, the model, which predicted considerable modulus reduction and accumulation of strain locally (at trabecular level), produced little apparent modulus reduction and negligible apparent accumulated strain. A probable reason for this could be the difference in the behaviour of trabecular and cortical bone at tissue level.

There are similar two dimensional cellular level models of cancellous bone, which have studied the effect of modulus reduction due to resorption of trabeculae and the effect of fractures and microcracking on apparent modulus reduction[204, 203]. Similarly, many theoretical studies on fatigue and creep of foams were based on micromechanism of deformation at cellular level (Chapter 2, section 2.4.2.1). However, none of these models have attempted for a simultaneous simulation of modulus reduction and accumulated strain along with damage accumulation; hence the need for the development of a continuum level model as described in the chapter.

Taylor et al.[183] used a combined finite element and continuum damage mechanics concept to simulate the tensile fatigue behaviour of cortical bone at global level. The iterative simulation method adopted was computationally efficient with no need to simulate each single cycle. In addition, the model had incorporated both modulus reduction and accumulation of strain along with damage accumulation. The model was based on uniaxial test results of the material (details of the method is given in section 6.2.1). A similarity in the fatigue behaviour of cortical bone and cancellous bone (at apparent level) has been noted in many studies. The present method used for the fatigue simulation of cancellous bone, is an extension of techniques used for fatigue simulation of cortical bone.

The fatigue simulations of uniaxial fatigue models of analogue foams, using a combined FE and CDM concepts were able to represent the given fatigue behaviour at the local and global level. However, a smooth transition for the variables was necessary through-out the analysis, especially at the beginning and towards the end of life, to avoid localisation of damage growth. Provided such localisation issues are avoided, the model was capable of reproducing a given input representation of the behaviour. The technique was unable to reproduce high stress/low cycle behaviour if the foam was assumed to be linearly elastic. However, the success of the model depends on its applicability to simulate migration. The present model was based on uniaxial results and a scalar damage parameter. On applying the model to a different stress state as in the case of migration model, further implementation in the model is required to account for the multiaxial stress state and direction oriented damage accumulation.

Chapter 7

Simulation of Migration Using Implant-Analogue Material Models

The previous two chapters have described the methods/procedures chosen to characterise and analytically simulate the fatigue behaviour of analogue materials using uniaxial models. In this chapter, the implementation of these methods to a model of implant-bone construct is discussed. In order to assess the applicability of the method in simulating migration of implant-bone models, a simplified model in terms of geometry and mechanical loading is introduced.

7.1 Experimental Model for Implant Migration

In its simplest form, neglecting the complexities of the shape and material property distribution, an implanted tibial component can be represented as a relatively stiff material plate resting on top of a foam block. An axial cyclic loading can be used to represent loading of the joint; this would impose an axial compressive stress in the foam. There was no attempt to model the effects of the cortical bone which surrounds the cancellous bone, as these models are meant to use for the verification of the chosen methods to simulate migration.

An Aluminium plate on foam block construct was chosen for the experimental and FE simulation of migration (Figure 7.1). Aluminium has a modulus of 69-70 GPa and a Poisson's ratio of 0.35. A very thin layer of araldite epoxy resin was used to glue the plate to the foam block, and the construct was modelled as a bonded material model in the finite element analysis. A contact model was not used due to the computational time for each simulation and the effort required to select the correct contact options,

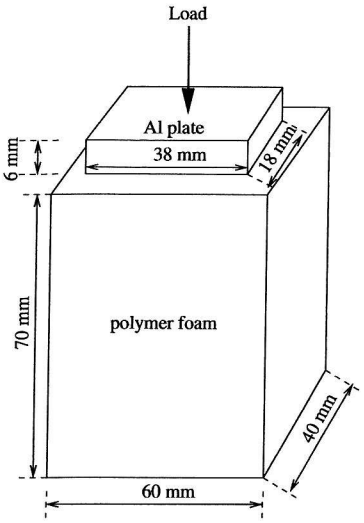

FIGURE 7.1: The model for experimental/FE simulations of migration. An aluminium plate glued on to the foam was used as a representative model of tibial plate on tibial cancellous bone. The construct was subjected to axial cyclic loading.

which could be very non-linear. In addition, the modelling and analysing options are more straightforward with a bonded model.

7.1.1 Experimental Simulation of Implant Migration

The experimental set-up for the migration test is shown in Figure 7.2. The plate-foam block was held in position using a vice and load was applied through a cylindrical loading pin on the centre of the metal plate. A computer controlled servo-hydraulic loading frame with a load cell capacity of 10 kN was used for testing and data collection. A cyclic compressive load was applied as sine wave at a frequency of 2Hz. The axial position of the loading pin was recorded at various cycle intervals using the

FIGURE 7.2: The experimental set up used for the migration studies. A computer controlled hydraulic loading frame was used for load application and data collection.

data acquisition system. The change in displacement with time, recorded as a change in position of the loading pin and hence the plate, was due to two components, accumulated strain and modulus degradation. The permanent strain caused permanent displacement or migration of the plate, while modulus degradation caused an increase in the elastic displacement during a loading cycle. The relative vertical displacement of the unloaded position as a function of time was calculated and reported as vertical migration. Similarly the relative change in the elastic displacement, with time was reported as elastic displacement.

7.1.2 Results from Experimental Simulation of Migration Using Herex ® C70.55 Foam

Tests were conducted at three different loads, 0.3, 0.35 and 0.4 kN respectively. Assuming a uniform axial stress distribution, which can be calculated as the ratio of the load to the plate area, the respective axial stress on foam at the interface region for these loads are 0.438, 0.51 and 0.58 MPa. Figure 7.3 shows the vertical migration and elastic displacement for up to 40,000 cycles. Some of the tests had to stop earlier than 40,000 cycles because the Instron was unable to control the load amplitude even though tuning the machine was conducted prior to each test. The tests were conducted to the lower end of the load cell sensitivity and this created control problems in some of the tests. The effect of a voltage spike, which resulted in a set permanent displacement in the position reading, was accounted for in one of the test.

7.1.3 Results from Experimental Simulation of Migration Using Solid Rigid PU Foam

A similar testing procedure to that used for Herex®C70.55 foam was followed for the Solid Rigid PU foam. Tests were carried out for two load cases of 1.08 kN and 1.24 kN. These loads caused average stresses of 1.58 and 1.81 MPa at the interface. The vertical migration and elastic displacements observed are shown in Figure 7.4 and Figure 7.5.

7.1.4 Discussion on Results of Migration Tests

In the initial stage, up to approximately 5000 cycles, the rate of migration was higher for both the foams; this then slowed down to a steady stage, i.e. exhibiting a constant

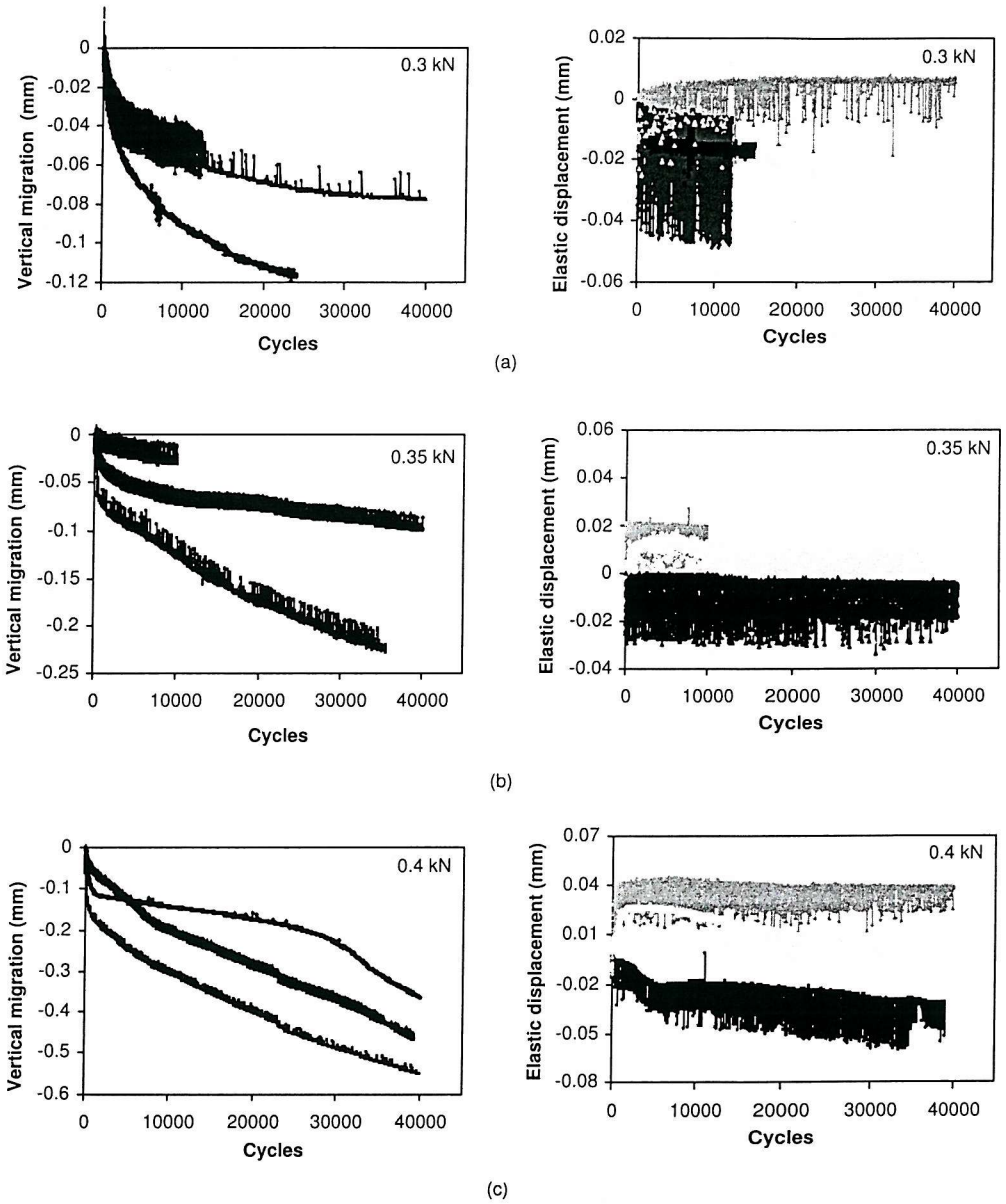

FIGURE 7.3: Patterns of vertical migration and elastic displacement from the migration tests with Herex®C70.55 foam for (a) cyclic load 0.3 kN (b) cyclic load 0.35 kN and (c) cyclic load 0.4 kN.

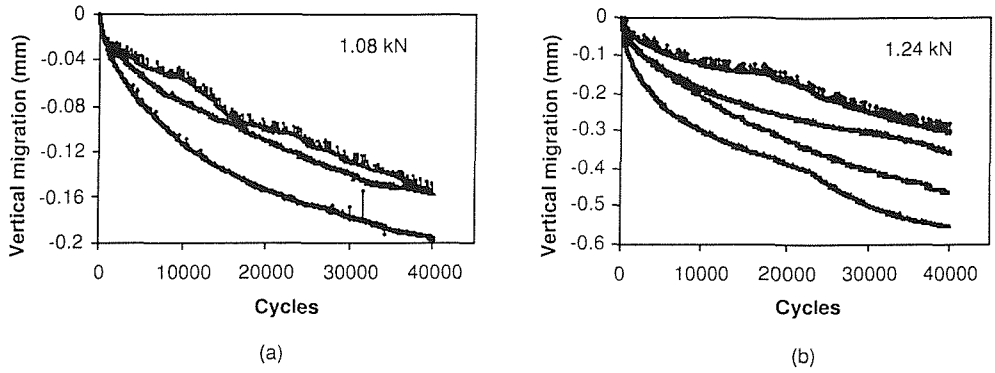

FIGURE 7.4: Patterns of vertical migration from the migration tests with Solid Rigid PU foam for (a) cyclic load of 1.08 kN (b) cyclic load of 1.24 kN

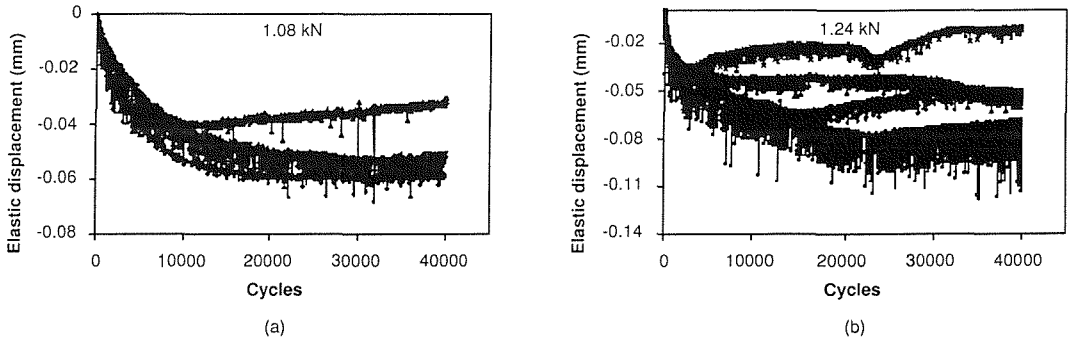

FIGURE 7.5: Patterns of elastic displacement from the migration tests with Solid Rigid PU foam for (a) cyclic load of 1.08 kN (b) cyclic load of 1.24 kN

rate of migration. Some of these tests were continued beyond 40,000 cycles, approximately up to 100, 000 cycles and they remained in a steady state. The amount of migration at the end of 40,000 cycles and the rate of migration in the linear stage between cycles 5000 to 40,000 are presented in Table 7.1. 40,000 cycles was chosen in these comparisons on the basis that, in the FE simulation of migration, the fatigue behaviour was to be simulated for 40,000 cycles.

In terms of vertical migration, the subsidence increased with increase in load for both foams. A relatively small increase in load (less than 20%) almost doubled the amount of subsidence for both the foams. The migration in the initial 5000 cycles constituted half of the total migration at the end of 40,000 cycles. In general the average migration was coincidentally similar in the order and magnitude for both the foams.

In terms of the elastic displacement, there was a large scatter in the recorded data, mainly due to the machine sensitivity to the lower load levels at which the tests were conducted. The scatter reduced for higher load ranges. For Herex®C70.55 foam a clear pattern for elastic displacement could not be identified, i.e. no modulus degradation appeared to occur at least at the global level; however, in general, there was a

change in elastic displacement only during the first 5000 to 10,000 cycles, and afterwards it remained constant. For Solid Rigid PU foam, although there was a scatter in the data there appeared to be a clearer trend, with some initial degradation early in the test, which again settled to near zero for the remainder of the test. There appear to be some elastic displacement recovery in some of the tests. However, considering the magnitude of the displacement recovery and the lower machine sensitivity for the test load levels, it can be neglected or considered negligible.

TABLE 7.1: Combined results from migration tests on two different foams

Foam & test load	Range of vertical migration after 40000 cycle (mm)	Range for rate of vertical migration between 5000 to 40000 cycles (mm/cycle)
HerexC70.55 at 0.35 kN	0.14-0.22	$(4.14 - 4.58) \times 10^{-6}$
HerexC70.55 at 0.40 kN	0.36-0.55	$(8.7 - 14.1) \times 10^{-6}$
Solid Rigid PU foam at 1.08 kN	0.16-0.20	$(2.97 - 3.35) \times 10^{-6}$
Solid Rigid PU foam at 1.24 kN	0.3-0.55	$(5.47 - 8.12) \times 10^{-6}$

7.2 FE Simulation of Implant Migration

The migration experiments showed that under cyclic loading migration of the idealised tibial plate occurred, with an initial period of rapid subsidence followed by a steady rate of migration. The fatigue simulation model developed for the FE models on uniaxial fatigue was extended to the analytical simulation of migration. The justification of the FE model in terms of geometry and mesh density are discussed in the following section.

7.2.1 The FE Model for Simulation of Implant Migration

The geometry of the FE model is shown in Figure 7.6. The metal plate and foam were glued together in the experimental work. In the FE model the foam and metal plate were directly bonded together at the interface and it was assumed that the contribution of glue to the structural behaviour of the construct was minimal. The migration was assumed to be solely due to fatigue damage of the supporting foam

material; the material properties of the metal plate were considered to be unaffected by the cyclic loading. The changes in properties under fatigue were simulated for within the valid range of normalised stress (Chapter 6, Table 6.1). Based on this, the

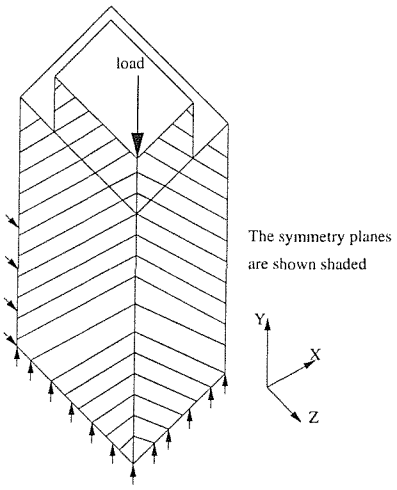

FIGURE 7.6: The FE model for the simulation of migration. Due to symmetry of the geometry and boundary condition only a quarter model need to be modelled. The boundary condition includes symmetry boundary conditions and constraints to movements in the normal direction of lower face and of half the length of one side representing the grip of the vice used to hold the foam.

regions which would be in this stress range, for fatigue simulation, could be identified for mesh descretization of the geometry; this would reduce the computational time and cost of analysis. Initially, a few static FE analyses were carried out to determine the stress distribution pattern in the construct, regions of possible fatigue damage, the effect of mesh size, and an effectively meshed volume for the analyses. Linear static analyses were carried out using the Solid Rigid PU foam -metal plate model, for an applied load of 1.24 kN. The Young's modulus and Poisson ratio were 68.4 MPa and 0.3, and 69 GPa and 0.35 respectively for the foam and the metal. The model was meshed with tetrahedral elements with an element edge size of 2mm. Figure 7.7 shows the contour plots of axial compressive stress and von Mises stress distribution in the foam. A stress range of 1.0 to 2.5 MPa was used for the contour plots; this gave a 20% extra bound to the upper and lower limits of normalised stress levels (see Table 6.1 in Chapter 6, Section 2) within which all accumulated strain and modulus reduction occurred. The roughness or irregularities in the contour plots were due to the fact that nodal averaging of results was not carried out while post processing, in order to show the results in the foam independent of the metal plate. Analysing the same model with the material properties of Herex®C70.55 foam, for an applied load of 0.4 kN (the highest load applied in the migration tests with Herex®C70.55 foam) gave similar patterns of stress and displacement distribution, although the magnitudes were different. From these plots, the material volume which could be expected to undergo fatigue damage was very small and directly below to the metal plate and in particular it was localised to the boundary edges of the bi-material interface. There was high stress concentration at the edge regions of material interfaces. Mesh refinements, to

study the effect of mesh size, were necessary only for the volume of foam close to the metal plate. There was a difference in the distribution of compressive stress and von Mises stress (Figure 7.7), for a given range, due to the multiaxial stress state in the material.

In Marc, an option for glued contact between two deformable bodies exist such that no tangential motion between the bodies can occur. This option was useful for joining two dissimilar, independently meshed volumes. Appropriate constraint conditions were automatically generated between the meshes to satisfy this condition. In the next stage of the analysis, mesh descretization of the FE model was carried out by dividing the geometry into a number of volumes and meshing them independently. Figure 7.8 shows the details of these mesh refinements. Tetrahedral elements of edge length 4mm were used for the coarse mesh and the rest were meshed with elements of edge length 2mm. A glued contact option was assigned between the metal plate and foam; this resulted in two sets of nodes at the interface belonging to each material rather than common nodes shared by materials. Thus the nodal values of parameters of interest on the foam surface were not averaged with that of the metal plate. Both the glued model and bonded model predicted the same displacement and a similar stress distribution pattern at regions of interest. The fine mesh was further refined in two more models. The first was meshed with elements of size 1mm. The other used 0.5 mm elements for the boundary regions of the interface and the rest of the volume was meshed with elements of 1mm size. A model completely meshed with a very coarse mesh (elements of 4mm size) was also analysed. The details of the number of elements for the various mesh refinements are given in Table 7.2. refinements.

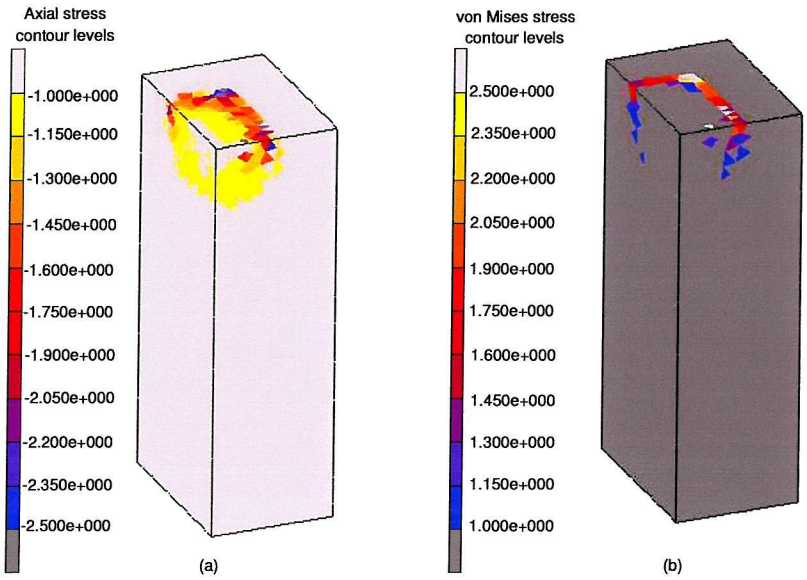

FIGURE 7.7: The contour plots of (a) axial compressive and (b) von Mises stress distribution from the FE analysis of foam-metal plate model of Solid Rigid PU foam for an applied axial load of 1.24kN. Only those regions are shown which falls in the stress range of 1.0 to 2.5 kN.

TABLE 7.2: Details of mesh refinement in terms of number of elements in the mesh for metal plate and foam for the chosen element sizes.

Element size	Number of elements in the mesh			
	Metal plate	Fine mesh region of foam	Coarse mesh region of foam	Total
4 mm	84	3296		3380
2 mm	843	3028	2834	6675
1 mm	25908	18192	2834	25908
1&0.5 mm	54017	41535	2834	54017

The equivalent stress distribution over the foam volume of interest, for a stress range of 1.0 to 2.5 MPa is shown in Figure 7.9. The finer the mesh, the smoother and better the representation of stress distribution. The pattern and magnitude were very similar for meshes of element size 1 mm and below. As the mesh density was increased, the magnitude of the stresses at the edges were also seen to increase. It was difficult to gain convergence in this region, due to the numerical singularity that occurs at such an abrupt edge between the two materials. Figure 7.10 shows a comparison of vertical displacement, equivalent stress distribution and axial compressive stress along the boundaries and mid regions (along the symmetry planes) of the interfacial region (the location on the foam is marked as ABCD). The displacements were uniform across the width and slightly increased towards the midsection of the length. The von Mises stress and compressive stress distribution patterns were the same and the magnitude of compressive stress was higher than the von Mises stress. Examination of the stress plots along edges DA or AB showed that towards the boundaries (towards D or A) the stresses increased and at the boundaries there was stress concentration; the stress was

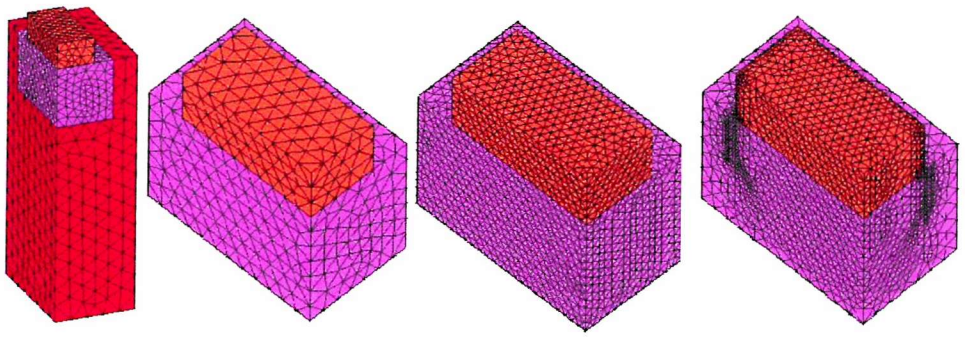

FIGURE 7.8: Details of the mesh refinements of the FE models for migration studies.

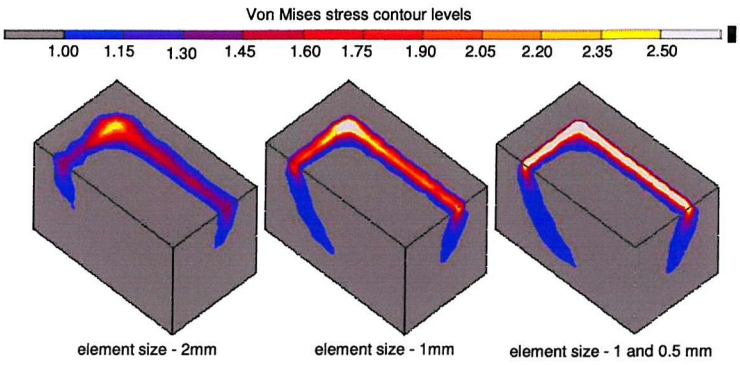

FIGURE 7.9: Von Mises stress distribution over the Solid Rigid PU foam for a stress contour range of 1. to 2.5 MPa for various mesh refinements. The applied axial load was 1.24 kN.

much higher than the observed material strength. The stress concentration effect on the geometric/material boundaries was more clear for stress plots along BC and CD, with the corner C showing the peak stress. At the same time, the nominal stress for the model (i.e. the ratio of the applied load to plate area), for the applied load of 1.24 kN was 1.81 MPa. Considering the fact the observed stresses were unrealistically high compared to the strength of the material and rather a numerical problem in dealing the change in geometry and difference in material properties, further refining was not carried out. Besides there is a limiting size to the elements in order to still satisfy the continuum assumption[64]. The model with elements of size 1mm was chosen as the default model in further analyses.

The choice of a rectangular cross section for the metal plate against a circular one was arbitrary. However, for the stiffness difference and edge effect, a circular section would not have made any difference except for the magnitudes of the stress concentration observed at the corners of the plate.

7.2.2 Procedure for FE Simulation of Migration

The FE simulation of migration used an extension of the method to describe the uniaxial fatigue tests described in Chapter 6. However, the migration model was different from the comparatively simple geometry and uniformly stressed uniaxial models, as it had a bi-material geometry and a non-uniform stress distribution. In this respect, the simulation of migration, using the method developed with uniaxial models, indicate its applicability to models of different geometries/materials and stress distributions. The expectation was that, the migration models would be able to provide global results (subsidence and elastic displacement as a function of time) comparable to experimen-

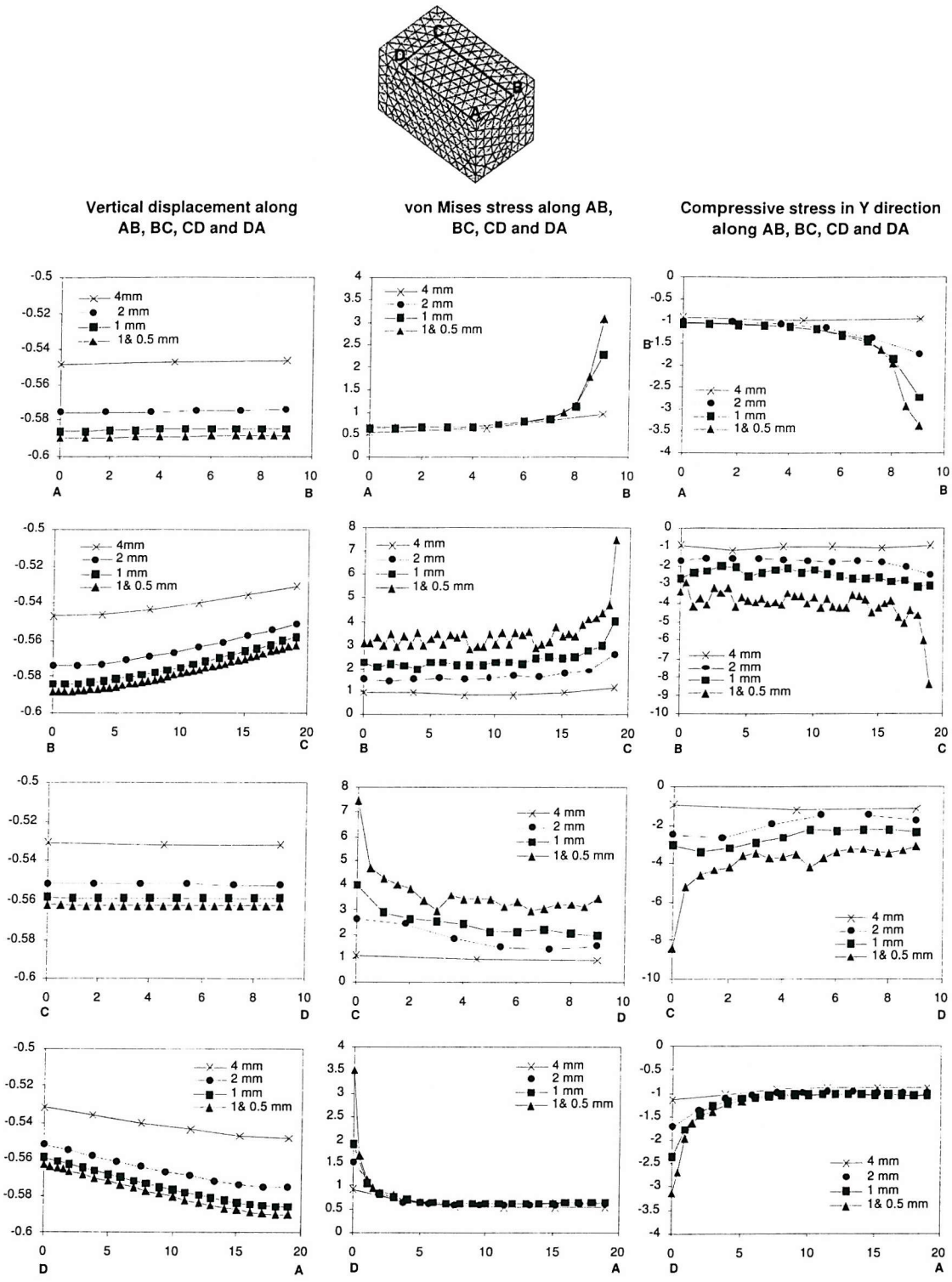

FIGURE 7.10: Variation of vertical displacement, von Mises stress and axial compressive stress over Solid Rigid PU foam surface along the metal plate boundaries (ABCD). For the applied axial load of 1.24 kN, the nominal stress is 1.81 MPa.

tal results. Since the material is non-uniformly stressed in the migration model, a local variable (at element level) cannot provide any direct information on the global variable (migration and elastic displacement), different to the uniaxial model. Again, as verified with uniaxial models, it was expected that the model would be able to satisfactorily reflect the element level changes to a known, measurable and comparable global variable.

7.2.2.1 The Procedure and Results of Simulation with Default Model Options

The default model simulations were carried out iteratively; in each iteration the model was subjected to a loading and unloading cycle. The load was applied axially through the center node of the plate (refer Figure 7.6). However the FE model with 1mm elements was chosen as the default FE model, the models of 2mm elements and 1mm elements with the finer mesh at the boundaries (0.5 mm) were also analysed, in order to assess the effect of mesh density. In the iterative simulation, the FE models were analysed for the stress distribution in the materials at peak load and at each iteration the accumulated strain and modulus degradation were determined and updated in the model. Once an element reached failure (or damage $\omega = 1$) the modulus of that element was kept the same and no permanent strain was allowed to accumulate in further iterations. The cycle step factor for each iteration was 0.02% and the von Mises stress was used for the calculation of normalised stress. The relationships for calculating number of cycles to failure, accumulated strain and modulus reduction in terms of life fraction and normalised stress were those derived from the uniaxial tests (Chapter 6, Table 6.2).

The models were analysed for the axial loads of 1.24 kN and 1.08 kN used in the migration experiments on the Solid Rigid PU foam. The axial displacement at the load application node on the metal plate was monitored; this reflected the element level variations in the accumulated strain (global migration) and modulus degradation (elastic displacement) respectively. The relative variation of axial displacement at unloading over time was referred to as migration. The difference between axial displacement at each iteration was referred to as the elastic displacement.

The progression of migration, for the three meshes and for the two load cases are shown in Figure 7.11. The magnitude of migration was unexpectedly very small, by one order of magnitude as compared to the experimental results (experimental results in Table 7.1). Comparing the difference in migration between meshes, differences were apparent. At the same time, compared to the expected magnitude of migration from experiments, the results from the different meshes were in same order, and in this

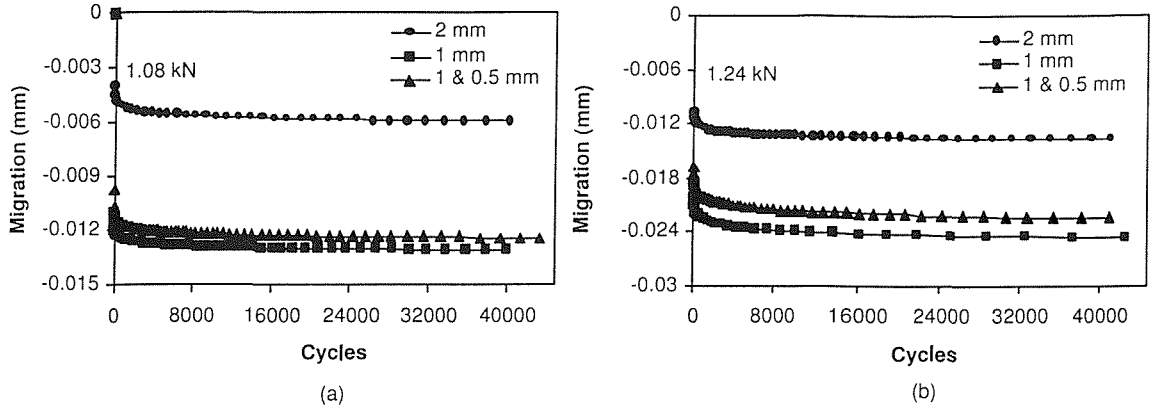

FIGURE 7.11: Variation of migration from the results of simulation with default model options for the migration model with Solid Rigid PU foam, with three mesh sizes for an applied load of (a) 1.08 kN (b) 1.24 kN

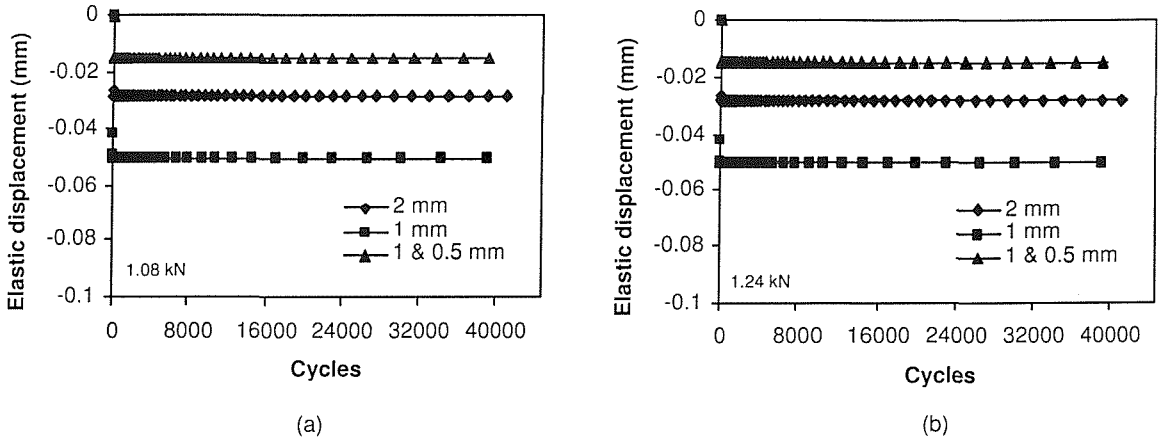

FIGURE 7.12: Variation of elastic displacement from the results of simulation with default model options for the migration model with Solid Rigid PU foam, with three mesh sizes for an applied load of (a) 1.08 kN (b) 1.24 kN

respect the considerable difference in migration with the experiments was not an effect of the mesh. In general, migration was lowest, for the 2 mm mesh, and the results appeared to converge with refinements in the mesh density. All simulations produced a rapid accumulation of displacement in the initial cycles, which then slowed down to a comparatively steady rate. There was some similarity with the experimental results in that the rapid phase was within the first 5000 cycles followed by a steady rate of migration. The degree of migration increased with load similar to the experimental observations. The variation in elastic displacement with cycles is given in Figure 7.12. There was a sudden change in the elastic displacement in the initial few cycles, which then became a constant. It appeared like there was no effective change in the elastic displacement in the FE simulation. The change of elastic displacement was different

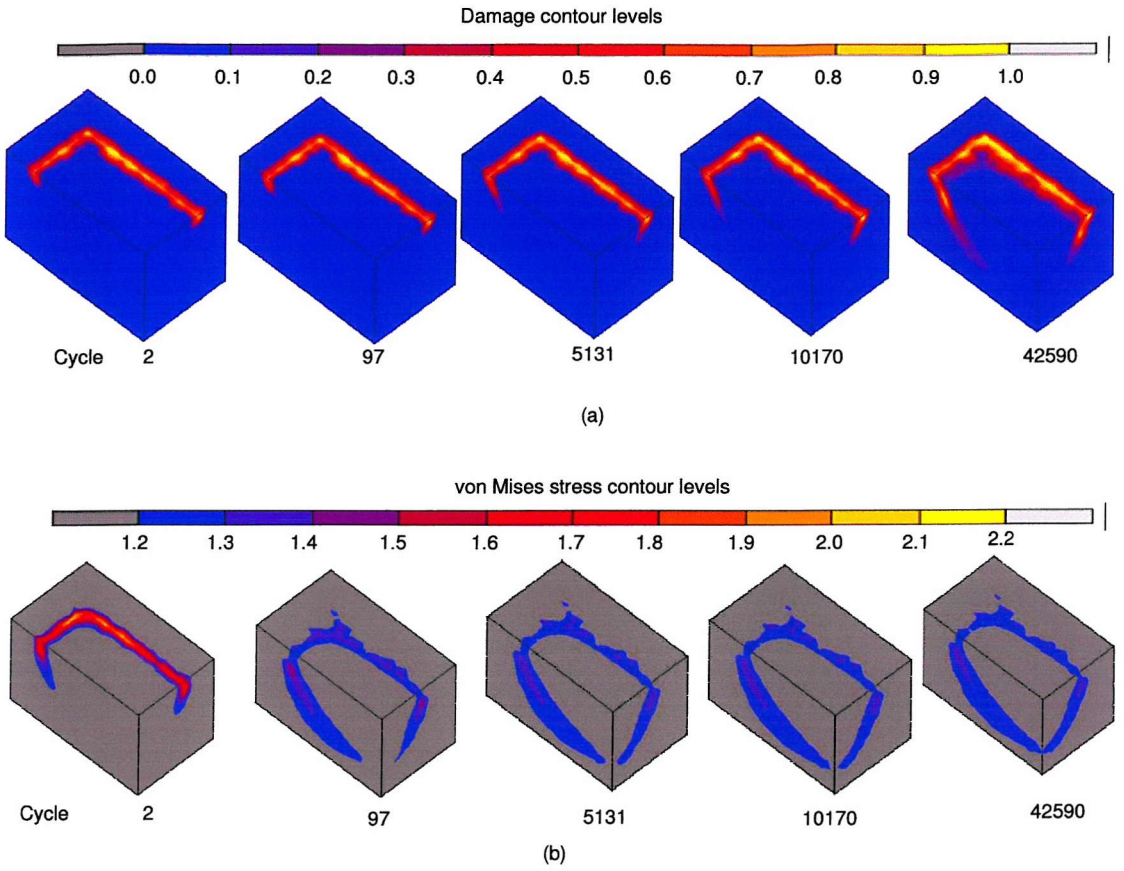

FIGURE 7.13: Variation of (a) damage accumulation and (b) von Mises stress at various stages of simulation with default model options for the migration model with Solid Rigid PU foam. A large amount of damage got accumulated in the initial cycles which then gradually progressed. The rate and accumulation of damage followed the amount and pattern of von Mises stress distribution.

in the experiments, with a gradual increase in the initial 5000 cycles, and no change with further cycles. The progression of damage with number of cycles and the von Mises stress distribution at various stages of the simulation is shown in Figure 7.13. It can be seen that the damage accumulation was very rapid in the first few cycles, particularly at the stress concentration which occurred at the boundary between the foam and metal plate. Once the layer of elements at high stress had failed, further progression of damage occurred at approximately 45 degrees to the interface plane; the von Mises stress in the foam fell to a lower value after the boundary elements had failed, and the range of stress in which any damage accumulation was possible existed in a shear plane (the plane at 45 degrees to the interface plane). However, in the experiments, failure was observed as a uniform subsidence of the metal plate into the foam.

The damage accumulated at the interface boundaries first, where there was a high

TABLE 7.3: Details of analyses carried out to compare the sensitiveness of the model to various parameters in migration simulation.

Analysis number	Parameters				
	stress component	Accumulated strain	Modulus reduction	Element modulus once its damage=1	$\triangle N$, cycles simulated per iteration
1	von Mises	updated	updated	unchanged	$= 0.02 \times N_{f_{min}}$
2	global axial compression	updated	updated	unchanged	$= 0.02 \times N_{f_{min}}$
3	global axial compression	updated	not updated	unchanged	$= 0.02 \times N_{f_{min}}$
4	global axial compression	updated	not updated	unchanged	$= 0.005 \times N_{f_{min}}$
5	global axial compression	updated	not updated	95% of E_{N_f}	$= 0.005 \times N_{f_{min}}$
6	minimum prini--cipal stress	updated	not updated	unchanged	$= 0.02 \times N_{f_{min}}$
7	minimum prini--cipal stress	updated	not updated	90% of E_{N_f}	$= 0.02 \times N_{f_{min}}$

stress concentration as observed from the static analyses. As explained in Chapter 6, such unrealistic stress could result in localisation of damage which over shadowed or dominated the expected function of the simulation through gradual variation of the variables. In general the default model options were able to simulate the general pattern of migration but significantly underestimated the magnitude. This effect was investigated by altering a number of parameters within the modelling algorithm.

The results of static analysis showed that the axial compressive stress and its area of distribution were higher than the corresponding von Mises stress. Although similar results were observed for the fatigue simulation of uniaxial tests with both stress components this may not be the same for the multiaxial stress situation of the migration model. Analyses were carried out to determine the effect of the chosen stress component on the results. The effect of independently updating of accumulated strain was also checked. In further analyses, only the results from the model with a mesh of element size 1 mm are reported unless any commendable difference was observed between the meshes. A summary of these analyses are given in brief in Table 7.3. Analysis 1 in Table 7.3 was the same as the default model option.

7.2.2.2 Results of Analysis 2

In this analysis axial compressive stress was used in the calculation of fatigue parameters; otherwise the models were analysed in the same manner as in Analysis 1. The rate of migration in the initial few cycles was rapid which then slowed down, for both the load cases (Figure 7.14). The magnitudes of migration were higher, compared to the default model, but still smaller as compared to experimental results. Again, there was an increase in migration with increase in load similar to the trend observed in experiments. The change in elastic displacement was rapid and only in the initial few cycles, similar to the previous analysis.

Figure 7.15 shows the pattern of damage accumulation and axial compressive distribution at various stages of the simulation. The first region to fail was the interface boundary, similar to Analysis 1 (default model). The progress of damage was, however different. The top layer of elements failed towards the center of the plate, followed by the elements underneath. The region of possible fatigue failure, outlined by the stress contours matched the damage pattern. The stress variation from the boundaries to the inside of the foam was smooth in the initial few cycles; this changed to a slightly irregular pattern after a few cycles.

In general, the rapid increase in displacement in the initial few cycles could be attributed to the stress concentration at the interface boundaries. At the same time an increase in the area/volume of possible region of fatigue failure with axial compression increased the magnitude of migration. This showed that an increase in the volume of possible failure and the stress magnitude to which these volumes were subjected could influence the observed pattern of migration.

The effect of modulus reduction and number of cycles simulated in each iteration were also assessed in the following analyses.

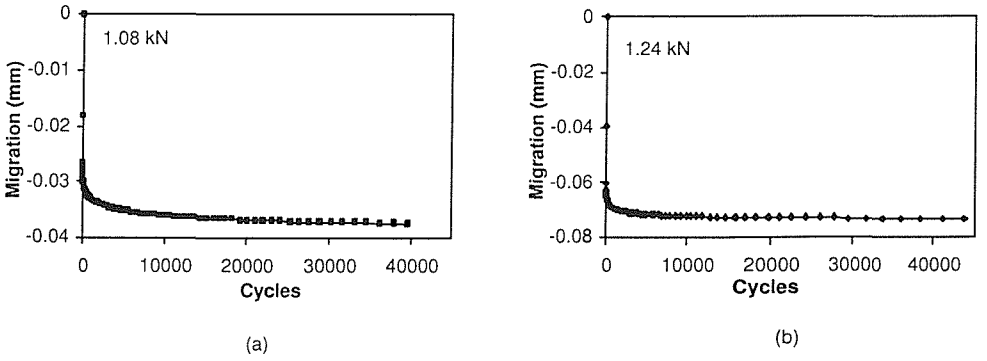

FIGURE 7.14: Variation of migration from **Analysis No: 2**, for an applied load of (a) 1.08 kN (b) 1.24 kN. The variation in migration in the initial few cycles were very high.

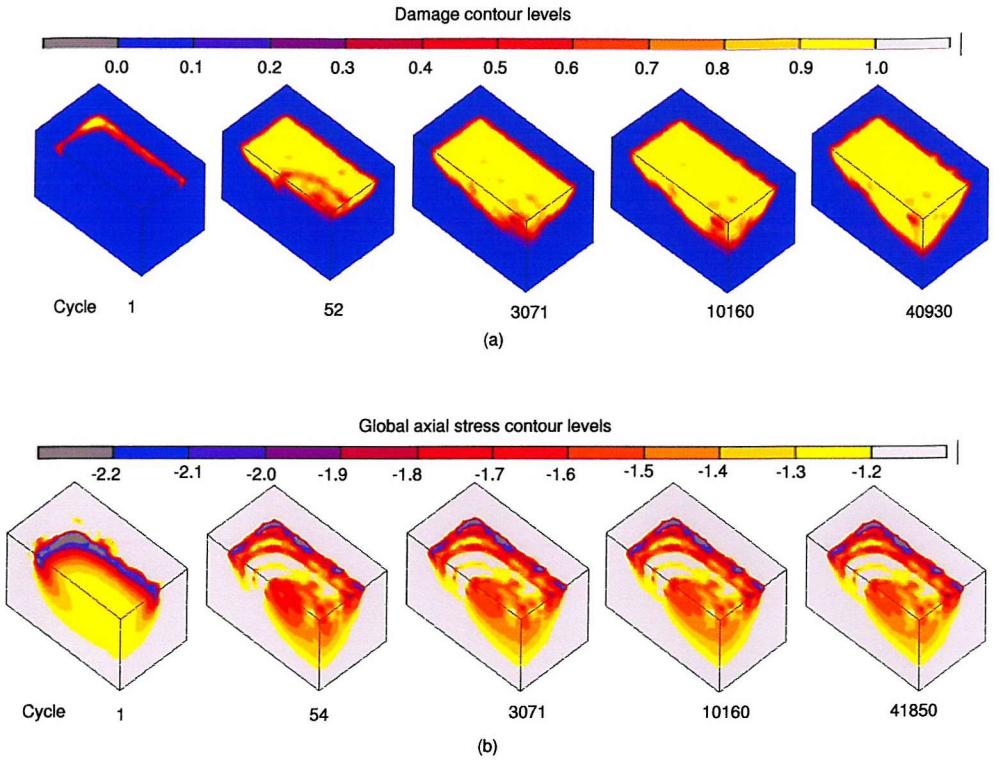

FIGURE 7.15: Variation of damage accumulation with number of cycles from the results of **Analysis No: 2**, for an applied load of applied load of 1.24 kN.

7.2.2.3 Results of Analysis 3 to 7

In these analyses the modulus reduction as a result of fatigue degradation was not updated in the model, as other than in the initial few cycles there was no apparent influence of modulus degradation. Axial compressive stress was used as the stress variable in analyses 3 to 5, while for the other two the minimum principal stress was chosen as the stress variable.

In Analysis 3, the model assumed that the material exhibited no modulus degradation. Figure 7.16 shows the variation of migration for the two load cases, from this analysis. The magnitude of migration was of a similar order as the previous analyses, and so was its relationship with the applied load. A comparison of migration, for an applied load of 1.24 kN, with the two previous analyses is shown in Figure 7.17. The migration pattern from the present analysis fell between the magnitudes from the analyses for the von Mises stress and axial compressive stress. The results from these three analyses showed the impact of modulus reduction and the stress variable on migration in the initial cycles. The pattern of damage accumulation and the pattern of changes in compressive stress with cycles are shown in Figure 7.18. In comparison with the updated modulus model there was a smooth transition of compressive stress from the

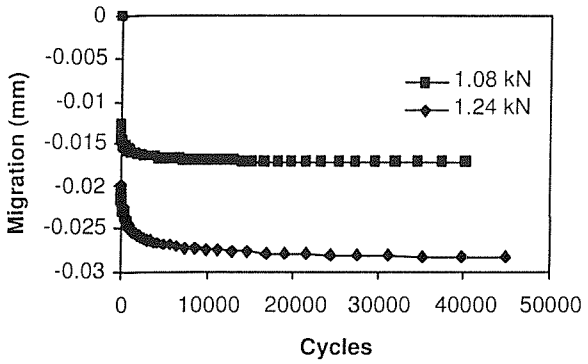

FIGURE 7.16: Variation of migration for two loads, from the results of **Analysis 3**

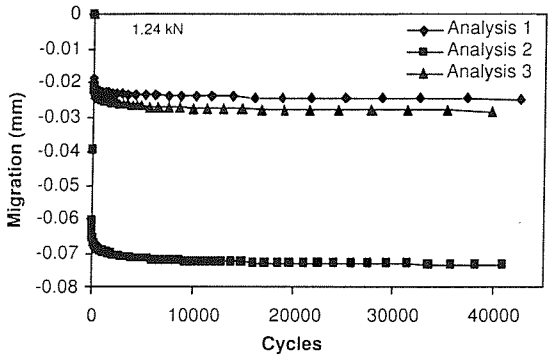

FIGURE 7.17: A comparison of the variation of migration from **Analysis 1, 2 and 3** for a load of 1.24 kN.

edge to the centre. The considerable migration in the initial few cycles could be due to the unrealistically high stress manifested as a high amount of accumulated strain. The modulus reduction factor probably caused an even higher stress concentration and subsequent accumulated strain as observed from the results of Analysis 2. In further analyses modulus reduction was not considered. There was no difference in the results for cycle step factors of 0.02 or 0.005 for the models (from Analysis 3 and 4). However, it had to be noticed that with high stress at the boundaries, it was only one cycle that was simulated in each iteration.

From the experiments, there was some variation in the elastic displacement with the number of cycles, particularly for the initial 5000 cycles, indicative of modulus reduction. In Analysis 3, there was no variation in the elastic displacement as modulus degradation was not simulated. In order to avoid the instantaneous rapid reduction in modulus and displacement, while inducing some modulus reduction, the modulus was reduced by 5% once the element had failed (Analysis 5). Again this resulted in an increase in the elastic displacement in the early loading cycles, but as seen before resulted in no further increase in elastic displacement thereafter; the analysis results were no different to those from Analysis 3. In Analysis 6, the principal stress was used as the driving variable, and no modulus updating was carried out. In Analysis 7 the modulus after the damage had reached one, was reduced to 90% of the modulus at failure. Again there was no significant difference in the results.

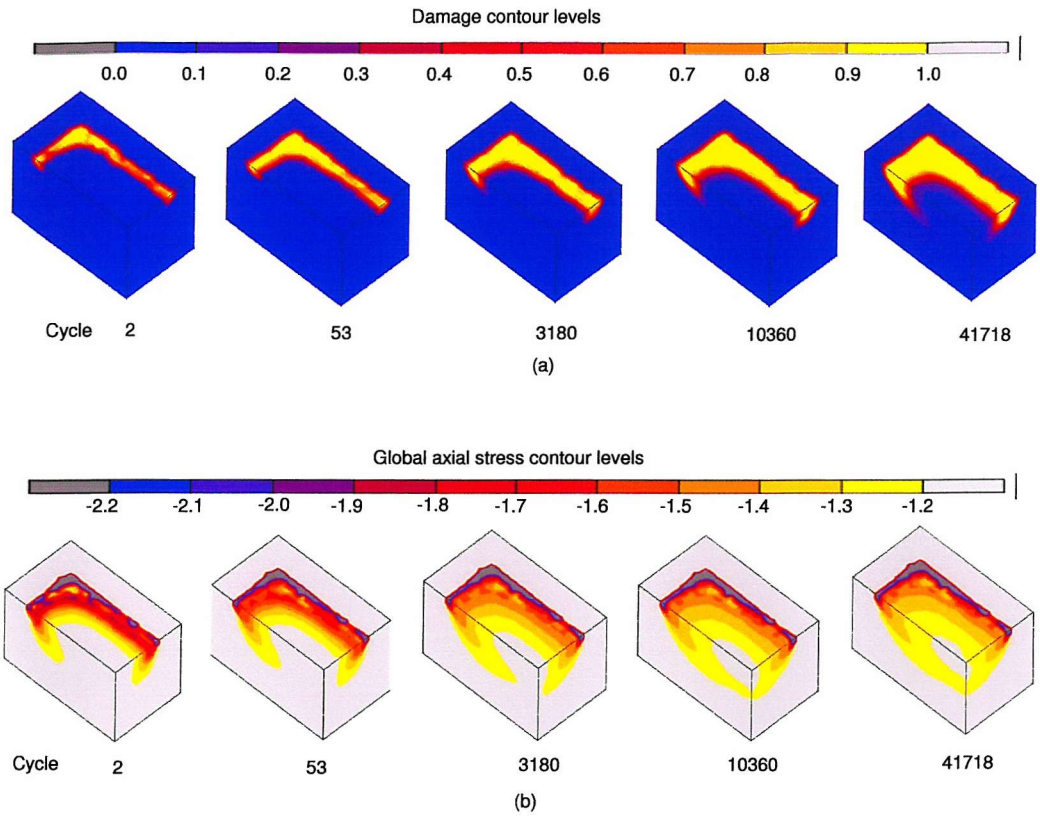

FIGURE 7.18: Variation of damage accumulation and axial compressive stress distribution at various stages of migration simulations, from **Analysis No: 3**.

A comparison of the simulated values of migration with the experimental results for the two load cases are shown in Figure 7.19. The results from Analysis 2 which gave the highest amount of migration, were used in the comparison. The analyses carried out so far showed that the model overestimated the initial variation in displacements, and after that underestimated the rate of the migration observed in the experiments. Slight variations occurred in the amount of migration according to the chosen stress variable and methods of updating the modulus, while in general the migration was underestimated compared to experimental results. The variation of migration with load levels followed a similar pattern to that of the experiments.

As discussed in Chapter 6 (Section 6.4), the algorithm is developed to analyse the model as linear elastic, with the update of additional non-linear strain in the material through the modulus reduction and accumulated strain. As long as these changes are gradual, as observed and discussed in the results of uniaxial models (Chapter 6), the model behaviour should be satisfactory. The higher stresses caused the models to have localised damage in the boundary regions and this would have resulted in a stress magnitude/distribution in the model, different from reality. A few initial analyses, shown a similar stress concentration effect and underestimation of migration for the Herex

foam model as well (Appendix B), and further detailed analyses with this model were not carried out.

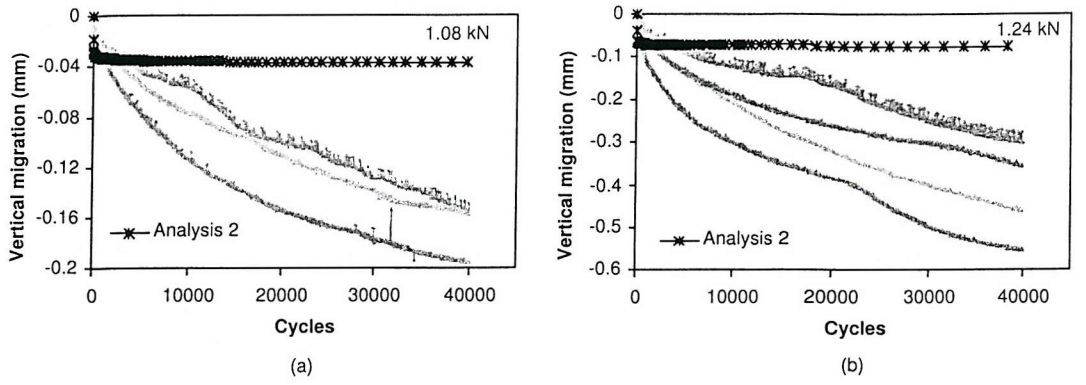

FIGURE 7.19: Comparison of the migration pattern from FE simulation and experiment using Solid Rigid PU foam for an applied load of (a) 1.08 kN and (b) 1.24 kN. The FE simulations results from **Analysis 2** is used for the comparison.

7.2.2.4 Creep Analysis of the Models

The CDM concept used in the previous fatigue simulations assumed that there was no accumulation of strain or modulus reduction once the number of cycles had reached the theoretical value of failure, N_f. It is possible that permanent strain was accumulating in the material continuously, with strain as a time dependent property. This could explain the underestimation in migration. However, the recovery of creep during sleeping or other transient stages of normal life are not considered in the present analysis, again considering it as a worst case scenario with continuous creep. A creep analysis of the model was used to verify this. As the stress concentration still existed, an initial rapid phase was expected. At the same time, in the next phase, the continuous creep assumption was expected to increase the rate of migration as compared to that from fatigue simulation.

In creep analysis, the accumulated strain for an applied load over a chosen period of time is calculated. The equation for the rate of accumulated strain from the experimental results was used for the calculation of creep increment at each time step. The secondary strain rate equation from the experiments was

$$\frac{d\epsilon_{acc}}{dN} = 6.85 \times 10^{48}(\sigma/E_*)^{33.169} \tag{7.1}$$

As the tests were conducted at a frequency of 2 Hz, the time dependent rate of creep accumulation and the accumulated strain per time increment for the model could be

written as

$$\frac{d\epsilon_{acc}}{dt} = 1.37 \times 10^{49}(\sigma/E_*)^{33.169} \tag{7.2}$$

The accumulated strain per increment was therefore updated to the model as

$$\triangle\epsilon_{acc} = 1.37 \times 10^{49}(\sigma/E_*)^{33.169} \times \triangle t \tag{7.3}$$

where $\triangle t$ is the time step. The algorithm for the fatigue analysis was modified to include this and was assumed that there was no modulus reduction. The total time was divided into suitable time steps. With a chosen constant time step of 5 seconds, the model was analysed. Using these equations, it was observed that the model accumulated a large amount of creep in the very initial time steps; this caused a large amount (1-2mm) of subsidence of the metal plate. The effect of time step caused a high creep strain evident from the Equation 7.3, especially for elements at the boundaries which were at high stress. Considering this, a cut off value for the total accumulated strain was imposed (a strain value of of 0.05) close to the maximum accumulated strain at failure (see fig 5.24, Chapter 5). The cut off option worked in the algorithm such that if the total strain accumulated at any integration point, k, at any particular time, exceeded the limit, there was no further creep added to that integration point. An extract of the subroutine, dealing with the above concept is given below.

```
if(totep(k).le.0.05) then
        deltaep(k)  =  1.37096e49*(str**33.169)*timinc
             else
        deltaep(k)  =  0.0
             endif
          totep(k)  =  deltaep(k) + totep(k)
```

Where, totep(k) is the total accumulated strain at that integration point, and deltaep (k) is the accumulated strain calculated for that particular time step at that integration point. A few analyses were carried out with set time steps and accumulated strain cut off values of total accumulated strain as variables.

7.2.2.5 Results of Creep Analysis 1 to 3

For a time step of 5 seconds, and with a cut off accumulated strain of 0.05, the total displacement rapidly increased in the very few initial cycles. This was possibly due to the value of creep increment (calculated from Equation 7.3) being very high for this

time step, resulting in an extremely high accumulated strain.

In creep analysis 2, the time step was further reduced to 1 second; this resulted in stable and realistic values for the subsidence. In analysis 3, the *totep (k)* was checked against the cut off limit; if exceeded, the creep increment ceased to update. A change in the cut off strain to 0.06 or 0.08 did not make any difference for the smaller time step of 1 second.

Comparisons of the observed migration from analyses 2 and 3 are shown in Figures 7.20 and Figure 7.21 respectively. A rapid subsidence was evident in the initial cycles, followed by a gradual subsidence. The magnitudes of migration were comparable to that observed from the fatigue simulations. Thus the underestimation in migration observed was not due to the chosen description of creep/accumulated strain, but rather it was due to the inability to contain the stress concentration effect.

A single attempt was made to restrict the maximum normalised stress in the model to a lower value, than 0.030 (as used throughout the analyses). This would have the effect of reducing the maximum strain accumulated in the elements at the stress concentration, in theory reducing the initial large displacements to a lower value. Figure 7.22 shows the pattern of migration observed from the results of this analysis. The observed large

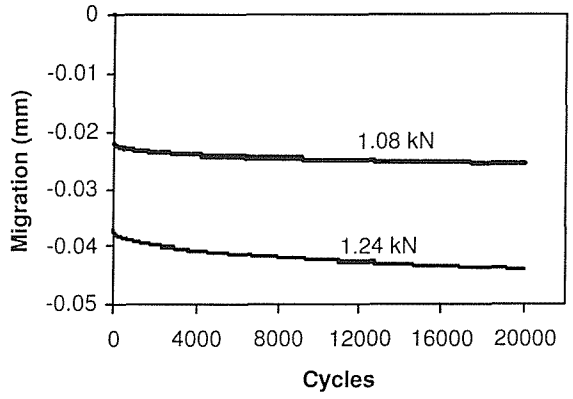

FIGURE 7.20: Comparison of migration from **creep analysis 2**, for two load cases.

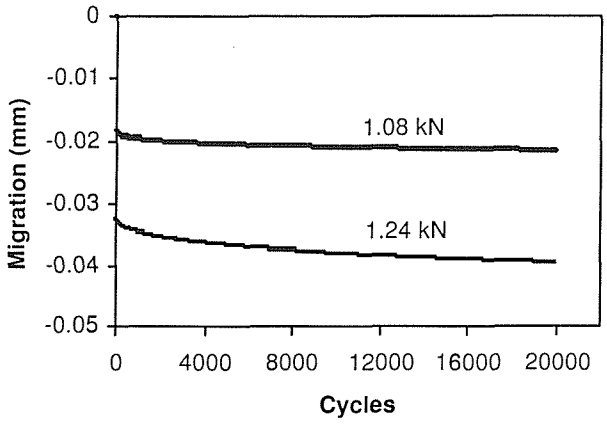

FIGURE 7.21: Comparison of migration from **creep analysis 3**, for two load cases.

initial displacements were reduced as compared to previous analyses. This supported the fact that the boundary regions and the stress state there needs to be addressed

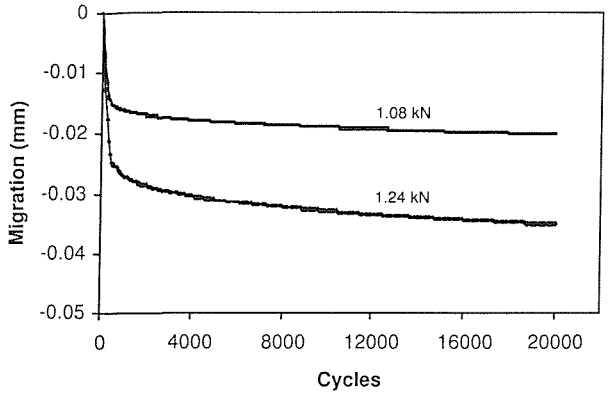

FIGURE 7.22: Pattern of migration by restricting the maximum normalised stress for the creep calculation to 0.026, for an applied load of 1.24 kN.

further.

7.3 Discussion

The migration model developed in this work was based on the assumption of the fatigue failure of the supporting cancellous bone. The development of a validated *in vitro* tool for prediction of migration, should enable the assessment of the effect of various fixation designs and loading combinations on migration. In view of the fact that this was a preliminary work towards achieving the aim, an effort was made to keep the models simple in terms of modelling options. To date, the model has been able to predict the general trends, but as compared to the experimental model, the simulations significantly underpredicted the migration.

Shirazi et al.[168] has used similar models of metallic plate on PU foam block in experimental and finite element comparisons of fixation designs for tibial trays. Their studies concentrated on the comparison of various fixations designs of tibial trays for various combined loading using experiments. In the FE simulations of the experiments various friction models were used to reproduce the experimental results. Most of these tests were performed under static loading. The experiments under fatigue loading was conducted only for 4000 cycles. The patterns of displacement from these tests showed an initial faster rate which then steadied down to a slower rate, with differences in magnitude for different fixation designs and combinations of loading. An FE simulation of the fatigue test was not carried out.

A similar metal-plate on foam model was chosen in the present study. A bonded model of the materials was chosen rather than a contact model, because of the computational time and effort required in selecting the appropriate contact parameters in

the FE model. When the model was subjected to axial compressive loading, it was considered that the major factor of influence on the mechanical behaviour of the system would be the fatigue behaviour of the substrate material.

The load cases applied in the experiment study were chosen such that the average axial stress under peak load (calculated as the ratio of the applied load to the area of the plate) was in a range of 70 to 90% of the foam strength. The materials exhibited accumulated strain under fatigue loading (Chapter 4) and the models were expected to show permanent displacement of the plate at these loads. Although there were some scatter in the results, when the loads were at the lower end of the machine sensitivity, in general the trends could be identified. The experimental results demonstrated a pattern of permanent displacement (migration) of the plate similar to that of a creep curve. The patterns were similar for both materials studied and the magnitudes of migration increased with increase in load. The degree of migration was not comparable to that observed for implants *in vivo*, due to the different geometry and applied loads; however they were similar, qualitatively, in terms of the pattern of migration. The variation in elastic displacement, compared to migration was very small. For Herex®C70.55 foam a clear pattern for the variation in elastic displacement (due to modulus reduction) could not be identified; however for Solid Rigid PU foam there was an initial increase in elastic displacement within 5000 cycles which then became constant.

The method of combined Finite Element Analysis (FEA) and Continuum Damage Mechanics (CDM) was validated through uniaxial fatigue tests (Chapter 6), and was extended to simulate migration. The expectation was that on simulation, the FE model would yield results comparable to the experiments.

The experiment models were reproduced in terms of the geometry and boundary conditions within the FE model. First, static analyses were carried out to gain convergence for the stress pattern and displacement. The initial analysis showed that it was the volume of foam directly below the plate that would undergo significant fatigue damage, with the rest of the volume of the model not considerably stressed. The effect of mesh densities was studied only for the volume of interest while the remaining volumes was descretized with a coarse mesh. In general there was stress concentration effect at the boundary region of the material interface which increased with mesh refinement. The discontinuity at the plate edges was expected to cause stress concentration and further mesh refinements were not carried out as the current mesh gave converged results at the interior regions. In the case of the uniaxial models, the stress concentration effect at the transition region did not influence the model behaviour; the stress concentration there underwent softening with the accumulated strain and modulus reduction, which shifted the high stress region into the midsection. A similar process was expected in

the migration model, where the elements at the boundary on accumulating strain and modulus reduction would transfer the loads towards the interior.

The finite element simulation of the fatigue model was carried out using the material behaviour of Solid Rigid PU foam as an input. The default model options were kept the same as the uniaxial models (as specified in Table 6.2, Chapter 6). However, unexpectedly, the simulations were unable to validate the experimental models; with FE analysis results fell short by nearly one order of magnitude. The models underwent rapid changes in the initial iterations, with damage accumulation at the interface boundaries and accumulation of large displacement. The stress concentration effects were affecting the model behaviour. Although unable to predict the absolute magnitude, the pattern of migration and its variation with load were comparable to the experiments in all the analyse. A number of analyses were carried out by varying the parameters in modelling algorithm. Creep analyses were also carried out by assigning a time dependent accumulated strain behaviour to the material, which was not dependent on the fatigue damage. There were differences in behaviour, with these changes, but these were not considerable changes in terms of the observed large difference with the experiments. The effect of the stress concentration at the edge of the plates dominated the performance of the model.

From the simulations of uniaxial tests it was observed that at higher stress/low cycle tests, a linear FE analysis and changes in the material behaviour by large increments, could result in very high stresses in the elements (as discussed in Chapter 6, Section 6.4). It caused the underprediction of life and simulations were unable to reproduce the non-linear material behaviour through the gradual changes in accumulated strain and modulus degradation. In the case of migration models, the effect of the stress concentration at the edges produced very high stresses, higher than the material strength. As explained before, in the fatigue simulation, updating of the accumulated strain and modulus degradation represented the magnitude of non-linear strain in the material at each cycle. However, the path dependent nature of the non-linear stress-strain behaviour was not represented, as these changes were updated at the end of each iterations, as a quantity. It resulted, in situations of unrealistically high stresses like the edge effect, underprediction of life with elements at edges failing in a single step; this hindered the stress redistribution in the elements through the gradual changes in accumulated strain and modulus reduction. In the case of uniaxial models, including the non-linear material properties in the FE analysis, predicted the material behaviour correlated with the analytical results; however, it caused a set permanent displacement. Due to various reasons, further implementation of the non-linear FE analyses was not included in the present study as explained in Chapter 6, Section 6.4. A method to address the path dependent stress-strain behaviour needs to be addressed in future

studies. While the edge effect and related high stress regions caused a large quantitative difference from the expected migration model behaviour, it is worth discussing other factors and methods/approaches that may need to be considered in future.

Another factor which was not considered is the 'stress volume' effect. It has been shown that the probability of failure for a larger volume of material as compared to a smaller volume of materials tested under the same stress[179]. In the case of migration model very small volume of the material is subjected to fatigue damage, compared to the uniformly stressed volume of the uniaxial model. It would imply that the fatigue life of these elements in the migration model, could be higher than that predicted by the uniaxial model. Accounting for this could effectively result in an increased life for the elements, and thus more time/increments for accumulated strain and modulus reduction; this would have allowed a gradual stress redistribution in the elements.

Localisation of damage is another issue to be addressed. A localised area of material damage is physically not possible, as in reality the damage get distributed among the surrounding material. In a local concept, the damage which accumulated under loading reaches a critical value for that material at which a crack in considered to initiate, or the material fails at that location[30, 108]. The further progress of damage is by a process of stress redistribution and damage growth around the crack. Peerling et al.[148] discusses the localization effect that could occur in an FE analysis on implementing it, and compares different methods to account the localisation effect. While the continuum damage variable presumes a local smoothness of the microstructural damage distribution, the continuum models allow discontinuous solutions causing damage localising in an area with unaffected surrounding material, affecting the physical relevance of damage modelling. The most promising strategies proposed to deal with such situations are local and gradient approach [147, 148]. The methods use spatial interaction terms in the constitutive models, either using an integral relation (non-local) or gradients of some constitutive variable (gradient method). The additional terms work in such a way that it smoothes the effect of damage field in the chosen interactive field, and thus avoids localisation. Stolk et al.[173] applied the non-local approach to avoid the mesh dependent damage growth in FE simulations of fatigue in bone cement. The method works in such a way that the stress value at any integration point is reassigned with a spatially averaged stress value. Using a weighing function a weighted average of the stress values was determined within the chosen averaging volume of that element.

Another issue which needs to be addressed in further studies on migration is the methods to represent the material after damage has reached unity. In the present simulations, further changes in modulus reduction and accumulated strain were terminated after damage has reached unity. However, in reality the material could be undergoing further deformation, and modulus reduction and accumulation of strain

than represented in the simulation as (i) the tertiary phase is not included in the simulation and (ii) the material has a large non-linear regime in compression after yield. An attempt was made in the present analysis to represent the element status after complete damage, by reducing its modulus by a factor. However, that approach was not successful in the present frame work of algorithm, as it caused unrealistic stress rise in some elements.

In the present migration model, the edge effect was a reality and could have influenced the experimental results, as compared to a model without the edge effect. An FE simulation was carried out to study the difference in behaviour by avoiding the edge effect by choosing a different metal plate geometry. The metal plate was extended to cover the whole top surface of the foam such that comparatively uniform stress would exist in the material. The applied load on the plate was increased proportionally to the increased area of contact at interface. Figure 7.23 compares the axial stress distribution of this model with the original migration model. For the model with an extended plate, the stress was evenly distributed over the foam. A fatigue simulation of the extended plate model was carried out. The results showed that the metal plate subsided rapidly in the foam by an order of magnitude higher than the experiments, within the first 100 cycles (Figure 7.24). Simulations with modulus reduction caused an even faster accumulation of permanent displacement. These results suggest that the experimental model was influenced by the edge effect.

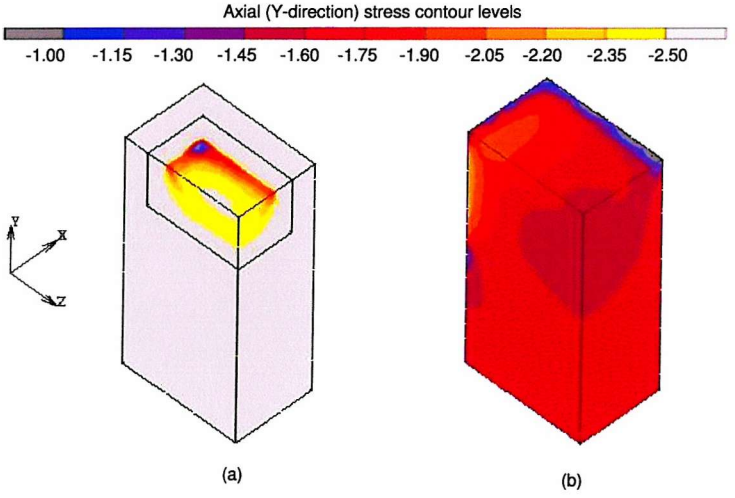

FIGURE 7.23: The contour plots axial stress distribution from the FE analysis of foam-metal plate model of Solid Rigid PU foam for an applied axial load of 1.24kN (a) the model of experimental work (b) model with an extended metal plate.

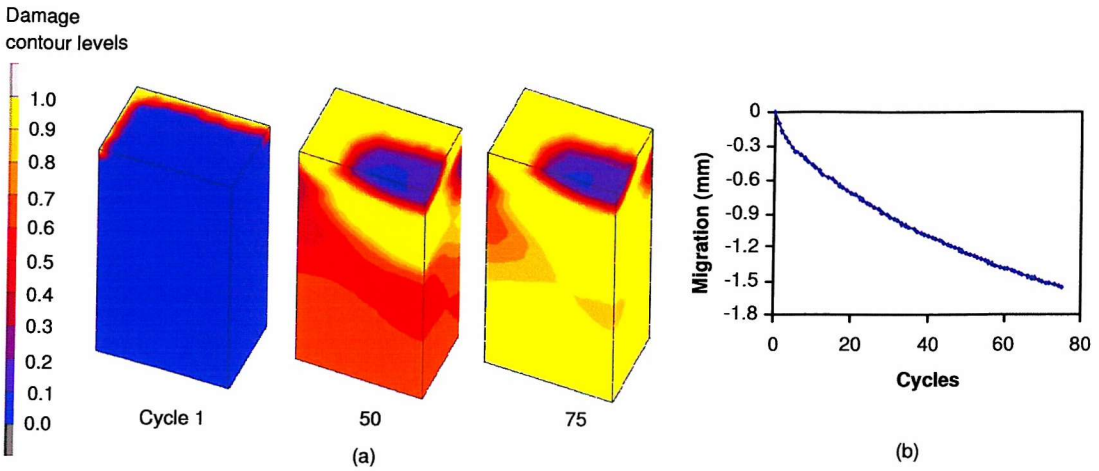

FIGURE 7.24: The results of fatigue simulation of foam-big metal plate model of Solid Rigid PU foam (a) the contour plots of damage distribution (b) migration of metal plate.

7.4 Conclusions

The presented research work proposes a methodology for the simulation of migration. The experimental models of migration exhibited a similar pattern of migration as observed *in vivo*, with an initial rapid phase of migration followed by a steady state rate of migration. The rate of migration was a function to the applied load level. In the FE simulation, the geometry of the chosen model produced some problems which were not anticipated either on selection of the model or the method of analysis. While the edge effect for the chosen geometry was a reality, the FE model amplified it by an unrealistic amount. The inability to deal with regions of localised damage in the CDM approach may be hindering the successful description of fatigue behaviour and its variation over the elements. A more detailed and complex mathematical damage models may be required as the simple damage mechanics approach used in the present study has shown a limited capacity in dealing with the localisation of damage growth and model sensitivity. The present study was able to provide a qualitatively validated FE model for fatigue simulation, and also highlighted many areas that, if addressed, should enable a more accurate simulation of implant migration.

Chapter 8

Discussion and Conclusions

8.1 Discussion

Aseptic loosening, the gradual process of loosening of the total joint replacement, is the major cause of revisions for hip and knee replacements. According to arthroplasty registries aseptic loosening accounts for 75% and 45% of hip and knee revisions respectively [68, 176]. There are various mechanical failure scenarios which lead to the failure of knee and hip replacements(Chapter 1, section 1.1.7). Studies on migration of implants have shown that irrespective of the type of implant, the method of fixation or the location, all implants show some form of migration (Chapter 3). These studies have shown that migration could be used as an *in vivo* predictive tool for aseptic loosening[53, 159]. The likelihood of failure of an implant was high, when excessive migration was evident in the initial years after implantation[5, 92, 101, 128, 129]. However, migration studies only report the end result and not the possible process by which it occurs.

Cancellous bone is the biological structure which is in direct contact with the prosthetic components. The mechanical properties of cancellous bone vary widely and are influenced by factors such as age, location, deformities and degenerative diseases[8, 50, 60, 83, 94]. Considering the fact that joints are subjected to millions of cycles of load as a result of daily activities, a knowledge of the fatigue behaviour of cancellous bone is important for predictive models. *In vitro* studies have shown that cancellous bone exhibits considerable modulus reduction and accumulation of strain as well as a strength reduction on cyclic loading and these are related to the stress levels and material properties of bone[13, 63, 124](Chapter 2). In mechanical terms the effect of accumulated strain is to cause a permanent displacement in the material. The observed pattern of accumulated strain with time from the *in vitro* studies, and migration curves are

qualitatively similar. *In vitro* studies have reported that a changed mechanical environment exists for an implanted joint compared to the intact bone (Chapter 3, section 3.2.3 and 3.2.4). Some of these studies have reported concern over the elevated stress levels in the supporting bone for some implanted joints. Variation in bone stress levels appear to be dependent on the type of fixation and researches have been able to match the ranking of implants, considering the risk of failure in terms of stress levels, with clinical migration rates [140, 81, 149, 180, 182, 193]. Bone, being a biological structure, is continuously being remodelled according to the mechanical environment; thus it attempts to repair any fatigue damage that accumulates in the material. However, the situation could arise, where the cancellous is unable to compensate for this and fatigue failure may occur; this has been suggested as a possible cause of migration[181, 182]. A worst case scenario in a changed mechanical environment would be a situation of no biological influence; i.e. no bone remodelling.

The aim of this thesis was to explore the possibility of developing an *in vitro* model which could explain migration through a study of mechanical behaviour of the cancellous bone. This is important as although *in vivo* studies have shown migration to be the most successful predictive tool for aseptic loosening, there are no preclinical tools to describe patterns of migration and their differences between prosthetic designs. In this respect, with (i) a known fatigue behaviour and (ii) an analytical technique to express the behaviour of the substrate material, it would be possible to develop an analytical model of migration. Research on both of these aspects are lagging at present. The project aim was to develop a validated *in vitro* tool for simulating migration using a simplified model and approach. A validated powerful pre-clinical tool would be useful in the performance prediction of implants, detecting the differences in patterns and magnitudes of migration of various designs and fixations, for different combinations of load.

Fatigue Characterisation of Analogue Materials

The proposed analytical tool would need a material model with known fatigue characteristics, thus an analogue material model was used in the present work. Analogue materials for cancellous bone are used in many *in vitro* studies[37, 37, 41, 168, 170, 177, 178] as they are cheap, easy to work with and consistent in properties. In composite synthetic models of the femur and tibia cancellous bone is replaced by PU foam. These models which are a popular replacement for cadaveric specimens, are used in many studies including fatigue tests and migration studies of cemented implants[116, 117, 168]. However, none of these studies have attempted to compare the fatigue behaviour of the analogue materials to that of cancellous bone. The analogue materials are normally chosen based on a similar structure and similar material

properties compared to cancellous bone, as determined from static tests. Cancellous bone exhibits complex fatigue behaviour with a gradual degradation of its strength, modulus and with accumulation of strain; thus it would be appropriate to ensure the analogue material has a comparable fatigue behaviour.

In the present work two commercially available polymer foams (Herex foam and Solid Rigid PU foam) were used as analogue materials. Although the chosen analogue materials had been used in previous studies, the fatigue characterisation of the materials had not been undertaken. The protocol for fatigue testing and data analysis were defined (Chapter 4), using similar procedures followed in cortical and cancellous bone studies [13, 95, 139]. A reduced section geometry and uniaxial load was assumed to produce a uniform stress in the midsection. The global displacement over the gaugelength was used for calculating the modulus reduction and accumulated strain variation with number of cycles. In the studies on bone, a particular percentage of reduction in modulus was normally used for determining the cycles to failure in compression [13, 124], with no standard rule for choosing this percentage. The present study defined a failure criteria as a percentage reduction in modulus or a visual observation of failure when the total strain started to increase rapidly (i.e., has reached a tertiary stage of dynamic creep). Fatigue studies on cancellous bone have reported relationships for S-N curve and secondary stage creep rate (Chapter 2, Table 2.3) and only general observations on modulus reduction and accumulated strain. While some relationships have been reported for cortical bone there are no similar studies for cancellous bone which have attempted to relate the applied stress level to the variation of modulus/accumulated strain in fatigue (Chapter 2, Table 2.2).

In general, the fatigue behaviour of the foam materials was comparable to that of cancellous bone, exhibiting both modulus reduction and accumulation of permanent strain. At the same time, quantitative differences existed between the foams and cancellous bone, and between the foams themselves. The analogue materials showed modulus reduction and accumulated strain less than the reported trends for cancellous bone. The nature of accumulated strain and modulus reduction were comparable for the two chosen analogue materials, in terms of the magnitude and their dependency on normalised stress; however, there were quantitative differences. The tensile and compressive fatigue behaviour of Herex foam was different with distinct relationships for the S-N curve and secondary stage accumulated strain rate. Further analysis of the tensile fatigue behaviour of the materials was not carried out, as the migration model was based on compressive axial cyclic loading results. The uniaxial static tests of the material showed a non-linear stress strain behaviour for the materials at higher stress levels. The secant modulus and accumulated strain was used to represent the non-linear behaviour of the material in the migration model. The modulus reduction

and accumulated strain variation during compressive fatigue were best described by power-law relationships. of the form $A\omega^B$; the constant A indicated the amount of accumulated strain/modulus reduction at the time of failure (or when $\omega = 1$) and the constant B indicated the rate by which accumulated strain/modulus reduction reach the value A. A linear fit best represented the relation of these constants with the normalised stress levels. Although these relationships were not strong in some cases, there were comparatively better correlations observed for the Solid Rigid PU foam between the constants and the normalised stress levels. Although the S-N data produced reasonable well fitted curves, if more test data can be obtained for each stress level, further correlations and conclusions on their dependence on stress levels may be possible. The nature of the relationships derived for life and secondary strain rate as functions of normalised stress were similar to that of cancellous bone. A similar pattern of variation was observed for both modulus reduction and accumulated strain, with life fraction, at all the tested stress levels. In this respect, there was no distinction made between low and high cycle tests in the analysis. However, with a very rapid deformation, no usable data was recorded, for tests carried out at very high stress level. The derived relationships with the rest of the test data was thus extrapolated to represent the material behaviour at these high stress levels.

In short, as well as providing the relationships for developing and validating the migration model, the study emphasized the need for fatigue characterisation of the materials. A lack of prior knowledge of the fatigue behaviour of the analogue material could lead to over/under estimation of the performance of an implant and erroneous interpretation of the results. In experiments, where both tensile and compressive fatigue are important, a knowledge of behaviour under both cases is important, as the material showed distinct relationships in tension and compression. While the analogue materials used in the present study are not completely representative of cancellous bone, they are appropriate for developing and validating a technique for simulation of migration.

FE Simulation of Uniaxial Fatigue

Finite Element (FE) analysis is a powerful analytical tool which has found wide application in many fields of engineering. The success of the method relies on the definition of the problem and the selection of appropriate approximations and assumptions in the definition and representation of the model. In this context it is important to validate the model against known results and data.

Continuum Damage Mechanics (CDM) is used to describe the gradual or progressive accumulation of damage in a material and the degradation of material strength. Using a damage parameter to represent the macrolevel effect of microlevel mechanisms of damage, and a cumulative law to describe its evolution of damage[30, 110], CDM tech-

niques can be used to determine the damage level and failure of structures. Damage can be taken as a scalar or vectorial parameter. An assumption of homogenous distribution of microcracks/defects in the material provides a scalar measure for damage. With different mechanisms associated with the damage process in different materials, a large number of damage parameters have been defined [48, 103, 202, 110]. In many cases it is easiest to use a simple damage parameter, the life fraction, and Palmgren-Miner linear cumulative damage law. However, studies have shown the non-linear dependence of damage accumulation on the load and damage history[31].

The present model used the scalar linear damage parameter (life fraction) and linear cumulative law in the simulations. The damage level varied from 0 to 1, indicating a no damage state to a completely damaged model. A brief introduction to the methods of Finite Element (FE) analysis and Continuum Damage Mechanics was given in Chapter 5. With damage represented as a field variable, it is possible to relate the changes in mechanical behaviour to the damage parameter and represent them in the constitutive relationships; this is referred to as coupled analysis. The advantage of the coupled analysis is that besides predicting the damage level, it also predicts the effect of changes in mechanical behaviour of the materials. Thus, for the analogue materials, a coupled analysis is required to predict the mechanical effect of accumulated strain/-modulus reduction with damage accumulation.

There are a few studies in the orthopedic field based on the application of CDM to model fatigue[184, 173, 183, 189, 190, 191]. Most of these studies have dealt with predicting the tensile fatigue life of bone cement and the performance of cemented hip replacement. The earlier analyses were uncoupled analysis with the assumption of a brittle nature for cement, where the mechanical properties of the materials were assumed to remain the same until fracture [190]. Some of these studies coupled creep with damage while simulating fatigue[173, 174, 190, 191]. Life fraction was used as the damage parameter, and either a linear or non-linear cumulative law was used to describe the accumulation of damage. These studies did not consider the fatigue behaviour of the surrounding bone in the analysis, and the behaviour of the model and hip stem movements were explained in terms of the creep and fatigue damage of the bone cement. Taylor et al. [183] used a combined FE and CDM concept to model the uniaxial tensile fatigue behaviour of cortical bone, along with the modulus reduction and accumulated strain coupled with the linear damage variable life fraction. Relationships, derived from the experiments, were used to describe modulus and accumulated strain coupled with damage. The models were satisfactory in reproducing the uniaxial experimental results. The advantage of the method was in its ability to predict the changes in material properties and mechanical behaviour as the damage accumulated in bone. For the present model a similar concept was used. The success of the method

in predicting the uniaxial behaviour of the analogue material could be a justification for its use in the migration model, by predicting the effect damage and coupled accumulated strain on global migration.

The working concept of the algorithm was detailed in Chapter 6. The method adopted an iterative procedure, where each iteration represented the fatigue simulation of a chosen number of cycles; this would reduce the computational time/cost by avoiding the simulation of each single cycle. In each iteration the FE analyses were carried out for loading and unloading increments. The number of cycles to failure (N_f) at each integration point was determined from the respective peak stress values on loading. The number of cycles simulated in each iteration (or the cycle step $\triangle N$) was defined as a particular percentage of the lowest of these number of cycles to failure($N_{f_{min}}$) determined. The damage ($\triangle\omega$) sustained at each integration point in that iteration ($\frac{\triangle N}{N_f}$) was determined. The total damage sustained until the previous iteration was updated with the damage increment in the current iteration. The amount of modulus reduction and accumulated strain were determined at each integration point as a function of the respective damage, and these values were updated into the model. The accumulated strain was updated at the unloading increment of the iteration while the new modulus was updated into the model at the beginning of the next iteration; this facilitated monitoring the effect of each parameter on the model behaviour independently. An element was assumed to be failed, once the total damage had reached a value of 1. The algorithm made use of the choice of user defined subroutines in MSc. Marc.

The preliminary development of the model used simple uniaxial models, so that it was easier to address the problems and understand the limitations of the models. Initial analyses were carried out to determine the sensitivity of the algorithm towards various model based parameters including mesh density, Poisson's ratio, chosen stress component and the chosen cycle step in each iteration. The chosen FE model, based on convergence study using static analyses, was satisfactory in the fatigue simulations as well in terms of the mesh density, chosen stress component and Poisson's ratio. With a linear damage cumulation law and linear FE analysis smaller cycle steps were required to represent the non-linear variations in mechanical behaviour. The models gave converged results for smaller cycle increment in the iterations; but were sensitive to larger increments as as the model was not able to produce a gradual non-linear variation of the fatigue parameters (damage, modulus reduction and accumulated strain). In general, the models were satisfactory in reproducing, locally and globally, the described material behaviour for high cycle low stress fatigue regime.

In cases where the changes in the model were occurring rapidly (for example the cases of N_f less than 100 in the Solid Rigid PU foam, or the use of reduction in modulus

after damage=1), there was significant increase in stress at some points, which were unacceptable considering the material strength. The high stresses caused a rapid accumulation of damage, and its progression, causing a premature failure of the model. As explained in Chapter 6, the assumption of a linear material, as opposed to a non-linear material, could result in a very high stress levels in the FE analysis, in the non-linear stress-strain regime of the material. This was due to the fact that there was no possibility to relax the stress levels, through non-linear deformation. For high stress/low cycle tests, the models were unable to reliably predict the fatigue behaviour. With a linear elastic model the life was underpredicted, whereas if an elastic-plastic model was used, the life was correctly predicted, but the amount of accumulated strain was over predicted.

In the iterative methods the changes in modulus and accumulated strain were applied at the end of each iteration. A sudden and large change in the system with the linear model could result in unrealistic stress changes at these locations, causing damage localisation, further stress concentration and faster progression of damage and failure. A non-linear stress-strain material behaviour was expected to smooth the variation of the stress. However, this resulted in additional permanent strain due to the non-linear displacement(Chapter 6). At the same time, the modulus reduction and accumulated strain updated to the model at each iteration also accounted for the total non-linear strain in the model through a linear analysis, and in this respect the permanent strain from the non-linear analysis was overpredicted. Future work should therefore aim to produce a gradual variation in accumulated strain and modulus reduction by either using sub steps of load increments in each iteration or by adopting methods to include the non-linear stress strain material behaviour in the FE simulations. Another factor which affected the model sensitivity was the definition of the cycle step factor. The algorithm was developed such that a single cycle was the least possible cycle increment that could be simulated in an iteration. In the case of low cycle tests, this resulted in a large damage increments, and consequently large changes in the material behaviour. This catalysed the damage growth at regions of damage localisation and stress concentration.

Experimental and Analytical Simulation of migration using a simplified model

Chapter 7 discussed the various aspects and procedures for experimental and finite element simulation of the migration using an idealised model of the implanted tibia. Similar models have been used in previous studies to represent the implanted tibia, but with different objectives. Shirazi et al.[168] used a metal plate on PU foam model in their studies, which were aimed to stress the need for non-linear friction models to

represent the contact condition at implant-bone interface. The models were analysed under static loading. Although the model was studied for its cyclic behaviour (for cycles less than 4000), no attempt was made to reproduce them computationally.

In the present study, a model of a metal plate bonded and supported by the foam cube was used for the experimental and FE models. A bonded model was preferred to a contact model, considering the computational time and effort needed in choosing the right contact parameters and analysis. On testing, it was observed that the experimental construct showed an expected migration pattern. There was an initial phase of rapid migration (in the initial 5000 cycles) which then changed to a steady state. The magnitude and rate of migration increased with increased in stress levels. RSA studies have reported a similar pattern of migration with an initial rapid phase of migration which then either ceased or reduced to a steady rate. If the rate of the steady state was higher than a critical amount, this resulted in loosening. In the present model, with all other conditions remaining the same, an increase in load (an increase in the stress level of the substrate material) caused an increase in the migration rates. An increase of load by a maximum of 20% resulted in almost a doubling of migration (Chapter 7, Table 7.1). A direct comparison of the rates or magnitudes with RSA studies were not possible due to the differences in the loading and geometry of the model. The elastic displacement showed an increase (due to modulus reduction) in the initial 5000 cycles, which then remained a constant. In general the experimental model of migration reflected the global effect of any modulus reduction and accumulated strain occurring in the substrate material under cyclic loading.

The experimental model was recreated in FE. Initial static analyses were carried out and volumes of expected fatigue damage were descretized with a finer mesh and a coarse mesh was used elsewhere. The glued model option in MSc.Marc was used for combining the independently meshed volumes. The static stress convergence analyses showed the boundary regions as locations of high stress. Default model options were set the same as used in uniaxial model, except that in the present model only the meshed volume of foam below the metal plate was of importance in terms of undergoing any fatigue damage. Unexpectedly, the analyses with the default model underpredicted the migration by an order of magnitude compared to the experiment. The simulations showed an initial rapid phase of migration, which compared to the migration in the rest of the life was very high. In the experiments the migration in the initial 5000 cycle was nearly the same as the migration in secondary stage (from 5000 to 40,000 cycles). The damage zone was confined to the boundary regions in the early period. The further progression and distribution of damage was very slow. The models were analysed by varying many parameters in the modelling algorithm, like the stress component, cycle steps and mode of updating modulus. While these factors resulted in

minor changes in the predicted magnitudes of migration, they could not bridge the gap with the experimental results. The chosen stress component had an effect on the amount of migration and on the damage progression and distribution. The use of von Mises stress component depicted the damage zone in a shear plane, while the axial compressive stress gave a damage zone as the volume below and adjacent to the metal plate. Multiaxial test data is required to define the stress component/criteria for failure prediction. Assigning accumulated strain as a time dependent property also did not make any significant difference in predicting migration.

In short, the migration models underpredicted migration in the simulations. However, an initial rapid phase and a constant rate secondary stage was observed in the analyses, with the amount of migration increasing with increase in load. Thus, these models were qualitatively similar to the experiments. There were issues on applying the algorithm to the migration model, which were not anticipated earlier on choosing the geometry. The models included a significant stress concentration, which resulted in stresses much higher than uniaxial models. The edges are expected to cause a high stress, however, with the linear model assumptions for the material, and on refining the mesh, these stress values were unrealistically high. A model of an extended plate, without the edge effect, showed a uniform distribution of stress in the foam, and migrated at a rate an order of magnitude higher than the experiments. In this respect, possibilities are that the realistic stress distribution and amount of migration from the simulations could be in between the model with and without the edge effects. Although the strainrange in which the models worked was specified, the first cycle produced many elements which failed, at the boundaries. The effect of these affected regions dominated, in overshadowing the slight differences made in the default options in terms of mesh density, the cycle step, stress component, and updating options.

While the edge effect caused a significant underprediction of the model, there are many other factors which could have influenced the performance of the migration model. Also there are many other methods/approaches which may need to consider in further investigation of the model, as mentioned in chapter 7 (Section 7.4).

The are many factors which need to be considered in the representation of the fatigue behaviour of the material. The simple material model used may have under/overestimated the material behaviour in the simulation, on applying it to the migration model. The damage cumulative law for the material was taken as linear, which is independent of the load sequence effect, while in reality it may not be the case. Chaboche et al. [31] proposed a nonlinear damage law in which the damage rate was expressed as a function of the present damage; the mean stress level and the maximum stress level by $dD = f(\sigma_m, \overline{\sigma}, D)dN$, i.e., a non linear evolution of damage. He formulated a damage

evolution equation:

$$D = 1 - [1 - r^{1/(1-\alpha)}]^{1/(1+\beta)} \tag{8.1}$$

Where β is a material constant and α is a stress dependent function and r is the life fraction. The function had unseparable variables σ_m and D which described the non linear damage accumulation and load sequence effects. It would require a further experimental tests to determine these material constants and damage evolution law for the materials.

Similarly there was no distinction made between low and high cycle fatigue performance of the materials. Although uniaxial test data was not available at very higher stress levels, the relationships derived from the tested stress range was extrapolated to represent the material behaviour at very high stress levels. It could be possible that the material had a different behaviour at these stress levels and which was not represented in the present situations. In compression fatigue simulation, another issue is how to deal with an element after it had failed theoretically (damage =1), and to represent its further contribution to the structural integrity. In the present algorithm the material was considered to undergo no more modulus reduction and accumulation of strain, once damage has reached unity. However, the material could take further load and undergo deformation as showed by the tertiary region of deformation in fatigue and a large non-linear stress-strain regime in static tests (from the experiments). However, with both the tertiary region and non-linear stress-strain behaviour not accounted in the numerical model, the performance of the migration model may be under predicted. In this respect further experiments and methods to represent the material behaviour are required to represent the material behaviour more accurately in the numerical models. Methods to represent the tertiary region of the deformation and degradation of materials would be helpful. Mao and Mahadevan [120] proposed a non-linear function to represent the fatigue damage for composites. This non-linear function accounted the initial rapid damage development, secondary and tertiary final failure stages observed in the modulus degradation pattern.

$$D = q(\frac{n}{N})^{m_1} + (1-q)(\frac{n}{N})^{m_2} \tag{8.2}$$

where $q, m1, m2$ are material constants, n, N are the applied number of cycles and fatigue life. Applicability of such representation for the cancellous/analogue materials need to be investigated.

Memon et al.[123] used a method to account the elastic and elastic-plastic material behaviour (or low and high cycle fatigue) in the FE simulations. The method works in such a way that, if the stress level in the critical zone is above yield limit, an additional nodal force vector is considered in the model to represent the reduction in

stiffness due to plastic effect. The applicability of the method to the present model is worth addressing.

In the case of migration model very small volume of the material is subjected to fatigue damage, compared to the uniformly stressed volume of the uniaxial model. With a higher probability of failure for a larger volume of material as compared to a smaller volume of materials tested under the same stress[179] the fatigue life of these elements could have been higher than the predicted life; this would have allowed a gradual stress redistribution in the elements. Taylor and Kuiper [179] has suggested methods to account for the stressed volume effect, by combining a probability analysis with the FE model.

In the present model damage is considered as a scalar quantity, which was a reasonable for a uniaxial model along with the assumption of homogeneously distributed defects in the material. However, for more complex models and multiaxial stress state, a vectorial representation for damage is required. A tensorial representation for damage, to account the three-dimensional stress situation, have been applied in the tensile fatigue simulation of bone cement [174, 190], where damage can accumulate in multiple directions.

The results of this study have highlighted the need to deal with situations of stress concentration and localisation. Damage localisation without sufficient damage smoothness with the surrounding materials can cause pathological localisation of damage and it results highly mesh sensitive results in FE analyses. Non local and gradient models[147, 40] have been suggested as methods of avoiding the localisation and mesh sensitivity of the model. Both methods use a spatial interaction term in their constitutive relationships either using integral relations or using gradients of some constitutive variables which gives a smoothing effect on the deformation and damage variables. For example, Stolk et al.[173] used an averaging technique in their CDM approach to model fatigue damage accumulation in bone cement. They observed that while the location and orientation of the crack was similar to the experimental results the crack growth rate was higher with increased mesh refinement. In order to contain this they used a spatially averaged stress component given by

$$\overline{\sigma}_{ij}^{k} = \frac{\sum_{n=1}^{m} \sigma_{ij}^{n} \phi(d_{crit}, d_{kn}) V_n}{\sum_{n=1}^{m} \phi(d_{crit}, d_{kn}) V_n} \tag{8.3}$$

The function $\phi(d_{crit}, d_{kn})$ is a weight function given by the optimal value of critical distance

$$\phi(d_{crit}, d_{kn}) = exp(-(d_{kn}/d_{crit})^2) \tag{8.4}$$

where m represents the total number of integration points over which stresses are averaged, within a spherical volume centred around integration point k. The parameter

V_n represents the volume belonging to the integration point n that lies within the averaging volume.

8.2 Conclusions

While migration has been projected as powerful tool for *in vivo* predictions of aseptic loosening, there is a lack of representative *in vitro* studies which attempt to understand the mechanical cause of migration and consequently develop methods which could simulate migration. Among the possible causes of migration, the hypothesis of fatigue failure of supporting cancellous bone appears to be acceptable in terms of its ability to explain the patterns of migration. Using this as a basis, the present research was a preliminary step towards developing an analytical model for simulating migration. The approach was to use a simple model as basis and incrementally improve it through numerical validation. In this respect established methods were used wherever possible than developing new models.

The present work emphasized the need for an adequate fatigue characterization of substitute materials to cancellous bone before using them in *in vitro* studies involving cyclic loading. The materials used in this study had a qualitative similarity with cancellous bone; thus they may not be entirely appropriate as an absolute replacement for cancellous bone models. However, for the development and validation of the analytical models, the analogue material models were satisfactory as an approximate *in vitro* model of cancellous bone, with their qualitative similarity in the fatigue behaviour to that of cancellous bone.

While the general concept of the chosen approach to simulate migration was satisfactory, there are issues of concern in the mathematical description of the problem in assuring gradual damage growth and gradual variations of the fatigue parameters. A more detailed material analysis in various aspects, especially the non-linear material models and their effect on fatigue behaviour is required.

In the uniaxial models the failure criteria was not important due to the uniaxial stress nature. In the migration model with the models being sensitive to edge effects, it was not able to detect the effect of various failure criteria. However, it was observed that the von Mises criteria was not valid for the multiaxial stress state of the migration model. The FE models of migration projected the problem of dealing with the edge effect within the available material model and CDM techniques used for the simulation. Disregarding the effect from these region, the trend of migration and its variation with loads were satisfactory, as compared to the experimental model. The major conclusions of this study can therefor be summarised as follows:

1. A preliminary level migration model has been developed based on the argument of fatigue failure of cancellous bone causing migration.

2. With no established data on fatigue characteristics of the analogue materials to cancellous bone, the present study has proposed a methodology for the fatigue characterisation of analogue materials.

3. The study results emphasized the need for fatigue characterisation of analogue materials.

4. The chosen analogue materials showed qualitative similarity in their fatigue behaviour as compared to cancellous bone.

5. In the framework of a combined FE and CDM method, an algorithm was implemented for the FE simulation of uniaxial fatigue of analogue materials.

6. The uniaxial models were satisfactory in reproducing the given input behaviour in a high cycle, low stress regime. However, the models were poor predictor in low cycle, high stress regime.

7. The analyses of the results indicate the adverse influence of the linear material model and local approach chosen in the CDM algorithm, at very high stress levels, and during faster damage growth.

8. The experimental model of migration showed the possible effect of fatigue on observed pattern of migration.

9. The FE simulation models for migration showed a pattern of migration and load dependency comparable to the experiments; however, they underpredicted the rate and magnitude of migration due to the edge effect in the model.

10. The study has highlighted areas that need to be addressed in further migration simulation.

8.3 Future Work

The present work was a preliminary attempt towards filling the gap between the *in vivo* and *in vitro* studies on migration. Considering the fact that there are no preclinical methods on predicting the risk of migration, the research has highlighted the scope for future work in the field. The immediate future work required based on the present model, would be to expand the CDM concepts to take into account the localisation

of damage, validated again with the uniaxial models. The description of accumulated strain and modulus are based on a particular failure criteria, and input models can be derived using various failure criteria. It would be worth exploring other factors, other than the normalised stress which is influential on the variation of accumulated strain and modulus reduction. The effect of the non-linear nature of the material, and the differences in the accumulated strain patterns for linear and non-linear regimes of the applied stress would also be informative. While the present fatigue model is based on a uniaxial data, it would be interesting to see the fatigue test results on the material for a different geometry, for example a four point beam test, from both experimental and analytical point of view. The damage variable is assumed to vary from 0 to 1, and also with a linear cumulative damage rule, both these aspects can be explored further while testing the models for varying stepped amplitude loading. The application of methods using a vectorial representation of damage is another possible field of study. The stress/strain failure criteria of the material is also required.

The chosen migration model was satisfactory in terms of conducting experiments, while the FE analysis created numerical problems due to the geometric and material discontinuities. Immediate future work on the migration model could use a change of geometry. A model with the plate extended over the foam would be numerically easier to solve in the FE analysis. The application of an updated uniaxial model to the modified model of migration is expected to exhibit the behaviour similar to the experimental observations. This model can then be verified with a different material model and also for different load combinations.

References

[1] **Andrews, E. W., and Gibson, L. J.**, '*The role of cellular structure in creep of two-dimensional cellular solids*', Materials Science and Engineering, A303, 120-126, 2001.

[2] **ASTM F1839-97**, 1998,'*Standard Specification for Rigid Polyurethane Foam for Use as a Standard Material for Testing Orthopaedic Devices and Instruments*', ASTM standards, 1278-1283.

[3] **Ahleberg, A. and Linden, B.**, '*The radioluscent zone in arthroplasty of the knee*', Acta Orthopaedica Scandinavica, 48, 687-690, 1977.

[4] **Albrektsson, B. E. J., Ryd, L., Carlsson, L. V., Freeman, M. A. R., Herberts, P., Regner, L. and Selvik, G.**, '*The effect of a stem on the tibial component of knee arthroplasty. A roentgen stereophotogrammetric study of uncemented tibial components in the Freeman-Samuelson knee arthroplasty*', The Journal of Bone and Joint Surgery, 72-B, 252-258, 1990.

[5] **Albrektsson, B. E., Carlsson, L. V., Freeman, M. A. R. and Ryd, L.**, '*Proximally cemented versus uncemented Freeman-Samuelson knee arthroplasty-A prospective randomized study*', The Journal of Bone and Joint Surgery, 74-B, 233-238, 1992.

[6] **Arthur, T., Pierce, R., and Gibson, L**, 2000, '*Microdamage in creep and monotonic compression of bovine trabecular bone*', 46th Annual Meeting, Orthopaedic Research Society, March12-15, Orlando, Florida.

[7] **Ashman, R. B., and Rho, J. Y.**, '*Elastic modulus of trabecular bone material*', Journal of Biomechanics, 21, 177-181, 1988.

[8] **Ashman, R. B., and Rho, J. Y. and Turner, C. H.**, '*Anatomical variation of orthotropic elastic moduli of the proximal human tibia*', Journal of Biomechanics, 22, 895-900, 1989.

[9] **Bathe, K. J.**, '*Finite Element Procedures*', Prentice Hall, 1996.

[10] **Behrens, J. C., Walker, P. S., and Shoji, H.**, '*Variations in strength and structure of cancellous bone at the knee*', Journal of Biomechanics, 7, 201-207, 1974.

[11] **Boeree, N. R. and Bannister, G. C.**, '*Cemented total hip arthroplasty in patients younger than 50 years of age. Ten- to 18- year results.*', Clinical Orthopaedics and Related Research, 287, 153-159, 1993.

[12] **Bourne, R. B. and Finlay, J. B.**, '*The influence of tibial component intramedullary stems and implant-cortex contact on the strain distribution of the proximal tibia following total knee arthroplasty. An in vitro study.*', Clinical Orthopaedics and Related Research, 208, 95-99, 1986.

[13] **Bowman, S. M., Keaveny, T. M., Gibson, L. J., Hayes, W. C. and McMahon, T. A.**, '*Compressive creep behaviour of bovine trabecular bone*', Journal of Biomechanics, 27, 301-310, 1994.

[14] **Bowman, S. M., Guo, X. E., Cheng, D. W., Keaveny, T. M., Gibson, L. J., Hayes, W. C. and Mc Mohan, T. A.**, '*Creep contributes to the fatigue behaviour of bovine trabecular bone*', Journal of Biomechanical Engineering, 120, 647-654, 1998.

[15] **Bowman, S. M., Gibson, L. J., Hayes, W. C. and McMahon, T. A.**, '*Results from demineralised bone creep tests suggest that collagen is responsible for the creep behaviour of bone*', Journal of Biomechanical Engineering, 121, 253-258, 1999.

[16] **Brown, T. D., Ferguson, A. B., Jr.**, '*Mechanical property distribution in the cancellous bone of the human proximal femur*', Acta Orthopaedica Scandenevica, 51, 429-437, 1980.

[17] **Bugbee, W. D., Culpepper 2nd, W. J., Engh, C. A., Jr. and Engh, C. A., Sr.**, '*Long term clinical consequences of stress-shielding after total hip arthroplasty without cement*', Journal of Bone and JointSurgery, 79, 1007-1012, 1997.

[18] **Burr, D. B., Martin, R. B., Schaffler, M. B. and Radin, E. L.**, '*Bone remodeling in response to in vivo fatigue microdamage*', Journal of Biomechanics, 18, 189-200, 1985.

[19] **Burman, M. and Zenkert, D.**, '*Fatigue of foam core sandwich beams-1: undamaged specimens*', International Journal of Fatigue, 19, 551-561, 1997.

[20] **Burman, M. and Zenkert, D.**, '*Fatigue of foam core sandwich beams-2: effect of initial damage*', International Journal of Fatigue, 19, 561-578, 1997.

[21] **Cameron, H. U. and Hunter, G. A.**, '*Failure in total knee arthroplasty: Mechanisms, revisions and results*', Clinical Orthopaedics and Related Research, 170, 141-146, 1982.

[22] **Carlsson, L. V., Albrektsson, B. E. J., Freeman, M. A. R., Herberts, P., Malchau and Ryd, L.**, '*A new radiographic method for detection of tibial component migration in total knee arthroplasty*', The Journal of Arthroplasty, 8, 117-123, 1993.

[23] **Callaghan, J. J., Dysart, S. H, Savory, C. F. and Hopkinson, W. J.**, '*Assessing the results of hip replacement: A comparison of fifteen rating systems*', The Journal of Bone and Joint Surgery, 72-B, 1008-9, 1990.

[24] **Carter, D. R., Schwab, G. H. and Spengler, D. M.**, '*Tensile fracture of cancellous bone*', Acta Orthopaedica Scandinavica, 51, 733-741, 1980.

[25] **Carter, D. S. and Hayes, W. C.**, '*The compressive behaviour of bone as a two-phase porous structure*', The Journal of Bone and Joint Surgery, 59-A, 7, 954-962, 1977.

[26] **Carter, D. R. and Hayes, W. C.**, '*Fatigue life of compact bone-I Effects of stress amplitude, temperature and density*', Journal of Biomechanics, 9, 27-34, 1976.

[27] **Carter, D. R. and Hayes, W. C.**, '*Compact bone fatigue damage-I. Residual strength and stiffness*', Journal of Biomechanics, 10, 325-337, 1977.

[28] **Carter, D. R. and Caler, W. E.**, '*A cumulative damage model for bone fracture*', Journal of Orthopaedics Research, 3, 84-90, 1985.

[29] **Carter, D. R. and Caler, W. E.**, '*Uniaxial fatigue of human cortical bone: The influence of tissue physical characterisitcs*', Journal of Biomechanics, 14, 461-470, 1981.

[30] **Chaboche, J. L.**, '*Continuum Damage Mechanics: Part 1 and 2- General Concepts*', Journal of Applied Mechanics, 55, 59-72, 1988.

[31] **Chaboche, J. L. and Lesne, P. M.**, '*A non-linear continuous fatigue damage model*', Fatigue and Fracture of Engineering Materials and Structures, 11, 1-17, 1988.

[32] **Chafetz, N., Baumrind, S., Murray, W. R, Genant, H. K, and Kron, E. L.**, '*Subsidence of the femoral prosthesis*', Clinical Orthopaedics and related research, 201, 60-67, 1985.

[33] **Chang, W. C. W., Christensen, T. M., Pinilla, T. P. and Keaveny, T. M.**, '*Uniaxial yield strains for bovine trabecular bone are isotropic and asymmetric*', Journal of Orthopaedic Research, 582-585, 1999.

[34] **Cheal, E. J., Hayes, W. C., Lee, C. H., Snyder, B. D. and Miller, J.**, '*Stress analysis of a condylar knee tibial component: Influence of metaphyseal shell properties and cement injection depth*', Journal of Orthopaedic Research, 424-434, 1985.

[35] **Cheng, Y. S. and Huang, Y.**, '*Measurement of continuous damage parameter*', Engineering Fracture Mechanics, 31, 199-209, 1988.

[36] **Choi, K., and Goldstein, S. A.**, '*A comparison of the fatigue behaviour of human trabecular and cortical bone tissue*', Journal of Biomechanics, 25, 12, 1371-1381, 1992.

[37] **Cristofolini, L., Viceconti, M., Cappello, A. and Toni, A.**, '*Mechanical validation of whole bone composite femur models*', Journal of Biomechanics, 29, 525-535, 1996.

[38] **Cristofolini, L. and Viceconti, M.**, '*Mechanical validation of whole bone composite tibia models*', Journal of Biomechanics, 33, 279-288, 2000.

[39] **Desai, C. S. and Abel, J. F.**, '*Introduction to the Finite Element Method - A numerical method for engineering analyis*', Van Nostrand Reinfold, 1972.

[40] **de Vree, J. H. P., Brekelmans, W. A. M. and van Gils, M. A. J.**, '*Comparison of nonlocal approaches in continuum damage mechanics*', Computers and Structures, 55, 581-588, 1995.

[41] **Dammak, M., Shirazi-adi, A. and Zukor, D. J.**, '*Analysis of cementless implants using interface nonlinear friction - Experimental and finite element studies*', Journal of Biomechanics, 30, 121-129, 1997.

[42] **Donnelly, W. J., Kobayashi, A., Freeman, M. A. R., Chin, T. W., Yeo, H., West, M. and Scott, G.**, '*Radiological and survival comparison of four methods of fixation of a proximal femoral stem*', Journal of Bone and Joint Surgery, 79-B, 351-360, 1997.

[43] **Ducheyne, P., Kagan, A. and Lacey, J. A.**, '*Failure of total knee arthroplasties due to loosening and deformation of the tibial component*', Journal of Bone and Joint Surgery, 60-A, 384-391, 1978.

[44] **Duparc, J., and Massin, P.**, '*Results of 203 total hip replacements using a smooth, cementless, femoral component*', The Journal of Bone and Joint Surgery, 74-B, 251-256, 1992.

[45] **Ewald, F. C.**, '*The Knee Society Total Knee Arthroplasty Roentgenographic Evaluation and Scoring System*', Clinical Orthopaedics and Related Research, 9-12, 248, 1989.

[46] **Engh, C. A., Massin, P. and Suthers, K.**, '*Roentgenographic Assessment of the Biologic Fixation of Porous-Surfaced Femoral Components*', Clinical Orthopaedics and Related Research, 257, 107-128, 1990.

[47] **Engh, C. A., Bobyn, J. D. and Glassman, A. H.**, '*Porous Coated Hip Replacement: The factors governing bone ingrowth, stress-shielding and clinical results*', The Journal of Bone and Joint Surgery, 69-B, 45-55, 1987.

[48] **Fatemi, A. and Yang, L.**, '*Cumulative fatigue damage and life prediction theories: a survey of the state of the art for homogeneous materials*', International Journal of Fatigue, 20, 9-34, 1998.

[49] **Fehring, T. K. and Valadie, A. L.**, '*Knee instability after total knee arthroplasty*', Clinical Orthopaedics, 299, 157-164, 1994.

[50] **Finlay, J. B., Bourne, R. B., Kraemer, W. J., Moroz, T. K. and Rorabeck, C. H.**, '*Stiffness of bone underlying the tibial plateaus of osteoarthritic and normal knees*', Clinical Orthopaedics and Related Research, 247, 193-201, 1989.

[51] **Fondrek, M., Bahniuk, E., Davy, D. T. and Phakey, P. P.**, '*Some viscoelastic characteristics of bovine and human cortical bone*', Journal of Biomechanics, 21, 623-630, 1988.

[52] **Ford, C. M. and Keaveny, T. M.**, '*The dependence of shear failure properties of trabecular bone on apparent density and trabecular orientation*', Journal of Biomechanics, 29, 1309-1317, 1996.

[53] **Freeman, M. A. R. and Plante-Bordeneuve, P.**, '*Early migration and late aseptic failure of proximal femoral prostheses*', Journal of Bone and Joint Surgery, 76-B, 432-438, 1994.

[54] **Garellick, G., Malachu, H. and Herberts, P.**, '*Survival of Hip Replacements: A Comparison of Randomized trial and a registry*', Clinical Orthopaedics and Related Research, 375, 157-167, 2000.

[55] **Garg, A. and Walker, P. S.**, '*The effect of the interface on the bone stresses beneath tibial components*', Journal of Biomechanics, 19, 957-967, 1986.

[56] **Gibson, L. J.**, '*The mechanical behaviour of cancellous bone*', Journal of Biomechanics, 18, 317-328, 1985.

[57] **Gibson, L. J. and Ashby, M. F.**, '*Cellular Solids: Structure and Properties* ', in Cancellous bone, Second Edition, Cambridge University Press, UK, 1997.

[58] **Grewal, R., Rimmer, M. G. and Freeman, M. A. R.**, '*Early migration of prostheses related to long-term survivorship*', Journal of Bone and Joint Surgery, 74-B, 239-242, 1992.

[59] **Griffin, L.**, '*Model of flexural fatigue damage accumulation of cortical bone*', Journal of Orthopaedic Research, 15, 607-614, 1997.

[60] **Goldstein, S. A., Wilson, D. L., Sonstegard, D. A. and Mathews, L. S.**, '*The mechanical properties of human tibial trabecular bone as a function of metaphyseal location*', Journal of Biomechanics, 16, 965-969, 1983.

[61] **Gruen, T. A., McNeice, G. M. and Amtustz, H. C.**, '*Modes of failure of cemented stem type femoral components: A radiographic Aanalysis of loosening*', Clnical Orthopaedics and Related Research, 141, 17-27, 1979.

[62] **Guo, X. D. E., McMohan, T. A., Keaveny, T. M., Hayes, W. C. and Gibson, L. J.**, '*Finite element modelling of damage accumulation in trabecular bone under cyclic loading*', Journal of Biomechanics, 27, 145-155, 1994.

[63] **Haddock, S. M., Yeh, O. C., Mummaneni, P .V., Rosenberg, W. S. and Keaveny, T. M.**, 2000, '*Fatigue behaviour of human vertrebral trabecular bone*', 46 th Annual Meeting, Orthopedic Research Society, March12-15, Orlando, Florida.

[64] **Harrigan, T. P., Jasty, M., Mann, R. W. and Harris, W. H.**, '*Limitations of the continuum assumption in cancellous bone.*', Journal of Biomechanics, 21, 269-275, 1988.

[65] **Hager, S. L. and Craig, T. A.**, '*Fatigue testing of high performance flexible polyurethane foam.*', Journal of Cellular Plastics, 28, 284-303, 1992.

[66] **Harris, W. H., McCarthy, J. C., Jr. and O' Neill, D. A.**, '*Femoral component loosening using contemporary techniques of femoral cement fixation*', The Journal of Bone and Joint Surgery, 64-A, 1063-1067, 1982.

[67] **Harte, A. M., Fleck, N. A. and Ashby, M. F.**, '*Fatigue failure of an open cell and a closed cell aluminium alloy foam.*', Acta Materiallica, 47, 2511-2524, 1999.

[68] **Havelin, L. I., Espehaug, B., Lie, S. A., Engesaeter, L. B., Furnes, O. and Vollset, S. E.**, 2000, '*Prospective studies of hip prostheses and cements : A presentation of the Norwegian arhroplasty register 1987-1999*', Scientific Exhibition presented at the 67th Annual Meeting of the American Academy of Orthopaedic Surgeons, March 15-19, Orlando, Florida, USA.

[69] **Hayes, W. C. and Carter, D. R.**, '*Post-yield behaviour of subchondral trabecular bone*', Journal Biomedical and Material Research, 10, 537-544, 1976.

[70] **Herberts, P. and Malachu, H.**, '*Long term registration has improved the quality of hip replacement*', Acta Orthopaedica Scandinavica, 71, 111-121, 2000.

[71] **Herberts, P., Ahnfelt, L., Malachu, H., Stromerg, C. and Andersson, G. B. J.**,'*Multicenter clinical trials and their value in assessing total joint arthroplasty*', Clinical Orthopaedics and Related Research, 249, 48-55, 1989.

[72] **Hilding, M. B., Lanshammer, H., and Ryd, L.**, '*Knee joint loading and tibial component loosening. RSA and gait analysis in 45 osteoarthritic patients before and after TKA*', The Journal of Bone Joint and Surgery, 78-B, 66-73, 1996.

[73] **Hilding, M. B., Yuan, X. and Ryd, L.**, '*The stability of three different cementless tibial components*', Acta Orthopaedica Scandinavica, 66, 21-27, 1995.

[74] **Hodgeskinson, R. and Currey, J. D.**, '*Young's modulus, density and material properties in cancellous bone over a large density range*', Journal of Materials Science: Materials in Medicine, 3, 377-381, 1992.

[75] **Huang, J. S. and Lin, J. Y.**, '*Fatigue of cellular materials*', Acta Materiallica, 44, 289-296, 1996.

[76] **Huang, J. S. and Gibson, L. J.**, '*Creep of Polymer foams*', Journal of Materials Science, 26, 637-647, 1991.

[77] **Huang, J. S. and Liu, S. Y.**, '*Fatigue of isotropic open-cell foams under multiaxial loads*', International Journal of Fatigue, 23, 233-240, 2001.

[78] **Huang, J. S. and Gibson, L. J.**, '*Creep of open-cell Voronoi foams*', Materials Science and Engineering, A339, 220-226, 2003.

[79] **Huiskes, R. and Kaastad, T. S.**, '*Management of fracturres in severely osteoporotic bone: Orthopaedic and pharmecological strategies*', in Biomechanics, Bone quality and Strength, Edited by Obrant, K., 54-72, Springer Verlag, 2000.

[80] **Huiskes, R., and Verdonschot, N.**, '*The Adult Hip*', in Failure Scenarios and the Innovation Cycle, Edited by Callaghan, J. J., Rosenberg, A. G., and Rubash, H. E., 171-186, Lippincott-Raven Publishers,, 1998.

[81] **Huiskes, R.**, '*Stress patterns around femoral stems*', Clinical Orthopaedics and Related Research, 261, 27-38, 1990.

[82] **Huiskes, R.**, '*Biomechanics of Artificial Joint Fixation*', in Basic Orthopaedic Biomechanics, Edited by Mow, V. C., and Hayes, W. C., Raven Press, 1993.

[83] **Hvid, I.**, '*Trabecular bone strength at the knee*', Clinical Orthopaedics and Related Research, 227, 210-221, 1988.

[84] **Ibijola, E. A.**, '*On some fundamental concepts of continuum damage mechanics*', Computer methods in Applied Mechanics and Engineering, 191, 1505-1520, 2002.

[85] **Joshi, M. G.**, '*Survey of stress analysis of the femoral hip prostheses*', ASME - Applied Mechanics Review, 53, 1-18, 2000.

[86] **Kachanov, L. M.**, '*On creep rupture time*', Proc. Acad. Sci. USSR Div. Engng. Sci, 8, 26-31, 1958.

[87] **Kachanov, L. M.**, '*Introduction to Continuum Damage Mechanics*', Martinus Nijhoff, 1986.

[88] **Kanny, K., Mahfuz, H., Carlsson, L. A., Thomas, T. and Jeelani, S.**, '*Dynamic and mechanical analyses and flextural fatigue of PVC foams*', Composite Structures, 58, 175-183, 2002.

[89] **Kanny, K., Mahfuz, H., Carlsson, L. A., Thomas, T. and Jeelani, S.**, '*Static and dynamic characterization of polymer foams under shear loads*', Journal of Composite Materials, 38, 2004.

[90] **Kaplan, S., Hayes, W. C., Stone, J. L. and Beaupre, G. S.**, '*Tensile strength of trabecular bone*', Journal of Biomechanics, 18, 723-727, 1985.

[91] **Karrholm, J., Borssen, B., Lowenhelm, G. and Snorasson, F.**, '*Does early micromotion of femoral stem prostheses matter?*', The Journal of Bone and Joint Surgery, 76-B, 912-917, 1994a.

[92] **Karrholm, J., Malchau, H., Gothenberg, Snorrason, F., and Herberts, P.**, '*Micromotion of femoral stems in total hip arthroplasty*', The Journal of Bone and Joint Surgery,76-A, 1692-1705, 1994.

[93] **Kawamura, H., Dunbar, M. J., Murray, P., Bourne, R. B. and Rorabeck, C. H.**, '*The Porous Coated Anatomic Total Hip Replacement: A ten to fourteen years follow-up study of a cementless total hip arthroplasty*', The Journal of Bone Joint and Surgery, 83-A, 1333-1338, 2001.

[94] **Keaveny, T. M.and Hayes, W. C.** '*A 20-Year Perspective on the mechanical properties of trabecular Bone*, Transaction of ASME - Journal of Biomechanical Engineering, 115, 534-542, 1993.

[95] **Keaveny, T. M., Guo, X. E., Wachtel, E. F., McMohan, T. A. and Hayes, W. C.**,'*Trabecular bone exhibits fully linear elastic behaviour and yields at low strains*, Journal of Biomechanics, 27(9), 1127-1136, 1994.

[96] **Keaveny, T. M., Borchers, R. E., Gibson, L. J. and Hayes, C. H.**, '*Theoretical analysis of the experimental artifact in trabecular bone compressive modulus*', Journal of Biomechanics, 26, 599-607, 1993.

[97] **Keaveny, T. M., Wachtel, E. F., Ford, C. M. and Hayes, W. C.**, '*Differences between the tensile and compressive strengths of bovine tibial trabecular bone depend on modulus*', Journal of Biomechanics, 27, 1137-1146, 1994.

[98] **Keller, T. S.**, '*Predicting the compressive mechanical behavior of bone*', Journal of Biomechanics, 27, 1159-1168, 1994.

[99] **Kelser, O., Crews, L. K. and Gibson, L. J.**, '*Creep of sandwich beams with metallic foam cores*', Materials Science and Engineering, 27, A341, 264-272, 2003.

[100] **Khaw, F. M., Kirk, L. M. G. and Gregg, P. J.**, '*Survival analysis of cemented press-fit condylar total knee arthroplasty*', The Journal of Arthroplasty, 16, 161-167, 2001.

[101] **Kiss, J., Murray, D. W., Turner-Smith, A. R., Bithell, J. and Bulstrode, C. J.**, '*Migration of cemented femoral components after THR-Roentgen stereophotogrammetric analysis*', The Journal of Bone Joint and Surgery, 78-B, 796-801, 1996.

[102] **Kopperdahl, D. and Keaveny, T. M.**, '*Yield strain behaviour of trabecular bone*', Journal of Biomechanics, 31, 601-608, 1998.

[103] **Krajcinovic, D. and Mastilovic, S.**, '*Some fundamental issues of damage mechanics*', Mechanics of Materials, 21, 217-230, 1995.

[104] **Krismer, M., Beidermann, R., Stockl, B., Fischer, M., Bauer, R. and Haid, C.**, '*The prediction of failure of the stem in THR by measurement of early migration using EBRA-FCA*', Journal of Bone and Joint Surgery, 81-B, 2, 273-280, 1999.

[105] **Lee, R. W., Volz, R. G. and Sheridan, D. C.**, '*The role of fixation and bone quality on the mechanical stability of tibial components*', Clinical Orthopaedics and Related Research, 273, 177-183, 1991.

[106] **Lee, T. Q., Barnett, S. L. and Kim, W. C.**, '*Effects of screw types in cementless fixation of tibial tray implants: stability and strength assessment*', Clinical Biomechanics, 14, 258-264, 1999.

[107] **Lemaitre, J. and Dufially, J.**, '*Damage measurements*', Engineering Fracture Mechanics, 28, 643-661, 1987.

[108] **Lemaitre, J.**, '*Local approach to fracture*', Engineering Fracture Mechanics, 25, 523-537, 1986.

[109] **Lemaitre, J.**, '*A continuous damage mechanics model for ductile fracture*', Journal of Engineering Materials and Technology, 107, 83-89, 1985.

[110] **Lemaitre, J.**, '*How to use damage mechanics*', Nuclear Engineering Design, 80, 233-245, 1984.

[111] **Linde, F., Norgaard, P., Hvid, I., Odgaard, A., and Soballe, K.**, '*Mechanical properties of trabecular bone. Dependency on strain rate*', Journal of Biomechanics, 24, 803-809, 1991.

[112] **Linde, F.**, '*Elastic and viscoelastic properties of trabecular bone by a compression testing approach*', Danish Medical Bullettin, 41, 119-138, 1993.

[113] **Liow, R .Y and Murray, D. W.**, '*Which knee replacement?*', Annals of the Royal College of Surgeons of England, 79(5), 335-340, 1997.

[114] **Loudon, J. R., and Charnley, J.**, '*Subsidence of the femoral prostheses in total hip replacement in relation to the design of the stem*', The Journal of Bone Joint and Joint Surgery, 62-B, 4, 450- 453, 1980.

[115] **Lucht, U.**, '*Danish Hip Arthroplasty Register*', Acta Orthopaedica Scandinavica, 71, 433-439, 2000.

[116] **Maher, S. A., Prendergast, P. J., and Lyons, C. G.**, '*Measurement of the migration of a cemented hip prostheses in an in vitro test*', Clinical Biomechanics, 16, 307-314, 2001.

[117] **Maher, S. A. and Prendergast, P. J.**, '*Discriminating the loosening behaviour of cemented hip prostheses using measurement of migration and inducible displacement*', Journal of Biomechanics, 35, 257-265, 2002.

[118] **Malachu, H., Herberts, P., Soderman, P. and Oden, A.**, 2000, '*Prognosis of Total Hip Replacement: Update and validation of results from the Swedish National Hip Arthroplasty Registry 1979-1998*', Scientific Exhibition Presented at the 67th Annual Meeting of the American Academy of Orthopaedic Surgeons, March15-19, Orlando, USA.

[119] **Malachu, H., Karrholm, J., Wang, Y. X., and Herberts, P.**, '*Accuracy of migration Analysis in hip arthroplasty: Digitized and conventional radiography, compared to radiostereometry in 51 patients*', Acta Orthopaedica Scandinevica, 66(5), 418-423, 1995.

[120] **Mao, H. and Mahadevan, S.**, '*Fatigue damage modelling of composite materials*', Composite structures, 58, 405-410, 2002.

[121] **Martens, M., Van Audekercke, R. L., Delport, P., de Meester, P. and Mulier, J. C.**, '*The mechanical characteristics of cancellous bone at the upper femoral region*', Journal of Biomechanics, 16, 971-983, 1983.

[122] **McBeath, A. A., Schopler, S. A. and Narechania, R. G.**, '*Circumferential and axial strain in the proximal femur- Effect of Prothesis type and position*',Clinical Orthopaedics and Related Research, 150, 301-305, 1980.

[123] **Memon, I. R., Zhang, X. and Cui, D.**, '*Fatigue life prediction of 3-D problems by damage mechanics with two-block loading*', International Journal of Fatigue, 24, 29-37, 2002.

[124] **Michel, M. C., Gou, X. E., Gibson, L. J., McMahon, T. A. and Hayes, W. C.**, '*Compressive fatigue behaviour of bovine trabecular bone*', Journal of Biomechanics, 26, 453-463, 1993.

[125] **Miner, M. A.**, '*Cumulative fatigue damage in fatigue*', Journal of Applied Mechanics - Trnasactions of ASME, 67, 159-164, 1945.

[126] **Mitts, K., Muldoon, M. P., Gladden, M. and Padgett, D. E.**, '*Instability after total knee arthroplasty with the Miller-Gallante II total knee*', The Journal of Arthroplasty, 16, 422- 427, 2001.

[127] **Mjoberg, B.**, '*Fixation and loosening of hip prostheses- A review*', Acta Orthopaedica Scandinavica, 62, 500-508, 1991.

[128] **Mjoberg, B., Selvik, G., Hansson, L. I., Rosenqvist, R., and Onnerham, R.**, '*Mechanical loosening of total hip prostheses- A radiographic and roentgen stereophotogrammetric study*', The Journal of Bone and Joint Surgery, 68-B, 770-774, 1986.

[129] **Mjoberg, B., Franzen, H. and Selvik, G.**, '*Early detection of prosthetic-hip loosening- Comparison of low and high viscosity bone cement*', Acta Orthopaedica Scandinavica, 61(3), 273-274, 1990.

[130] **Moore, T. L. A. and Gibson, L. J.**, '*Microdamage accumulation in bovine trabecular bone in uniaxial compression*', Journal of Biomechanical Engineering, 124, 63-71, 2002.

[131] **Morgan, E. F. and Keaveny, T. M.**, '*Dependence of yield strain of human trabecular bone on anatomic site*', Journal of Biomechanics, 34, 569-577, 2001.

[132] **Morrison, J. B.**, '*The mechanics of the knee in relation to normal walking*', Journal of Biomechanics, 51-61, 1970.

[133] **Murray, D. W., Carr, A. J., and Bulstrode, C. J.**, '*Which Primary Total Hip Replacement?*', Journal of Bone and Joint Surgery, 877-B, 4, 520-527, 1995.

[134] **Nafei, A., Nielsen, S., Kristensen, O. and Hvid, I.**, '*The press-fit kinemax knee prostheses: High failure rate of non-cemented implants*', Journal of Bone and Joint Surgery, 74-B, 243-46, 1992.

[135] **Nistor, L., Blaha, J. D., Kjelstrom, U., Selvik, G.**, '*In vivo Measurements of relative motion between an uncemented femoral total hip component and the femur by roentgen stereophoyogrammetric analysis*', Clinical Orthopaedics and Related Research, 269, 220-227, 1991.

[136] **Odgaard, A. and Linde, F.**, '*The underestimation of Young's modulus in compressive testing of cancellous bone specimens*', Journal of Biomechanics, 24, 691-698, 1991.

[137] **Oh, I. and Harris, W. H.**, '*Proximal strain distribution in the loaded femur*', The Journal of Bone and Joint Surgery, 60-A, 75-85, 1978.

[138] **Paas, M. H. J. W., Schreurs, P. J. G. and Janssen, J. D.**, '*The application of continuum damage mechanics to fatigue failure mechanisms*', Integration of Theory and Applications in Applied Mechanics, Kluwer Academic Publishers, 49-63, 1990.

[139] **Pattin, C. A., Caler, W. E., and Carter, D. R.**, '*Cyclic mechanical property degradation during fatigue loading of cortical bone*', Journal of Biomechanics, 29, 69-79, 1996.

[140] **Perillo-Marcone, A., Ryd, R., Johnsson, K. and Taylor, M.**, '*A combined RSA and FE study of the implanted proximal tibia: correlation of the post-operative mechanical environment with implant migration*', Journal of Biomechanics, Article in Press.

[141] **Philips, T. W. and Messieh, S. S.**, '*Cementless hip replacement for arthritis: Problems with a smooth surface Moore stem*', Journal of Bone and Joint Surgery, 70-B, 750-755, 1988.

[142] **Philips, T. W., Nguyen, L. T. and Munro, S. D.**, '*Loosening of cementless femoral stems: A biomechanical analysis of immediate fixation with loading vertical, femur horizontal*', Journal of Biomechanics, 24, 37-48, 1991.

[143] **Philips, T. W., Messieh, S. S. and McDonald P. D.**, '*Femoral stem fixation in hip replacement: A biomechanical comparison of cementless and cemented prostheses*', Journal of Bone and Joint Surgery, 72-B, 431-434, 1990.

[144] **Pidaparti, R. M. V., Merril, B. A. and Downton, N. A.**, '*Fracture and material degradation properties of cortical bone under accelerated stress*', Journal of Biomedical and Materials Research, 37, 161-165, 1997.

[145] **Pilliar, R. M., Lee, J. M. and Maniatopoulos, C.**, '*Observation on the effect of movement of bone ingrowth into porous-surfaced implants*', Clinical Orthopaedics and Related Research, 208, 108-113, 1986.

[146] **Pitter, M. A., Faris, P. M., Keating, E. M. and Meding, J. B.**, '*Post-operative alignment of total knee replacement: Its effect on survival* ', Clinical Orthopaedics and Related Research, 299, 153-156, 1994.

[147] **Peerlings, R. H. J., Brekelmans, W. A. M., de Borst, R. and Geers, M. G. D.** , '*Gradient enhanced damage modelling of high cycle fatigue* ', International Journal for Numerical Methods in Engineering, 49, 1547-1569, 2000.

[148] **Peerlings, R. H. J., de Borst, R., Brekelmans, W. A. M. and Geers, Spee, I.**, '*Some observation on localisation in non-local and gradient damage models*', European Journal of Mechanics. A/Solids, 15, 937-953, 1996.

[149] **Ramamurti, B. S., Orr, T. E., Bragdon, C. R., Lowenstein, J. D. and Jasty, M.**,'*Factors influencing the stability at the interface between a porous surface and cancellous bone: A finite element analysis of a canine in vivo micromotion experiment*', Journal of Biomedical Material Research, 36, 374-380, 1997.

[150] **Rakotamanana, P. F., Curnier, A., Leyvraz, P. F., Heeggard, J. H. and Rubin, P. J.**, '*A finite element model for evaluation of tibial prosthesis-bone interface in total knee replacement*', Journal of Biomechanics, 25, 1413-1424, 1992.

[151] **Reilly, D., Walker, P. S., Ben-Dov, M. and Ewald, F. C.**, '*Effect of tibial components on load transfer in the upper tibia*', Clinical Orthopaedics and Related Research, 165, 273-282, 1982.

[152] **Rice, J. C., Cowin, S. C. and Bowman, J.**, '*On the dependence of the elasticity and strength of cancellous bone on apparent density*', Journal of Biomechanics, 21, 155-168, 1988.

[153] **Van Rietbergen, B., Muller, R., Ulrich, D., Ruegsegger, P. and Huiskes, R.**, '*Tissue stresses and strain in trabeculae of a canine proximal femur can be quantified from computer reconstructions*', Journal of Biomechanics, 32, 165-173, 1999.

[154] **Rimnac, C. M., Petko, A. A., Santner, T. J. and Wright, T. M.**, '*The effect of temperature, stress and microstructure on the creep of compact bone* ', Journal of Biomechanics, 26, 219-228, 1993a.

[155] **Robertsson, O., Lewold, S., Knutson, K. and Lidgren, L.**, '*The Swedish Knee Arthroplasty Project*', Acta Orthopaedica Scandinevica, 71, 7-18, 2000.

[156] **Rohl, L., Larsen, E., Linde, F., Odgaard, A., and Jorgensen, J.**, '*Tensile and compressive properties of cancellous bone*', Journal of Biomechanics, 24(12), 1143-1149, 1991.

[157] **Ryd, L.**, '*Micromotion in knee arthroplasty: A rontegen stereophotogrammetric analysis of tibial component fixation*', Acta Orthopaedica Scandinavica, 1986, Supplement 220.

[158] **Ryd, L., Albrektsson, B. E. J., Herberts, P., Lindstrand, A. and Selvik, G.**, '*Micromotion of noncemented Freeman-Samuelson knee prostheses in gonarthrosis- A roentgen stereophotogrammetric analysis of eight successful cases*', Clinical Orthopaedics and Related Research, 229, 205-212, 1988.

[159] **Ryd, L., Albrektsson, B. E. J., Carlsson, L., Dansgard, F., Herberts, P., Lindstrand, A., Regner, L., Toksvig-Larsen, S.**, '*Roentgen stereophotogrammetric analysis as a predictor of mechanical loosening of knee prostheses*', The Journal of Bone and Joint Surgery, 77-B, 377-383, 1995.

[160] **Ryd, L., Linder, L.**, '*On the correlation between micromotion and histology of the bone- Cement Interface*', The Journal of Arthroplasty, 4, 303-309, 1989.

[161] **Ryd, L., Lindstrand, A., Rosenquist,R., and Selvik, G.**, '*Micromotion of conventionally cemented all polyethylene tibial components in total knee replacements- A roentgen stereophotogrammetric analysis of migration and inducible displacements*', Archieves of Orthpaedic and Traumatic Surgery, 106, 82-88, 1987.

[162] **Sala, M., Taylor, M. and Tanner, K. E.**, '*Torsional stability of primary total knee replacement tibial prostheses* ', The Journal of Arthroplasty, 14, 610-615, 1999.

[163] **Sauer, J. A. and Richardson, G. C.**, '*Fatigue of polymers*', International Journal of Fracture, 16, 499-532, 1980.

[164] **Shen, Y., Golnaraghi, F. and Plumtree, A.**, '*Modelling compressive cyclic stress-strain behaviour of structural foam*', International Journal of Fatigue, 23, 491-497, 2001.

[165] **Schneider, E., Eulenberger, J., Steiner, W., Wyder, D., Freiedman, R. J. and Perren, S. M.**, '*Experimental method for the in vitro testing of the initial stability of cementless hip prostheses*', Journal of Biomechanics, 22, 735-744, 1989.

[166] **Schroder, H. M., Berthelsen, A., Hassani, G., Hansen, E. B., Solgaard, S.**, '*Cementless porous coated total knee arthroplasty*', Journal of Arthroplasty, 16(5), 559-567, 2001.

[167] **Sharp, D. J. and Porter, K. M.**, '*The Charnely total hip arthroplasty in patients under age 40*', Clinical Orthopaedics and Related Research, 201, 51-56, 1985.

[168] **Shirazi-adi, A., Patenaude, O., Dammak, M. and Zukor, D.**, '*Experimental and finite element comparison of various fixation designs in combined loads*', Journal of Biomechanical Engineering, 123, 391-395, 2001.

[169] **Shenoi, R. A., Allen, H. G. and Clark, S. D.**, '*Cyclic creep and creep-fatigue interaction in sandwich beams*', Journal of Strain Analysis, 32, 1-18, 1997.

[170] **Simoes, J. A. Q., Vaz, M. A., Chousal, J. A. G., Taylor, M., and Blatcher, S.**, 1997, '*Speckle interferometry to measure the strain distribution within porous materials*', International Conference on Advanced Technology in Experimental Mechanics, JSME-MMD, Japan.

[171] **Soballe, K., Toksvig-Larsen, S., Gelineck, J., Fruensgaard, Hansen, E. S., Ryd, L., Lucht, U., and Bunger, C.**, '*Migration of hydroxiapatite coated femoral prostheses*', The Journal of Bone and Joint Surgery, 75-B, 5, 681-687, 1993.

[172] **Speirs, A. D., Slomczykowski, M. A., Orr, T. E., Seibenrock, K., Nolte, L. P.**, '*Three dimensional measurement of cemented femoral stability: an in vitro cadaver study*', Clinical Biomechanics, 15, 248-255, 2000.

[173] **Stolk, J., Verdonschot, N., Mann, K. A. and Huiskes, R.**, '*Prevention of mesh dependent damage growth in finite element simulations of crack formations in acrylic bone cement*', Journal of Biomechanics, 36, 861-871, 2003.

[174] **Stolk, J., Verdonschot, N., Murphy, B. P., Prendergast, P. J. and Huiskes, R.**, '*Finite element simulation of anisotropic damage accumulation and creep in acrylic bone cement*', Engineering Fracture Mechanics, 2004.

[175] **Stone, J. L., Beaupre, G. S. and Hayes, W. C.**, '*Multiaxial strength characteristics of trabecular bone*', Journal of Biomechanics, 16, 743-752, 1983.

[176] **Swedish Knee Arthroplasty Register**, 2002 '*Annual Report*', 1-23.

[177] **Szivek, J. A., Thomas, M., and Benjamin,J. B.**, '*Technical note: Characterization of a synthetic foam as a model for human cancellous bone*', Journal of Applied Biomaterials, 4, 269-272, 1993.

[178] **Szivek, J. A., Thomas, M. and Benjamin,J. B.**, '*Characterization of three formulations of a synthetic foam as models for a range of human cancellous bone types*', Journal of Applied Biomaterials, 6, 125-128, 1995.

[179] **Taylor, D. and Kuiper, J. H.**, '*The prediction of stress fractures using a 'stresed volume' concept*', Journal of Orthopaedic Research, 19, 919-926, 2001.

[180] **Taylor, M., Tanner, K. E., Freeman, M. A. R. and Yettram, A. L.**, '*Cancellous bone stresses surrounding the femoral component of a hip prosthesis: an elastic-plastic finite element analysis*', Med. Eng. Phys., 17, 544-550, 1995.

[181] **Taylor, M. and Tanner,K. E.**, '*Fatigue failure of cancellous bone: a possible cause of implant migration and loosening*', The Journal of Bone and Joint Surgery, 79-B, 181-182, 1997.

[182] **Taylor, M., Tanner, K. E., Freeman, M. A. R. and Yettram, A. L.**, '*Finite Element Analysis of the Implanted Tibia: A relationship between the initial cancellous bone stresses and implant migration*', Journal of Biomechanics, 31, 303-310, 1998.

[183] **Taylor, M., Verdonschot, N., Huiskes, R. and Zioupos, P.**, '*A Combined finite element method and continuum damage mechanics approach to simulate the in vitro fatigue behaviour of human cortical bone*', Journal of Materials Science: Materials in Medicine, 12, 841-846, 1999.

[184] **Taylor, M., Cotton, J. and Zioupos, P.**, '*Finite Element Simulation of the Fatigue Behaviour of Cancellous Bone*', Meccanica, 37, 419-429, 2002.

[185] **Tisakht, M., Eskandari, H. and Ahmed, M.**, '*Micromotion analysis of the fixation of total knee tibial component*', Computers and Structures, 56, 365-375, 1995.

[186] **Turner H. C**, '*Is yield strain in cancellous bone isotropic?*', Journal of Biomechanics, 28, 763, 1995.

[187] **Tsukayama, D. T., Estrado, R. and Ramon, B.**, '*Infection after total hip arthroplasty*', he Journal of Bone and Joint Surgery, 78-A, 512-522, 1996.

[188] **Volz, R. G., Lee, R. W. and McMurthy, G.**, '*The mechanical stability of various noncemented tibial components*', Clinical Orthopaedics and Related Research, 226, 38-42, 1988.

[189] **Verdonschot, N. and Huiskes, R.**, '*Subsidence of the THA stems due to acrylic cement creep in extremely sensitive to interface friction*', Journal of Biomechanics, 29, 1569-1575, 1996.

[190] **Verdonschot, N. and Huiskes, R.**, '*The effect of cement-stem debonding in THA on the long term failure of probability of cement*', Journal of Biomechanics, 30, 795-802, 1997.

[191] **Verdonschot, N. and Huiskes, R.**, '*The application of continuum damage mechanics to pre-clinical testing of cemented hip prostheses: The effects of cement/stem debonding*', 51-56.

[192] **Vince, K. G., Insall, J. N. and Kelly, M. A.**, '*The total condylar prostheses*', The Journal of Bone and Joint Surgery, 71-B, 793-797, 1989.

[193] **Visnic, C. D., Reid, R. H. and Di Gioia, A. M.**, '*Finite element preoperative simulation of cementless hip implant*', 1994, Proceedings of the 1994 Winter Simulation Conference, Edited by New, J. D., Manivannan, S., Sadowski, D. A. and Seila, A. F, 856-860.

[194] **Walker, P. S., Mai, S. F., Cobb, A. G., Bentley, G. and Hua, J.**, '*Prediction of clinical outcome of the THR from migration measurements on standard radiographs: A study of cemented Charnley and Stanmore Femoral Stems*', Journal of Bone and Joint Surgery, 77-B, 705-714, 1995.

[195] **Walker, Sathasivam, S., Cobb, A., Learmonth, I. D., Grobler, G. P., Pinder, I. M., Marchetti, N., Spinelli, M. D. and Welsby, A.**, '*A comparison between cemented, press-fit, and HA coated interfaces in Kinemax total knee replacement*', The Knee, 71-78, 2000.

[196] **Walker, P. S. Schneeweis, D., Murphy, S. and Nelson, P.**, '*Strains and micromotions of press-fit femoral stem prostheses*', Journal of Biomechanics, 20, 693-702, 1987.

[197] **Walker, P. S., Greene, M .S., Reilly, D., Thatcher, B. S. and Ewald, F. C.**, '*Fixation of tibial components of knee prostheses*', The Journal of Bone and Joint Surgery, 63-A, 258-267, 1981.

[198] **Wachtel, E. F. and Keaveny, T. M.**, '*Dependence of Trabecular Damage on Mechanical Strain*', Journal of Orthopaedic Research, 15, 781-787, 1997.

[199] **Whiteside, L. A. and Pafford, J.**, '*Load transfer characteristics of a noncemented total knee arthroplasty* ', Clinical Orthopaedics and Related Research, 239, 168-177, 1989.

[200] **Windsor, R. E, Scuderi, G. R., Moran, M. C., and Insall, J. N.**, '*Mechanism of failure of the femoral and tibial components in total knee arthroplasty*', Clinical Orthopedics and Related Research, 248, 15-20, 1989.

[201] **Wixson, R. L., Elasky, N., and Lewis, J.**, '*Cancellous bone material properties in osteoarthritic and rhuematoid total knee patients*', Journal of Orthopaedic research, 7, 885- 892, 1989.

[202] **Yang, L. and Fatemi, A.**, '*Cumulative fatigue damage mechanisms and quantifying parameters: A literature review*', Journal of Testing and Evaluation, 26, 89-100, 1998.

[203] **Yeh, O. C., and Keaveny, T. M.**, '*Relative roles of microdamage and microfracture in the mechanical behaviour of trabecular bone*', Journal of Orthopaedic Research, 19, 1001-1007, 2001.

[204] **Vajjhala, S., Kraynik, A. M. and Gibson, L. J.**, '*A cellular solid model for modulus prediction due to resorption of trabecular bone*', Journal of Biomechanical Engineering, 122, 511-515, 2000.

[205] **Zettle, B., Mayer, H., Stanzl-Tschegg, S. E. and Degischer, H. P.**, '*Fatigue properties of aluminium foams at high number of cycles*', Materials Science and Engineering, A292, 1-7, 2000.

[206] **Zilch, H., Rohlmann, A., Bergmann, G. and Klbel, R.**, '*Material properties of femoral cancellous bone in axial loading Part2: Time dependent properties*', Archieves of Orthopaedic and Traumatic Surgery, 97, 257-262, 1980.

[207] **Zioupos, P., Wang, X. T., and Currey, J. D.**, '*The accumulation of fatigue microdamage in human cortical bone of two different ages in vitro*', Clinical Biomechanics, 11, 365-375, 1996.

[208] **Zioupos, P., Currey, J. D., and Casions, A.**, '*Tensile fatigue in bone: Are cycles-, or time to failure, or both, important?*', Journal of Theoretical Biology, 210, 389-399, 2001.

Appendix A

The Algorithm for FE Simulation of Uniaxial Fatigue Tests

A.1 Introduction

A combined Finite Element and Continuum Damage Mechanics method for the simulation uniaxial fatigue tests was discussed in Chapter 6. The algorithm used for the simulation, made an effective use of the user defined subroutines in MSc.Marc. The option of user defined subroutine is provided in MSc.Marc for model definition, analysis and post-processing. The sequence of use of various subroutines in the the algorithm, their function in MSc.Marc and the purpose of use in the present fatigue simulation is presented pictorially (Figure B.1). The algorithm, coded in Fortran, for the uniaxial fatigue simulations, is also presented in this Appendix. Appropriate modification were made in the presented coding, for the creep analysis of uniaxial models and also for the migration simulations.

In Chapter 6, various aspects of fatigue simulations were discussed using the material model of Solid Rigid PU foam. The results from the simulation of uniaxial models of Herex foam are also presented in this Appendix. Only a brief discussion of the results was carried out, as the general characteristics of the model behaviour was similar to Solid Rigid PU foam models.

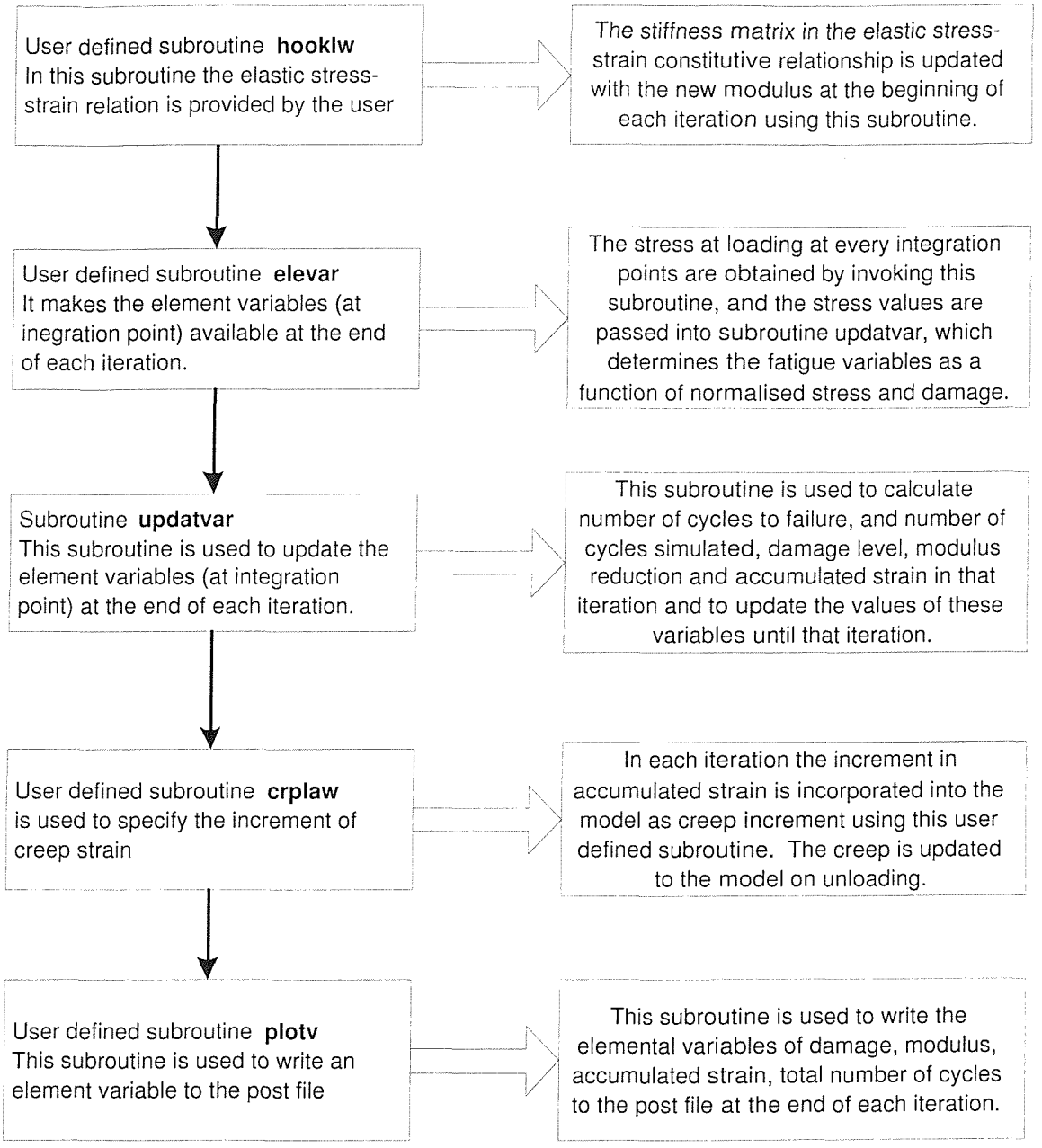

FIGURE A.1: A representation of the details of subroutines used in the algorithm, their purpose and application in the present analyses.

```
      Subroutine hooklw(m1,nn,lay,b,ngens1,dt,dtdl,e,pr, ndi,nshear,imod,rprops,iprops)
C     ******************************************************
C     SUBROUTINE IS CALLED BY Marc ISOTROPIC OPTION
C     FOR EACH INTEGRATION POINT
C     SUBROUTINE SET THE MODULUS OF THE MATERIAL TO INITIAL
C     THIS SUBROUTINE SET THE MODULUS OF THE MATERIAL TO INITIAL
C     SECANT MODULUS IN THE ZERO AND FIRST INCREMENT, OR UPDATE
C     TO THE NEW MODULUS IN THE LOADING INCREMENT OF EACH
C     ITERATION. THE STRESS-STRAIN CONSTITUTIVE RELATIONSHIPS
C     FOR AN ELASTIC ISOTROPIC MATERIAL IS ALSO DEFINED.
C     ******************************************************
      implicit real*8 (a-h,o-z)
      include 'far'
      include 'dimen'
      include 'matdat'
      include 'blnk'
      include 'concom'
      include 'creeps'
      include 'nzro1'
      logical vfthklw,vftelevar,vftimpd,vftposth,vftevec,schrijf
      dimension b(ngens1,ngens1),dt(1),dtdl(1),rprops(1),iprops(1),m1(2)
      common/usdam/usdama(1)
      common/usmod/usmoda(1)
      common/usmodnew/usmodnew(1)
      common/torc/torc(1)
      common/tx/tx(1)
      common/ ymod/ ymod
      common /modparams/pa1, pa2, pb1, pb2, pc1, pc2
      common /features/ iydamage, iymoddeg, iyplastic, nincpcycl
      common /einit/ einit(1)
      DIMENSION ps(3),str(3,3),varint(8),varnod(8)
      REAL maxschuif
C     *********************************************
C      m - element number
C      numel - total number of elements
C      nn - number of integration point
C      inc - increment number
C      e - Young's modulus
C      pr - Poisson's ratio
C      einit (k) - initial secant modulus
C      usmoda (k) - modulus of the material at integration point k
C      iymoddeg - variable assigned with a value of 1, so that
C      modulus get updated at the loading increment of each iteration
C      usdama(k) - total damage at integration point k
C     *********************************************
      if (m .eq. 1) write(*,*) 'in hooklw', nn
      k = m + (nn - 1)*numel
C     *********************************************
C     assigns initial modulus to the material in the
C     0 and 1st increment or updates modulus in the subsequent
C     iterations at the loading increment.
C     *********************************************
```

```
53.              if(inc .le. 1)then
54.                    ymod = e
55.                    einit(k) = e
56.                    usmoda(k)=ymod
57.              else
58.                    if (mod(inc,nincpcycl) .eq. iymoddeg) then
59.                          ymod = usmodnew(k)
60.                          usmoda(k) = ymod
61.                    else
62.                          ymod = usmoda(k)
63.                    endif
64.              endif
65. C            ***********************************************
66. C            provides the option to reduce the modulus once
67. C            the element is broken(usdama (k)=1). The
68. C            modulus is kept unchanged in the default model
69. C            ***********************************************
70.             if (usdama(k) .ge. 1.0 .and.
71.      +             mod(inc,nincpcycl) .eq. iydamage) then
72.                   ymod = usmoda(k)/1.
73.                   usmoda(k) = ymod
74.             endif
75. C            ***********************************************
76. C            defines the stress-strain constitutive matrix
77. C            for a linear isotropic material
78. C            ngens1 - number of stress strain components
79. C            ***********************************************
80.             gg= ymod/(2*(1+pr))
81.             b11 = 1/ymod
82.              b12 = -pr/ymod
83.             b33 = 1/gg
84.             if (ngens1.eq.3) then
85.             b(1,1)= b11
86.             b(1,2)= b12
87.             b(2,2)= b11
88.             b(3,3)= b33
89. c           symmetric and zero part of constitutive matrix
90.             b(1,3)= 0.0
91.             b(2,3)= 0.0
92.             b(2,1)= b12
93.             b(3,1)= 0.0
94.             b(3,2)= 0.0
95.             else
96.             if (ngens1.eq.4) then
97.             b(1,1)= b11
98.             b(2,2)= b11
99.             b(3,3)= b11
100.            b(1,2)= b12
101.            b(1,3)= b12
102.            b(2,3)= b12
103.            b(4,4)= b33
104. c          symmetric and zero part of constitutive matrix
```

```
105.            b(2,1)= b12
106.            b(3,1)= b12
107.            b(3,2)= b12
108.            b(1,4)= 0.0
109.            b(4,1)= 0.0
110.            b(2,4)= 0.0
111.            b(4,2)= 0.0
112.            b(3,4)= 0.0
113.            b(4,3)= 0.0
114.            else
115.            b(1,1)= b11
116.            b(2,2)= b11
117.            b(3,3)= b11
118.            b(1,2)= b12
119.            b(1,3)= b12
120.            b(2,3)= b12
121.            b(4,4)= b33
122.            b(5,5)= b33
123.            b(6,6)= b33
124.  c         symmetric and zero part of constitutive matrix
125.            b(2,1)= b12
126.            b(3,1)= b12
127.            b(3,2)= b12
128.            b(1,4)= 0.0
129.            b(4,1)= 0.0
130.            b(1,5)= 0.0
131.            b(5,1)= 0.0
132.            b(1,6)= 0.0
133.            b(6,1)= 0.0
134.            b(2,4)= 0.0
135.            b(4,2)= 0.0
136.            b(2,5)= 0.0
137.            b(5,2)= 0.0
138.            b(2,6)= 0.0
139.            b(6,2)= 0.0
140.            b(3,4)= 0.0
141.            b(4,3)= 0.0
142.            b(3,5)= 0.0
143.            b(5,3)= 0.0
144.            b(3,6)= 0.0
145.            b(6,3)= 0.0
146.            b(4,5)= 0.0
147.            b(5,4)= 0.0
148.            b(4,6)= 0.0
149.            b(6,4)= 0.0
150.            b(5,6)= 0.0
151.            b(6,5)= 0.0
152.            endif
153.            endif
154.            End
```

```
      Subroutine elevar(n11,nn11,lay,gstran,gstres,stress,pstran,cstran,vstran,cauchy
     +  eplas,equivc,swell,krtyp,prangdt,gsv,ngens1,ngen1,nstats,nstass,therm)
C     ******************************************
C     it is called by Marc 'udump' option, makes the
C     element variables available at the integration
C     point at the end of each load increment.
C     ******************************************
      IMPLICIT REAL*8 (a-h,o-z)
      DIMENSION gstran(ngens1),gstres(ngens1),stress(ngen1),pstran(ngen1),cstran(ngen1),
     +          vstran(ngen1),cauchy(ngen1),dt(nstats),gsv(1),therm(ngen1),krtyp(4)

      DIMENSION ps(3),str(3,3),varint(8),varnod(8)
      REAL maxschuif
      common/usdam/usdama(1)
      common/usmod/usmoda(1)
      common/torc/torc(1)
      common/princ/prinstress (1)
      common/strold/strold(1)
      common/fnoc/fnoc(1)
      common/fnocold/fnocold(1)
      common/strares/strares(1)
      common /lifeparams/pn1comp, pn2comp, pn1ten, pn2ten
      common /stepcontrol/omegatar, overshoot
      common /features/ iydamage, iymoddeg, iyplastic, nincpcycl
      common /einit/ einit(1)
      common /totnoc/ totnoc
      common/ ymod/ ymod
      common/efirst/efirst(1)
      include 'far'
      include 'dimen'
      include 'creeps'
      include 'nzro1'
      include 'matdat'
      include 'blnk'
      include 'lass'
      include 'concom'
      include 'elmcom'
C     ***********************************************
C      n11 - element number
C      numel - total number of elements
C      nn11 - integration point number
C      inc - increment number
C     ***********************************************
      if (n11.eq. 1) write(*,*) 'in elevar'
C     ***********************************************
C      The element variables are required from the
C      loading increment
C     ***********************************************
      if (inc.ge. 1 .and. mod(inc, nincpcycl) .eq. nincpcycl/2) then
        k = n11 + (nn11 - 1)*numel
C     ***********************************************
C      Sets the number of cycles at each integration
```

```
C      to a high value prior to the calculation
C      ********************************************
            if (k.eq.1) fminnoc=1.0e7
C      ********************************************
C      princv is a function in Marc which makes the
C      principal stress values available
C      ********************************************
        CALL princv(ps,str,stress,ndi,nshear,0,0,0,0)
C      ********************************************
C      Function vm is used to determine the Von Mises stress
C      from the stress components and normalised stress
C      at each integration point is determined.
C      ********************************************
        vm=vonmis(stress, ngens1)
        strares(k) = vm/einit(k)
C      ********************************************
C      determines the minimum and maximum principal
C      stress values.
C      ********************************************
        if (abs(ps(1)).gt.abs(ps(2)) .and. abs(ps(1)).gt.abs(ps(3))) then
            prinstress(k)=ps(1)
        else
            if (abs(ps(2)).gt.abs(ps(3))) then
                prinstress(k)=ps(2)
            else
                prinstress(k)=ps(3)
            endif
C      ********************************************
C      determines whether the maximum principal stress is
C      tensile/compressive and assigns the values of 1 and 2 for
C      flag torc (k) for tension and compression respectively.
C      ********************************************
                if (prinstress(k) .lt. 0) then
                    prinstress(k) = -1.0*prinstress(k)
                    torc(k)=2
                else
                    torc(k)=1
                endif
        prinstress(k)= max(prinstress(k), 0.1)
        fnocold(k) = fnoc(k)
C      ********************************************
C      calculates the number of cycles to failure
C      fnoc at an integration point using the input
C      S-N relationships for tension and compression. For the
C      present analysis input is given for only compression.
C      ********************************************
        if (torc(k) .eq. 1) then
            fnoc(k)=10**(pn1ten*log10(strares(k))+pn2ten)
        else
            fnoc(k)=10**(pn1comp*log10(strares(k))+pn2comp)
        endif
C      ********************************************
```

```
C          The following part represents the method to find
C          the minimum number of cycles to failure within
C          the whole model.
C          ********************************************
              xnoc = min(omegatar, 1.0+overshoot-usdama(k))*fnoc(k)
                 if (xnoc .lt. fminnoc) then
                     fminnoc = xnoc
                     keyelm = k
                 endif
           endif
C          ********************************************
C          Once the elements in the whole model has been
C          checked for the minimum number of cycles to failure
C          move on to updating the damage and related variables
C          through subroutine updatvar
C          ********************************************
           if (n11 .eq. numel .and. nn11 .eq. intel) call updatvar(fminnoc, keyelm)
           endif
 8888       format(3i5,7e13.5)
           return
           end
```

```
           Subroutine updatvar(fminnoc, keyelm)
           IMPLICIT REAL*8 (a-h,o-z)
           LOGICAL vftposth,vftelevar,vftevec,schrijf,vftimpd,vfthklw
           common/usdam/usdama(1)
           common/usmod/usmoda(1)
           common/usmodnew/usmodnew(1)
           common/torc/torc(1)
           common/princ/prinstress (1)
           common/fnoc/fnoc(1)
           common/totep/totep(1)
           common/deltaep/deltaep(1)
           common/strares/strares(1)
           common/strold/strold(1)
           common/incbrk/incbrk(1)
           common/efirst/efirst(1)
           common/logica/vftelevar,vftimpd,vfthklw,vftevec,vftposth,schrijf
           common /modparams/pa1, pa2, pb1, pb2, pc1, pc2
           common /plasparams/pd1, pd2, pe1, pe2
           common /einit/ einit(1)
           common /totnoc/ totnoc
           common /features/ iydamage, iymoddeg, iyplastic, nincpcycl
           include 'far'
           include 'dimen'
           include 'creeps'
           include 'nzro1'
           include 'matdat'
           include 'blnk'
           include 'lass'
           include 'concom'
           include 'elmcom'
```

```
C     ********************************************
C      sets the number of cycles simulated in the
C      first iteration to one and in the subsequent
C      iterations to the calculated minimum number of cycles
C     ********************************************
      if (inc .le. nincpcycl/2) then
          deltanoc = 1.
      else
          deltanoc = max(fminnoc, 1.)
      endif
C     ********************************************
C      sets the total number of cycles simulated in
C      the first increment to 0. In the consequent
C      iterations updates it with the deltanoc from
C      current iteration.
C     ********************************************
      if (vftelevar) then
          totnoc=0
          vftelevar=.false.
      endif
          oldnoc = totnoc
          totnoc = totnoc + deltanoc
      write(80,8888) inc,mod(keyelm,numel), keyelm/numel+1,totnoc, deltanoc, fminnoc,
     +     prinstress(keyelm),strares(keyelm),usmoda(keyelm)
C     ********************************************
C      calculates the increment in damage at each
C      integration point
C     ********************************************
      do k = 1, numel*intel
      if (usdama(k) .lt. 1.0) then
       olddam = usdama(k)
       daminc = deltanoc/fnoc(k)
C     ********************************************
C      checks to assure the additive nature of damage
C      increment
C     ********************************************
      if (daminc .lt. 0) write (80,*) 'dw negative: Element ',k,' inc',inc, '.'
      omega = usdama(k) + daminc
      if (omega .ge. 1.0) then
      incbrk(k) = inc
      omega = 1.0
      write (80,*) 'Element ',k,' breaks in increment', inc, '. (E = ', usmoda(k)
      endif
      usdama(k) = omega
C     ********************************************
C      defines the upper boundary for the normalised
C      stress, the given value is for Solid Rigid PU foam
C     ********************************************
      str = max(strares(k), 0.0)
      if(str.gt.0.030)then
      str=0.030
      else
```

```
 82.            endif
 83. C          ********************************************
 84. C           calculates the constants A(cnstd), B (cnste) at the integration point
 85. C           for the respective normalised stress and calculates
 86. C           the accumulated strain for the damage.
 87. C          ********************************************
 88.            cnstd = pd1*str + pd2
 89.            cnste = pe1*str + pe2
 90.            if (omega .eq. 0.) then
 91.            ep = 0.0
 92.            else
 93.            ep = cnstd*omega**cnste
 94.            endif
 95.            deltaep(k) = ep - totep(k)
 96. C          ********************************************
 97. C           checks the incremental nature of strain increment
 98. C           and the lower boundary of normalised stress
 99. C           the calculated incremental strain is later
100. C           used in the subroutine crplw
101. C          ********************************************
102.           if (deltaep(k) .lt. 0 .or. str.lt. 0.0188) then
103.           deltaep(k) = 0
104.           else
105.           totep(k) = ep
106.           endif
107. C         ********************************************
108. C          calculates the constants C (cnsta), D (cnstb) at the integration point
109. C          for the respective normalised stress and calculates
110. C          the modulus reduction for the damage.
111. C         ********************************************
112.           cnsta= pa1*str + pa2
113.           cnstb= pb1*str + pb2
114.           if (omega .eq. 0.) then
115.           dymod=0.0
116.           else
117.           totmod =cnsta*omega**cnstb
118.           endif
119.           dymod = usmoda(k)-totmod
120. C         ********************************************
121. C          checks the decremental nature of modulus increment
122. C          and the lower boundary of normalised stress
123. C         ********************************************
124.           if (dymod .lt. 0 .or. str.lt.0.01988) then
125.           dymod = 0
126.           endif
127. C         ********************************************
128. C          updates the modulus
129. C         ********************************************
130.           usmodnew(k) = max(usmoda(k) - dymod, 1.)
131.           endif
132.           enddo
133.           return
```

```
134.            end
```

```
 1.              Subroutine crplaw (eqcp, eqcpnc, str, crpe, t, dt, timinc, cptim, m,
    nn,kc,mats,ndi,nshear)
 2.              IMPLICIT REAL*8 (a-h, o-z)
 3.              DIMENSION t(1),dt(1),str(3),crpe(1)
 4.              common/deltaep/deltaep(1)
 5.              common/totep/totep(1)
 6.              common/usdam/usdama(1)
 7.              common/incbrk/incbrk(1)
 8.              common /features/ iydamage, iymoddeg, iyplastic, nincpcycl
 9.              include 'concom'
10.              include 'dimen'
11.              if (m.eq. 1) write(*,*) 'in crplaw'
12.  C           ********************************************
13.  C            at the unloading increment of each iteration
14.  C            updates the model with the accumulated strain
15.  C            increment as the equivalent creep strain increment
16.  C           ********************************************
17.              if (mod(inc, nincpcycl) .eq. iyplastic) then
18.              k = m + (nn - 1)* numel
19.              if (usdama(k) .ge. 1.0) then
20.              jinc = inc - incbrk(k)
21.              if (jinc .eq. 1) then
22.              eqcpnc = deltaep(k)
23.              else
24.              eqcpnc = 0
25.              endif
26.              else
27.              eqcpnc=deltaep(k)
28.              endif
29.              else
30.              eqcpnc = 0.0
31.              endif
32.    8888       format('CRPLAW:',3i5,7e13.5) c
33.              RETURN
34.              END
```

```
 1.              REAL*8 FUNCTION vonmis(stress, ngens1)
 2.              IMPLICIT REAL*8 (a-h,o-z)
 3.              DIMENSION stress(ngens1)
 4.              if (ngens1. eq. 3) then
 5.                                  vonmis=   sqrt(0.5*((stress(1)-stress(2))**2+  stress(2)**2+
    +       stress(1)**2+6*stress(3)**2))
 6.              else if (ngens1 .eq. 4) then
 7.                              vonmis=sqrt(0.5*((stress(1)-stress(2))**2+  (stress(2)-stress(3))**2+
    +       (stress(3)-stress(1))**2+ 6*(stress(4)**2)))
 8.              else
 9.                          vonmis=  sqrt(0.5*((stress(1)-stress(2))**2+  (stress(2)-stress(3))**2+
    +       stress(3)-stress(1))**2+6*(stress(4)**2+stress(5)**2+stress(6)**2)))
```

```
10.            endif
11.            RETURN
12.            END
```

```
1.          Subroutine PLOTV (v,s,sp,etot,eplas,ecreep,t,m,nn,layrer,ndi,nshear,jpltcd)
2.  C       **********************************************
3.  C        The variables like damage, modulus, accumulated strain
4.  C        and total number of cycles are written to the
5.  C        post file.
6.  C       **********************************************
7.           IMPLICIT REAL *8 (A-H, O-Z)
8.           DIMENSION S(1),SP(1),ETOT(1),EPLAS(1),ECREEP(1)
9.           include 'dimen'
10.          common/usdam/usdama(1)
11.          common/usmod/usmoda(1)
12.          common/totep/totep(1)
13.          common/totee/totee(1)
14.          common/torc/torc(1)
15.          common /totnoc/ totnoc
16.          if (m.eq. 1) write(*,*) 'in plotv'
17.          k = m + (nn - 1)*numel
18.          IF (JPLTCD.eq.1) v=usmoda(k)
19.          IF (JPLTCD.eq.2) v=usdama(k)
20.          IF (JPLTCD.eq.3) v=torc(k)
21.          IF (JPLTCD.eq.4) v=totep(k)
22.          IF (JPLTCD.eq.5) v=totnoc
23.          RETURN
24.          END
```

```
1.           block data
2.          implicit real*8 (a-h,o-z)
3.          logical vfthklw,vftposth,vftevec,vftelevar,vftimpd,schrijf
4.           logical interc,interp
5.           common/funit/icom,idat,iint,irho,ipos,iinl,ivol,imov,iwrd
6.           common/logica/vftelevar,vftimpd,vfthklw,vftevec,vftposth,schrijf
7.           common /lifeparams/pn1comp, pn2comp, pn1ten, pn2ten
8.           common /modparams/pa1, pa2, pb1, pb2, pc1, pc2
9.           common /plasparams/pd1, pd2, pe1, pe2
10.          common /stepcontrol/omegatar, overshoot
11.          common /features/ iydamage, iymoddeg, iyplastic, nincpcycl
12.          common /totnoc/ totnoc
13.          common /randdam/ iseed, dammaxinit, dslope
14.          common/einit/einit (400000)
15.          common/usdam/usdama (400000)
16.          common/usmod/usmoda (400000)
17.          common/usmodnew/usmodnew(400000)
18.          common/torc/torc (400000)
19.          common/tx/tx (400000)
20.          common/princ/prinstress (400000)
21.          common/strold/strold (400000)
22.          common/fnoc/fnoc (400000)
```

```
23.     common/fnocold/fnocold (400000)
24.     common/strares/strares (400000)
25.     common/totep/totep (400000)
26.     common/deltaep/deltaep (400000)
27.     common/incbrk/incbrk (400000)
28.     common/efirst/efirst (400000)
29.     data vfthklw/.true./
30.     data vftelevar/.true./
31.     data icom,idat,iint,irho,ipos,iinl,ivol,imov,iwrd /80,45,58,38,41,57,60,70,90/
32.     data pn1comp,pn2comp,pn1ten,pn2ten/-23.64,-35.368,-23.64,-35.368/
33.     data pa1, pa2, pb1, pb2, pc1, pc2/-4511.8,150.27,-10.891,0.2141, 0.0,0.0/
34.     data pd1, pd2, pe1, pe2/3.5083,-0.0647,62.177,-0.9488/
35.     data omegatar, overshoot/0.02, 0.02/
36.     data iydamage, iymoddeg, iyplastic, nincpcycl/ 1, 1, 0, 20/
37.     data iseed, dammaxinit, dslope /5963211, 0.0, 0.3/
38.     end
```

A.1.1 FE Simulation of Compressive Fatigue of Herex Foam

The FE model with similar geometry and mesh density, as described in Chapter 6, was used for the analyses with the material properties and relationships replaced with that for Herex foam. The details of the input relationships in the algorithm and the default model are presented in Table A.1 and Table A.2 respectively.
The models gave converged results for cycle step factors of 0.5 and 0.02 %. Similar to studies carried out with Solid Rigid PU foam, the choice of mesh density, Pois-

TABLE A.1: Details of the input relationships and constants in the CDM algorithm for fatigue simulation of Herex ®C70.55 foam.

Relationships	Constants	Comments
Life $logN_f = C_1\ log\frac{\sigma}{E_*} + C_2$	$C_1 = -29.4$ $C_2 = -52.66$	σ is von Mises stress and E_* is 43, initial Young's modulus assigned to the material
Accum. strain $A\omega^B$	$A = -0.6912\frac{\sigma}{E_*} - 0.0108$ $B = 75.578\frac{\sigma}{E_*} - 0.546$	The relationships are valid within a normalised stress range of 0.008 and 0.0156
Modulus $C\omega^D$	$C = -752.98\frac{\sigma}{E_*} + 41.275$ $D = -1.459\frac{\sigma}{E_*} - 0.0061$	The relationships are valid within a normalised stress range of 0.0058 and 0.0161

TABLE A.2: The default FE model details for fatigue simulation of Herex ®C70.55 foam.

The default FE model details	
Initial Young's modulus and Poisson ratio	43 MPa and 0.3
Number of load increments in each iteration	2, peak load applied at compressive load direction and opposite
Type of FE analysis	Linear static analysis
Chosen load cases	Five load cases such that axial compressive stress at the midsection over these five load cases varied from 0.63, 0.58, 0.53, 0.48,to 0.43 MPa, analytically
Stress component for normalised stress calculation	von Mises stress
Termination point of revising fatigue parameters at integration points	total damage till that increment, $\omega = \sum \triangle\omega_i = \sum \frac{n_i}{N_{f\,i}} = 1$

son's ratio and stress component were tested for their satisfactory performance. The analytical values for life, modulus reduction and accumulated strain for the five load cases were determined by substituting the respective axial stress in to the relationships given in Table A.1. A comparison of the number of cycles to failure with analytical results, from the simulations of the five load cases using default model, for two cycle step factors are presented in Table A.3.

The FE models prediction slightly overestimated the life, compared to the analytical values for all the load cases and there was no difference in the results with the cycle step factors. Again, while reproducing the analytical results a constant stress value was assumed throughout the test, which may not be strictly true.

With the default model options the simulations predicted the fatigue behaviour very similar to the input model, at all stress levels. Figure A.2 compares the global, local and analytical values of modulus reduction and accumulated strain for a given load case. Figure A.2 shows the gradual accumulation of damage in the model, at various

TABLE A.3: Comparison of number of cycles to failure from analytical and FE simulation results of Herex foam, for five load cases, using the default model.

Load case	Stress (MPa) (analytical)	N_f (analytical)	N_f at node B from FE simulation for cycle step factor	
			0.02	0.005
1	0.63	18	22	22
2	0.58	210	253	253
3	0.53	2515	2945	2949
4	0.48	54689	67198	66492
5	0.43	1745768	2029330	2016680

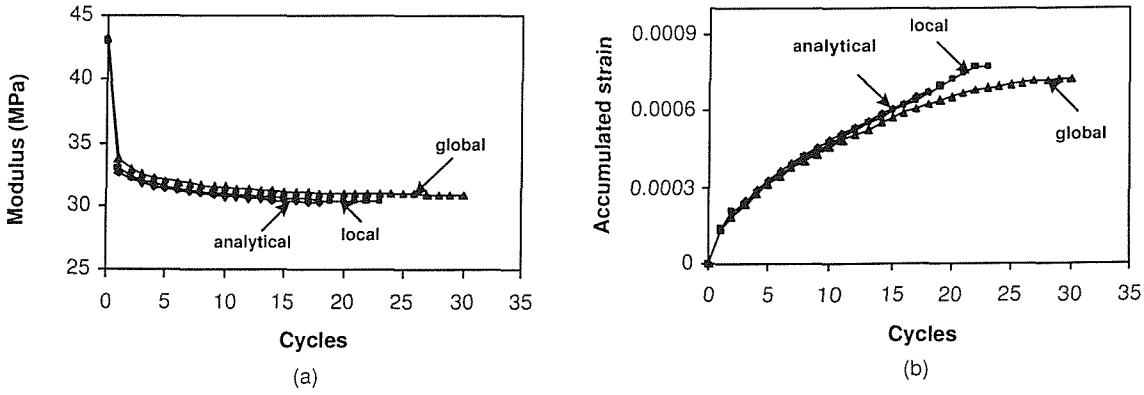

FIGURE A.2: Comparison of local, global and analytical values of (a) accumulated strain and (b) modulus reduction pattern from the fatigue simulation of herex foam. The axial stress was 0.63 MPa.

stages of the simulation for a particular load case. The first location of damage was at the neck, however, in the successive iterations the damage accumulation was shifted to the midsection. The pattern of its progression was more or less similar to that of Solid Rigid PU foam. However, differences are expected with the quantitative difference in the relationships describing the damage and properties coupled with it.

On applying a modulus reduction to the element, once it had failed, resulted in underestimation of life (Figure A.4). The tertiary stage of rapidly decreasing modulus were related to the factor by which modulus was reduced. The analysis showed that the change in element status by modulus reduction caused a very high stress in the surrounding elements and resulting in the faster damage growth and failure of the whole unit.

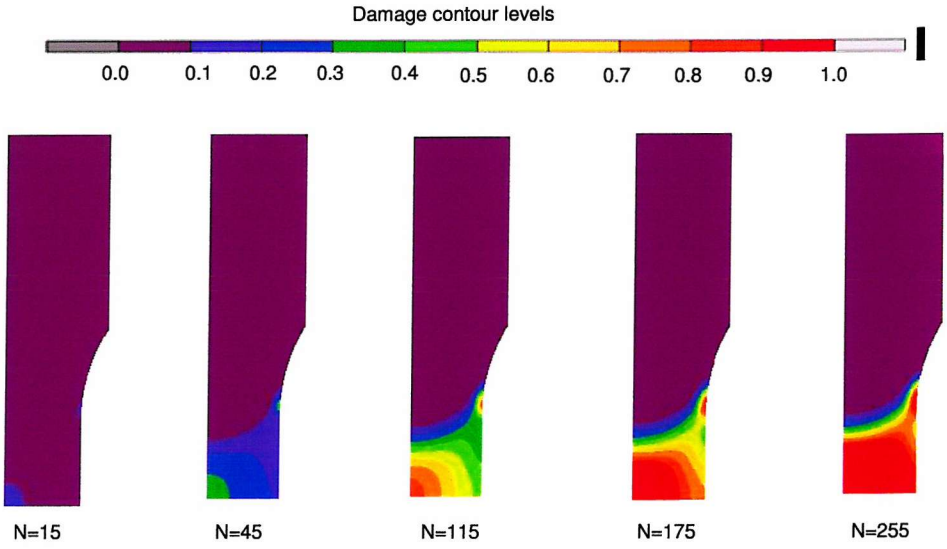

FIGURE A.3: Progression of damage pattern at various stages of the simulation of uniaxial fatigue of Herex foam. The axial stress was 0.58 MPa.

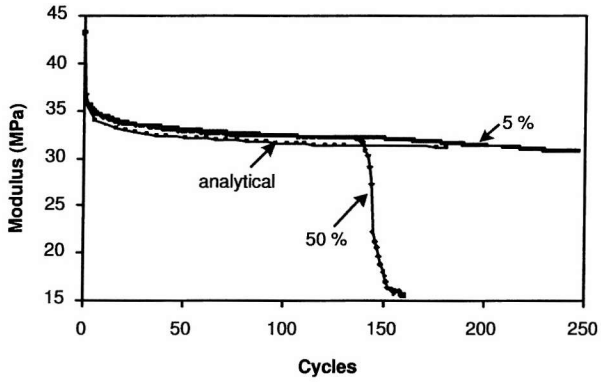

FIGURE A.4: Comparison of modulus variation at global level for modulus reduction factors from the fatigue simulation of Herex foam for for cases of default model and modulus reduction by 50 and 5%. Applied axial stress was 0.58 MPa.

Appendix B

The FE Simulation of Implant Migration Using Herex Foam

In Chapter 7, various aspects of FE simulation of migration using the material model of Solid Rigid PU foam were presented. The models underpredicted the migration behaviour, mainly due to the effect of stress concentration at the boundaries. A detailed discussion of the issues in the simulations and methods/approaches to be addressed in future work were discussed in Chapter 7. The analyses were carried out with the Herex foam model as well. The input relations were the same as for uniaxial models (Table A.1). However, initial migration simulations of the Herex foam model showed the edge effect and damage was occurring mainly at the boundaries. Again, there was an initial rapid phase of migration, followed by a steady rate. The magnitude of migration were directly related to the applied load. The simulations underpredicted migration significantly, as observed for Solid Rigid PU foam. Further detailed analysis of the model was not carried out. The results from FE simulations (using options for **Analysis 2** Table 7.3) for two load cases (0.35 kN and 0.4 kN) are presented here. Figure B.1 compares the migration pattern for the two load cases, and Figure B.2 show a comparison of the FE simulation results with experiments.

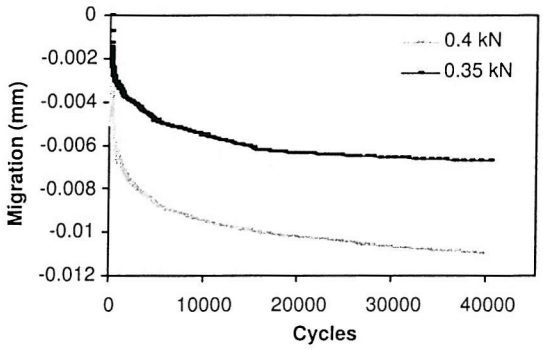

FIGURE B.1: Comparison of migration for two load cases using Herex foam model, from **Analayis 2**.

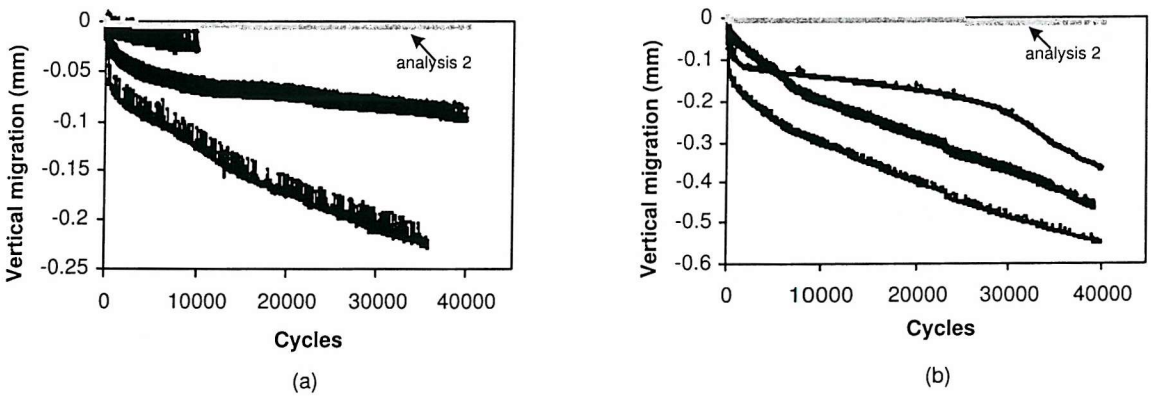

FIGURE B.2: Comparison of the migration pattern from FE simulation and experiment using Herex foam for an applied load of (a) 0.35 kN and (b) 0.4 kN. The FE simulations results from **Analysis 2** is used for the comparison.

Appendix C

Publications

Parts of the research work carried out in this thesis have been presented at International conferences and meetings. Some of the research work presented in Chapter 5 was published as a Journal paper. Besides, some of the collaborative work with outside researchers/groups has also appeared in conferences. A list of publications is given below, along with the journal paper.

SELECTED PUBLICATIONS AND PRESENTATIONS

1. V. Palissery, M. Taylor, M. Browne, "Characterisation of a Polymer Foam to Use as a Cancellous Bone Analogue Material in the Assessment of Orthopaedic Devices", Journal of Materials Science: Materials in Medicine, 15, 61-67, 2004.

2. V. Palissery, M. Taylor, M. Browne, 2002, "Characterisation of a Substitute Material to Model cancellous bone in *In Vitro* Implant Migration Studies", 4th World Congress Biomechanics, Calgary, Canada.

3. R. Hussein, J. A. N. Shepperd, V. Palissery, M. Browne, M. Taylor, 2002, "The effect of tapered pegs on tibial tray subsidence in closed cell foam", British Orthopaedic Association Annual Congress, Cardiff, UK.

4. V. Palissery, M. Taylor, M. Browne, 2001, "Characterisation of Static and Fatigue Behaviour of a Polyurethane Foam Material to Model Cancellous Bone", European Society of Biomaterials, London, UK.